Comparative Evaluation of Flax, Cattail, and Hemp Fiber Composites

by

MD. SHADHIN

A Thesis submitted to the Faculty of Graduate Studies of

The University of Manitoba

in partial fulfillment of the requirements of the degree of

MASTER OF SCIENCE

Biosystems Engineering

University of Manitoba

Winnipeg, Manitoba, Canada

ABSTRACT

Composite parts, used in transportation industries, are manufactured using VARTM (Vacuum Assisted Resin Transfer Molding) and glass fiber non-woven mats that are optimized for impregnation, fiber volume fraction (V_f), and composite properties. However, such optimized non-woven mats are commercially not available for natural fibers such as hemp and flax. Fahimian (2013) has developed the knowledge on the effect of areal density (weight per unit area), needle punching used to bind the fibers together, and the pressure applied during manufacturing, on composite properties. Similar studies on flax fibers is not available. Such studies on Cattail fibers, with comparable properties and abundance, are lacking. Hence, the goal of this thesis to generate this knowledge and do a comparative evaluation of flax, cattail, and hemp fibers and their composites. The mat permeability as well as tensile strength and modulus of needle-punched (0-72P) flax composites, manufactured using VARTM pressure as well as compression molding pressures (subsequent to VARTM molding), were measured and evaluated. Similar studies were repeated on 50% Flax-50% hemp fiber mat. Cattail fibers were extracted from cattail leaf using alkali retting, characterized for properties, and used to manufacture 0-P mat. This was subsequently used to test for permeability as well as manufacture composites for mechanical testing. The results from these studies as well as that for hemp fiber (generated by Fahimian (2013)) were used in comparative evaluation of the three fibers as reinforcement in composites.

It was found that the V_f of flax mats changes with punch density that affects the permeability. V_f in flax mat composite dictates the modulus and strength which is a function of consolidation behavior that varies with punch density and pressure. Despite having similar tensile strength in all three fibers, cattail fibers possess higher specific strength than flax and hemp due to lower density values of cattail fiber; however, modulus and specific modulus increases as follows ($E_{flax} < E_{cattail} < E_{hemp}$); it should be noted that the weight of the composite

part decreases with increase in specific properties of the fiber. The transverse permeability of cattail fiber mat is the highest, followed by hemp fiber mat and the flax fiber mat's permeability was the least. At VARTM pressure (101 kPa) the properties of composites with three fibers are similar.

ACKNOWLEDGEMENT

He who does not thank the people, does not thank Almighty Allah.

–Prophet Muhammad (may peace be upon him)

First and foremost, praise is to Almighty Allah (SWT) for all his blessings for giving me patience and good health throughout my MSc degree.

I would like to express my sincere gratitude to my co-supervisor, Dr. Raghavan Jayaraman, for giving me the opportunity to work with Composites Materials and Structures Research Group (CMSRG) and department of Mechanical Engineering of the University of Manitoba, who has guided me with immense knowledge and inspiration throughout this journey.

I would also like to give my sincere thanks to my academic supervisor, Dr. Mashiur Rahman, who supported, guided, and encouraged me during my studies. I am grateful forever to him for providing me the opportunity to work under his supervision.

I would like to thank Mike Boskwick for his technical assistance and support during my research.

I extend my gratitude to URGP (University Research Grant Program), NSERC, and Dr. Danny Mann for their financial support.

I would like to thank my lab mates – Kaushal Sharma and Spence Cabel. I would also like to thank Ikra Iftekhar Shuvo, Mostafizur Rahman, and Masud Rana for their immense support while doing my studies at U of M. Finally, I would like to thank my parents, for all their support and patience.

TABLE OF CONTENTS

LIST OF TABLES

LIST OF FIGURES

CHAPTER I
INTRODUCTION

Polymer-matrix composites (PMC) are increasingly used in structural applications. PMC consists of a thermoset or thermoplastic matrix reinforced with reinforcing fibers. The higher modulus of reinforcing materials, when compared to the polymer matrix, makes fibers the main load-bearing component. The properties of polymer matrix composites can be tailored to meet the specific needs of an application.

PMC can be categorized as a particulate composite, a discontinuous or short fiber composite, and a continuous fiber composite. Continuous fiber composites are used in structural applications in the aerospace industry, for example, as components of civil and military aircraft such as box beam skins, flaps, fairings, vertical and horizontal stabilizers, components of forward, mid and rear fuselages, fuel tanks, engine doors, drive shafts, fences, and rotor blades for helicopters, where meeting the desired properties requirement is more significant than the cost. However, discontinuous fiber composites are usually used in semi-structural or non-structural applications such as doors, windows, furniture, gaskets, ceiling tiles, and automotive interior parts, where cost is the primary consideration. The selection of fiber as a reinforcement relies on the mechanical properties requirement of the final composite product and manufacturing process as well as increasing focus on biodegradability.

1.1 BACKGROUND

Natural fiber reinforced composites (NFRC) are preferable because of their low density, low manufacturing cost, flexibility, and renewability over synthetic composite products. Consumer preference has been growing in recent times towards new products from renewable

sources. The concept of green composite, biodegradability, new directives on recycling, and social influence have led the consumer towards eco-friendly products. The natural biomass fibers (BFs), such as flax, kenaf, jute, hemp, and sisal, are increasingly investigated as environmentally friendly alternatives to glass fibers for engineering applications (Fahimian, 2013; Nishino et. al., 2003; Karnani, 1997; Oksman, 2002; Wambua et. al., 2003; Wrobel et. al., 2012; Yan et. al., 2014).

Natural fibers can be plant-based or animal-based according to their sources. Plant-based fibers, commonly known as cellulosic fibers, and animal based-fibers are similar to protein fibers. Cellulose, hemicellulose, and lignin are the main constituents of plant-based fibers, which are usually extracted from bast (e.g. flax, hemp, jute), leaves (e.g. sisal), seed (e.g. cotton), fruit (e.g. coir), wood (e.g. hardwood, softwood), stalk (e.g. wheat, maize), and grass (e.g. bamboo) (Lau et. al., 2018).

The bast fibers are the most widely used natural fiber in composite applications. Among them, published research have mostly focused on composites made from flax, hemp, jute, kenaf, and ramie. Two other natural cellulosic fibers that have been extracted from waste biomass and are shown to be comparable with the currently used bast fibers, are: canola fiber from canola stems and cattail fiber from leaves whose physical and mechanical fiber properties have recently been published (Shuvo et. al., 2019). These fibers are comparatively easier to extract from their raw resources. The common extraction methods of bast fibers are by using water and chemical retting (Verma et. al., 2016).

Bast fibers have a few drawbacks that hinder their performance on composite applications. One drawback is that bast fibers are hydrophilic in nature, resulting in poor fiber-matrix interfacial adhesion (Mohanty et. al., 2001). Surface modification is needed to improve the fiber-matrix interfacial bond strength and to reduce the hydrophilic characteristic of bast

fibers. However, there have been large variations reported in the scientific literature regarding their mechanical properties.

Bast fibers extracted from plants are discontinuous. Dry spinning them into continuous yarns, for manufacturing continuous fiber composites, is costly. Hence, using them as discontinuous fibers is cost effective and has been the focus of the Composites Materials and Structures Research Group (CMSRG) at the University of Manitoba. Discontinuous glass fiber mats have been used along with VARTM (Vacuum Assisted Resin Transfer Molding) and thermoset resin to manufacture cost effective semi-structural applications such as panels for buses and coaches manufactured by New Flyer Industries and Motor Coach Industries in Winnipeg, MB. In order to successfully replace glass fiber mat in these composites with bast fibers such as Hemp and Flax grown in Canada, non-woven mats of these fibers are required. Currently, there are no commercial manufacturers and suppliers of these mats in North America.

Hence, the CMSRG group of Dr. Raghavan Jayaraman at the University of Manitoba have been studying the design of non-woven mats and their effect on manufacturability and properties of composites manufactured using VARTM for transportation applications. They have used the Pilot plant facility at NCSU, Raleigh, North Carolina, USA to manufacture mats of hemp, flax, and 50% hemp-50% flax. Unlike glass fiber mats where fibers are bound together using a binder, the hemp and flax mats are bound through needle punching. Punch density was veried from 0 to 72 and needle punch depth from 0 mm to 8 mm in this study for flax to identify the optimal mat manufacturing conditions.

Fahimian (2013) has correlated the effect of punch density on permeability, consolidation, compressibility of hemp mats during manufacturing as well as properties of manufactured composites. However, similar study of flax mats, manufactured by him, is

required to confirm the broader applicability of the mat design to natural fibers and hence is one focus of this study.

Another focus of this study is to investigate the suitability of a cattail fiber in composite application due to its many advantages over bast fibers. Unlike BFs that are grown as main crop, cattails grow naturally in bog and fen, lacustrine marshes, prairie pothole marshes, roadside ditches, riverine marshes, tidal marshes, and wet meadows. Total wetland in Canada is estimated to be 1.5 million km^2 and it is estimated that 23% of land in the Prairie Pothole Region is wetland (Euliss et al., 2006; Canadian Encyclopedia, n.d.). A comparison of cattail with flax and hemp is given in Table 1.1.

Table 1.1 Comparative Analysis of Cattail, Flax, and Hemp.

Fiber type	Fiber source	Water footprint (litre/kg)	Availability	[e]GHG emissions (CO_2-eq/tonne of fiber)	Density (g/cc)	Fiber yield (%)	Moisture regain (%)
Cattail	Waste/marginal land	N/A	Abundant[c]	202	1.26[f]	30-60[h]	8.3-12.5[m]
Flax	Main crop	3,783[a]	Limited ($800x10^3$tons)[d]	902	1.54[g]	10-15[g]	12.0[k]
Hemp	Main crop	3,783[b]	Limited ($214x10^3$ tons)[d]	846	1.54[g]	10-15[g]	8.0[l]

[a]:Hoeckstra 2013; [b]:Averink 2015; [c]:The Canadian Encyclopedia, n.d.; Euliss et al, 2006; [e]:from field operations to non-woven factory – de Beus al, 2019, calculation is based on fibre cultivation in Europe to the factory gate of the non-woven producer in Germany; [f]:Mortazavi and Moghadam, 2009; [g]:Shuvo et al, 2019; Rahman et al, 2020; [d]:Ngo 2018; [k]: Collier & Epps, 1999; [l]:Morrton & Hearle, 2008; [m]:Hasan, 2019

Table 1.1 demonstrates the advantages of cattail over flax and hemp fibers, which include lower density, abundant supply without any cost in growing them, and higher fiber yield (%). Lower density would help to save energy when used as reinforcement in composite used in automobile applications. Further, the production of cattail does not require any water during plant growing; therefore, the greenhouse emission would be much lower than that of flax and hemp as mentioned in Table 1.1. However, the moisture regain of cattail fiber is

comparable with flax and hemp and high for composite applications and requires further surface treatment to enhance adhesion with the hydrophobic resins. Despite the advantages of cattail fibers over flax and hemp, research on comparative evaluation with flax and hemp has not been done yet and is a second focus of this study. Nonwoven preform is required for manufacturing composite in VARTM and compression molding. Hence, manufacturing nonwoven from cattail is focused on this study as published studies on the same are also missing.

1.2 THESIS GOALS AND SCOPE

The goal of this thesis is to perform a comparative evaluation of properties of discontinuous natural fiber composites manufactured using flax, hemp, and cattail fibers.

The effect of punch density on permeability of the non-woven mat, as well as the effect of punch density and manufacturing pressure on properties of 100% flax and 50% flax-50% hemp fiber composites, manufactured through VARTM, were studied in this thesis and compared with the results generated by Fahimian (2013) for Hemp.

In order to investigate the suitability of cattail fiber for composite applications, the effect of humidity on the properties of the fibers as well as surface modification to enhance its suitability for impregnation by hydrophobic thermoset resin was first studied. Subsequently, cattail composites with zero-punch mat were manufactured with untreated and DIH (1,6-diisocyanatohexane) - HEA (2-hydroxyethyl acrylate) treated fiber, were manufactured using VARTM and compression molding and tested. Finally, tensile properties of hemp, flax, and cattail fiber composites are compared and evaluated.

1.3 ORGANISATION OF THESIS

The organisation of this thesis is arranged in the following order.

- Chapter 1: Introduction
- Chapter 2: Detailed Literature Review - In this chapter, published studies on natural fiber structure and mechanical properties, characterisation of nonwoven mat, effect of punch density and consolidation pressure on composite properties are presented and discussed to establish the knowledge gaps in support of the objectives of this thesis.
- Chapter 3: Experimental details - In this chapter, experimental details and methods involved in fiber evaluation, mat characterisation, manufacturing composite, and an analysis of mechanical properties for 100% flax, 50% flax/50% hemp fiber matt, cattail fiber composites are presented and discussed.
- Chapter 4: Results and discussion – Flax fiber characterization, evaluation of mat parameters, manufacturing flax composite from zero punched and various needle punched mat, correlation between mat manufacturing parameters and composite properties are presented and discussed in this chapter.
- Chapter 5: Results and discussion - Cattail fiber extraction, evaluation of fiber properties, fiber surface modification, preparing nonwoven cattail mat, manufacturing cattail composite, and evaluation of mechanical properties evaluation of composite are presented and discussed in this chapter
- Chapter 6 : Comparative analysis on flax, cattail, and hemp composites is presented in this chapter.
- Chapter – 7: Conclusions.

CHAPTER II

LITERATURE REVIEW

2.1 INTRODUCTION

Natural lignocellulose fibers, such as flax (bast/biomass), hemp (bast/biomass) and cattail (leaf/ biomass) are the interest of the current research for composite applications due to their biodegradability, availability, and lower cost. A composite may be defined as a physical mixture of two or more different materials and has properties, which are generally better than any one of the materials used. The composites from natural fibers are manufactured by infiltrating resin into the natural fiber non-woven preform (virgin and treated) at different consolidation pressures. The composite manufacturing pressures as well as the mat thickness, permeability, and fiber volume fraction determine the performance of natural fiber reinforced composites (NFRC).

However, mat manufacturing parameters, for example, density of needle punch and needle depth in flax and hemp mats that might affect the mat properties and NFRC performances have been comprehensively reviewed based on the published literatures to support the scope and objective of this research. Further, a novel biomass fiber from leaf (cattail) has been investigated for its suitability in composite applications. Finally, cattail fiber and composites have been investigated and compared with that of the other biomass fibers (flax and hemp).

2.2 BACKGROUND INFORMATION

2.2.1 Lignocellulosic fiber

In broad sense, fibers can be categorized as natural or man-made . Based on origin, natural fibers can be classified as plant, mineral, and animal fibers. The classification of natural fibers is shown in Table 2.1. Plant based fibers or vegetable fibres are mainly composed of cellulose, hemicellulose, and lignin and they are usually extracted from bast, leaf, seed, fruit, wood, stalk, and grass/reed (Pecas et. al., 2018). Bast fibers are produced around the globe. The world production of various lignocellulosic fibers and their geographical distribution is shown in Table 2.2 (Bharath & Basavarajappa, 2016).

Table 2.1. Classification of natural fibers based on their origin (Pecas et. al., 2018; Bharath & Basavarajappa, 2016).

	Origin	Fiber type	List of fibers
Natural fibers	Lignocellulosic	Bast	Flax, Hemp, Jute, Kenaf, Ramie
		Leaf	Abaca, Banana, Pineapple, Sisal
		Seed	Cotton, Kapok
		Fruit	Coir
		Wood	Hardwood, Softwood (e.g., Eucalyptus)
		Stalk	Wheat, Maize, Oat, Rice
		Grass / Reed	Bamboo, Corn
	Animal	Wool / hair	Cashmere, Goat hair, Horse hair, Lamb wool
		Silk	Mulberry
	Mineral	-	Asbestos, Ceramic fibres, Metal fibres

Table 2.2 World production of lignocellulosic fibers and their manufacturer. (Ramamoorthy et. al., 2015; La Mantia & Morreale, 2011; John & Thomas, 2008; Yan et. al., 2014).

Fiber type	Fiber name	World production (10^3 ton)	Largest producers
Bast	Flax	830	Canada, France, Belgium
	Hemp	214	China, France, Philippines
	Jute	2300	India, China, Bangladesh
	Kenaf	970	India, Bangladesh, USA
	Ramie	100	China, Brazil, Philippines, India
Leaf	Abaca	70	Philippines, Ecuador, Costa Rica
	Pineapple	74	Philippines, Thailand, Indonesia
	Sisal	378	Tanzania, Brazil
Seed	Coir	100	India, Sri Lanka
	Cotton	25000	China, India, USA
	Oil palm	40	Malaysia, Indonesia
Grass	Bagasse	75000	Brazil, India, China
	Bamboo	30000	India, China, Indonesia

Among all the lignocellulosic fibers, bast fibers are mostly used one as a reinforcement in discontinuous fiber composite. Flax (*Linum usitatissimum*) is a bast fiber mainly produced in Canada, France, and Belgium and is predominantly grown for the fiber and the linseed oil. Flax fibers were reported to be used for many applications well before 5000 BC in Egypt and Georgia. High grade long fibers are usually converted into yarns for textiles and the low-grade fibers are used as reinforcements/fillers in composites (Ramamoorthy et. al., 2015). The structure, morphology, and properties of flax fibers are explained in previous studies (Charlet et. al., 2007; Cristaldi et. al., 2010; Shadhin & Shuvo, 2019). Due to its high cellulosic content

and high specific properties, flax stands as a strong and potential candidate for the replacement of existing synthetic fibers.

Cattail (*Typha latifolia*) fiber is a newly recognized bast fiber to use as a reinforcement in discontinuous fiber composite. Cattail plant grows abundantly in swamplands and near the edge of ponds and lakes and becoming increasingly dominant wetland plants in North America (Shih & Finkelstein, 2008). The chemical composition of cattail is shown in Table 2.3 (Vetayasuporn, 2007). Cattail fibers are prevalent in nature and their mechanical properties are also promising like other bast fibers such as flax, hemp, and jute. The chemical composition of the bast fibers (flax, hemp, jute, kenaf, ramie) could be found in section 2.3.2 (Table 2.5).

Table 2.3. Chemical composition of cattail fiber (Vetayasuporn, 2007).

Fiber	Cellulose (%)	Hemi- cellulose (%)	Lignin (%)	Wax (%)	Ash (%)
Cattail	63	8.7	9.6	1.4	2

2.2.2 Key factors affecting natural fiber composite properties

The mechanical properties of Natural Fiber Reinforced Composite (NFRC) rely on the chemical constituents of fiber, reliable fiber supply chain, and important fiber characteristics, such as fiber geometry, fiber orientation, fiber moisture absorption, fiber porosity, permeability, and fiber volume fraction (Lau et. al., 2018; Ho et. al., 2012). The major fiber characteristics that affect the properties of natural fiber composite are illustrated in Figure 2.1. It may be possible to obtain the desired mechanical properties of NFRC by controlling and tailoring these properties.

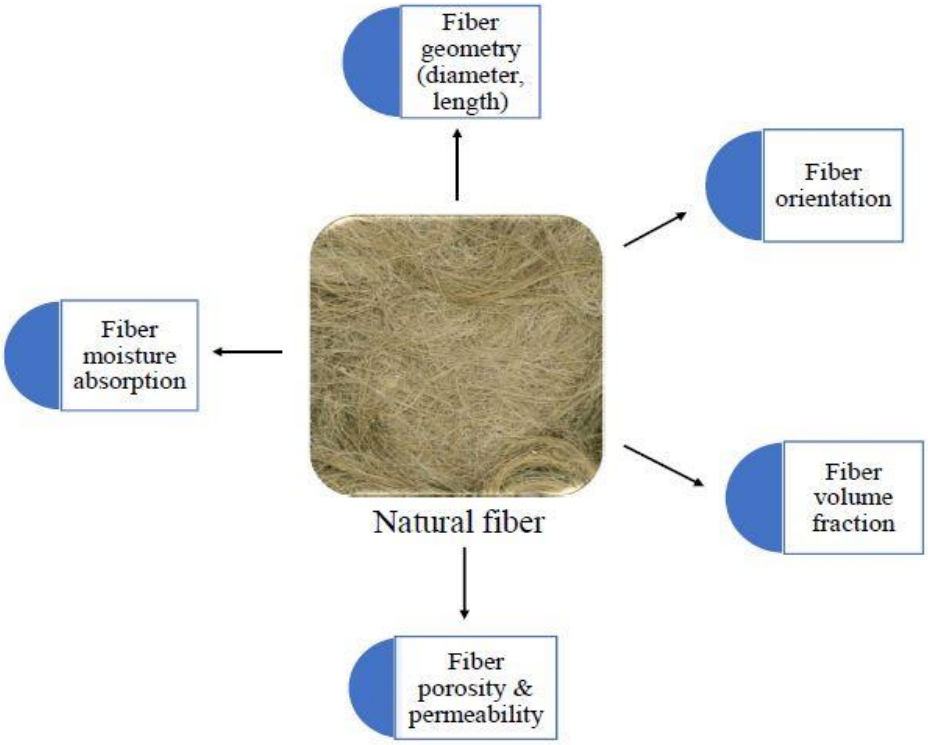

Figure 2.1 Key factors that affect the properties of natural fiber composite.

a) <u>Fiber geometry</u>

Variability in the natural fiber diameter is the major difference between natural fibers and synthetic fibers. The diameter of synthetic fibers can be designed to meet the end-use requirement during fiber spinning by choosing spinnerets with desired hole size; whereas the natural fiber diameter varies greatly (CV% can be as high as 20%) along the length of the fiber. However, the aspect ratio (l/d, where l is the length and d is the diameter of fiber) could be an important parameter to determine the properties of NFRC (Facca et. al., 2006).

The fiber diameter is the key to influence critical length (lc). In composites, the critical length, l_c is a parameter that indicates the amount of stress transferred to the fiber; a fiber whose aspect ratio is greater than the critical aspect ratio would strengthen the composite while

a fiber whose aspect ratio is smaller than the critical aspect ratio is more likely to weaken the material. For a given fiber diameter d and the critical fiber length l_c, the fiber-matrix interfacial bonding strength can be determined using Eq. (2.1) (Chawla, 2012).

$$\frac{l_c}{d} = \frac{\sigma_f^u}{2\tau_y} \tag{2.1}$$

where: l_c stands for the critical fiber length,

d for fiber diameter

σ_{fu} for fiber tensile strength, and

τ_y for fiber-matrix interfacial bond strength.

From Eq. (2.1) it can be stated that the fiber length l should be greater than the critical length lc for the fiber to be loaded to its maximum stress, σ_{fu}. The fiber critical length is important as it is known from the 'Shear lag model' (Chawla, 2012), which explains the mechanism of load transfer from the matrix to the fiber, and that composite failure would occur due to the fiber fracture followed by the matrix failure when $l > l_c$ while composite failure would occur due to fiber debonding followed by matrix failure when $l < l_c$ (Chawla, 2012). Figure 2.2 illustrates the variation in tensile stress and interfacial bond strength with different critical fiber lengths and aspect ratios.

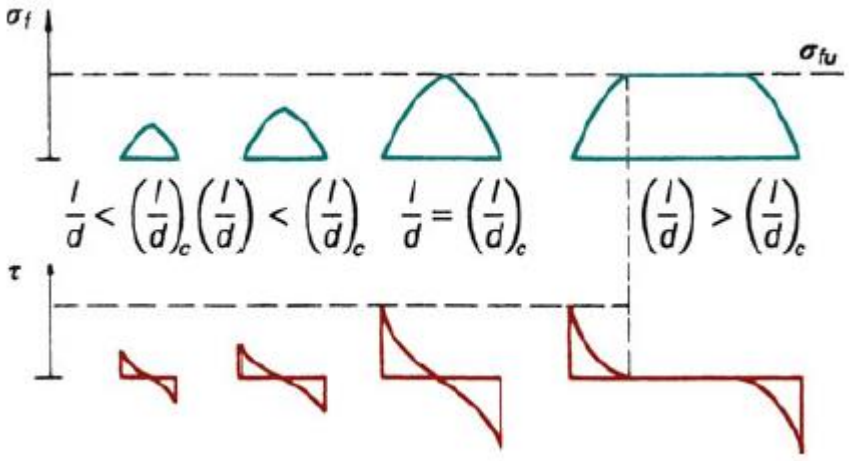

Figure 2.2 Schematic diagram of variation in tensile stress (σ_{fu}) and interfacial bond strength (τ_y) with different critical fiber lengths (l_c) and aspect ratios (l/d) (Chawla, 2012).

b) Fiber moisture absorption

Another drawback of natural cellulosic fibers such as flax, hemp, and cattail is the hydrophilicity, which degrades the fiber performance in PMC. Higher moisture content in the fiber results in poor fiber-matrix interfacial adhesion while manufacturing composites (Mohanty et. al., 2001). However, the hydrophilic properties of fiber can be reduced by chemical treatment (Qiu et. al., 2011).

c) Permeability

The manufacturing of the composite and the subsequent mechanical properties of composites manufactured from these fibers may vary due to permeability of the fiber preforms used while manufacturing composite. Permeability of fiber preform would depend on the fineness of fiber (fiber diameter), packing of fiber, and other manufacturing parameters (in case of needle punched preform) such as needle punch density and needle depth. Small inter-fiber spacing in case of smaller diameter fibers would result in low permeability, which in turn will affect the manufacturing process.

d) Fiber volume fraction

The fiber content or fiber volume fraction plays a key role to achieve the desired mechanical properties of PMC. The strength and stiffness of PMC will increase with the increasing fiber content in a reinforcement. However, too high fiber content or fiber volume fraction (%) would result in degradation of material properties due to insufficient filling of the matrix to hold the fibers together. Thus, an optimum fiber content is needed to achieve a balanced interface strength that is high enough to attain better mechanical properties.

e) Fiber orientation

The fiber orientation defines the orientation of the longitudinal axis of the fiber in a composite, with respect to the loading axis. During non-woven mat production, fibers are fed onto the conveyor belt by pneumatic pressure. Further, the fiber orientation could be changed by the moulding pressure and resin flowing pattern while manufacturing composites. The fiber orientation is quantified by the orientation factor (ξ). The relationship between the orientation factor and mechanical properties of composites can be determined using Eq. (2.2) (Chawla, 2012). The higher the orientation factor, the better the mechanical properties of the manufactured composite. $\xi = 1$ for aligned and continuous fiber composite and $\xi < 1$ for random fiber orientation.

$$Ec = \xi E_f V_f + E_m V_m \quad (2.2)$$

where: ξ is the orientation factor.

E_C, E_f, and Em denotes the modulus of composite, fiber, and matrix respectively.

V_f, and V_m denotes the fiber volume fraction of fiber and matrix respectively.

2.2.3 Nonwoven mat

Non-woven mats are also known as nonwoven or nonwoven fabric. Processes for converting fibers directly into a fabric or mat without involving the spinning and weaving operations are known as nonwoven processes. Nonwoven products have the potential to replace woven and knit materials due to their lower cost and ease of processing as the process of spinning for making yarn and weaving or knitting for making fabric is expensive, time consuming, and labour oriented when compared to nonwoven mat manufacturing process. Nonwoven products are being used in composite industries, apparel, home building, packaging, and geotextile industries because of their higher permeability, better friction, and better conformability when compared to woven products (Gillies, 1979; MARIENFELD, 1995).

Nonwoven mat manufacturing process consists of two major steps that include web formation and binding. Three methods of forming a web are (1) air laying, (2) wet laying, and (3) spun laying (MARIENFELD, 1995). Air laying technique is the focus of this study where fibers are separated by a mechanical comb, suspended in air, and dropped on to a moving conveyor belt to form the web of fibers. In wet laying, fibers suspended in water are collected on a screen, drained of any entrapped water, and dried to form the web. In spun laying, hot and continuous synthetic filaments extruded through the spinnerets are blown onto a moving belt where they are bonded together to form the web.

The various mat binding methods (Yan et. al., 2014). include thermal, mechanical and chemical. In thermal binding, the thermoplastic component of a mat softens upon application of heat and binds the fibers together. The mechanical binding includes hydro-entanglement and needle punching. Hydro-entanglement uses fine jets of highly pressurized water to entangle and bind the fibers. In needle punching, entanglement of fibers is achieved by a set of barbed needles punching through the web. This study has used a mat without a binding

material. This study has used a mat without a binding material and needle punching was used here to bind the fibers in the mat.

2.2.4 Needle punching

Natural fibers such as cotton, jute, wool, sisal and a few synthetic fibers such as polypropylene, polyethylene, rayon, and nylon have been used in manufacturing needle punched mats. Needle-punched nonwovens are felt-like and very flexible, with a fibrous network and distinctive pores that are entangled to form a complex 3D structure by random fibers. Needle punched nonwovens are accounted for its bulky nature and a wide range of pore size distribution.

Schematic diagram of needle punched flax fiber mat manufacturing process is illustrated in Figure 2.3. In the needle punching process, the web of fibers is formed by air-laying and fed into a needling press or needler using a conveyor belt. Needle board is fitted with needles which strike the web of fibers from the top, and the needles descend through the web by a pre-determined needle depth. During this downward stroke, the grooves in the needles pick up in-plane fibers (parallel to the surface of the web) and reorient them in the out-of-plane (i.e. along the thickness of the web) direction. These reoriented fibers mechanically interlock the rest of the fibers resulting in the mat. The punch density (P) is measured in punches per cm^2 and calculated usually from Eq. (2.3) [Hearle, J. W. S. (1972].

$$P = \frac{N_O X S}{V_x} \tag{2.3}$$

where N_O is the number of needles per unit length of the needle board (needles/cm), S is the number of strokes per unit time (Punches/sec) of the needle board, and V_x is the speed of the conveyor belt (cm/sec).

The structure of needle-punched fabric is not homogenous and structural anisotropy in the manufactured needle punched nonwoven mat arises due to rearrangement of fibers while processing. The shape and number of holes depends on the number of needles in the needle board, the size of needles, advances per stroke, punching density and fiber type (Das et al., 2012; Jinlian, 2008). Key parameters that influence the performance characteristics of a nonwoven needle-punched mat are – properties of the fiber used in mat; needle density; depth of penetration of needle, needling rate, and mat areal density (Venkatappa & Banerjee, 1997).

In this study, the punch density was varied from 0 and 72 to understand its effect on the structure of the mat and manufactured composite. Needle depth is the distance travelled by the needle beyond the bottom surface of the web. For a given areal density of the mat, the structural parameters could be altered when depth of needle penetration is varied which influences the subsequent properties of mat and composite. In this study, needle punching was executed on nonwoven flax mat only and the needle depth was varied between 2 and 8 mm.

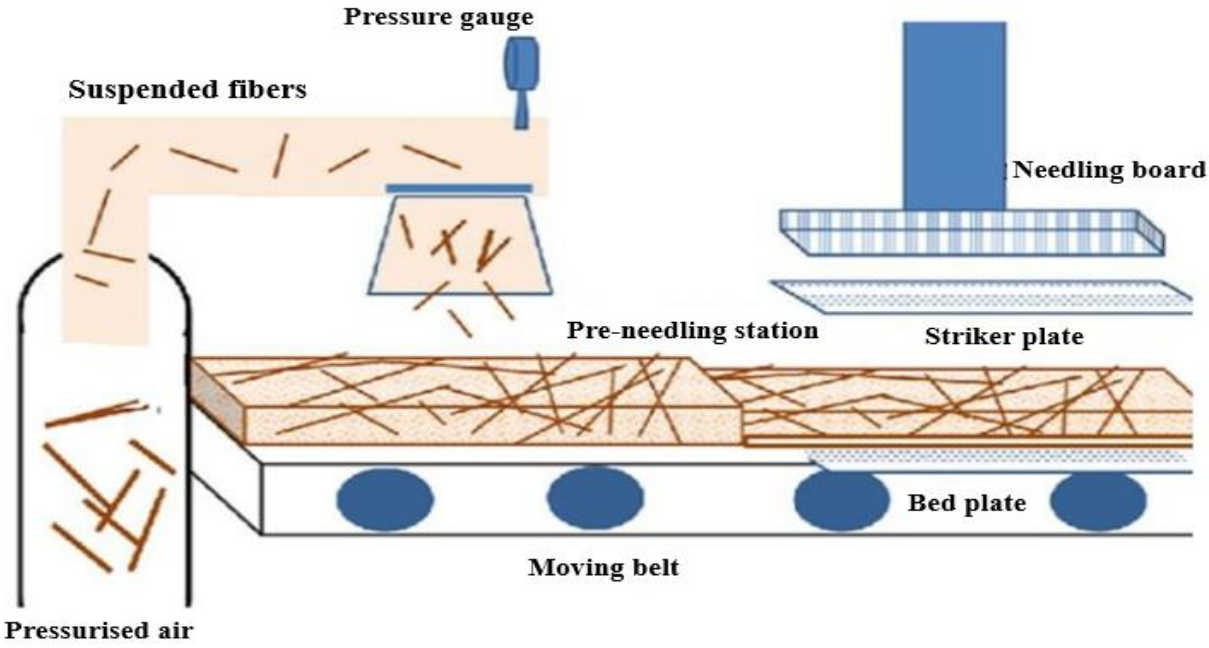

Figure 2.3 Schematic diagram of needle punched flax fiber mat manufacturing process (Fahimian, 2013).

2.2.5 Mat permeability

Permeability is a measure of the amount of void spaces between the fibers and how they are connected within the mat. The resin flows through void spaces among the fibers of the mat during mold filling with a purpose of impregnating the entire mat.

In this study, out of plane (through the thickness or transverse) permeability of the flax fiber mats, cattail fiber mats, and mats blended with flax and hemp fiber were measured and compared to understand the effect of mat manufacturing parameters. Manufacturing a good composite plate in VARTM process is mostly dependent on the uniformity in permeability across the mat. The knowledge on the permeability would allow prediction of resin flow path in a mat of given shape which could further be used for location adjustment of resin inlets and vacuum outlets for complete impregnation of a mat without any dry spots. In addition, the resin filling time could be determined from mat permeability to adjust the get time of resin matrix. As the resin stops flowing when it reaches gel point during manufacturing, the fill time has to be less than the gel time to manufacture quality composites without any dry spots. The resin flows through a fibrous mat could be described from Darcy's Law as presented in Eq. (2.4).

$$k = \frac{Q \eta L}{A \Delta P} \tag{2.4}$$

where Q is the volumetric flow rate (m^3/sec), is the viscosity of the fluid (Pa.s), ΔP is the pressure gradient in flow direction (MPa), k is the permeability of the mat (m^2), A is the cross-sectional area perpendicular to flow (m^2) and L is the length of mat parallel to the flow (m).

2.2.6 Composite manufacturing

Selection of appropriate manufacturing process is important for transformation of the raw materials to the flawless final product. There are key factors that influences the selection of composite manufacturing process that include size and geometry of final composite part, desired properties, raw materials processing, production speed, and manufacturing cost.

Common techniques of manufacturing NFRC are hand lay-up, spray lay-up, liquid moulding, compression moulding, and injection molding. Liquid moulding and compression moulding are used for manufacturing the thermoset composite, and injection moulding is used for the thermoplastic composite (Facca et. al., 2006). Manufacturing thermoset composites from short ($20<l/d<1000$) and discontinuous natural fibers (e.g., 100% flax, 50% flax-50% hemp, 100% cattail) is the focus of this study.

Manufacturing the thermoset composite includes several steps such as fiber impregnation, lay-up of the part, consolidation, curing, and part removal, which is the removal of the manufactured composite from the mold after curing, regardless of whether it is a continuous fiber or a discontinuous fiber. Consolidation of the composites is the important and complex part while manufacturing. Consolidation can be defined as the reduction in the thickness of the composite during manufacturing. The rate of consolidation is influenced by resin viscosity, applied pressure, and fiber permeability. The level of consolidation determines the fiber volume fraction and void content in the laminate and thus the properties of the composite. Good control of the resin flow (setting the optimum injection point, resin injection strategy, e.g. point/edge/peripheral) and pressure while the manufacturing process is happening are essential to reduce the void content and achieve the desired fiber volume fraction.

Vacuum assisted resin transfer moulding (VARTM) and the compression moulding process will be used in this study for manufacturing short NFRC. VARTM is one of the variants of the liquid moulding process which is commonly used to manufacture short (i.e. discontinuous) fiber thermoset polymer composites. In VARTM, a vacuum is used for both resin injection and curing. VARTM is less expensive and it is used for manufacturing large structural parts e.g. ship hulls.

Compression molding, another process or technique for manufacturing thermoset composite, will be used in the study. For manufacturing a discontinuous fiber composite with compression molding, the resin impregnated fiber preform is transferred to the hydraulic press where release film, metal platen, and silicon pad is placed in sequence on either side of the impregnated nonwoven preform. The platen with fiber preform is then compressed with pre-determined pressure.

2.3 REVIEW OF PUBLISHED LITERATURE

2.3.1 Fiber extraction and retting techniques of bast fibers

Previous studies report that an increasing number of mechanical processing steps during fiber extraction and processing results in the reduction in degree of polymerisation of the cellulose chains, formation of kink bands, and finally degradation in mechanical properties of fiber (Hughes, (2012). Good quality composites and high quality fibers could be obtained with minimally-processed fibers that undergoes retting and hackling (Miao & Finn, 2008).

Retting is the very first process to obtain high-quality fibres from the plant. Retting is a biological process that include removal of non-cellulosic materials sticking to the fibre bundle by enzymatic activities, consequently yielding detached cellulosic fibres (Lee et. al., 2019). Fiber retting is a complex process, and fiber properties are highly dependent on the

type of retting and retting conditions. Under-retted fibers result in less productive fiber separation and over retting causes fibre weakening (Preisner et. al., 2014). Several retting processes have been introduced for fiber extraction. Retting could be categorized as chemical retting, enzyme retting, water retting, and dew retting (Sadrmanesh & Chen, 2019). Chemical retting results in comparatively more controllable bast fiber within a short retting duration whereas enzyme retting is popular for its mild process conditions, specificity, and high selectivity (Lee et. al, 2019). A brief comparison among different retting process is listed in Table 2.4.

Apart from these techniques, there are few other less used and non-commercial retting process such as microwave retting process (applied on flax fiber) (Nair et. al., 2013), gel-retting method (Pandey, 2016), and microbial retting (Ramaswamy et. al., 1994). The supply chain for bast fibers are strong as they are annual crops. Bast fibers are extracted from the phloem located at the stem of the fibrous plant (Lee et. al., 2019).

Chakma (2018) attempted several retting techniques to extract cattail fibers from cattail leaf. They used water, acid, enzyme, alcohol, and alkali to find out a suitable extraction process for cattail fibers. The use of water, acid, enzyme, and alcohol didn't work on cattail and alkali retting was found to be a suitable process for cattail fiber extraction as concluded by Chakma (2018). However, no clear result was concluded in Chakma (2018) for optimum retting conditions (e.g. concentration, time, and temperature) of cattail fiber. Hasan (2019) further investigated the optimum retting conditions for cattail fiber extraction. Here, the extraction parameters such as extraction time, temperature, and concentration of alkali were optimized using desirability function analysis (DFA) for cattail fiber. 7% (w/v) concentration of NaOH, 10 hours treatment duration, and 90°C treatment temperature was concluded by Hasan (2019) as the optimum retting conditions for cattail fiber extraction. Both Chakma (2018) and Hasan (2019) attempted to extract cattail fiber in a very small scale (1 – 3 gm).

However, large scale production of cattail fiber is required for manufacturing nonwoven cattail preform. Hence, published studies on appropriate conditions and suitable techniques for large scale extraction process of cattail fibers are missing.

Table 2.4 The comparison among different retting process of bast fiber (Paridah et. al., 2014).

Retting methods	Description	Duration of retting
Water retting	Plant stems are submerged in water and checked periodically until complete retting is done	7–14 days
Dew retting	The plant stems are spread evenly onto the fields to get enough sunlight, atmospheric air, and dew for fungal colonisation which result in breakdown of cellular stem tissues and adhesive substances to release the single fibre	2-3 weeks
Enzymatic retting	Controllable retting conditions with higher retting efficiency that uses enzymes to hydrolyse the gum and pectin material in the stem	12–24 hours
Chemical retting	In chemical retting, fibers are usually extracted using hydrogen peroxide, sodium benzoate, or sodium hydroxide.	60–75 minutes

2.3.2 Chemical composition of bast fibers

The primary chemical components of bast fibers are cellulose, hemicellulose, and lignin. The percentage of these compounds in the extracted bast fiber varies and depends on plant age, species, retting process, and extraction conditions. Cellulosic content determines the physical and mechanical properties of the bast fiber. Bast fiber contains a large amount of hydroxyl group (- OH) in its cellulosic structure providing hydrophilic nature (Shadhin & Shuvo, 2019) to bast fiber. The waxy substances of bast fiber affect the fiber wettability and adhesion properties (Yan et. al., 2014). Although the structure of cellulose remains same for all the bast

fibers, the degree of polymerization changes. The degree of polymerization was found higher in bast fiber than any other plant fibers (Lewin & Pearce, 1985). The chemical composition different bast fibers are listed in Table 2.5.

Table 2.5 Chemical composition of different bast fiber (Akil et. al., 2011; Yu, 2015; Faruk et. al., 2012; Martí-Ferrer et. al., 2006; Varma et. al., 1984).

Fiber	Cellulose (%)	Hemi- cellulose (%)	Lignin (%)	Pectin (%)	Wax (%)
Flax	62 - 71	16 - 20	2.0 – 4.5	1.8 – 2.0	1.5 – 1.7
Hemp	67- 75	16 – 22.4	3.0 – 5.7	0.8	0.7 – 0.8
Jute	59 - 71	12 – 20.4	11.8 – 12.9	0.2 – 4.4	0.5
Kenaf	39 - 57	21.5	15 – 19	3.0 – 5.0	-
Ramie	68 - 76	13	0.6 – 2.0	1.9 – 2.1	0.5

2.3.3 Mechanical properties of bast fibers

The mechanical properties of bast fibers are listed in Table 2.6. As discussed in section 2.3.2, the chemical composition of bast fiber varies for plant age, species, retting process, and extraction conditions. For the same reason variations in bast fiber properties are observed as well. Each stage of processing the fiber have several influencing factors that affect the mechanical properties of natural fiber. The percentage of cellulose content, fiber diameter, density, and aspect ratio influence the mechanical properties of plant based natural fibers. While evaluating the mechanical properties of natural fiber, change in natural fiber strength and modulus with change in fiber diameter was observed in previous studies. Mwaikambo (2006) observed increase in fiber strength and modulus with the decrease in fiber diameter where the diameter of fibers was reported to be around 120 μm.

Table 2.6 Mechanical properties of different bast fiber (Faruk et. al., 2012; Hoareau et. al., 2004; Wang et. al., 2018; Fan & Weclawski, 2017).

Fiber	Tensile modulus (GPa)	Tensile strength (MPa)	Elongation at break (%)
Flax	27.6	345 - 1100	2.7 – 3.2
Hemp	30 - 60	690 - 720	1.6 – 1.7
Jute	13 – 26.5	393 - 773	1.2 - 1.5
Kenaf	53	240 - 930	1.6
Ramie	61 - 128	400 – 938	1.2 – 3.8

2.3.4 Nonwoven mat manufacturing and characterization

There are limited studies on the mat manufacturing process, permeability measurement methodology, and evaluation of mat structure and properties. Niu et al. (2010) investigated the effect of operating parameters like carding method involved during manufacturing of nonwoven flax mat on the mechanical properties of flax composite. However, they did not study the effect of needle punch density. Fahimian (2013) investigated the effect of mat manufacturing parameters such as needle punching density, depth of needle penetration on mat structure and properties for hemp. Similar studies for flax are missing. Although, Dev (2018) found deterioration in mechanical properties of composite with increase in needling density manufactured from flax-polypropylene needle punched nonwovens, but effect of punch density is still unknown for the composites manufactured from flax fiber alone. Andre (2017) studied the effect of the needle-punching direction on the tensile properties of the resin transfer molded nonwoven kenaf fiber/epoxy composites which revealed that mechanical interlocking of nonwoven Kenaf were responsible for improvements in the modulus and composites at both the needle-punching direction exhibited isotropy in tensile properties. Sengupta (2018) concluded that punch density and depth of needle penetration are two controlling factors of Mesta needle punched nonwoven fabrics by help to result in a compact

and entangled nonwoven structure initially; however, decrease in compactness of Mesta mat structure showed up after certain value of needle punching and needle depth. A detailed investigation of needle punched flax mat structure and manufacturing parameters is missing. Also, no previous study has been found to manufacture either zero punched or needle punched nonwoven mat from cattail fiber.

2.3.5 Mat permeability

Xue et. al. (2011) investigated the permeability of different nonwoven flax mat structure and found a higher overall compressibility in parallel-laid flax mats than the cross-laid flax mats resulting in lower porosity, and lower overall permeability in parallel-laid flax mats. Merhi (2007) studied the transverse permeability of 25 mm-long chopped glass fiber bundle bed and found porosity content of fiber beds as a main factor that defines its permeability. Niya (2018) investigated the statistical correlation between permeability, porosity, tortuosity and conductance in random mat structure which concluded that permeability is a function of porosity; however, the permeability estimation would only be reliable for a medium or mat structure having porosities greater than 0.8. Scholz et. al. (2007) studied transverse permeability measurements over a wide range of materials and implemented a permeability cell which can be used both with gaseous and fluid flow. 8% deviation in the permeability measurement result was reported in this study while using air and water for permeability measurement.

Fahimian (2013) studied the effect of punch density on needle punched hemp mats. Fahimian used water in the experimental setup of transverse permeability measurement where transverse permeability of hemp mats decreased with the increase in punch density. However, published studies to determine the effect of punch density on needle punched flax mats are

missing. Also, no previous studies reported the permeability results of zero punched cattail and flax-hemp hybrid nonwoven preform.

2.3.6 Composite manufacturing and properties (effect of punch density and consolidation pressure)

The tensile modulus increases as the fiber content increases in discontinuous fiber composites (Ku et al., 2011). Current literatures are available for glass fiber composite and other synthetic fiber composite. However, published literatures on discontinuous and natural fiber composites are limited. Even a very few them studied the combined effect of needle punch density and manufacturing pressure on composite properties.

Huang and Young (2019) studied the properties of untreated and treated bamboo epoxy composite. This study reveals that the alkaline treated bamboo epoxy composite showed enhanced flexural strength of 182.29 MPa when compared to untreated composite strength of 141.30 MPa. The effect of hemp fiber content and anisotropy in needle punched hemp mats were studied by Hargitai et al., (2006 & 2008). In this study, hemp fibers were blended with polypropylene fibers in different weight fractions (30, 40, 50, and 70%) and mats were manufactured using carding and needle punching process. The needle punched mat composites were manufactured using compression molding. Maximum value of tensile modulus was reported 6.5 GPa at 50% fiber weight fraction. Composites with double-carded mats had lower modulus. The modulus of 30% hemp fiber composite was 5 GPa for double carded mat composites. However, the needle punch density and needle depth of mat were not reported on this study. Fahimian (2013) studied in detail the effect of mat manufacturing parameters (needle punch density) on hemp mat properties and manufacturing pressure on composite properties and the relationship between mat design and composite properties. Tensile strength and modulus of needle punched hemp mat composite increased with the increase in punch

density as concluded by Fahimian (2013). For a given punch density tensile strength and modulus increased at 260 or 560 kPa when compared to VARTM pressure due to increase in Vf at higher pressures. However, there are no previous research that studied the combined effect of needle punch density and consolidation pressure on flax mat composite properties. Published studies on the effect of consolidation pressure on cattail composite properties are also missing.

2.4 KNOWLEDGE GAP AND MOTIVATION

Existing non-woven glass mats are already characterized and optimized for manufacturing the glass fiber reinforced composite to yield good impregnation, desired permeability, compaction, final part thickness, and fiber volume fraction. However, optimized natural fiber non-woven mats are not available yet. Composite Materials and Structures Research Group of Dr. Jayaraman has generated this knowledge for hemp fibers. This research is the continuation of this study to generate such knowledge for Flax fibers and Flax-Hemp hybrid fibers. In addition, such studies on Cattail fibers, with comparable properties and abundance, are lacking. Also, no previous study has been focused on manufacturing nonwoven mat and fiber reinforced composites and understanding on how mat parameters influences composite properties from 100% cattail fiber.

Bridging the knowledge gaps, identified above, with respect to the design of flax fiber and cattail fiber nonwovens, in order to enable comparative evaluation of the various natural fibers as reinforcements in composites is the motivation of this thesis.

2.5 THESIS OBJECTIVES

Hence, the goal of this thesis to perform a comparative evaluation of properties of discontinuous natural fiber composites manufactured using flax, hemp, and cattail fibers. In order to realize this goal, the following objectives were identified and pursued.

1. Study the effect of punch density on permeability of the non-woven mat, as well as the effect of punch density and manufacturing pressure on properties of 100% flax and 50% flax-50% hemp fiber composites, manufactured through VARTM and compression molding.

2. Investigate the suitability of cattail fiber for composite applications by studying,

   (i) the effect of extraction process on fiber properties,

   (ii) the effect of humidity on the properties of the fibers,

   (iii) the effect of surface modification to enhance its suitability for impregnation by hydrophobic thermoset resin, and

   (iv) properties of composites with Cattail fibers.

3. Comparative evaluation of properties of composites manufactured with 100% Flax, 100% Cattail, 50%flax – 50% hemp, and 100% hemp (generated by Fahimian (2013)).

CHAPTER III

EXPERIMENTAL DETAILS

3.1 MATERIALS

Flax fiber non-woven mats and 50%Flax-50% Hemp fiber non-woven mats, used in this study were supplied by Dr. Raghavan Jayaraman of Composites Materials and Structures Research Group. They had used the fibers supplied by Stemergy Renewable Fiber Technology Inc. in Ontario, Canada and the Non-woven pilot plant facility at North Carolina State University, Raleigh, USA to manufacture the mats. Green cattail plants were collected from the roadside ditches along the Provincial Highway 3 near Winnipeg, Canada in early October 2019 for extracting fibers and to make nonwoven cattail mats from the extracted fiber. For cattail fiber extraction, KOH was used for retting and acetic acid was used for the neutralization of the fiber after retting and both were procured from Fisher Scientific, Ontario, Canada.

Unsaturated polyester resin (Stypol 8086) was used as the thermoset polymer matrix and was purchased from Composite Envisions LLC, Wausau, USA. Stypol resin is manufactured to be used in closed-mold processes such as RTM. It is a low-viscosity resin, which starts reacting with the addition of a curing initiator. The curing initiator chosen for this study was Luperox 224 (2,4-Pentanedione peroxide), purchased from Sigma Aldrich (Oakville, Ontario, Canada). The surface modification chemicals 1,6-diisocyanatohexane (DIH), 2-hydroxyethyl acrylate (HEA), and anhydrous ethyl acetate were purchased from Sigma Aldrich (Oakville, Ontario, Canada). These chemicals were used for the surface modification of cattail fiber and nonwoven mats

3.2 MANUFACTURING OF FIBERS AND FIBER MATS

3.2.1 Manufacturing nonwoven flax and flax-hemp hybrid mats

Flax and hybrid mats, manufactured by Composite Materials and Structures Research Group at the University of Manitoba, were used in this study. The mats were manufactured at the pilot plant at North Carolina State University, USA. The needle punch density varied between 0 and 72 needles per cm^2 and the needle punch depth varied between 2 and 8 mm. In order to make the needle punch non-woven mat, flax fibers were converted into a web of fibers on a moving conveyor belt through an air lying technique. The web of fibers was further fed to a needler and needle punched to form nonwoven mats as shown in Figure 3.1. The manufactured needle-punched nonwoven flax mats were finally wound on a 48-inch wide take-up roller and shipped back to the University of Manitoba.

Figure 3.1 Manufacturing needle-punched flax mat (Courtesy – Dr. Raghavan Jayaraman).

Manufacturing of 0 punch flax, flax-hybrid, cattail fiber mats are discussed below. First extraction of cattail fibers from cattail leaves are presented.

3.2.2 Cattail fiber extraction

(a) Plant preparation for alkali retting

The collected cattail leaves, shown in Figure 3.2, were dried for 48 hrs at room temperature. The dried leaves were precut to 6-10 cm in length and weighed using an electronic balance.

(b) Alkali retting in water-bath

Cattail fiber was extracted using a bath (Figure 3.3) in alkaline medium. The 12 L bath is equipped with the temperature and oscillation control systems as shown in Figure 3.3. The following list indicates the optimum condition for alkali retting of cattail fiber.

- Chemical – 5 % (w/v) KOH solution
- Temperature – 90 °C
- Time – 4 hrs
- M : L – 1 : 25 (plant and KOH ratio)

Figure 3.2 Cattail plants collected from wetlands in Winnipeg.

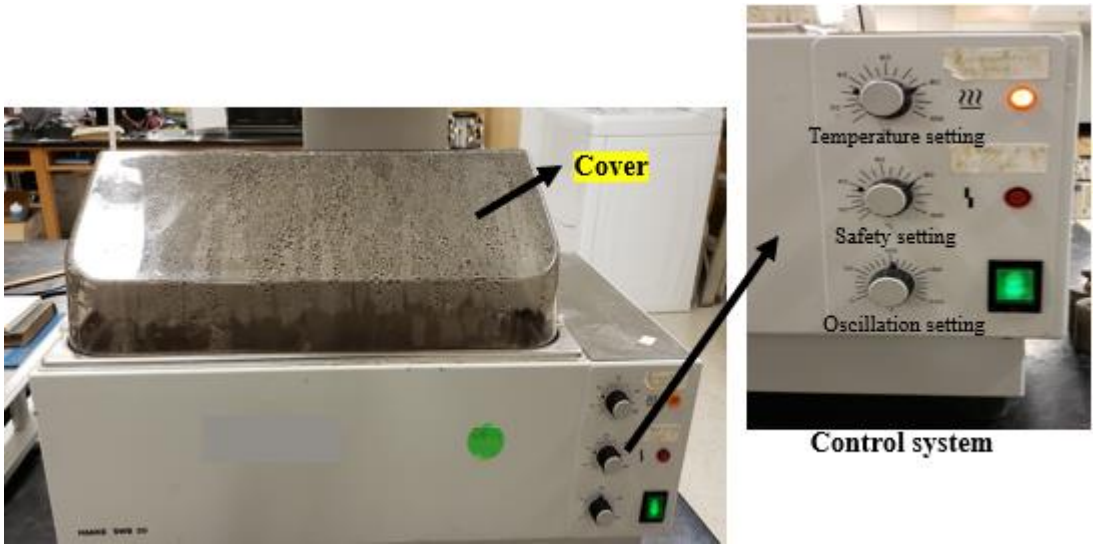

Figure 3.3 Temperature and oscillation-controlled water bath for cattail fiber extraction.

A stock solution of 5 % (w/v) KOH was prepared and the required amount was added into the bath. The temperature of the bath was set and raised to 90°C. 250 gm of dried and cut (6-8 cm) cattail leaves or plants (Figure 3.4 a) were added to the 10 L KOH (M:L = 1:25) solution in the bath and closed with a cover as shown in Figure 3.3. The oscillation speed of the bath was set at 100 rpm. A thermometer was used to check the temperature of the bath at regular intervals and stirring was done every hour to maintain uniform retting of the cattail plants. Figure 3.4(b) indicates the alkali retted cattail plant in the bath after 3 hours. After 4 hours, once the retting was completed, the bath was turned off. The left-over KOH solution was reused for the next retting of cattails as shown in Figure 3.5.

It is worth mentioning here that at the beginning of the cattail fiber extraction, retting with 5 % (w/v) KOH solution was conducted at 70, 80 and 90°C for 2, 3 and 4 hrs. However, 90°C retting temperature and 4 hrs retting time were picked as optimum conditions for cattail fiber extraction.

(c) Neutralization

The retted cattail plant was rinsed in cold distilled water and neutralized in 2 % (v/v) acetic acid solution for 30 minutes.

(d) Washing and drying

The retted and neutralized cattail fibers were washed progressively in cold, hot and cold distilled water and left for drying at room temperature. The washed and dried cattail fibers are illustrated in Figure 3.6.

(a) (b)

Figure 3.4 (a) Cattail plant pieces before retting (b) alkali retted cattail plant in bath after 3 hrs.

Figure 3.5 Cattail fiber extraction using reused KOH solution.

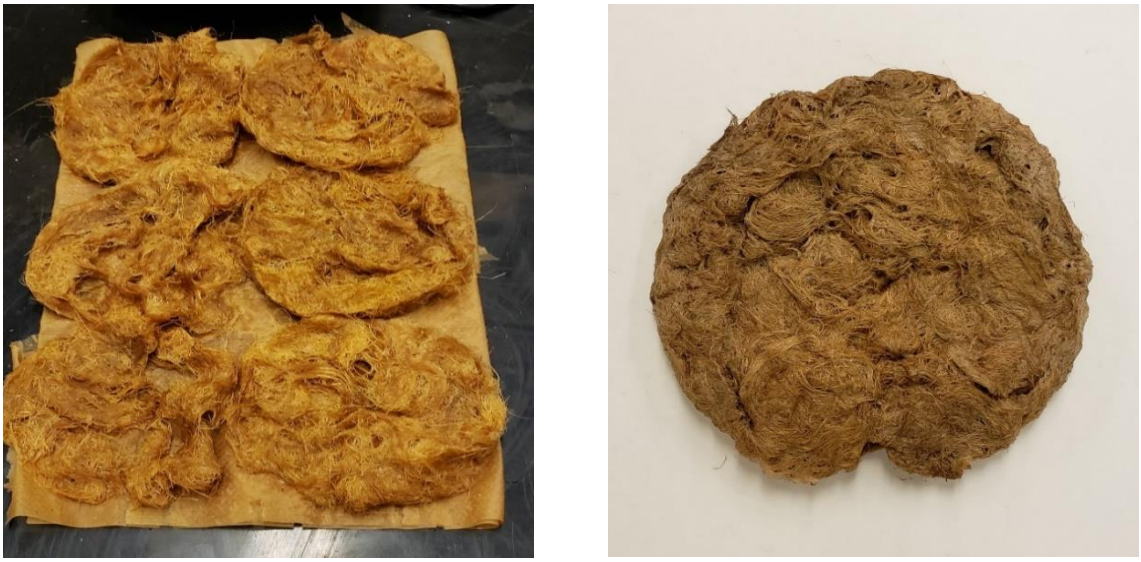

(a) (b)

Figure 3.6 KOH retted cattail fibers after (a) washing and (b) drying.

3.2.3 Manufacturing zero punch nonwoven mat

I. Fiber individualization

Cattail fibers extracted from cattail plants using alkali retting were further individualised, parallelised, and oriented using a modified laboratory carding machine as shown in Figure 3.7. During carding, cattail fibers were passed through a pair of spiked rollers of the carding machine while a combing operation was conducted during the passing by each spiked roller. The spike roller also helps to individualize the entangled fibers obtained from extraction and the combing operation helps to orient the individual cattail fibers parallel to one another.

Figure 3.7 Side view of a mini carding machine.

II. Mat preparation

Although the needle punched flax non-woven mat was manufactured at the North Carolina State University, the zero punched non-woven mat was prepared in the lab. In order to do so, a template was designed with a metal plate having a dimension of 8.5”x8.5” for laying up the individualized fibers. The sides of the metal plate were covered by a paper board for the ease of thickness control of the mat. Desired volume fraction and thickness of the mat was obtained by laying up different layers of fibers in the template as illustrated in Figure 3.8 (a). Once the fiber lay-ups were done, a metal plate with same dimensions was placed on the top layer of the mat and a dead weight of 3 kg was applied to compress the mat layers as shown in Figure 3.8 (b). Finally, the zero punched nonwoven cattail mat was removed from the mold as shown in Figure 3.8 (c).

Similarly, the zero punched flax mat and zero punched flax-hemp hybrid mats were prepared by repeating the above procedure.

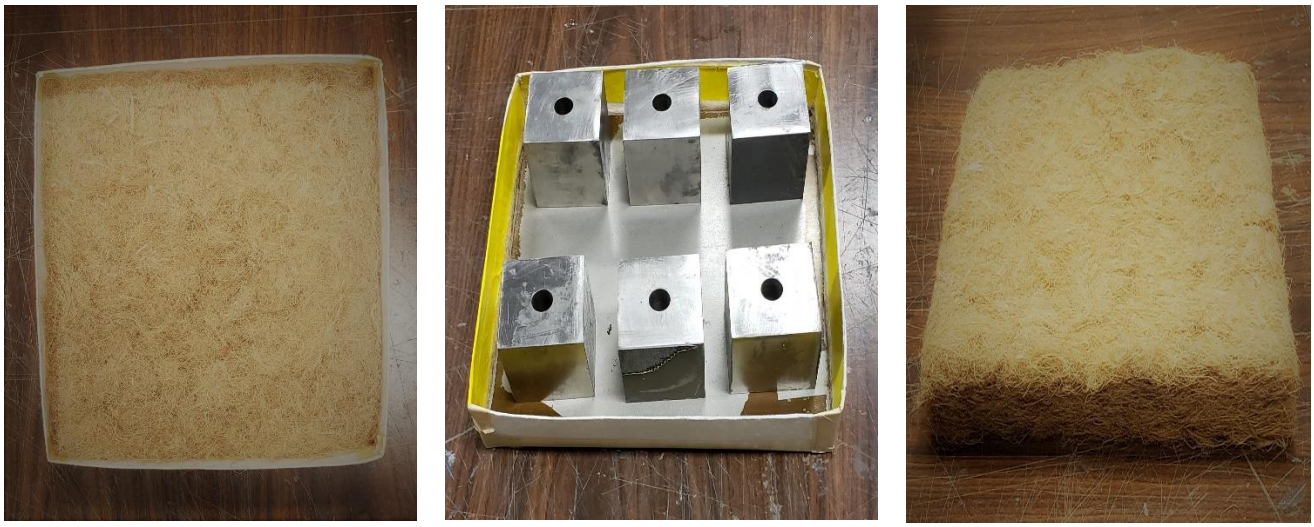

(a) (b) (c)

Figure 3.8 Preparation of nonwoven cattail mat (a) laid up fibers (b) dead weight application (c) prepared mat.

3.3 FIBER CHARACTERIZATION

The equipment and methods used in determining the cattail and flax fiber properties such as fiber length, diameter, yield percentage, and mechanical properties are listed in Table 3.1.

Table 3.1 The equipment and methods used to determine the properties of cattail and flax fiber.

Fiber properties	Equipment/Method	Standard test method	Fiber type
Yield (%)	Thermo scientific oven and weighting machine	(Gravimetric method) standard: NF G 08-001	Cattail
Length	Forceps, precision scale	ASTM D5130	Cattail and flax
Diameter (μm)	Bioquant life science image analyzer	France standard NF G 07- 004 (1983)	Cattail and flax
Mechanical properties of cattail fiber	Instron Tensile Tester	ASTM D3822	Cattail and flax
Moisture regain (%)	Humidity chamber and Thermofisher scientific oven	ASTM D2564	Cattail

3.3.1 Yield measurement

The yield (%) of the fibers is the ratio of the oven dried mass of the fibers extracted after chemical treatment (M_a) and the oven dried mass of the cattail plants before chemical treatment (M_b). Yield (%) is calculated using Eq. (3.1).

$$\text{Yield (\%)} = \frac{M_a}{M_b} \text{ X } 100 \tag{3.1}$$

3.3.2 Moisture Regain (%) Measurement

The moisture regain of the cattail fibers was measured using the constant weight principle. In this method, fibers in an aluminum pan were dried in the oven, maintained at 100ºC for 12 hours. At the end of 12 hours the oven dry weight of the samples was measured (M0). The complete drying of fiber samples was deemed reached when the difference in weights was obtained less than 0.05% of the weight in a sample between the two successive weighing within a 15-minute interval. The weighing was carried out using an electronic balance.

Subsequently, the fibers were conditioned according to ASTM D 1776- 4 (2008) in the desiccators at the Textile lab of the University of Manitoba. The relative humidity of the desiccator or humidity chambers will rely on the desiccants used. The detail on different desiccants and their corresponding relative humidity (%) [R.H%] is discussed in section 3.3.5. The moisture regain (%) was calculated as a percentage of the ratio of the weight of moisture absorbed by the sample to the oven dry weight of the sample as expressed in Eq. (3.2).

$$\text{Moisture regain (\%)} = \frac{M_w - M_0}{M_0} \text{ X } 100 \tag{3.2}$$

Where, M_w is the weight of the samples after conditioning and M_0 is the oven dry weight of the samples.

3.3.3 Fiber length measurement

Individual cattail and flax fibers were separated from the extracted fiber bundle and needle-punched mat respectively, and the fiber length was measured using ASTM D 5130 method. Both ends of the fiber were gripped with forceps perpendicular to the axis of the fiber keeping the fiber ends in line with the tips of the forceps. The tip of the forceps was placed at a reference point on the measuring scale. The other gripping end of the forceps was moved to full extension without stretching the fiber to remove the crimp. The fiber length was observed and recorded through a measuring scale.

3.3.4 Fiber diameter measurement

A rectangular paper frame (25 mm in length) was made for measuring the fiber diameter and preparing the sample for tensile testing as illustrated in Figure 3.9. 400 cattail fibers and 100 flax fibers were selected randomly for diameter measurement and tensile testing. The fibers whose length was already measured were marked with individual identifications and attached to the middle of this rectangular frame using an adhesive. The inside length of the frame was 25 mm. Then the frame along with the fiber was placed on a glass slide and the fiber was observed using 10x magnification using Bioquant life science image analyzer (Bioquant life science - Motic, BA310l, 2010), which was connected with a projection microscope and camera. The schematic diagram of the projection microscope and camera set-up attached with Bioquant analyzer is shown in Figure 3.10 (a). The diameter of the single fiber attached inside the frame was measured following France standard NF G 07- 004 (1983) and the unit of measurement was in micrometer (μm). The diameter was measured in five different places across the length of the cattail fiber as shown in Figure 3.10 (b) and the average diameter was recorded.

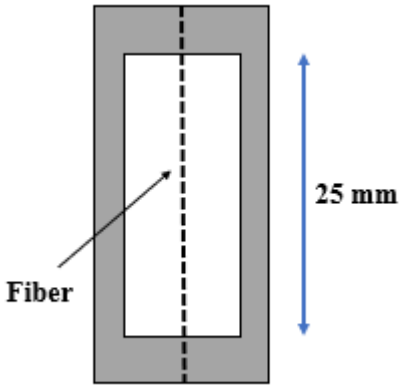

Figure 3.9 Rectangular fiber attachment frame for tensile testing.

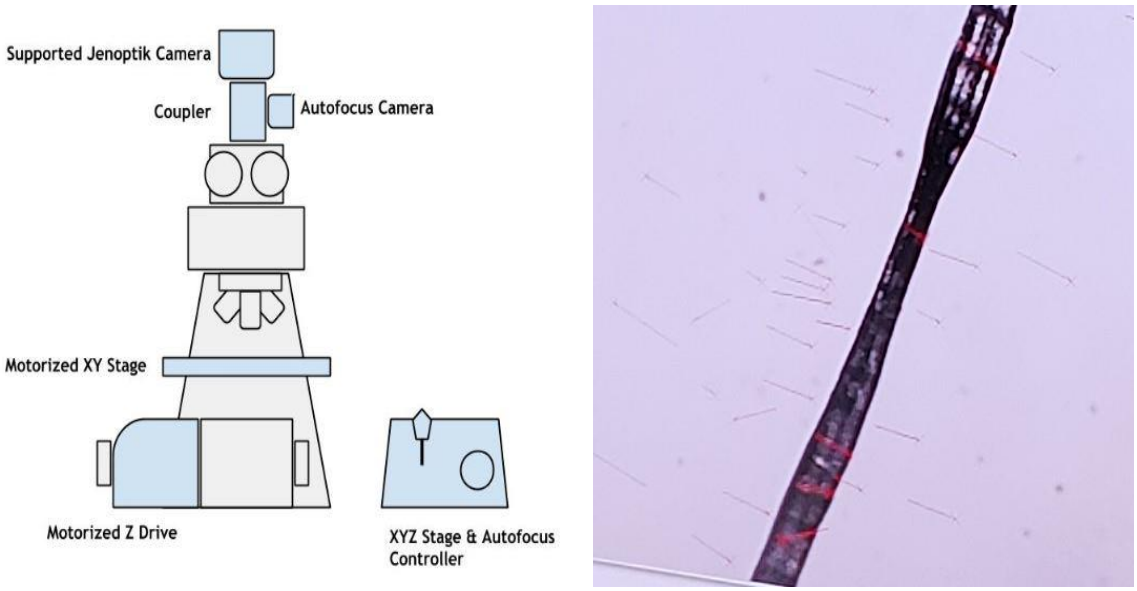

(a) (b)

Figure 3.10 (a) Schematic diagram of projection microscope and camera set up connected with Bioquant analyzer (b) microscopic view of fiber while diameter measurement in Bioquant analyzer.

3.3.5 Mechanical properties of fiber

I. Humidity Conditioning (cattail fiber)

Tensile testing of cattail fibers was carried out at different relative humidity conditions. Desiccators were used as a humidity chamber and different types of salt and water were used

as desiccants to create different environmental conditions for the cattail fibers. Prior to testing, the rectangular frames holding the single fibers were dried in an oven at 50°C for 12 h, which was necessary to avoid any hysteresis effect After drying, the fiber containing frames was kept together in a glass plate and suspended in desiccators as shown in Figure 3.11. Fifty fibers were tested at each relative humidity condition. The name of chemicals used as desiccant and their corresponding relative humidity (%) are listed in Table 3.2.

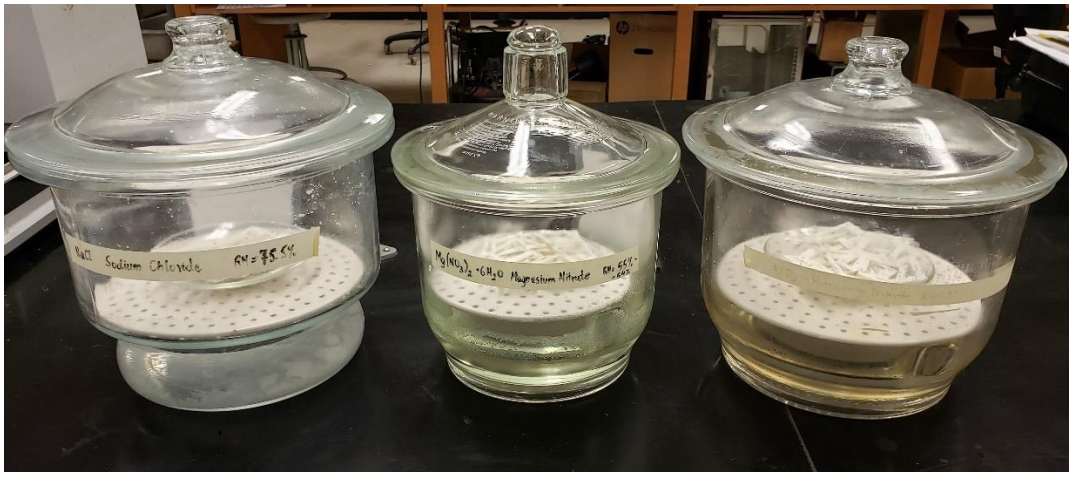

Figure 3.11 Cattail fiber kept in desiccators containing different relative humidity condition.

Table 3.2 Different types of desiccants and corresponding relative humidity (%).

Name of chemical	Relative Humidity (%)
Lithium Chloride [LiCl. H_2O]	11
Magnesium Chloride [$MgCl_2.6H_2O$]	33
Magnesium Nitrate [$Mg(NO_3)_2$]	55
Sodium Chloride [NaCl]	75
Potassium Chloride [KCl]	84
Potassium Nitrate [KNO_3]	93
Water [H_2O]	100

II. Single fiber tensile testing (flax and cattail)

The mechanical properties, i.e. tensile strength, modulus of elasticity, and strain at break (%), were evaluated using the Instron Tensile Tester (Model# 5965, Sl#VS02075661, manufactured by INSTRON, Norwood, USA) following the ASTM D3822 method. The desiccant container with the rectangular frames, holding the fibers, were brought to Instron Tensile Tester before tensile testing. The frames were taken from the desiccators one by one just before testing to prevent change in the moisture level in the fiber. The length of the fiber inside the frame (i.e. 25 mm) acted as a gage length. After the clamping the frame with the fibers between the clamps of the Instron tester, the paper frame was cut in the center so that the tension was applied only on the fiber.

'Pretest' and 'Auto-balance' functions in the 'Instron Bluehill 3' software were selected to remove any crimp in the fiber acquired during extraction process. The 'Pretest' function allows the machine to extend the fiber, but no data is reported until a small amount of load is experienced by the load cell, which was chosen as 0.3 N for this experiment. When the load cell experiences the specified amount of load (0.3 n), the extension up to this point is considered due to the crimp and the 'Auto-balance' function adds this length with the initial length of the fiber and then the actual test begins. All the 400 fiber samples were tested using this procedure. The crosshead was moved at a speed of 20 mm/min, and a 1 KN load cell was used to conduct the tensile testing. The raw data, stress-strain curve, and summary of tensile testing were directly obtained from the 'Instron Bluehill 3' software and the tensile strength, elastic modulus, and strain at break of the cattail were calculated.

Flax fiber samples were conditioned at 21°C temperature and 50% relative humidity for 48 hours. Once the conditioning was done, single fiber tensile testing was executed by repeating the above procedure.

3.4 MAT CHARACTERIZATION

3.4.1 Areal density and thickness of nonwoven mat

As the area of the prepared zero punched nonwoven mat is fixed (8.5 x 8.5 inch), the weight of the mat is measured using a weighing balance and the weight per unit area or areal density of the mat is calculated. The thickness of each nonwoven mat was measured using a caliper. For the needle punched mat, circular mat samples of 14 cm diameter were cut at different locations using cutter and the weight of the sample was recorded to determine areal density (gsm – gram per square meter).

3.4.2 Transverse permeability measurement of nonwoven mat

Frazier Permeability Tester manufactured by Fraizer Precision Instrument Co. Inc. Hagerstown, MD. U.S.A was used in this study to determine the volumetric flow rate in nonwoven mat following the ASTM D-737 method. In this method, the rate of airflow passing perpendicularly through a known area of nonwoven mat is adjusted to obtain a prescribed air pressure differential between the two mat surfaces. The transverse mat permeability is then determined using Darcy's law from the recorded rate of air flow.

A schematic diagram of the Frazier Permeability Tester is shown in Figure 3.12 indicating the essential parts of the machine (Schiefer & Boyland, 1942). The clamp for holding the nonwoven mat as shown in Figure 3.12 against the orifice is pivoted in its supporting frame so that it can press uniformly against the upper surface of the orifice. The inclined manometer filled with oil indicates the pressure drop across the nonwoven mat and the vertical manometer indicates the pressure drop across the orifice for measuring the rate of air flow. A set of nine orifices has orifice diameters from 1 mm to 16 mm that covers the range of flow rate from 1 to 700 cubic feet per minute per square foot of fabric. The volumetric flow rate table for different orifices and corresponding vertical manometer reading is provided in Appendix.

For permeability measurement, the rate of air flow was determined in this study for a pressure drop (across the mat) of 0.5 inch of water according to ASTM D-737. Finally, the mat permeability was calculated using Darcy's law in Eq. (3.3). Fahimian (2013) investigated the out-of-plane permeability of hemp mats using water. Hence, it is expected to have difference in permebaility results while using two different media (Scholz et al., 2007). For comparison, the transverse permeability of zero punched hemp mat was also investigated in this study which is tabulated in Table 6.2.

$$k = \frac{Q\,\eta\,L}{A\,\Delta P} \tag{3.3}$$

Where, k = Out of plane or transverse permeability,

Q = volumetric flow rate

η = viscosity of air = 1.81×10^{-5} Pa s

A = Area of the specimen perpendicular to flow direction = 0.003788 m^2

ΔP = Pressure difference and L = length of mat parallel to the flow direction.

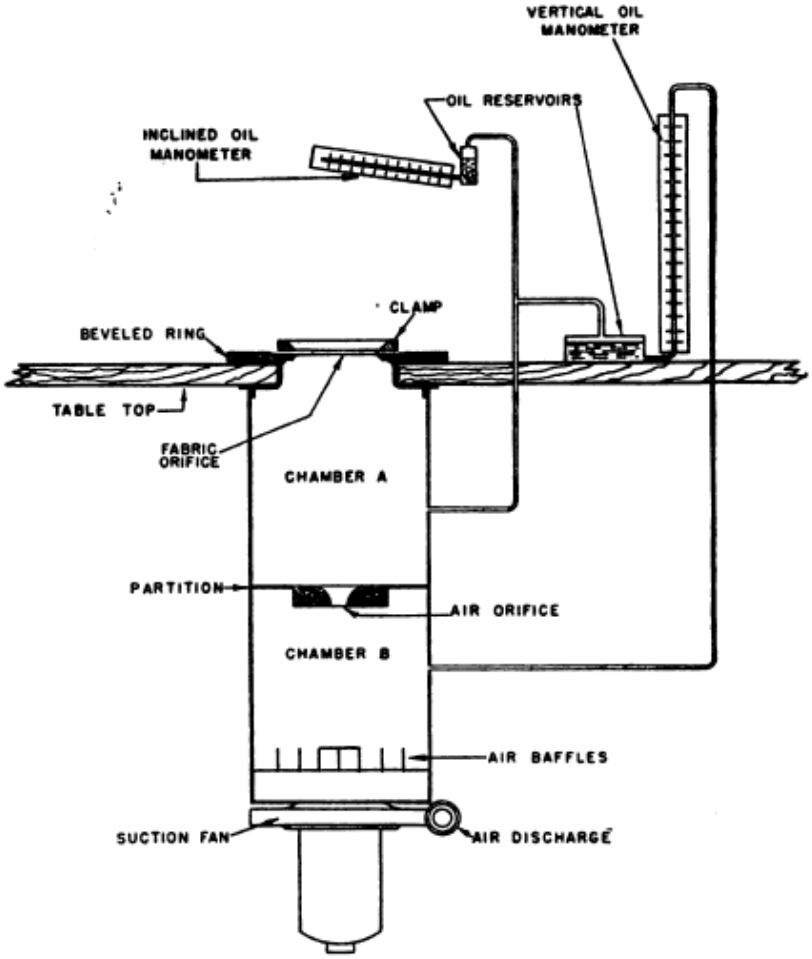

Figure 3.12 Schematic diagram of mat permeability measurement using air (Schiefer & Boyland, 1942).

3.5 SURFACE MODIFICATION OF CATTAIL

3.5.1 Surface modification of cattail fiber

Solution preparation: 2.5 ml of DIH and 2.5 ml of HEA were added to 95 ml of ethyl acetate solution to prepare 2.5% DIH+HEA solution for the surface modification of cattail. Similarly, 5 ml and 10 ml of DIH and HEA were added to 90 ml and 80 ml of ethyl acetate solution respectively, to prepare 5% and 10% DIH+HEA solution.

Pad-dry-cure: For cattail fiber treatment with DIH and HEA, oven dried (100ºC for 12 hrs) fibers were immersed in 2, 5, and 10% solution of DIH and HEA (dissolved in ethyl acetate) for 20 min. After that, excess chemicals were squeezed out from the treated fibers using a padding machine (Model# D394, manufactured by SDL ATLAS USA). with 4 padding cycle and 2 kg force applied on it. Once the padding was done, cattail fibers were then dried in an oven at 50ºC for 5 hrs. The FTIR-ATR analysis of the chemically treated cattail fiber was done. In addition, the change in moisture regain % in treated cattail fiber was evaluated using the procedure as described in section 3.3.2.

3.5.2 Surface modification of cattail mat

Cattail fibers were individualized using a carding machine and a nonwoven cattail mat was manufactured following section 3.2.3. The prepared mat was dried in an oven at 100^0C for 12 hrs. 5 % (v/v) of 1,6-diisocyanatohexane (DIH), 5 % (v/v) of 2-hydroxyethyl acrylate (HEA) were prepared by dissolving them in anhydrous ethyl acetate solution. The resulting solution was evenly sprayed on the cattail mat. The nonwoven cattail mat coated with DIH-HEA was then dried in an oven at 50^0C for 5 hrs.

3.5.3 FT-IR analysis

The surface modification of cattail fibers, caused by treating them with DIH and HEA was investigated through Fourier-transform infrared (FT-IR) analysis using NICOLET 6700 spectrometer manufactured by Thermo Fisher Scientific, Inc. USA. The machine was synchronised with OMNIC software for analysing the spectral data and equipped with a single reflection Diamond ATR cell as shown in Figure 3.13. A spectral resolution of 4 cm-1 in the mid-infrared range (500–4000 cm^{-1}) with 120 scans was used in the analysis.

Figure 3.13 NICOLET 6700 spectrometer for FT-IR analysis.

3.6 COMPOSITE MANUFACTURING

Composite manufacturing was facilitated by Dr. Raghavan Jayaraman in the advanced composite processing laboratory of Mechanical Engineering department at the University of Manitoba. Fahimian (2013) investigated hemp composites using three different pressures (101, 260, and 560 kPa). Same consolidation pressures are also used in this study so that the results can be compared. 101 kPa pressure (VARTM) was used to manufacture composite without any additional compaction and 560 kPa has been chosen to achieve a much higher V_f in manufactured composite without bleeding a lot of resins from mat and 260 kPa has been chosen as a middle value between 101 kPa and 560 kPa.

3.6.1 Manufacturing composites using VARTM (vacuum assisted resin transfer molding)

The needle punched nonwoven flax mat, hybrid flax-hemp mat, and prepared nonwoven cattail fiber mat (8.5” X 8.5”) were placed on the mold surface that was already coated with a mold release agent. The mold release agent helps for the easy removal of the cured composite part

from the mold. A chopped glass mat was placed at the opposite edge of the mat connecting the mat to the vacuum port. The glass mat provides the path for the air to flow from the mat to the vacuum port. Tacky tape was placed along the longitudinal edge of the mat to prevent race tracking and dry spots. A re-usable silicon pad was placed over the mat to cover it and sealed along the edges to the bottom mold using appropriate seals as illustrated in Figure 3.14 (a, b). This silicon pad isolates the mat from the surrounding atmosphere creating a bag containing the mat, to which vacuum could be applied. Vacuum is applied at one end of the mat and the thermoset resin is introduced at the opposite end. STYPOL 8086 thermoset resin was prepared in a beaker and mixed with the LUPEROX 224 curing initiator, degassed, and injected into the mat under the action of vacuum. When the flow front, as shown in Figure 3.14 (c), traverses the entire mat and impregnates it, the resin inlet was closed and the impregnated mat was maintained under vacuum until the resin gelled (2 hours). Subsequently, the vacuum port as closed and the composite was allowed to cure at room temperature overnight (24 hours).

3.6.2 Manufacturing composites by compression molding

The pressure used in VARTM is ~101 kPa. In order to study the effect of pressure, additional mats were cured under various compression pressures. The mats impregnated using the VARTM set-up, were removed from the mold, right after resin impregnation, and were compression molded in a hydraulic press using different pressures. The impregnated mat sample from VARTM was sandwiched between two release films, which were subsequently sandwiched between two metal plates and two silicone pads and subjected to pressures of 260 and 560 kPa, using a G50 H- 24-CLX hydraulic press manufactured by WABASH MPI, IN, USA as shown in Figure 3.15 (a). After gelation (2-3 hours) the sandwiched samples were left inside the press for 8-10 hours to cure at room temperature (Figure 3.15 b). The cured composite is shown in Figure 3.15 (c).

(a) (b)

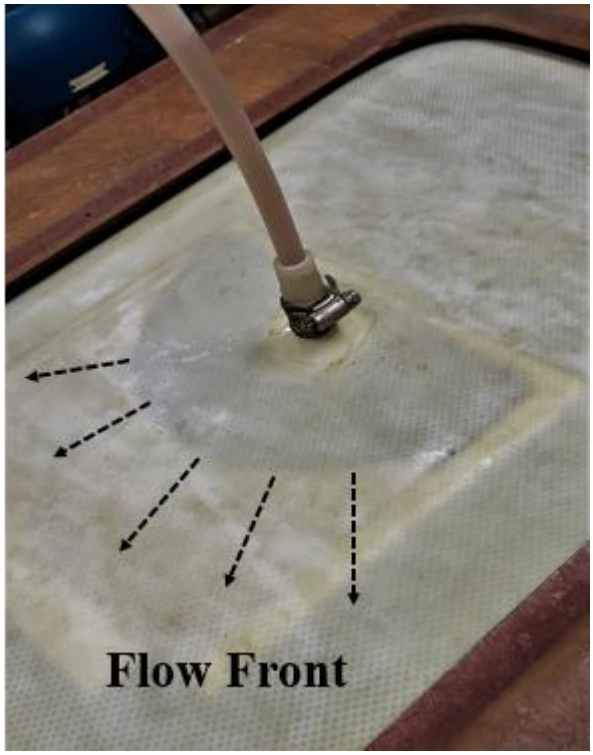

(c)

Figure 3.14 Vacuum Assisted Resin Transfer Molding process – (a) nonwoven mat laid up in mold (b) VARTM setup before resin impregnation (c) flow front of resin while impregnation.

(a) (b) (c)

Figure 3.15 (a) G50 H- 24-CLX hydraulic press machine for compression molding (b) resin impregnated mat sandwiched among release film, metal plate, and silicon pad (c) cured composite plate in compression molding.

3.7 DENSITY MEASUREMENT

The density of the cattail fiber, flax fiber, hemp fiber, Stypol resin, and the manufactured composites were measured in the grain storage lab of the University of Manitoba, using Helium Pycnometer (Model#UPY-32, UPY-32T; v-5.04 manufactured by Quantachrome INSTRUMENTS) according to ASTM D4892-89. The Helium Pycnometer used in this study for density measurement is shown in Figure 3.16. The calibration of Helium Pycnometer is needed prior starting the density measurement trials. Initially, composite samples were weighed using a very precise balance and placed further in the pycnometer using the smallest cell. Various run parameters (target pressure, Equilibrium time, purge mode, and run mode) and sample parameters (weight) were selected before starting the test. Three different trials were done for each experiment and the final results were shown in pycnometer display that include average volume, average density of composite, and standard deviation.

Figure 3.16 Helium Pycnometer for density measurement.

3.8 FIBER VOLUME FRACTION MEASUREMENT

3.8.1 Fiber volume fraction in nonwoven mat

The fiber volume fraction in the nonwoven mat was determined using Eq. (3.4).

$$\text{Fiber volume fraction, } V_f \ (\%) = \frac{W}{A \,.\, h \,.\, \rho_f} \tag{3.4}$$

Where, W is weight of reinforcement specimen, A is the reinforcing area, h stands for thickness, and ρ_f is the density reinforcing fiber.

3.8.2 Fiber volume fraction of composite

The volume fraction of fibers (V_f %) in composite can be calculated using the density of composite measured following the procedure described in section 3.9. V_f % is calculated using Eq. (3.5), assuming 100% dense composite.

$$\text{Fiber volume fraction, } V_f \ (\%) = \frac{\rho_c - \rho_m}{\rho_f - \rho_m} \text{ X } 100 \tag{3.5}$$

Where, ρ_f, ρ_m, ρ_c are the density of the fiber, resin, and composite respectively.

3.9 PREPARATION OF TENSILE TEST COUPONS

Composite test specimens, 127 mm in length and 20 mm in width were cut from the manufactured panels which were tabbed, and polished before tensile testing. Prepared composite specimens ready for tensile testing are shown in Figure 3.17.

Figure 3.17 Composite specimen (127 mm X 20 mm) sandwiched between carbon epoxy laminates for tensile testing.

3.9.1 Tabbing

The composite panels manufactured in VARTM and the compression molding was bonded to the gripped ends to avoid crushing the gripping ends while tensile testing. Tabs cut from carbon fiber epoxy composite laminates were bonded to the edges of the composites using a room temperature curing adhesive. Marine Epoxy (made by Lepage) glue was used in this case as it has the capacity to endure maximum shear stress while tensile testing. The adhesive was applied on both the carbon epoxy and composite specimen and they were allowed to cure under 15 psi pressure for 24 hrs in G50 H-24-CLX hydraulic press.

3.9.2 Cutting

127 mm long and 20 mm wide composite test specimens were cut from the panels with bonded tabs using Micro-Matic Precision Wafering Machine manufactured by Micromech Mfg. Corp. The bonded panels were attached to the cutting bed using double-sided tape during the cutting process. A slow feed rate of 10 mm/min was used to prevent excessive heat formation in the saw and damaging of the edges of test specimens.

3.9.3 Polishing

Edges of the prepared testing coupons were ground progressively using 80, 180, 240, 320, and 400 grit silicon carbide papers and polished further using alumina powder to remove all adhered particles. The polished test coupons were stored in lab atmosphere until testing.

3.9.4 Manufacturing carbon epoxy laminate tabs

The manufacturing process of carbon-epoxy composite tabs includes following steps.

I. Cutting prepreg

The carbon fiber epoxy composite laminates were fabricated using 4 plies of woven carbon epoxy prepregs (supplied by SAE International). The woven carbon-epoxy prepreg roll was removed from a freezer, just before use, and allowed to warm up at room temperature for 3-4 hrs. 12” X 12” prepreg layers were cut from the prepreg roll using a template.

II. Prepreg lay-up process and vacuum bag assembly

After cutting, the woven prepregs were laid up manually on an Aluminum plate. Release film, peel ply, bleeder (Supplied by Airtech), and breather were cut to size (12” X 12”) and placed on either side of stacked prepreg layup as shown in Figure 3.18. Before the lay-up procedure, the tool part was coated with non-stick coating 5-6 times with a 5-minute drying interval between each coat. The peel plies provide texture to the cured laminate surface and the bleeder layer enables excess resin to bleed-out. The lay-up mold was then taken in the autoclave plate, covered by a silicon pad and then placed in the G50 H- 24-CLX hydraulic press (manufactured by WABASH MPI, IN, USA). The lower autoclave platen was connected to a vacuum pump and the upper platen was connected to a nitrogen tank as shown in Figure 3.19.

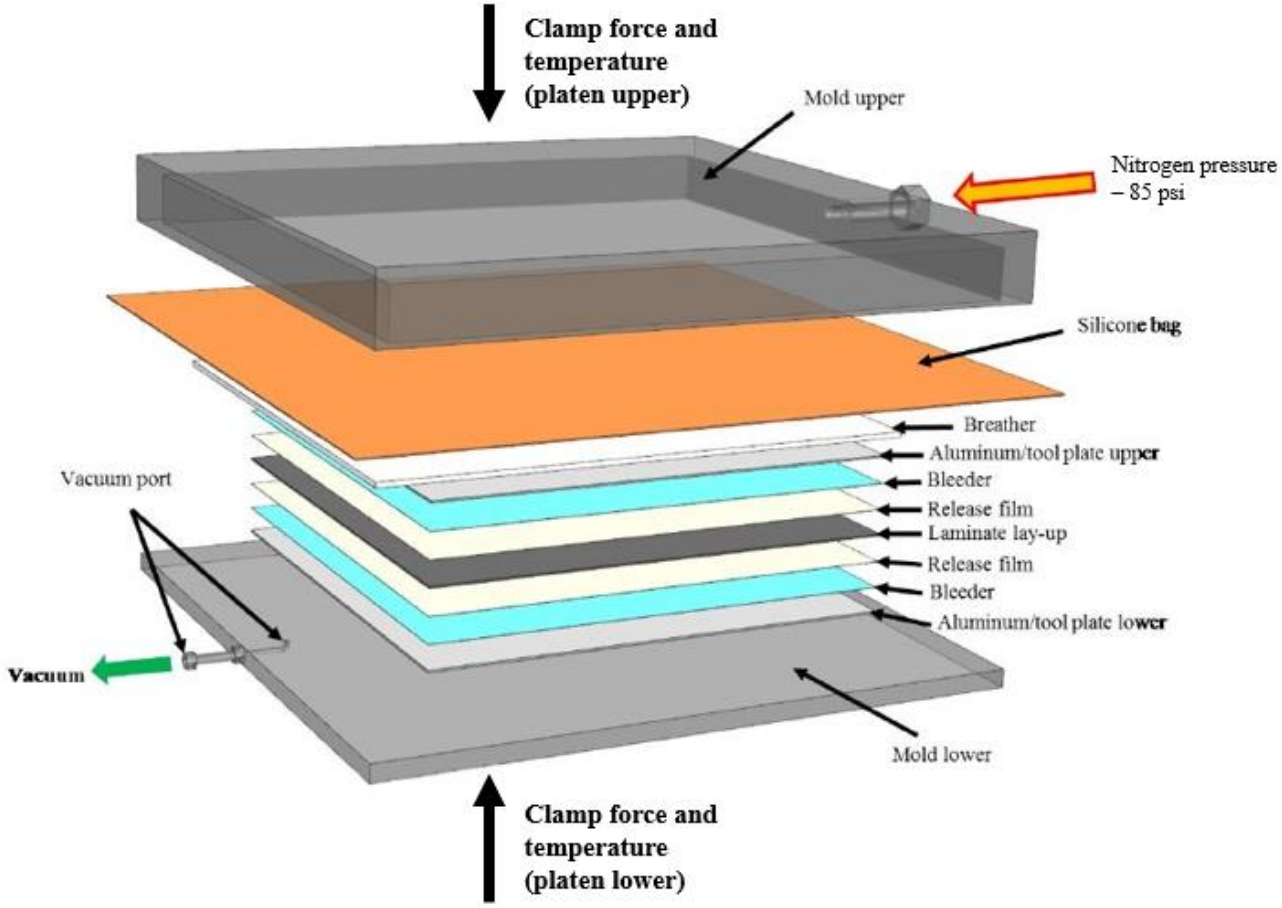

Figure 3.18 Prepreg layup and vacuum bag assembly for manufacturing carbon-epoxy composites (Chekurthi, 2018).

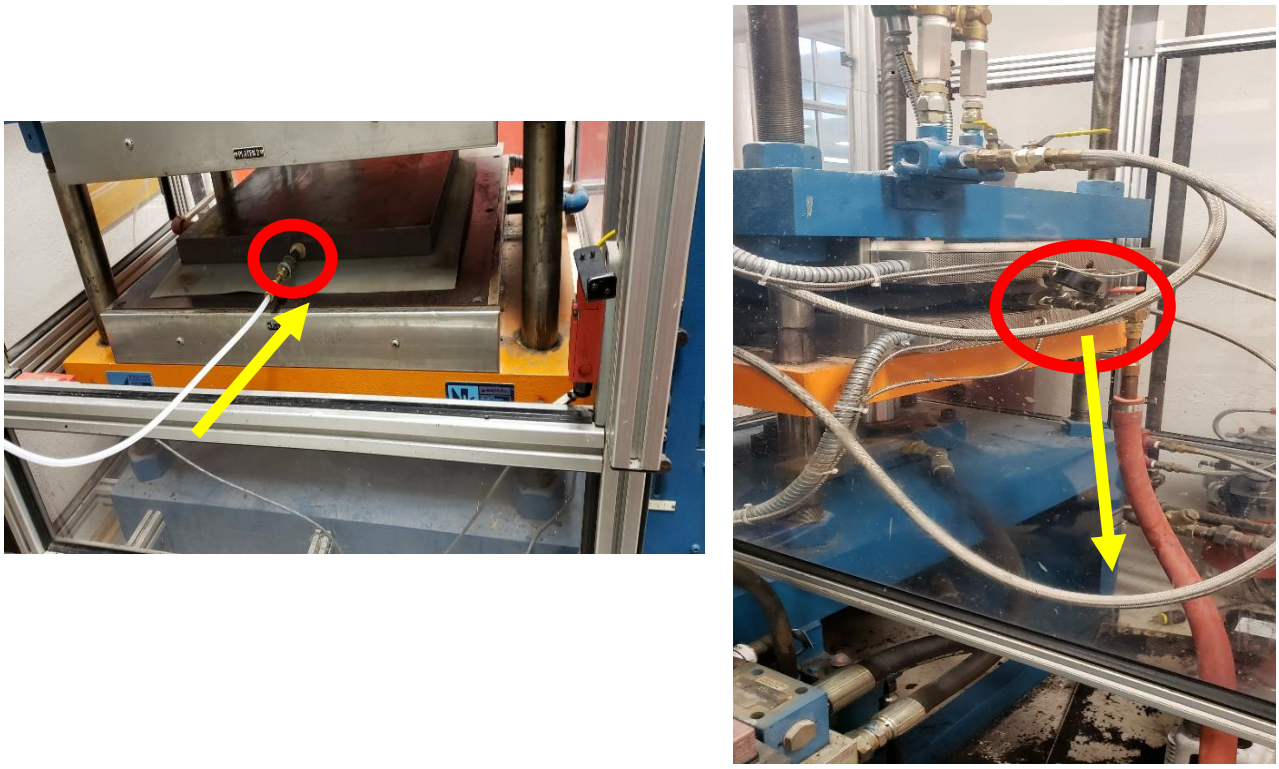

(a) (b)

Figure 3.19 Autoclave plate is connected to (a) nitrogen tank and (b) vacuum pump – while manufacturing carbon-epoxy laminates.

III. Autoclave curing

The laid-up carbon-epoxy composite lay-up was cured using a mold simulating the autoclave and a one-step cure cycle shown in Figure 3.20. The press was clamped down and the clamp force was set to 23 Ton-force. The valve of the nitrogen tank was turned on and adjusted to 85 psi. The Nitrogen tank valve was turned off once the adjustment was made. The vacuum pump was now turned on and the temperature was set to 180^0C. When temperature of platens reached 80^oC, the vacuum pump was turned off, the lower half was vented to atmosphere, and the pressurized nitrogen gas was channeled into the upper part of autoclave mold to maintain a constant pressure of 85 Psi. The epoxy resin or matrix system started flowing at 80^0C. The mold

was held at 180^0C under nitrogen pressure for 120 minutes. The silicon pad created a negative pressure on laminates and Nitrogen pressure helped the resin to flow.

After completion of the holding time (120 minutes), heating was turned off and the platens were allowed to cool down to room temperature freely (i.e. without any imposed cooling rate). The nitrogen pressure was cut off after reaching 100^0C during the cooldown process. The cured carbon epoxy laminate is illustrated in Figure 3.21. The cured carbon-epoxy laminate was post cured in an oven at 220^0C for 4 hrs to complete the cross-linking of monomers in the laminate.

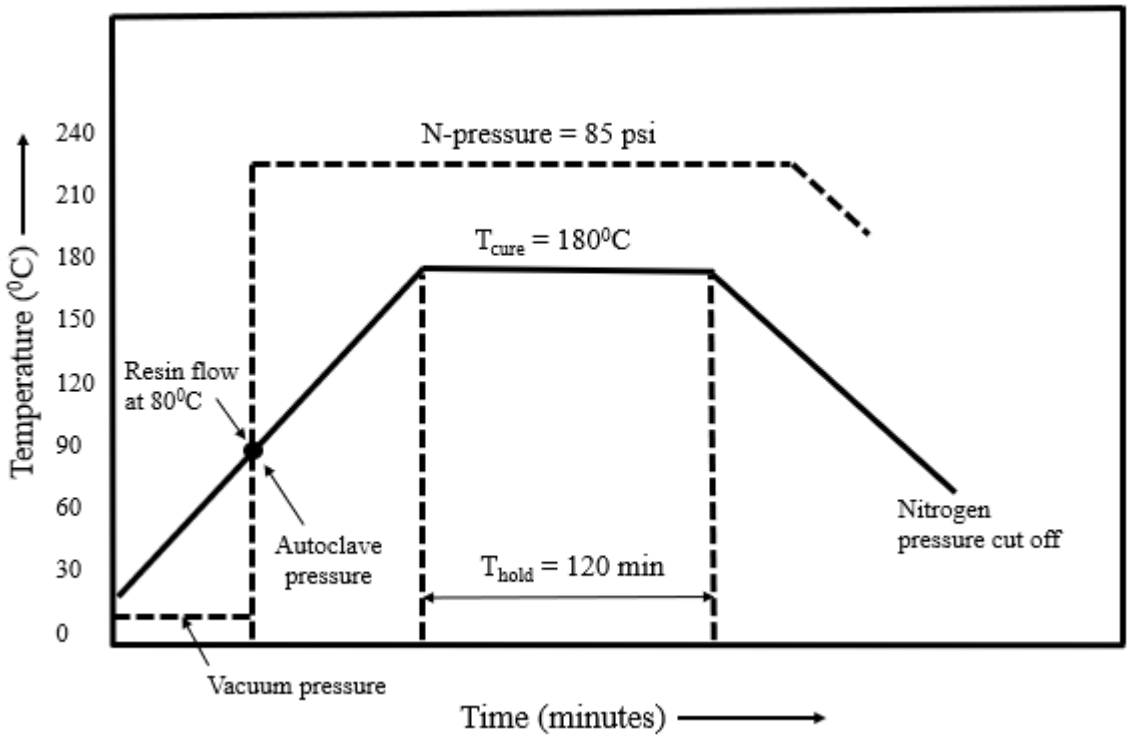

Figure 3.20 Cure cycle in autoclave processing for carbon-epoxy composite.

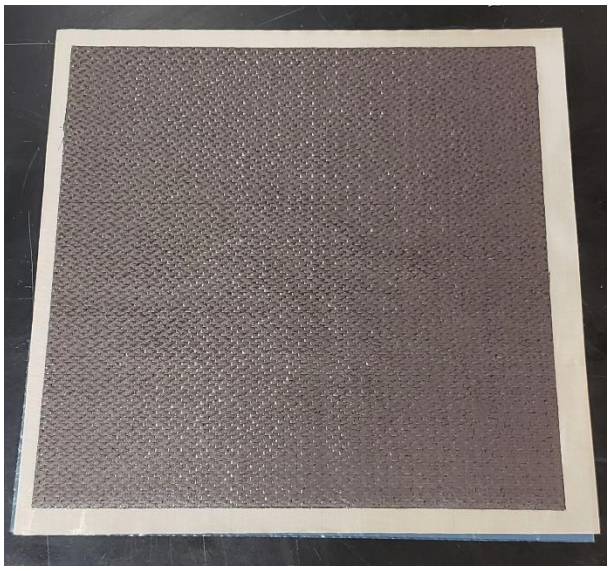

Figure 3.21 Cured carbon-epoxy laminates.

3.10 TENSILE TESTING OF COMPOSITE

The mechanical properties of manufactured composite were determined using an MTS tensile testing machine with 30 KN Load cell and 2-inch extensometer, following the ASTM D3039 method. The machine set-up for tensile testing of composite specimens in MTS with extensometer is shown in Figure 3.22. All samples were stored in the lab atmosphere after preparation until testing. The testing was done at a crosshead speed of 2 mm/min. Five samples were tested for each consolidation pressure. The tensile modulus of the manufactured mat composite was calculated from the slope of the stress-strain curve in the strain range of 0.1%.

It is to be noted that only longitudinal modulus of composite was measured in this study as samples prepared were cut along the length of the mats. Also, the modulus of the samples cut along the width of the mats is referred as transverse modulus. Fahimian (2013) observed difference in experimental results between longitudinal modulus and transverse modulus for hemp mat composite where transverse strength was more than longitudinal strength confirming the bias in fiber orientation distribution. Hence, it is expected to get such difference for the discontinuous fiber composites investigated on this study. Also, evaluation of modulus in each direction is important to find out the lowest modulus value which is the key to design a material.

Therefore, measurement for transverse mechanical properties of flax, cattail, and flax-hemp hybrid mat composite is recommended for future research of this study.

Figure 3.22 Tensile testing of composite specimens in MTS with extensometer.

3.11 MICROSCOPIC ANALYSIS OF MATS AND COMPOSITE

The manufactured composite surface was analysed in a microscope to understand and examine the fiber geometry, fiber orientation, and any voids. In this study, the needle punched flax mat and composite surface were analysed using VHX Digital Microscope - VHX-S770E (manufactured by KEYENCE CORPORATION, Osaka, Japan) as shown in Figure 3.23.

Figure 3.23 VHX Digital Microscope.

3.12 SEM ANALYSIS OF COMPOSITE

The fractured surfaces of the composite specimens from the tensile test were examined in a SEM at an accelerating voltage of 10.0 kV. A scanning electron microscope (SEM) in the Manitoba Institute for Materials (MIM), at the University of Manitoba, was used in this study to analyse the cross-section of the fractured surface of composite specimens. The scanning electron microscope used in this study was FEI Quanta 650 FEG ESEM from Thermo Fisher Company, USA as shown in Figure 3.24.

Prior to the SEM analysis, the fractured composite specimens were coated with a thin layer of gold-palladium film (20 nm) using DESK II COLD SPUTTER ETCH UNIT under the chamber pressure of 30 mTorr. Figure 3.25 shows that the coating operation is in progress while depositing the Au-Pd film on the fractured surface of the composite samples.

After coating, the samples were mounted on the SEM stub for examination. The image was collected with ETD (Everhart-Thornley detector) in HiVac at low pressure for coated

(100% cattail, 100% flax, and 50% flax-50% hemp fiber reinforced) composite samples. The SEM was used for imaging at different magnifications from low to high (40x - 1000x) for the morphological analysis of fractured surface.

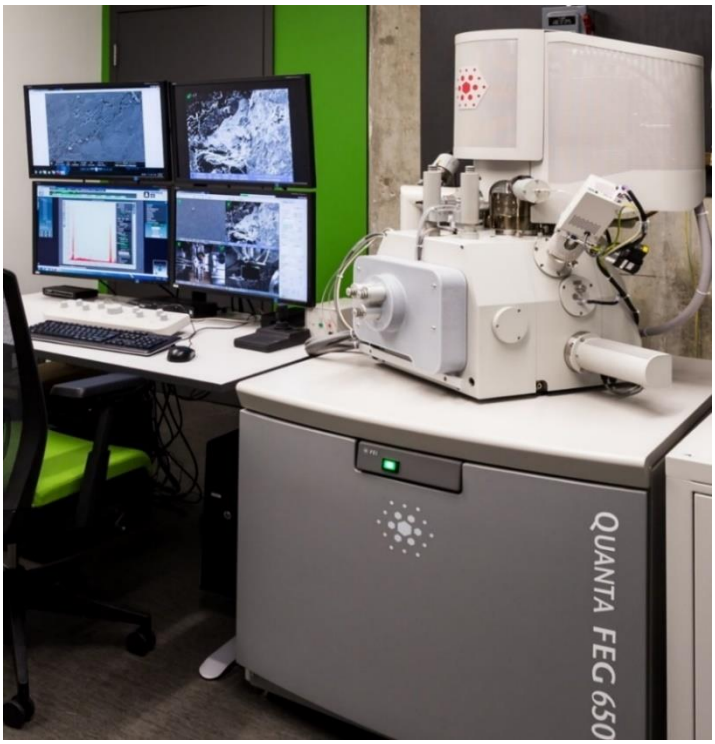

Figure 3.24 Scanning electronic microscope (Courtesy – Manitoba Institute for Materials, University of Manitoba).

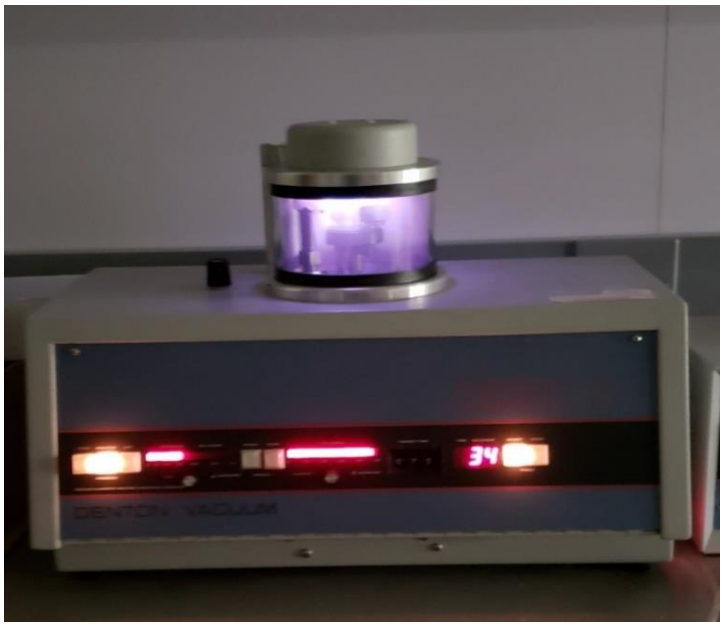

Figure 3.25 Coating operation of fractured composite samples.

CHAPTER IV

FLAX FIBER COMPOSITES – RESULTS AND DISCUSSION

In this chapter, the experimental results for flax fiber properties, characterisation of needle punched flax mat, properties of flax mat composite, and properties of flax-hemp hybrid mat composite are presented. The effect of mat manufacturing parameters on flax mat structure and evaluation of mat properties such as the areal density (GSM), thickness, fiber volume fraction, permeability are discussed by analysing the experimental results. Subsequently, the experimental results for the tensile modulus and the tensile strength of flax mat composite and flax-hemp hybrid mat composite are presented and relationship between mat design and composite properties are highlighted.

4.1 PHYSICAL AND MECHANICAL PROPERTIES OF FLAX FIBER

Random flax fibers were pulled out from different needle punched mats and physical and mechanical properties were determined experimentally. Figure 4.1 and Figure 4.2 illustrate the frequency distribution of fiber length and diameter respectively. Similarly, frequency distribution for experimental tensile strength, modulus, and strain at break (%) of flax fiber are shown in Figure 4.3, 4.4, and 4.5, respectively.

The normal frequency distribution model can be used to determine the mean value of corresponding fiber properties (fiber length, diameter, tensile strength, modulus, and strain at break) using Eq. (4.1), (4.2), (4.3), (4.4), and (4.5); where n_f is the frequency of fibers for a given fiber properties. The mean values of fiber length, diameter, tensile strength, modulus, and

strain at break (%) determined from these equations are shown in Figure (4.1), (4.2), (4.3), (4.4), and (4.5), respectively and it could be used further for predicting properties of flax-polyester composite.

The length of the flax fiber pulled out from nonwoven flax mat varied from 2.25 to 12.77 cm and the diameter of flax fiber varied from 20 to 192 μm. The experimental tensile strength of flax fiber varied from 16 MPa to 597 MPa, modulus of elasticity from 1 GPa to 26 GPa, and strain at break (%) from 0.9 to 8 %. The calculated mean tensile strength and tensile modulus value of flax fiber using normal frequency distribution is 201.54 MPa and 11.72 GPa, respectively.

$$Avg.fiber\ length, \bar{L} = \frac{\sum nf\ Lf}{\sum nf} \tag{4.1}$$

$$Avg.fiber\ diameter, \bar{D} = \frac{\sum nf\ Df}{\sum nf} \tag{4.2}$$

$$Avg.tensile\ strength, \bar{\sigma} = \frac{\sum nf\ \sigma f}{\sum nf} \tag{4.3}$$

$$Avg.tensile\ modulus, \bar{E} = \frac{\sum nf\ Ef}{\sum nf} \tag{4.4}$$

$$Avg.\ strain\ at\ break\ (\%), \bar{\varepsilon} = \frac{\sum nf\ \varepsilon f}{\sum nf} \tag{4.5}$$

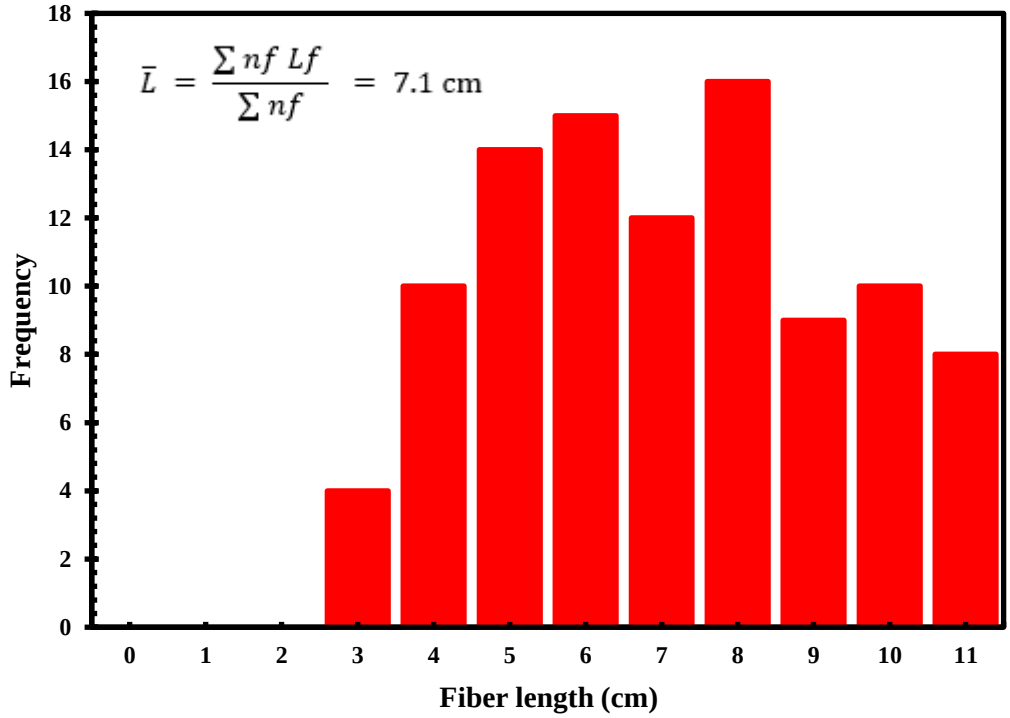

Figure 4.1 Distribution in length of fibers in needle punched flax mat.

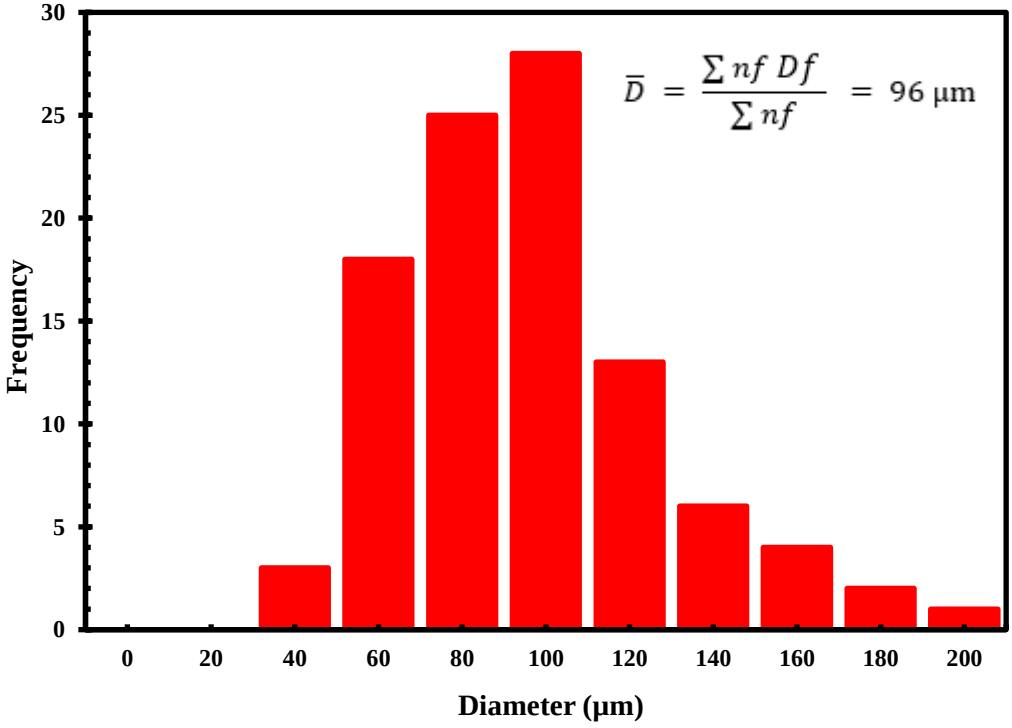

Figure 4.2 Distribution in diameter of fibers in needle punched flax mat.

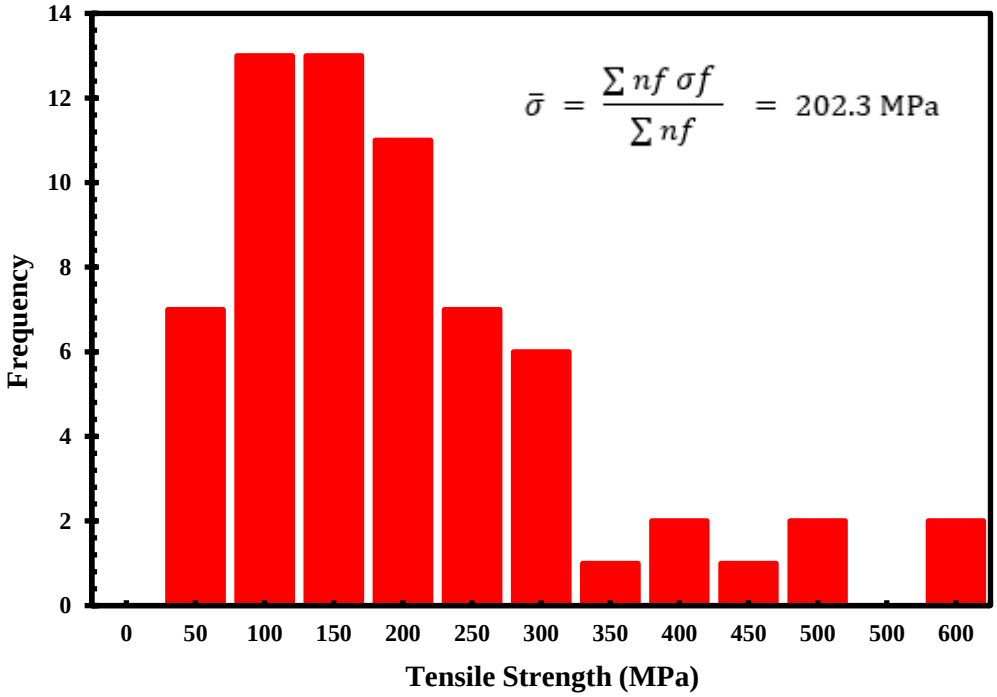

Figure 4.3 Distribution in tensile strength of fibers in nonwoven flax mat.

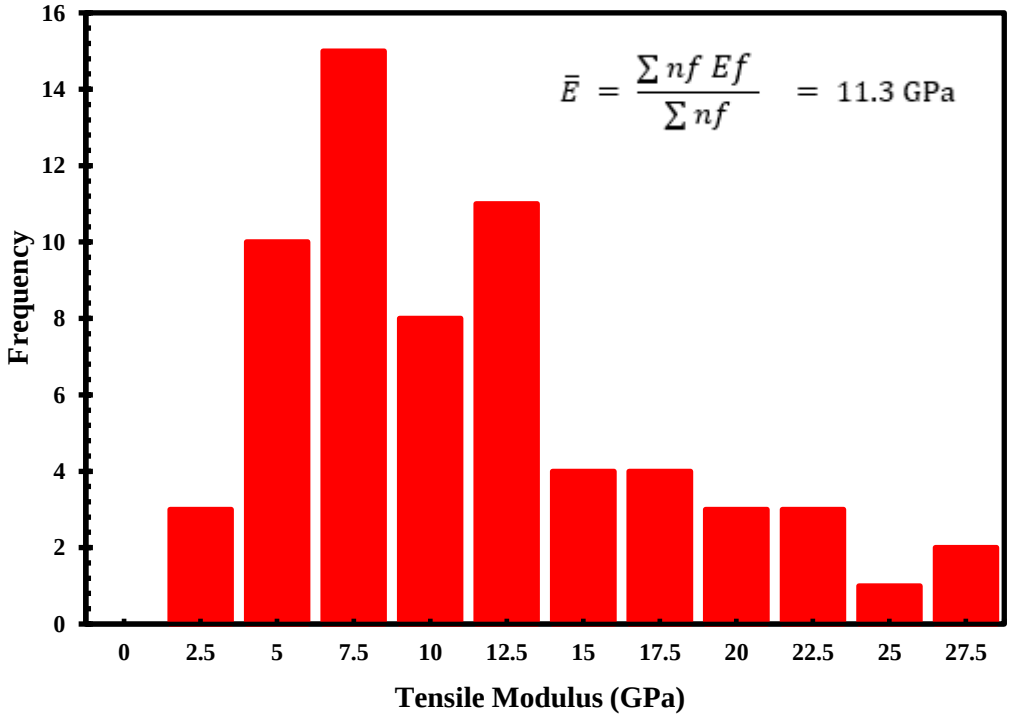

Figure 4.4 Distribution in tensile modulus of fibers in nonwoven flax mat.

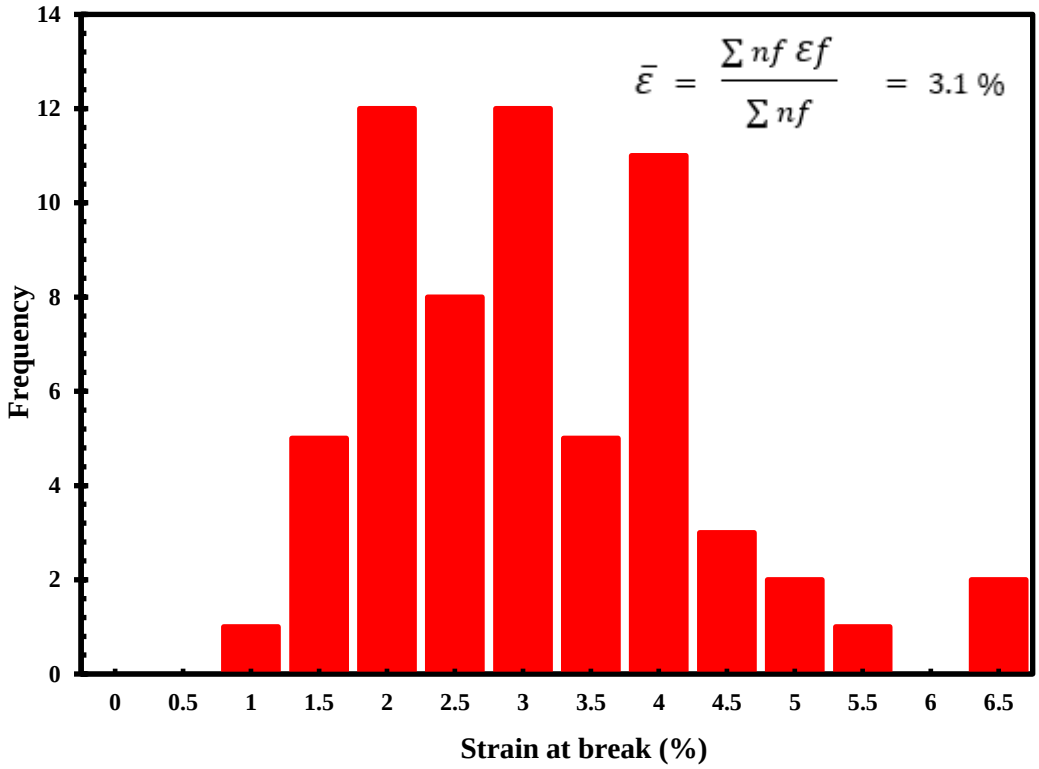

Figure 4.5 Distribution in strain at break (%) of fibers in nonwoven flax mat.

4.2 EFFECT OF DIAMETER ON THE MECHANICAL PROPERTIES OF FLAX FIBER

The experimentally measured tensile modulus or modulus of elasticity of flax fibers (E_f) varied with the variation in diameter of fibers (D_f) due to the change in the chemical composition of fibers and number of defects with diameter. These variations are illustrated in Figure 4.6 by plotting the tensile modulus as a function of flax fiber diameter. The tensile modulus of flax fiber varied from 1 GPa to 26 GPa for a fiber diameter variation from 20 to 192 μm. The experimental data points in Figure 4.6 were empirically fitted using non-linear regression function and an equation was derived with the fitted values for predicting flax fiber modulus. The derived equation is shown in Eq. (4.6). A decreasing trend in elastic modulus is observed with increase in flax fiber diameter which is in agreement with published results for hemp fibers (Fahimian, 2013). The correlation or R^2 value is found 0.78 from the regression analysis.

$$E_f = 46.92 \exp [- 0.018 (D_f)] \quad (4.6)$$

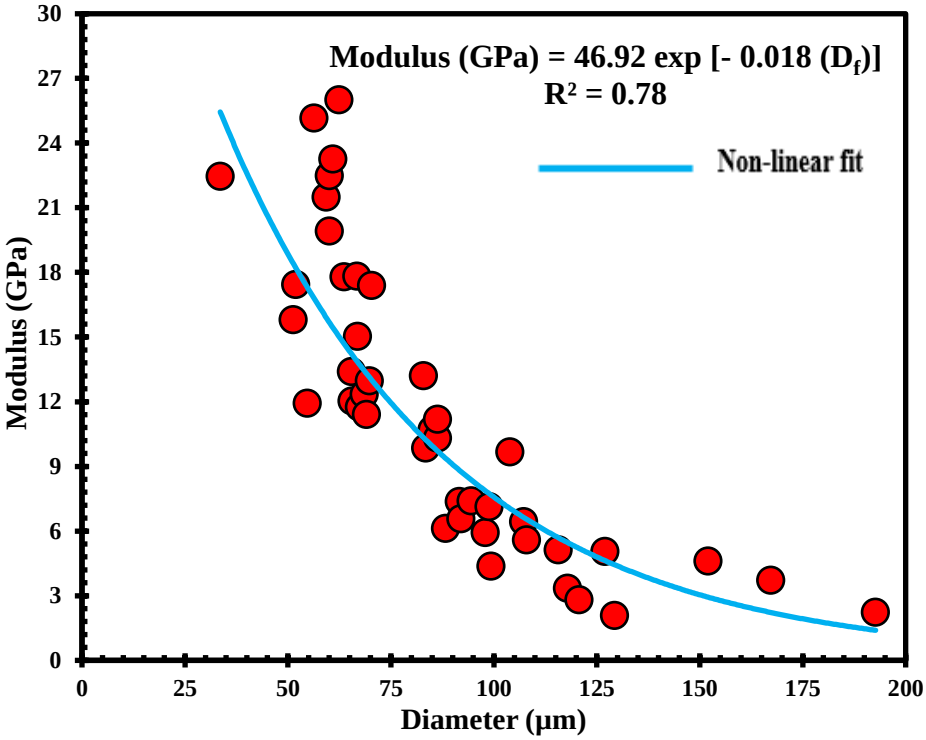

Figure 4.6 Variation in elastic modulus of flax fibers with diameter.

4.3 PHYSICAL PROPERTIES OF NONWOVEN FLAX MAT

The structure of needle-punched nonwoven mat is not homogenous as the rearrangement of fibers during processing increases the structural anisotropy when compared with the original web. That is why it is necessary to assess the physical properties of needle punched nonwoven mat. Key properties that determine the performance characteristics of a nonwoven needle-punched preform are: type of fiber used, fiber diameter and length, fiber quality, needle punch density; depth of penetration of needle, needling rate, permeability, and areal density of mat (Rao et al., 1997).

Microscopic images of 20-P, 30-P, and 72-P needle punched flax mat are shown in Figure 4.7, 4.8, and 4.9 respectively at 20X magnification. These images show that flax fibers are randomly oriented or not at all aligned at 20 needle punch density mats and the fiber

orientation changes when punch density increased from 20 to 72. Theoretically, 72-P flax mat should pick more number of in-plane fibers and re-orient them in the out-of-plane direction while manufacturing mat. Change in fiber orientation with the change in needle punch density could change the mechanical properties of manufactured composite. Effect of fiber orientation on the composite properties is already discussed in section 2.2.2.

Figure 4.7 Microscopic image of 20-P flax mat at 20X magnification.

Figure 4.8 Microscopic image of 30-P flax mat at 20X magnification.

Figure 4.9 Microscopic image of 72-P flax mat at 20X magnification.

The physical properties of needle punched nonwoven flax mat are tabulated in Table 4.1. Areal density and thickness of mat varies for different punch density and needle depth and the fiber volume fraction and mat permeability changes with the alteration in areal density and mat thickness. Fahimian (2019) studied and evaluated the same properties for nonwoven hemp mat where depth of needle penetration while needle punching process was kept constant to 8 mm. To compare these properties between nonwoven flax mat and hemp mat, the physical properties of nonwoven hemp mat are also tabulated in Table 4.2.

The large standard deviation in the areal density of the mat points to large variation in the areal density from one location to another location of the mat. Given the similar areal density with large standard deviation, increasing the punch density from 20 to 30 did not change the mat thickness. Initially flax mat thickness was higher when manufactured at zero punch density and thickness decreased with increase in punch density observed in 20P and 30P needle punched mat. So, it is clear that needle punching process reduces the thickness of the mats. However, the higher flax mat thickness for 72-P mat (Table 4.1) when compared to 20 and 30

is believed to be due to higher starting areal density of the flax fiber web (before needle punching) and smaller needle depth.

The fiber volume fraction of the flax mat certainly increases with needle punching when compared with zero punched flax mat (Table 4.1), due to packing of fibers as indicated by the lower mat thickness. However, among the needle punched flax mat, instead of increasing, the fiber volume fraction in the mat decreases with the increase in punch density as seen in Table 4.1. For a given punch density, fiber volume fraction varied in flax mat and hemp mat as V_f % of mat depends on the mat thickness and starting areal density.

Table 4.1 Physical properties of nonwoven flax mat.

Mat Content	Punch density (p/cm^2)	Depth of needle penetration (mm)	Areal density of mat (g/m^2), (SD)*	Mat thickness before consolidation (mm), (SD)*	Fiber volume fraction in mat, V_f %, (SD)*
100% Flax	0	0	931.1 (67.1)	16.3 (0.7)	3.8 (0.2)
100% Flax	20	8	814.7 (88.3)	4.6 (0.3)	11.6 (0.7)
100% Flax	30	8	823.6 (97.4)	4.7 (0.5)	11.4 (1.4)
100% Flax	72	2	885.2 (108.5)	6.8 (0.4)	8.7 (1.4)

(SD)* - Standard deviation, N = 9

Table 4.2 Physical properties of nonwoven hemp mat (Fahimian, 2015).

Mat Content	Punch density (p/cm^2)	Depth of needle penetration (mm)	Areal density of mat (g/m^2)	Mat thickness before consolidation (mm)	Fiber volume fraction in mat, V_f %
100% Hemp	0	8	941.3 (17.9)	12.5 (3.1)	6.6 (1.6)
100% Hemp	2.6	8	1021.6 (7)	8.1 (1.5)	8.7 (1.6)
100% Hemp	20	8	1014.8 (7)	5.75 (0.93)	11 (3.5)
100% Hemp	30	8	1113.9 (6.6)	5.39 (1.24)	15 (1.1)
100% Hemp	70	8	1241.3 (11.2)	6.8 (1.40)	12 (1.5)

4.4 FLAX MAT PERMEABILITY

Zero-punched and needle punched nonwoven flax mat structures are porous in nature and hence, they are permeable. Characterization of mat permeability is necessary to understand their effect on composite properties. The transverse permeability of the flax mat decreased initially when punch density increased from 0 to 20 as shown in Figure 4.10. However, permeability increased again when punch density increased further from 20 to 72. No clear trend was observed with needle punch density and hence, the data has to be analyzed in terms of change in void fraction with needle punching.

The experimental permeability values calculated at different punch density are plotted as a function of corresponding mat void fraction as shown in Figure 4.11. From Figure 4.11, a linear relationship observed in transverse permeability with the void fraction content of flax mat indicating an increase in permeability with increase in void fraction of mat. So, out of plane permeability investigated on this study is a function of fiber volume fraction or void fraction of nonwoven flax mat. Since the latter is a function of punch density, the out-of-plane permeability is a function of punch density; for a given areal density, an increase in punch density will decrease in out-of-plane permeability. This trend was observed by Fahimian (2013) in hemp mats. The experimental data in this figure was empirically fitted using linear regression function. The equation of the best fitted line is shown in Eq. (4.7). The correlation or R^2 value of this equation is 0.98. For a given fiber volume fraction (V_f %) of flax mat, transverse permeability can be predicted using Eq. (4.7).

$$\textit{Transverse permeability, } K_z = 0.27 \times (1 - V_f) - 23.08 \qquad (4.7)$$

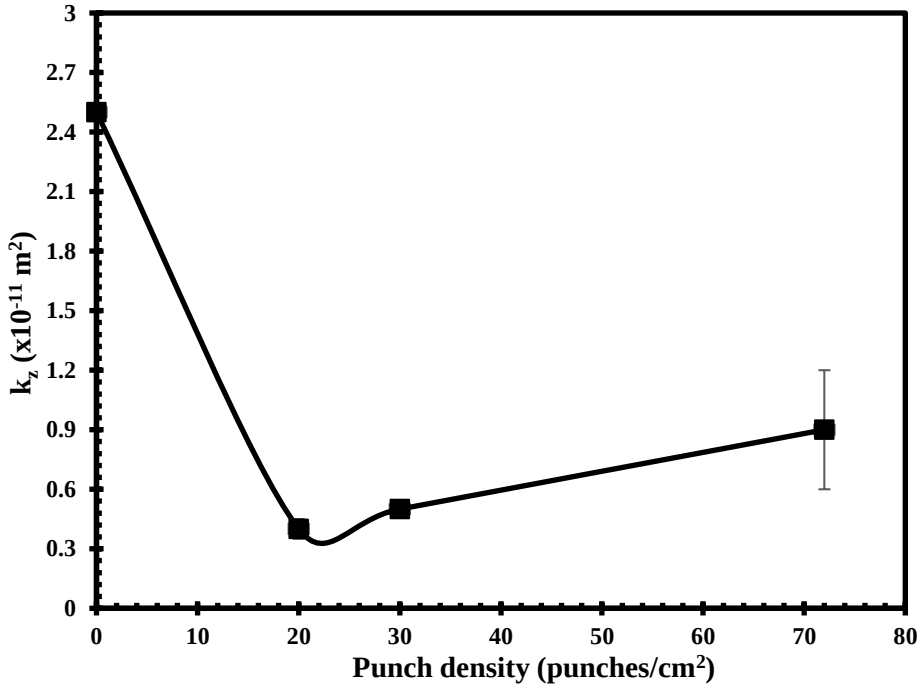

Figure 4.10 Effect of needle punch density on the transverse permeability of flax mat.

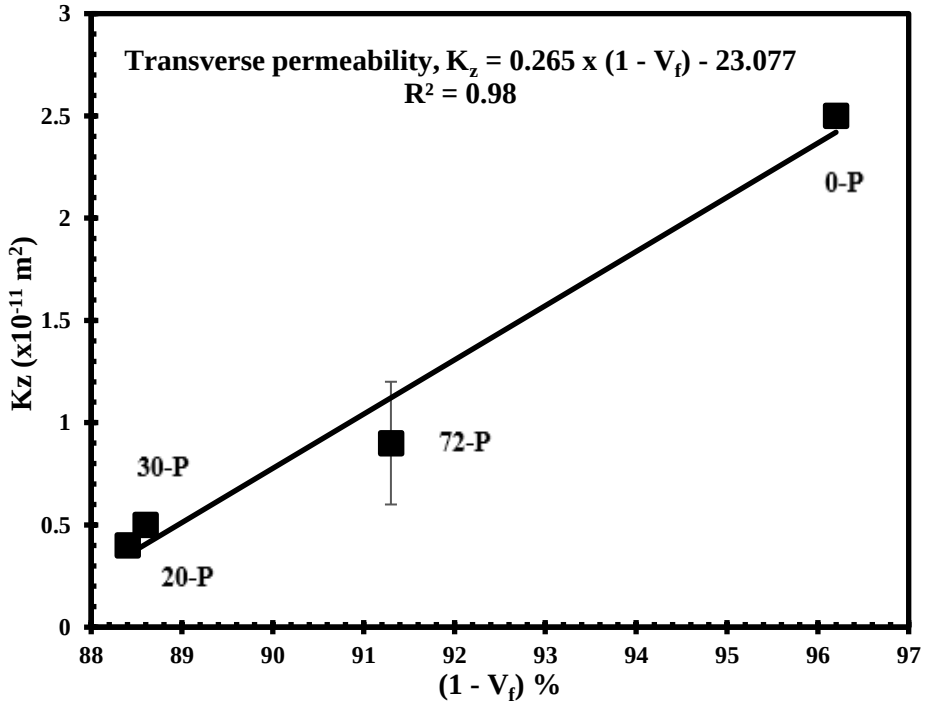

Figure 4.11 Effect of void fraction on the experimental transverse permeability of nonwoven flax mat.

The out-of-plane permeability of nonwoven flax mat can be analysed using well-known Kozney-Carman model. From well-known Kozney-Carman model, the value of C can be determined using Eq. (4.8) (Karaki et al., 2019).

$$C = 0.2 \times \text{Carmen - Kozeny constant} \tag{4.8}$$

However, the value of C an also be determined using Eq. (4.9).

$$C = \frac{r_f^2 (1 - V_f)^3}{4 V_f^2} \tag{4.9}$$

Where, r_f is the radius of fiber and V_f is the volume fraction of fiber. The experimentally measured permeability values of different flax mats were plotted as a function of C as shown in Figure 4.12. The value of C was determined using the data for 0-P, 20-P, 30-P, and 72-P mats with different fiber volume fraction. Although the fiber diameter in the mat exhibited a distribution, the lowest diameter value reported in Figure 4.2 was used in determining the value of "C" plotted in Figure 4.12. The relationship is smilar to that for void content.

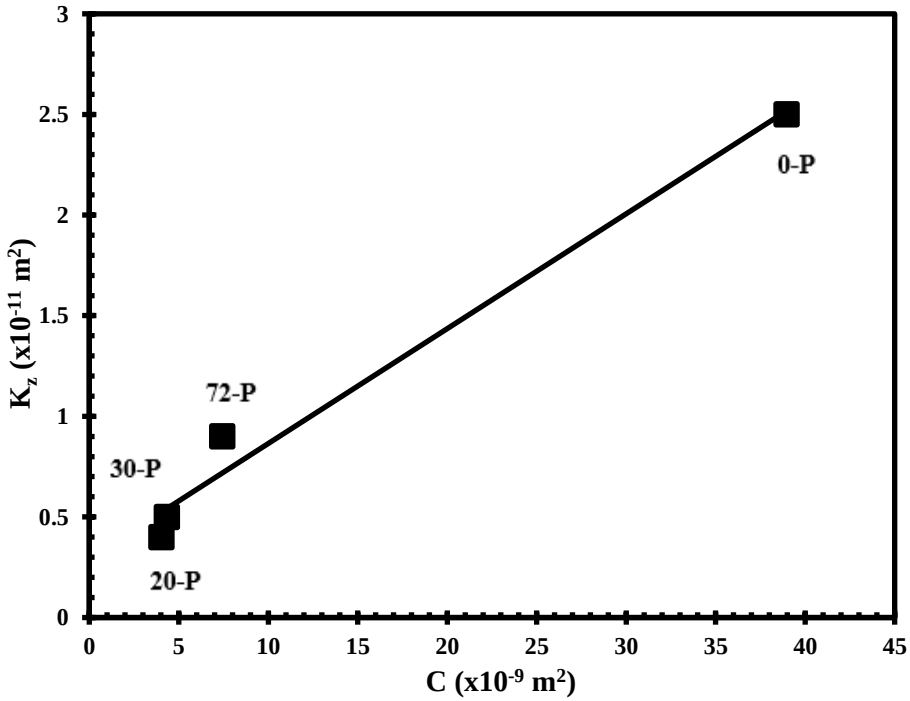

Figure 4.12 Out of plane permeability plotted as a function of C.

4.5 DENSITY OF REINFORCING FIBERS AND RESIN

The experimentally measured density of flax fiber, hemp fiber, and stypol resin are presented in Table 4.3. The density value of reinforcing fibers and resin matrix is required to determine the fiber volume fraction of nonwoven mat and manufactured composite. Apparently, the density of hemp fiber is higher than flax. Also, the recorded density value of Stypol resin in this study is lesser than previously reported density value (1.3 gm/cm^3) of stypol resin investigated by Fahimian (2013) which is believed to be due to different formulation of polyester and styrene unit while manufacturing.

Table 4.3 Density of reinforcing fibers and Stypol resin.

Content	Density (gm/cm^3)	S.D (N = 3)
100% Flax	1.49	0.004
100% Hemp	1.57	0.003
Stypol 8086	1.16	0.001

4.6 FLAX FIBER REINFORCED COMPOSITE PROPERTIES

4.6.1 Effect of consolidation pressure during composite manufacturing on structure of composite

I. Composite thickness

The consolidation pressure used in VARTM and compression molding had significant influence on the final part thickness and fiber volume fraction of composites manufactured using various flax mats. The measured thickness of cured plates is plotted as a function of molding pressures in Figure 4.13. The increase in consolidation, indicated by the decrease in

thickness, is highest when the pressure was increased from 101 kPa to 260 kPa and the increase was relatively gradual when the pressure was increased to 560 kPa.

Moreover, the consolidation level in cured composite varied with mat punch density as well. Maximum consolidation was observed for zero punched flax mat composite because of the loosely bound flax fibers in mat and decrease in consolidation observed until punch density increased to 30 punches/cm^2. However, 72-P flax mat composite exhibited higher consolidation than those of 20-P and 30-P composite which is believed to be due to higher starting areal density and shorter needle depth. The consolidation in 20-P and 30-P composites were found similar.

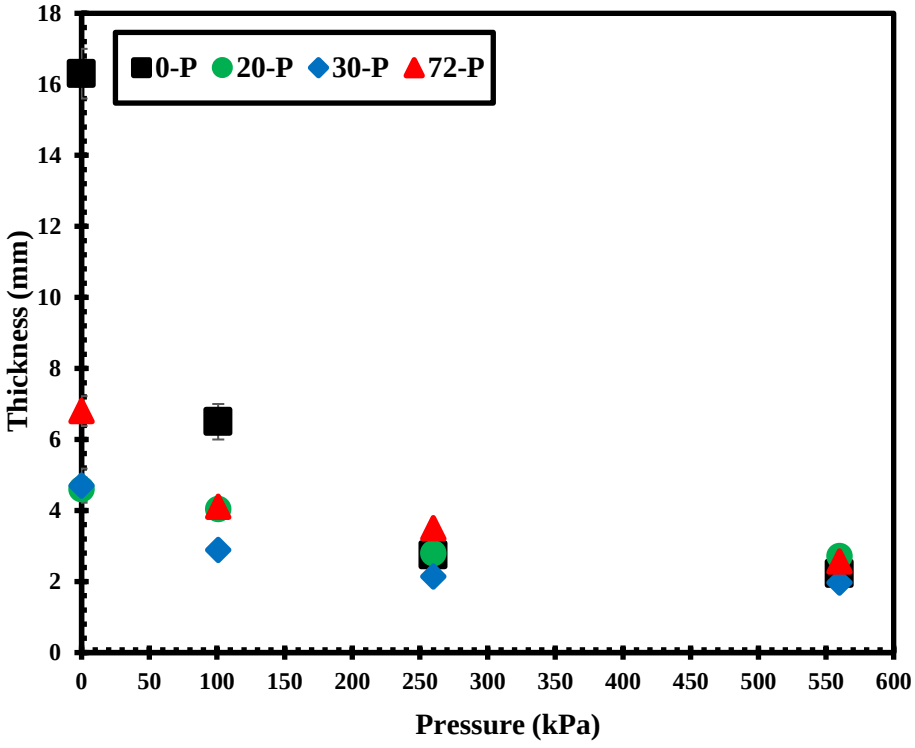

Figure 4.13 Effect of consolidation pressure on composite thickness for various flax mats.

II. Density and fiber volume fraction

The density results of flax mat composite manufactured at different molding pressures are tabulated in Table 4.4 along with their corresponding fiber volume fraction % values. The experimentally measured fiber volume fraction of the flax mat composites is plotted in Figure 4.14 as a function of consolidation pressure. The fiber volume fraction value at zero pressure here corresponds to Vf in zero punched dry mats before resin infiltration.

V_f of composite depends on the composite density, which in turn depends on the level of consolidation. Hence, V_f % also varied significantly with punch density and pressure. The fiber volume fraction increased with consolidation pressure. The rate of increase was higher until 260 kPa compared to the increase when the pressure was increased from 260 to 560 kPa. This is to be expected since the pressure required to compress the fiber bed would increase as the compaction increases. Due to relatively loose binding of fibers in 0-P and 72-P flax mats, the increase in fiber volume fraction from 0 to 560 kPa is linear and it is more than that with 20-P and 30-P flax composites. For 20-P and 30-P flax composites, maximum V_f is recorded at 260 kPa and after which didn't compress the mat further when pressure increased to 560 kPa resulting in no increase or decrease in V_f % 20-P and 30-P composites. At any consolidation pressure, the fiber volume fraction differed with punch density due to differences in starting fiber volume fraction percentage in the mat and in the consolidation behavior during manufacturing.

Table 4.4 Density and fiber volume fraction percentage of flax composite at different punch density and manufacturing pressure.

Mat content	Punch density (p/cm^2)	Consolidation pressure (kPa)	Density (gm/cm^3) (SD)*	Fiber volume fraction, V_f %
100% Flax	0	101	1.19 (0.004)	11.2
100% Flax	0	260	1.25 (0.005)	26.9
100% Flax	0	560	1.27 (0.005)	32.6
100% Flax	20	101	1.18 (0.005)	15.6
100% Flax	20	260	1.25 (0.004)	25.8
100% Flax	20	560	1.23 (0.004)	22.5
100% Flax	30	101	1.23 (0.004)	20.9
100% Flax	30	260	1.24 (0.002)	25
100% Flax	30	560	1.24 (0.004)	23.6
100% Flax	72	101	1.22 (0.006)	18.1
100% Flax	72	260	1.24 (0.004)	24.7
100% Flax	72	560	1.26 (0.001)	31.5

(SD)* - Standard deviation, N = 5

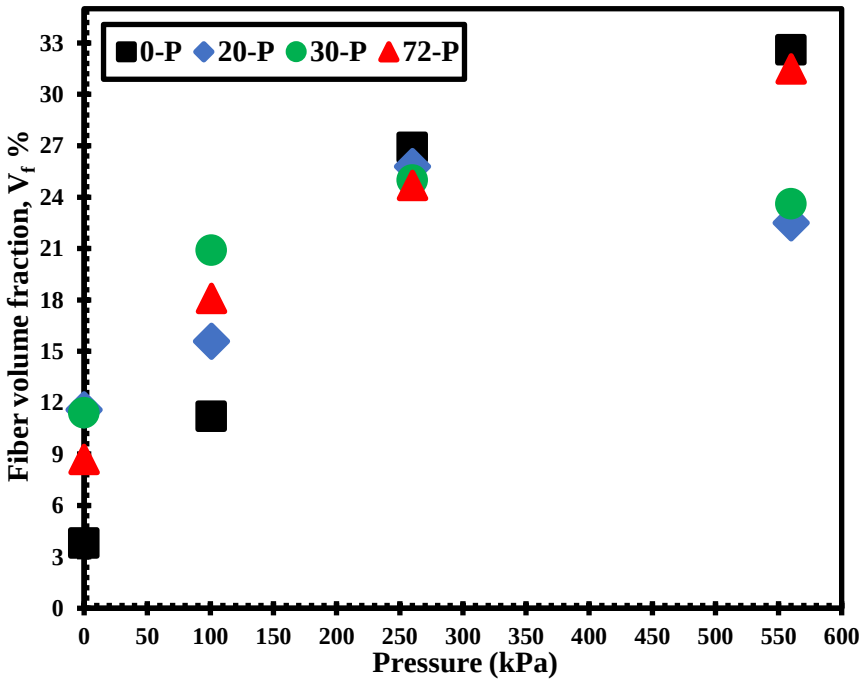

Figure 4.14 Effect of consolidation pressure on fiber volume fraction of flax mat composite.

4.6.2 Mechanical properties of flax fiber reinforced composite

The tensile stress-strain plots for flax fiber composites manufactured under three different pressures are plotted along with that for Stypol resin in Figure 4.15, 4.16, and 4.17.

Based on these plots, it can be stated that the flax fiber reinforces the unsaturated polyester resin (Stypol 8086) significantly. However, for a given manufacturing pressure the level of reinforcement changes with the change in needle punching density and needle depth of nonwoven flax mat as indicated by the lack of superposition among stress-strain curves for various punch densities. The tensile modulus of manufactured composite was calculated from the slope of the initial linear portion (in the strain range of 0.1%) of the stress-strain curve as indicated in Figure 4.15.

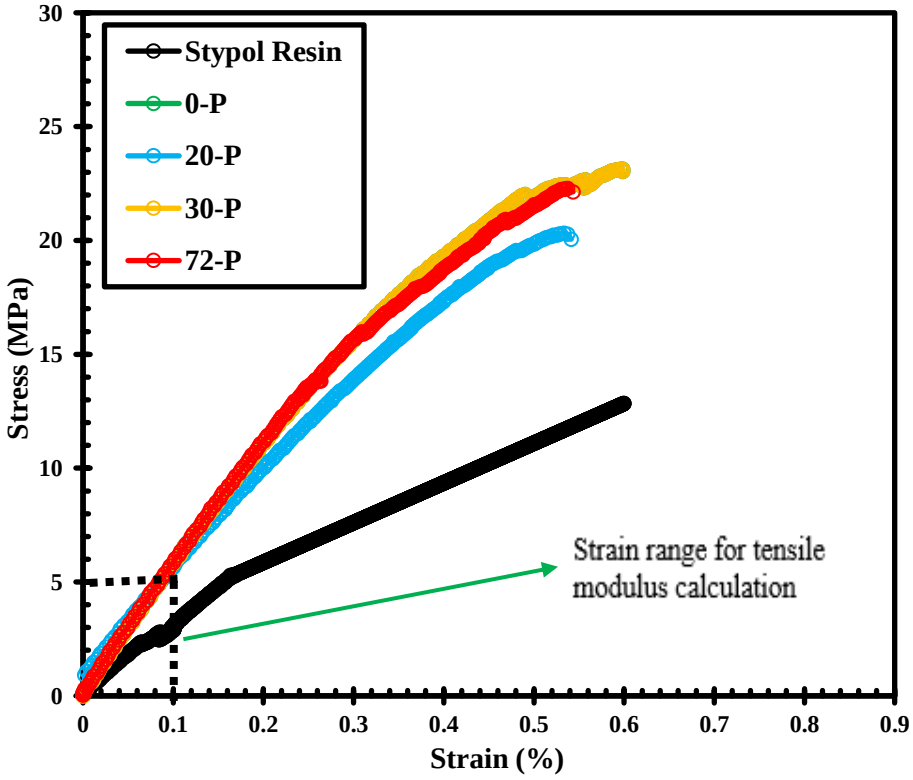

Figure 4.15 Stress-strain curve of flax composite manufactured at 101 kPa for different punch density.

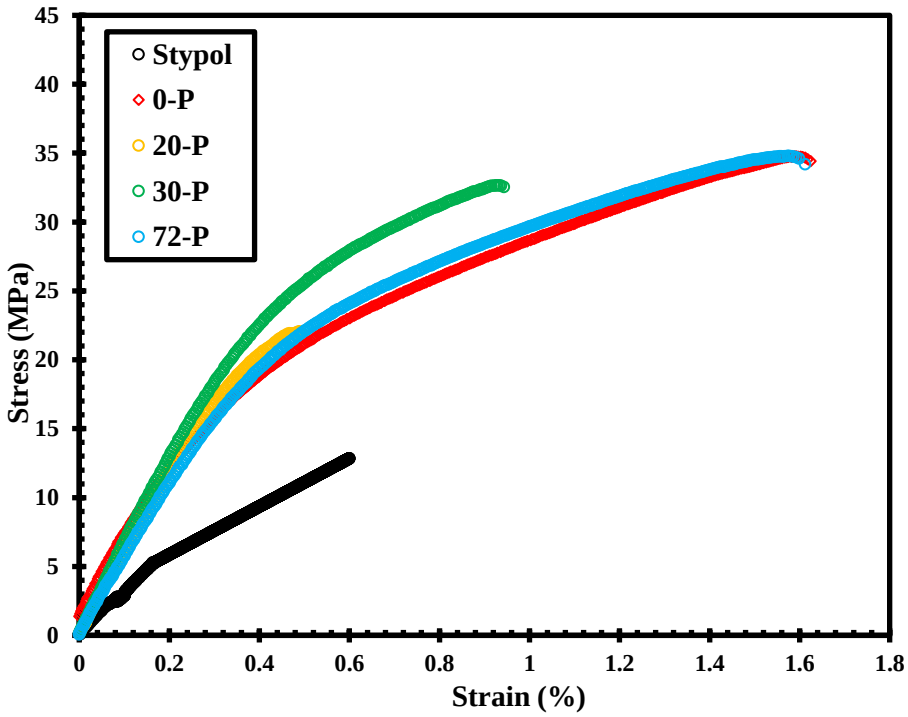

Figure 4.16 Stress-strain curve of flax composite manufactured at 260 kPa for different punch density.

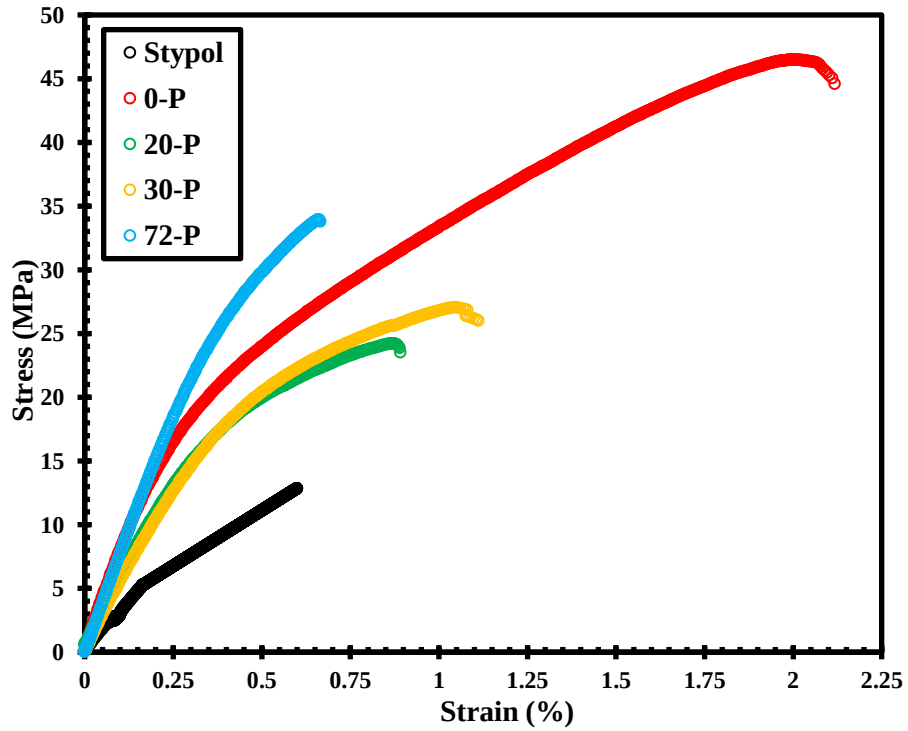

Figure 4.17 Stress-strain curve of flax composite manufactured at 560 kPa for different punch density.

The mechanical properties of flax fiber reinforced composite, obtained from these plots, are tabulated in Table 4.5.

Table 4.5 Mechanical properties of flax fiber reinforced composite.

Mat content	Needle Punch density (p/cm^2)	Consolidation pressure (kPa)	Longitudinal modulus (GPa) (SD)*	Tensile strength (MPa)	Strain at break (%)
100% Flax	0	101	4.6 (0.3)	18.6 (2.8)	0.6 (0.04)
100% Flax	0	260	6 (0.3)	40.4 (3.3)	2.1 (0.3)
100% Flax	0	560	7.1 (0.5)	42.5 (2.6)	1.9 (0.2)
100% Flax	20	101	4.9 (0.2)	23.2 (2.3)	0.6 (0.1)
100% Flax	20	260	6.1 (0.8)	27.4 (2.8)	0.5 (0.03)
100% Flax	20	560	5.6 (0.5)	26.2 (2.7)	0.9 (0.2)
100% Flax	30	101	5.9 (0.5)	22.7 (0.8)	0.6 (0.04)
100% Flax	30	260	6.9 (0.5)	33.8 (3.0)	1.1 (0.2)
100% Flax	30	560	6 (0.4)	26.2 (2.8)	0.9 (0.2)
100% Flax	72	101	5.9 (0.3)	23.9 (1.1)	0.5 (0.2)
100% Flax	72	260	6.2 (0.2)	33.3 (0.8)	1.4 (0.1)
100% Flax	72	560	8 (0.7)	41.4 (2.7)	1.0 (0.2)

(SD)* - Standard deviation, N = 5

4.7 EFFECT OF PUNCH DENSITY AND MANUFACTURING PRESSURE ON MECHANICAL PROPERTIES OF FLAX MAT COMPOSITE

In order to understand the effect of punch density and manufacturing pressure on the mechanical properties of flax mat composite, tensile modulus is plotted as a function of punch density in Figure 4.18 and as a function of manufacturing pressure in Figure 4.19. Similarly, tensile strength is plotted as a function of punch density in Figure 4.20 and as a function of manufacturing pressure in Figure 4.21. From these figures, it appears that it is difficult to

interpret the trend since the V_f changes with both punch density and consolidation pressure. So, in order to interpret the data, tensile modulus and tensile strength are plotted as a function of V_f and presented in section 4.7.1 and 4.7.2.

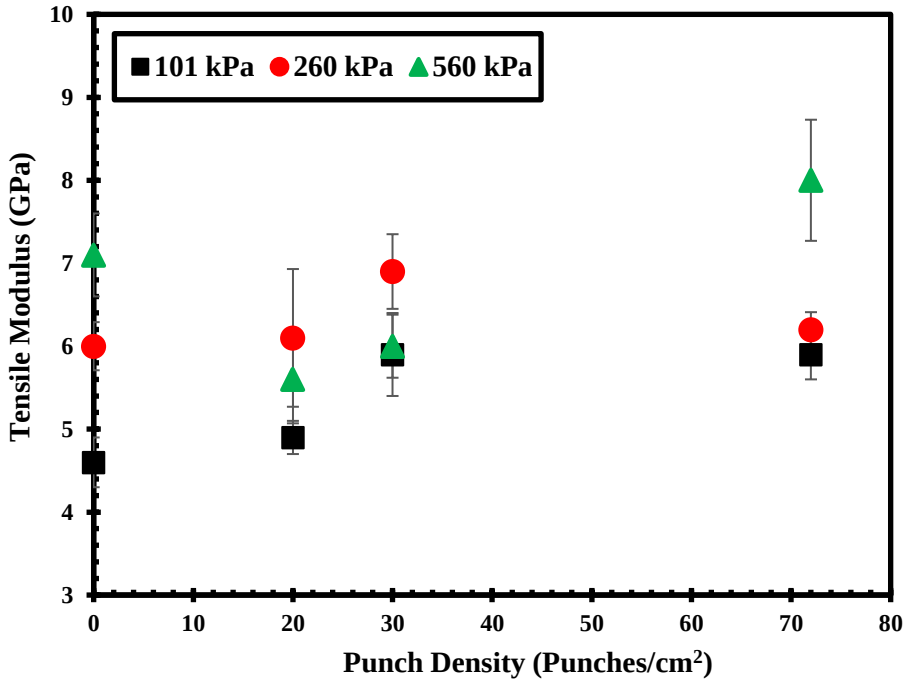

Figure 4.18 Variation in tensile modulus with change in punch density of flax mat composite at different pressures.

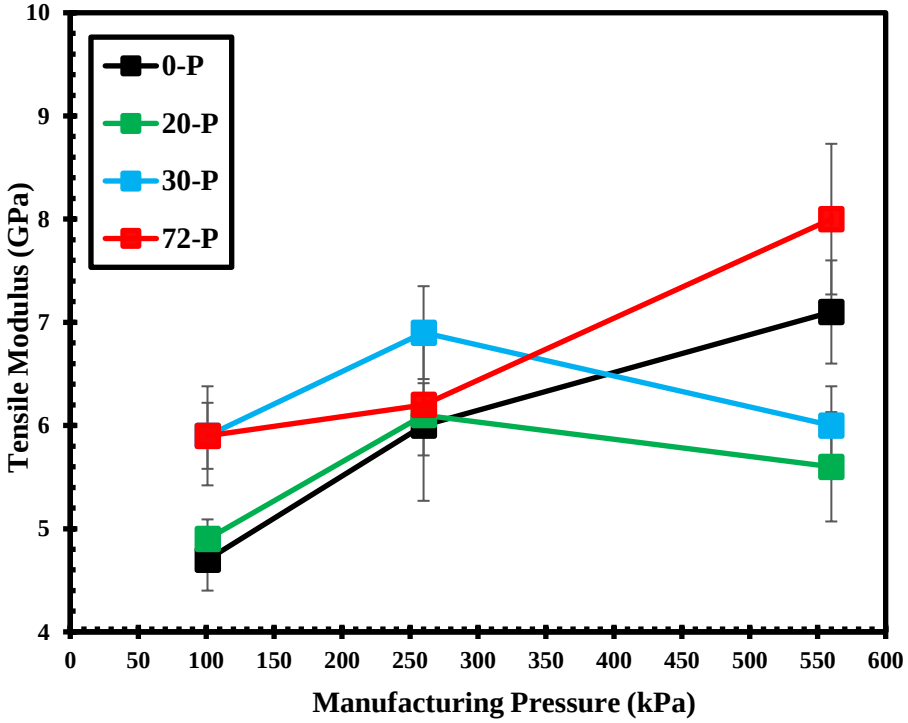

Figure 4.19 Variation in tensile modulus with change in manufacturing pressure for various punch density flax composite.

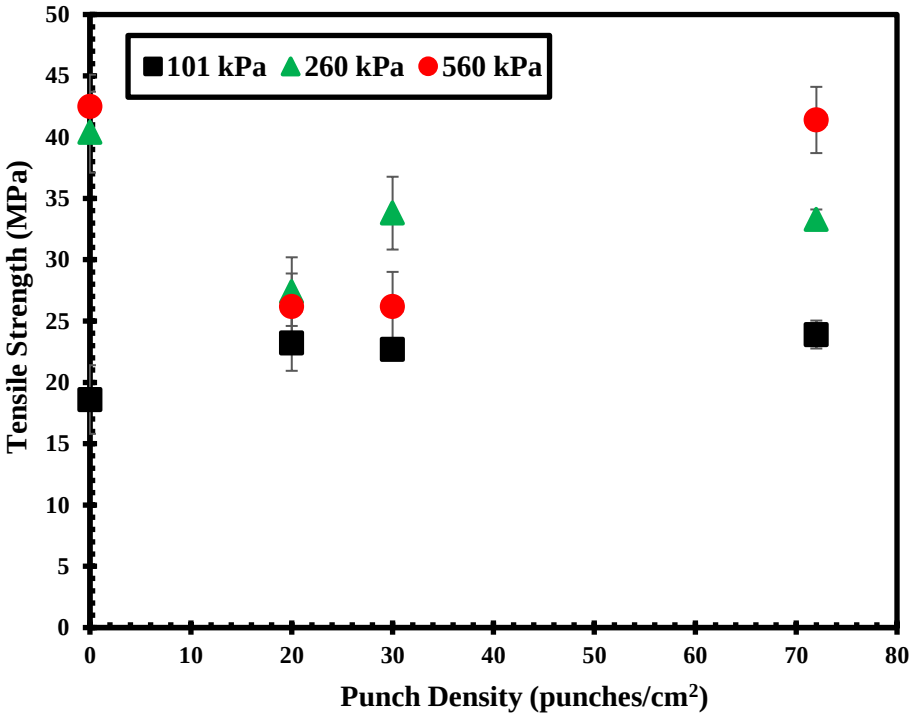

Figure 4.20 Variation in tensile strength with change in punch density of flax mat composite at different pressures.

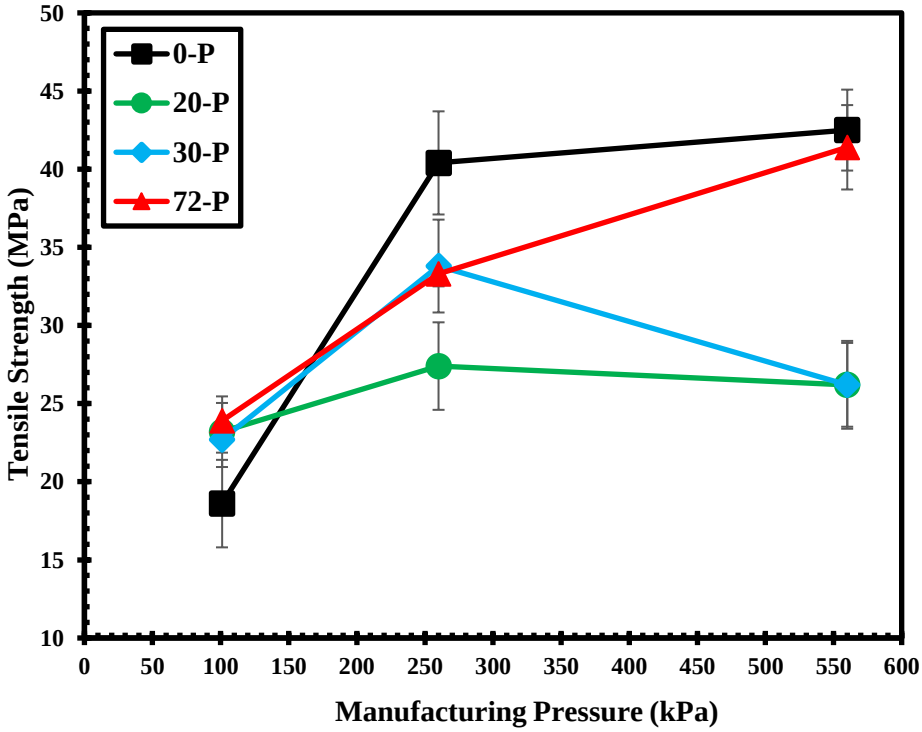

Figure 4.21 Variation in tensile strength with change in manufacturing pressure for various punch density flax composite.

4.7.1 Tensile modulus

Since V_f varies with punch density, the experimental tensile modulus is plotted in Figure 4.22, 4.23, 4.24, and 4.25 as a function of measured fiber volume fraction of flax composite. The data for tested each sample instead of plotting the average value for each pressure since the V_f varied from sample to sample. As discussed in section 4.6.1 (Table 4.4), the V_f increased monotonically with increase in pressure for 0-P and 72-P flax composite as shown in Figure 4.26; however, for 20-P and 30-P, V_f increased until the 260 kPa pressure and decreased when the consolidation pressure further increased from 260 to 560 kPa. The tensile modulus of flax composite followed the observed trend in V_f. For each consolidation pressure, the modulus of tested samples for a given punch density increased with V_f, as expected. The variation in modulus and V_f for samples manufactured and tested from the same manufactured plate, attests to inhomogeneity in fiber distribution within the non-woven mat.

These results demonstrate that the V_f in the composite, which dictates the modulus, is a function of consolidation behavior during manufacturing and the latter is a function of punch density and pressure. The trend in the presented results is complicated by the variation in the areal weight of the mat as well as heterogeneity in fiber distribution. However, for a given areal density, increasing the punch density and the manufacturing pressure results in increase in modulus.

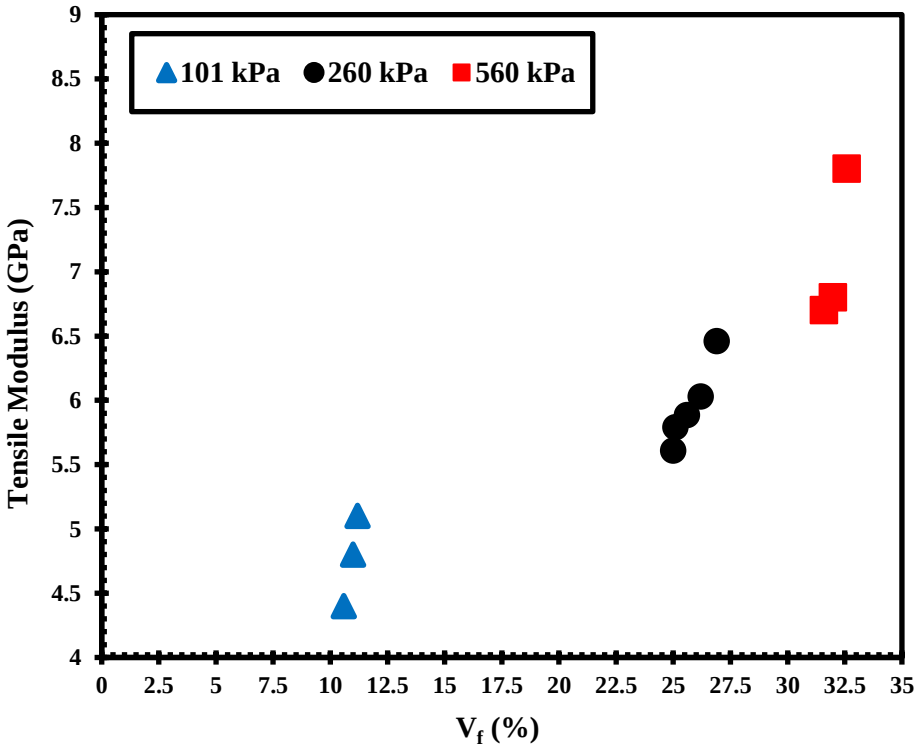

Figure 4.22 Experimental tensile modulus of 0-P flax composite.

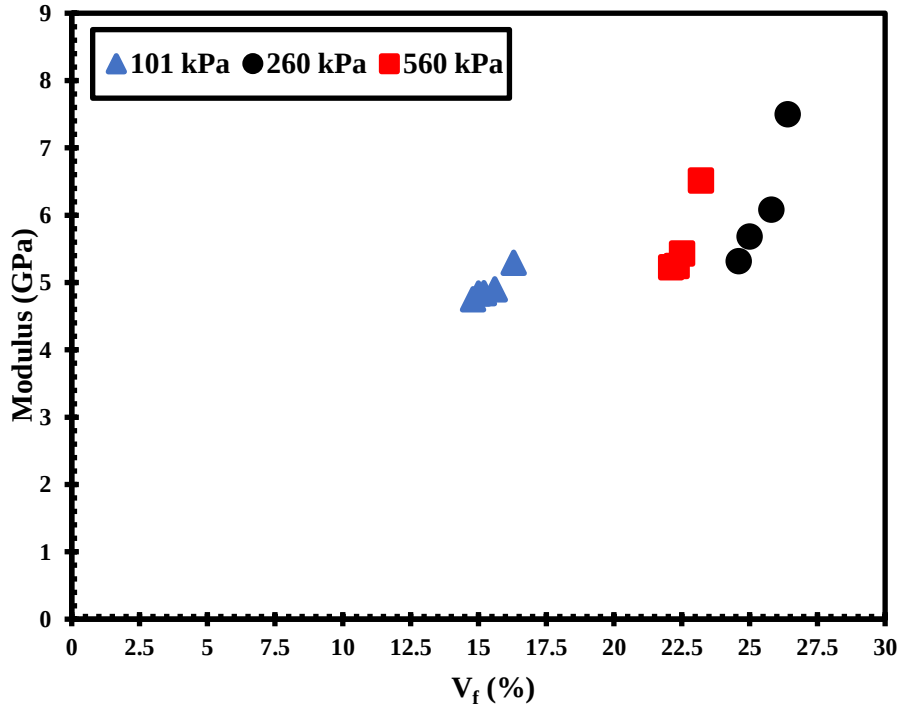

Figure 4.23 Experimental tensile modulus of 20-P flax composite.

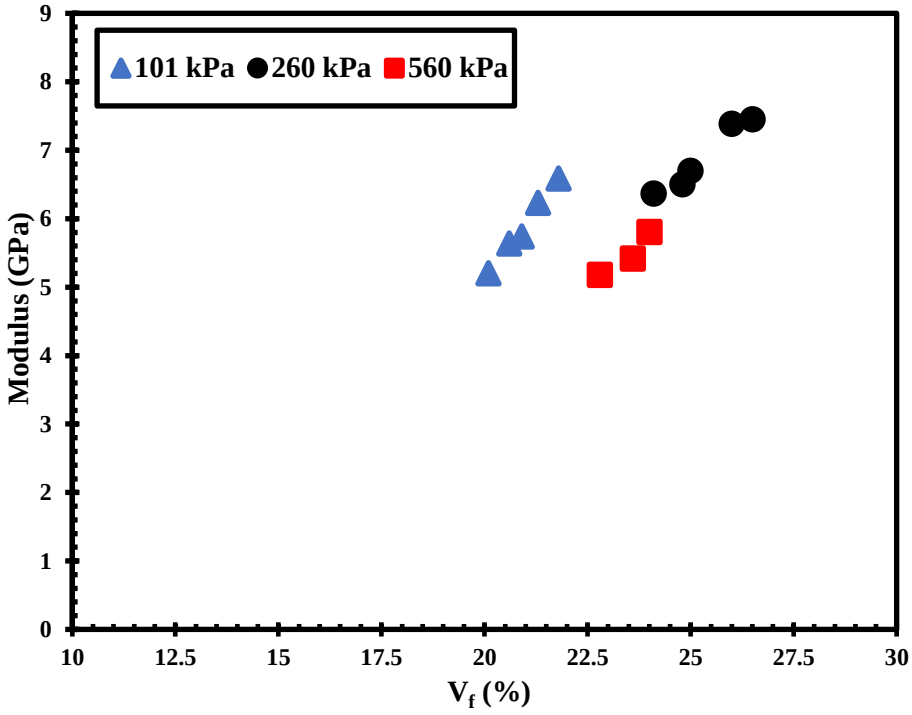

Figure 4.24 Experimental tensile modulus of 30-P flax composite.

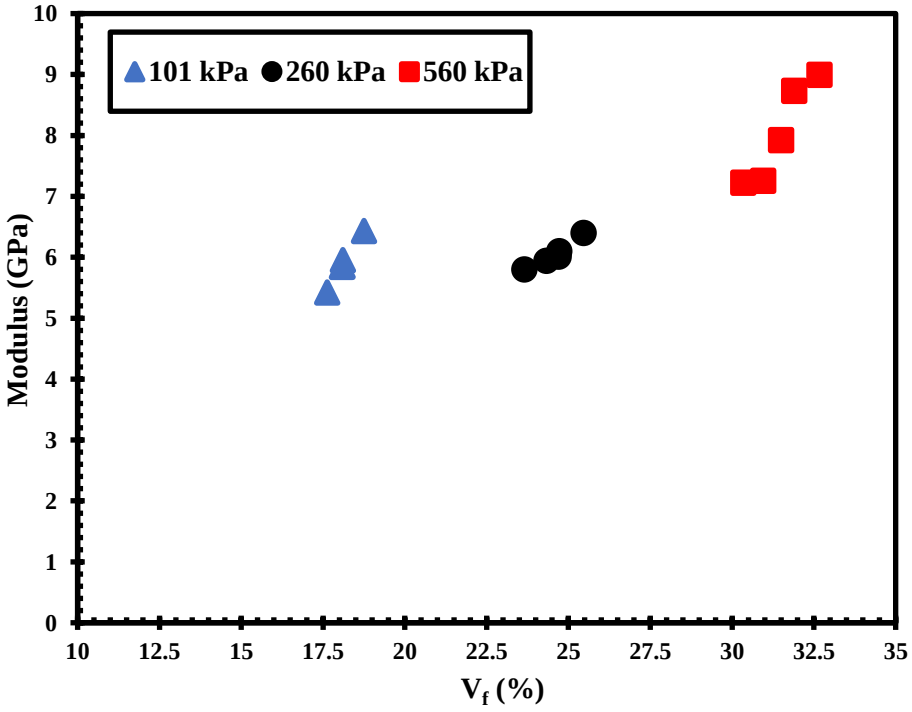

Figure 4.25 Experimental tensile modulus of 72-P flax composite.

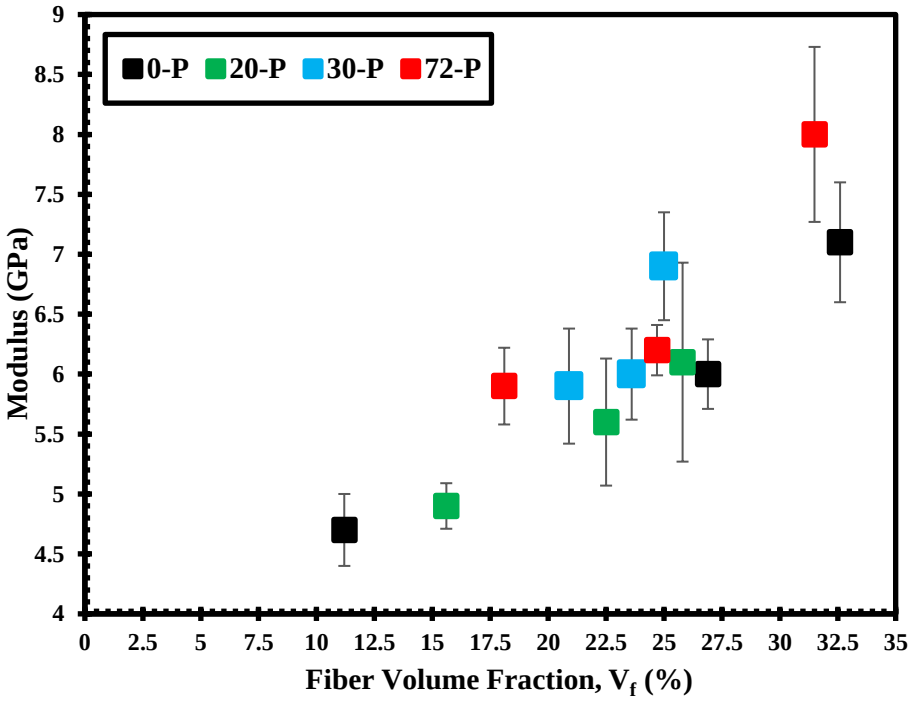

Figure 4.26 Relationship between tensile modulus and fiber volume fraction of flax mat composite at different punch density.

4.7.2 Tensile strength

The experimental tensile strength for each punch density and pressure is plotted in Figure 4.27, 4.28, 4.29, and 4.30 as a function of measured V_f of flax composite. The data for tested each sample are plotted here since the V_f varied from sample to sample for each punch density and pressure.

The trend in the effect of punch density and consolidation pressure on tensile strength are similar to that observed for the tensile modulus of flax composite. The tensile strength of tested samples varied by the following trend of V_f for each consolidation pressure and punch density. The 0-P flax mat composite showed lowest and highest tensile strength at VARTM and 560 kPa pressure, respectively as shown in Figure 4.31; since 0-P composite achieved minimum consolidation at VARTM pressure due to lower V_f of corresponding mat used while manufacturing and achieved maximum consolidation at higher pressure (560 kPa) due to loosely bound fibers in mat. Tested samples of 72-P flax mat composite exhibited a nearly

linear relationship between V_f and tensile strength while the manufacturing pressure advances as shown in Figure 4.30. From these results, it can be seen that tensile strength is a function of V_f which is the case for modulus as well, where V_f varied with punch density and pressure caused by the difference in consolidation behavior.

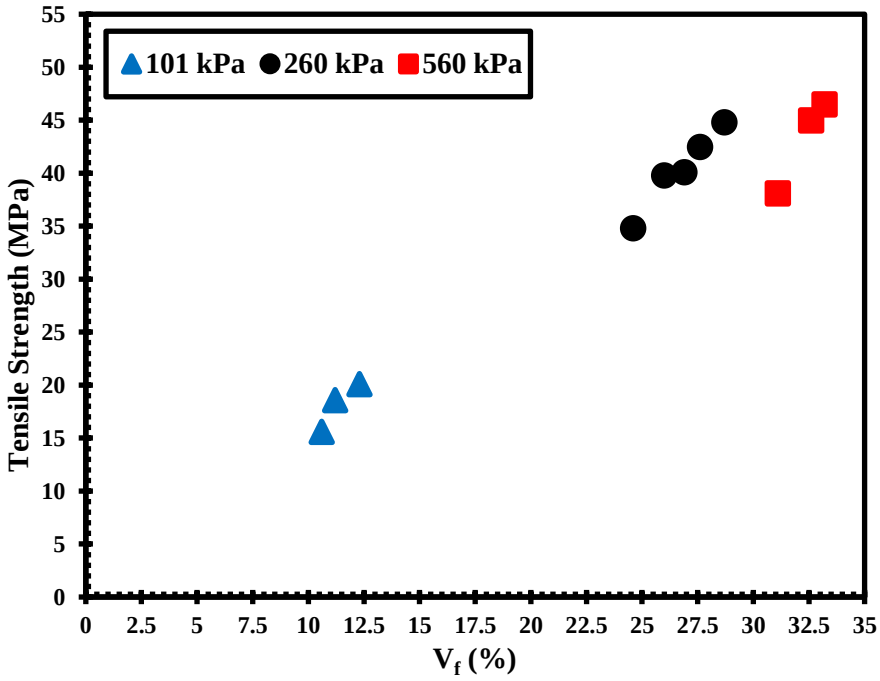

Figure 4.27 Experimental tensile strength of 0-P flax composite.

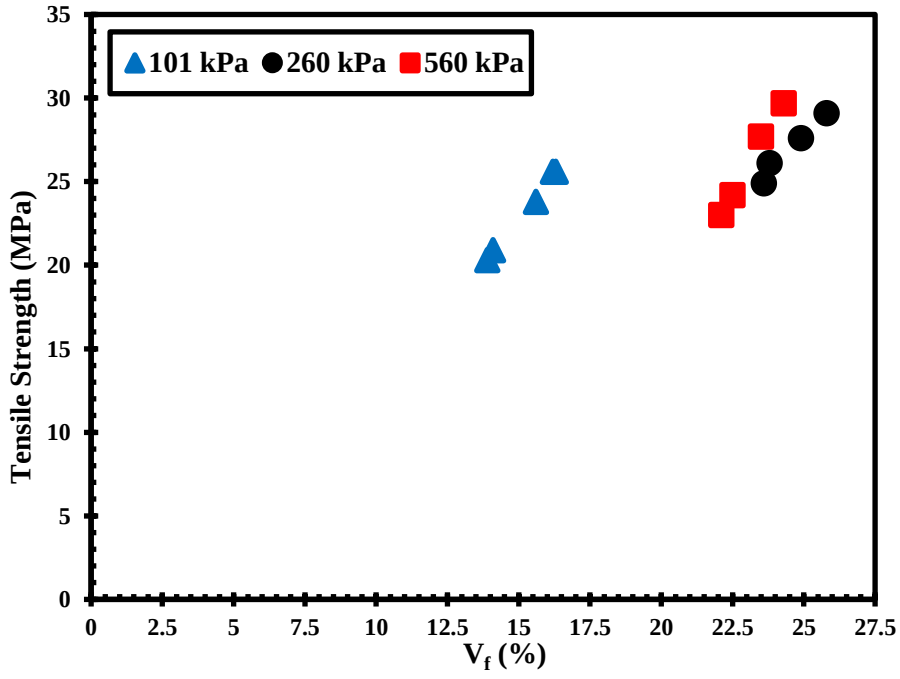

Figure 4.28 Experimental tensile strength of 20-P flax composite.

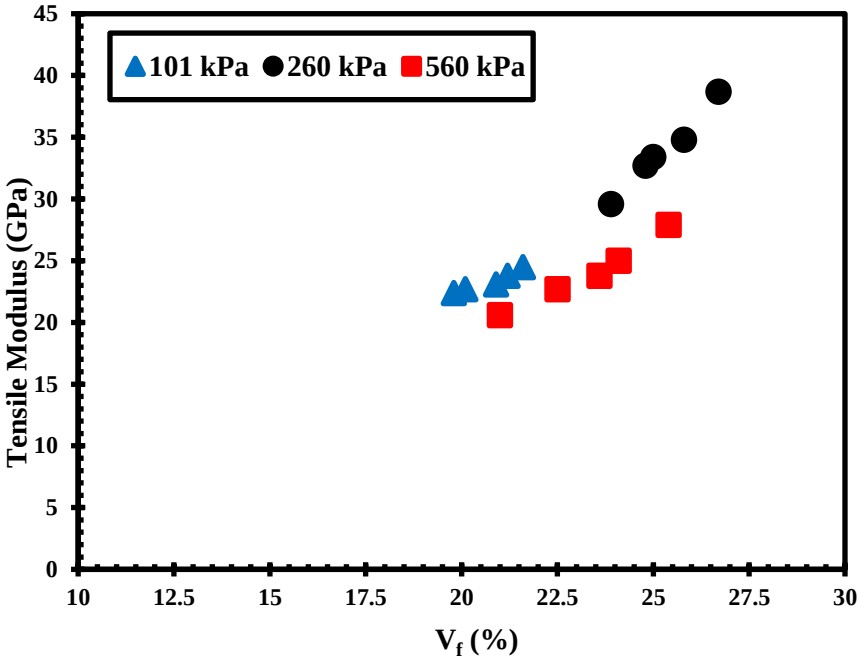

Figure 4.29 Experimental tensile strength of 30-P flax composite.

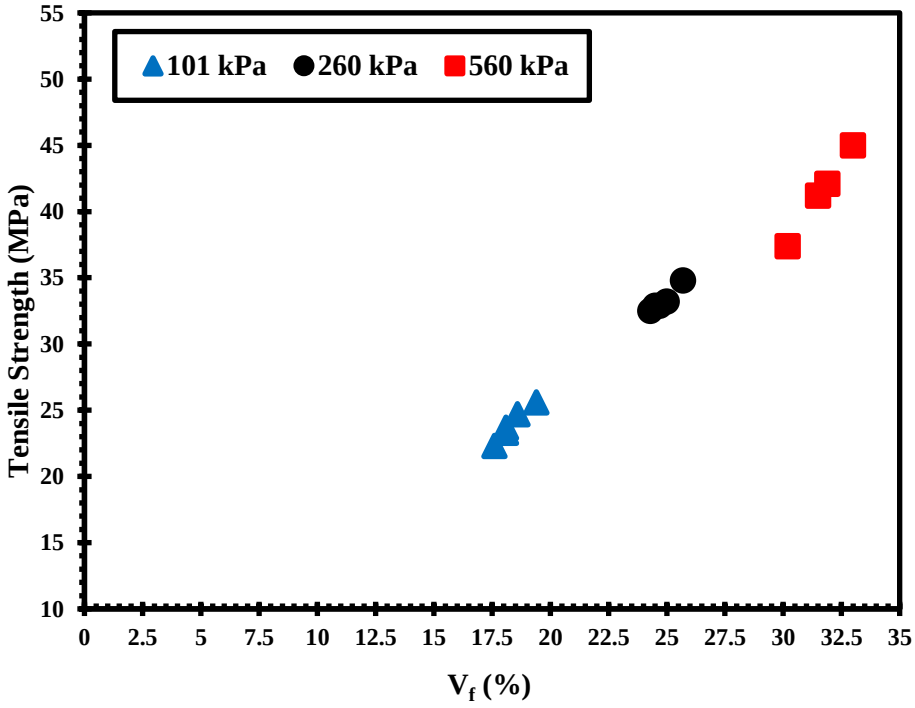

Figure 4.30 Experimental tensile strength of 72-P flax composite.

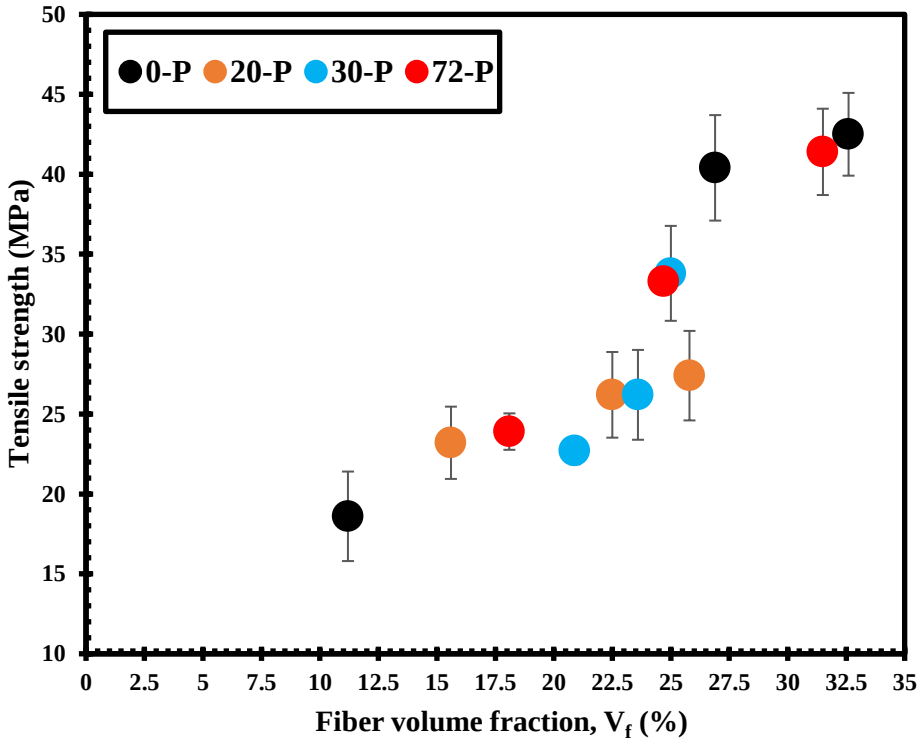

Figure 4.31 Relationship between tensile strength and fiber volume fraction of flax mat composite at different punch density.

4.8 IMAGE ANALYSIS OF FLAX COMPOSITE

Microscopic images of flax composite captured using VHX Digital Microscope at different punch density for a given pressure (560 kPa) are provided in Appendix (Figure B.1, B.2, B.3, and B.4). These images show a thin coat of resin at the top which exhibits a large variation in the diameter of flax fibers within a punch density or different. Also, these images are showing that more fibers are in-plane which increasingly orient perpendicular to plane of the image with increase in punch density. Also, the length of the fibers is reduced as the punch density is increased. The reduction in fiber length with increase in punch density as revealed in composite image analysis resulted in comparatively shorter fibers in 72-P flax mat which is one of the reasons of higher consolidation in 72-P composite than 20-P and 30-P flax composite as discussed in section 4.6.1.

4.9 STATISTICAL ANALYSIS

A two way ANOVA was performed to determine the significance of variation in tensile strength and tensile modulus of flax composite, manufactured using different punch density mats and pressure, with fiber volume fraction (V_f). The test of significance for two way ANOVA was carried out in SAS® University Edition software using Tukey's LS (Least Squares) means comparison. In this analysis, the tensile strength and tensile modulus were considered as dependent variables and V_f of flax composite was considered as independent variables. For pairwise comparison of the tensile strength or tensile modulus means, Tukey-Kramer GLM procedure (LS-means) was followed at $\alpha = 0.05$.

4.9.1 Tensile strength

The summary of two way ANOVA for variation of tensile strength of flax composite with V_f is tabulated in Table 4.6. From Table 4.6, F value is equal to 33.51 and P value is less than 0.001 (<0.05). So, the results of two way ANOVA for tensile strength of flax composite reject the null hypothesis and the variances are unequal which indicates that the effect of different V_f or fiber content % on tensile strength is significant. The interactions among all possible pairs of tensile strength means for different V_f is investigated and listed in Table 4.7 where $V_f = 11.2$ stands for 1, $V_f = 15.6$ for 2, $V_f = 18.1$ for 3, $V_f = 20.9$ for 4, $V_f = 22.5$ for 5, $V_f = 23.6$ for 6, $V_f = 24.7$ for 7, $V_f = 25$ for 8, $V_f = 25.8$ for 9, $V_f = 26.9$ for 10, $V_f = 31.5$ for 11, $V_f = 32.6$ for 12 in this table. The numerical values listed in Table 4.7 indicates the P value of corresponding pairs, respectively. For a given pair in Table 4.7, $P < 0.05$ indicates the tensile strength means are Significant, $P < 0.001$ indicates they are highly Significant, and $P > 0.05$ indicates they are not Significant. It appears that tensile strength means are significant or highly significant for higher V_f % of flax fiber composite or when V_f is 26.9 (0-P, 260 kPa), 31.5 (72-P, 560 kPa), and 32.6 (0-P, 560 kPa) as seen in Table 4.7.

Table 4.6 Summary of two way ANOVA for tensile strength of flax composite in respect to corresponding V_f.

Source	DF	Sum of Squares	Mean Square	F Value	Pr > F
Model	11	3096.58	281.51	33.51	<.0001[a]
Error	42	352.83	8.40		
Corrected Total	53	3449.42			

[a] P < 0.05 = Significant, P < 0.001 = Highly Significant, P > 0.05 = Not Significant (NS).

Table 4.7 The interactions among all possible pairs of tensile strength means for different V_f of flax composite.

Least Squares Means for effect Sample

Pr > |t| for H0: LSMean(i)=LSMean(j)

Dependent Variable: TS (Tensile Strength)

i/j	1	2	3	4	5	6	7	8	9	10	11	12
1		0.4106	0.2387	0.3934	0.0317	0.2222	<.0001	<.0001	0.1896	<.0001	<.0001	<.0001
2	0.4106		1.0000	1.0000	0.9333	1.0000	0.0001	<.0001	1.0000	<.0001	<.0001	<.0001
3	0.2387	1.0000		1.0000	0.9903	1.0000	0.0004	0.0002	1.0000	<.0001	<.0001	<.0001
4	0.3934	1.0000	1.0000		0.9417	1.0000	0.0001	<.0001	1.0000	<.0001	<.0001	<.0001
5	0.0317	0.9333	0.9903	0.9417		0.9928	0.0300	0.0134	0.9994	<.0001	<.0001	<.0001
6	0.2222	1.0000	1.0000	1.0000	0.9928		0.0005	0.0002	1.0000	<.0001	<.0001	<.0001
7	<.0001	0.0001	0.0004	0.0001	0.0300	0.0005		1.0000	0.0025	0.0158	0.0320	0.0015
8	<.0001	<.0001	0.0002	<.0001	0.0134	0.0002	1.0000		0.0010	0.0368	0.0706	0.0035
9	0.1896	1.0000	1.0000	1.0000	0.9994	1.0000	0.0025	0.0010		<.0001	<.0001	<.0001
10	<.0001	<.0001	<.0001	<.0001	<.0001	<.0001	0.0158	0.0368	<.0001		1.0000	0.9712
11	<.0001	<.0001	<.0001	<.0001	<.0001	<.0001	0.0320	0.0706	<.0001	1.0000		0.9171
12	<.0001	<.0001	<.0001	<.0001	<.0001	<.0001	0.0015	0.0035	<.0001	0.9712	0.9171	

4.9.2 Tensile modulus

The summary of two way ANOVA for tensile modulus of flax composite in respect to corresponding V_f is tabulated in Table 4.8. From Table 4.8, F value is equal to 12.21 and P value is less than 0.001 (<0.05). Similar to that of tensile strength, the results of two way ANOVA for tensile modulus of flax composite reject the null hypothesis and the variances are

unequal which indicates that the effect of different V_f or fiber content % on tensile modulus is significant. Likewise tensile strength, the interactions among all possible pairs of tensile modulus means for different V_f is investigated and listed in Table 4.9 where V_f = 11.2 stands for 1, V_f = 15.6 for 2, V_f = 18.1 for 3, V_f = 20.9 for 4, V_f = 22.5 for 5, V_f = 23.6 for 6, V_f = 24.7 for 7, V_f = 25 for 8, V_f = 25.8 for 9, V_f = 26.9 for 10, V_f = 31.5 for 11, V_f = 32.6 for 12 in this table. The numerical values listed in Table 4.9 indicates the P value of corresponding pairs, respectively. For a given pair in Table 4.9, $P < 0.05$ indicates the tensile strength means are Significant, $P < 0.001$ indicates they are highly Significant, and $P > 0.05$ indicates they are not Significant. It appears that tensile modulus means are significant or highly significant for higher V_f % of flax fiber composite or when V_f is 31.5 (72-P, 560 kPa) and 32.6 (0-P, 560 kPa) as seen in Table 4.9. However, V_f = 31.5 (72-P, 560 kPa) exhibited significant variations in tensile modulus means with more number of pairs than that of V_f = 32.6 (0-P, 560 kPa).

Table 4.8 Summary of two way ANOVA for tensile modulus of flax composite in respect to corresponding V_f.

Source	DF	Sum of Squares	Mean Square	F Value	Pr > F
Model	11	37.96	3.45	12.21	<.0001[a]
Error	39	11.02	0.28		
Corrected Total	50	48.98			

[a] $P < 0.05$ = Significant, $P < 0.001$ = Highly Significant, $P > 0.05$ = Not Significant (NS).

Table 4.9 The interactions among all possible pairs of tensile modulus means for different V_f of flax composite.

Least Squares Means for effect Sample

Pr > |t| for H0: LSMean(i)=LSMean(j)

Dependent Variable: TM (Tensile Modulus)

i/j	1	2	3	4	5	6	7	8	9	10	11	12
1		1.0000	0.5307	0.5589	0.9225	0.9884	0.8217	0.0035	0.2625	0.4470	<.0001	0.0028
2	1.0000		0.1810	0.2022	0.7452	0.9560	0.5075	<.0001	0.0562	0.1269	<.0001	0.0001
3	0.5307	0.1810		1.0000	0.9995	0.9925	1.0000	0.1711	0.9999	1.0000	<.0001	0.1198
4	0.5589	0.2022	1.0000		0.9997	0.9948	1.0000	0.1525	0.9998	1.0000	<.0001	0.1076
5	0.9225	0.7452	0.9995	0.9997		1.0000	1.0000	0.0382	0.9486	0.9973	<.0001	0.0295
6	0.9884	0.9560	0.9925	0.9948	1.0000		1.0000	0.0327	0.8720	0.9800	<.0001	0.0240
7	0.8217	0.5075	1.0000	1.0000	1.0000	1.0000		0.0416	0.9774	0.9996	<.0001	0.0334
8	0.0035	<.0001	0.1711	0.1525	0.0382	0.0327	0.0416		0.6471	0.2384	0.0600	1.0000
9	0.2625	0.0562	0.9999	0.9998	0.9486	0.8720	0.9774	0.6471		1.0000	0.0003	0.4591
10	0.4470	0.1269	1.0000	1.0000	0.9973	0.9800	0.9996	0.2384	1.0000		<.0001	0.1637
11	<.0001	<.0001	<.0001	<.0001	<.0001	<.0001	<.0001	0.0600	0.0003	<.0001		0.4419
12	0.0028	0.0001	0.1198	0.1076	0.0295	0.0240	0.0334	1.0000	0.4591	0.1637	0.4419	

From the above statistical results, it can be concluded that changes in V_f % resulted in significant variations in tensile strength and modulus within different pairs. Since, V_f changes with both needle punch density and consolidation pressure; therefore, the effect of punch density and consolidation pressure on tensile modulus and tensile strength of flax composite are significant.

4.10 PROPERTIES OF FLAX-HEMP HYBRID MAT COMPOSITE

4.10.1 Composite thickness, density, and fiber volume fraction

The thickness, density, and V_f % of flax-hemp hybrid mat composite at different consolidation pressure are tabulated in Table 4.10. In Table 4.10, thickness at 0 - pressure indicates the nonwoven mat (flax-hemp hybrid) thickness as received before consolidation. As observed in

flax composite (Figure 4.13), similar trend found in flax-hemp mat composite as the decrease in thickness is highest when the pressure was increased from 101 kPa to 260 kPa and the decrease was relatively gradual when the pressure was increased to 560 kPa. However, maximum consolidation for flax-hemp mat composite achieved at 560 kPa, indicated by the lowest thickness value of composite thickness resulting in highest composite density and fiber volume fraction recorded at 560 kPa. Thus, the change in consolidation behavior at different pressure would affect the mechanical properties of manufactured composite as discussed in section 4.7.

Table 4.10 Thickness, density, and fiber volume fraction of flax-hemp hybrid mat composite.

Mat content	Needle Punch density	Consolidation pressure (kPa)	Composite thickness (mm), $(SD)^1$	Density (gm/cm^3), $(SD)^1$	Fiber volume fraction, V_f %, $(SD)^1$
50% Flax - 50% Hemp	0-P	0	[a]13.9 (0.5)	-	[a]4.7 (0.2)
50% Flax - 50% Hemp	0-P	101	5.8 (0.2)	1.20 (0.004)	11.7
50% Flax - 50% Hemp	0-P	260	2.4 (0.07)	1.24 (0.006)	23.5
50% Flax - 50% Hemp	0-P	560	2 (0.05)	1.27 (0.007)	32.1

$(SD)^1$ – Standard deviation, N = 5

[a]Mat (as received) thickness and V_f %

4.10.2 Mechanical properties of flax-hemp hybrid mat composite

Figure 4.32 shows the stress-strain curve of stypol resin and the flax-hemp composites manufactured at 101, 260, and 560 kPa. The level of reinforcement in flax-hemp composite increases with the increase in pressure. Each stress-strain curve of flax-hemp composite was identical as no superposition was observed among the lines at different pressures. Maximum

consolidation achieved and highest tensile strength of flax-hemp composite was recorded (41-50 MPa) at 560 kPa.

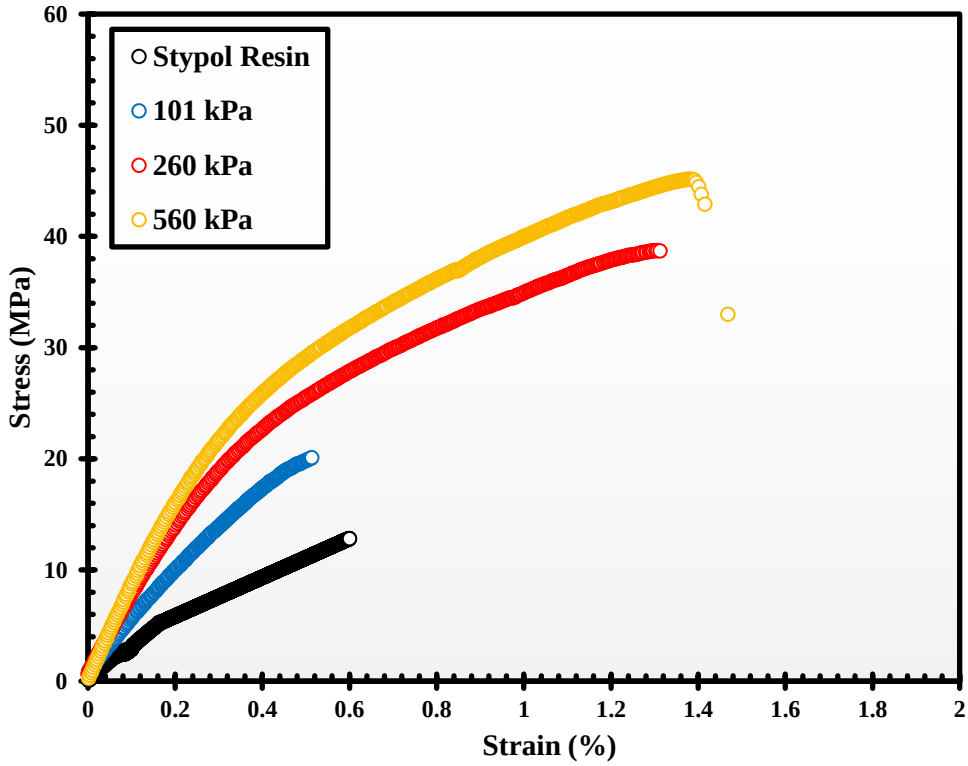

Figure 4.32 Stress-strain curve for stypol resin and 0-P flax-hemp mat composite manufactured at different pressure.

The mechanical properties of 0-P flax-hemp hybrid mat composite, obtained from these plots, are tabulated in Table 4.11.

Table 4.11 Mechanical properties of flax-hemp hybrid mat composite.

Mat content	Needle Punch density	Consolidation pressure (kPa)	Tensile modulus (GPa), (SD)*	Tensile strength (MPa), (SD)*	Strain at break (%), (SD)*
50% Flax - 50% Hemp	0-P	101	4.8 (0.8)	19.2 (2.1)	0.5 (0.1)
50% Flax - 50% Hemp	0-P	260	6.8 (0.3)	39.5 (1.0)	1.5 (0.2)
50% Flax - 50% Hemp	0-P	560	7.8 (0.7)	47.2 (2.0)	1.7 (0.3)

(SD)* - Standard deviation, N = 5

4.10.3 Tensile strength and modulus

The experimental tensile strength and tensile modulus of flax-hemp hybrid mat composite is plotted as a function of measured V_f % in Figure 4.33 and 4.34, respectively. An increase in tensile strength and tensile modulus observed with increase in fiber volume fraction ~~%~~ percentage of manufactured composite. A nearly linear relationship exists both in tensile strength and tensile modulus with V_f %. Also, the change in tensile strength and tensile modulus appears to be nearly linear with change in consolidation pressure as indicated in Figure 4.33 and 4.34, respectively. Hence, the tensile strength and tensile modulus of zero punched flax-hemp hybrid mat composite is found to be a function of both V_f and consolidation pressure.

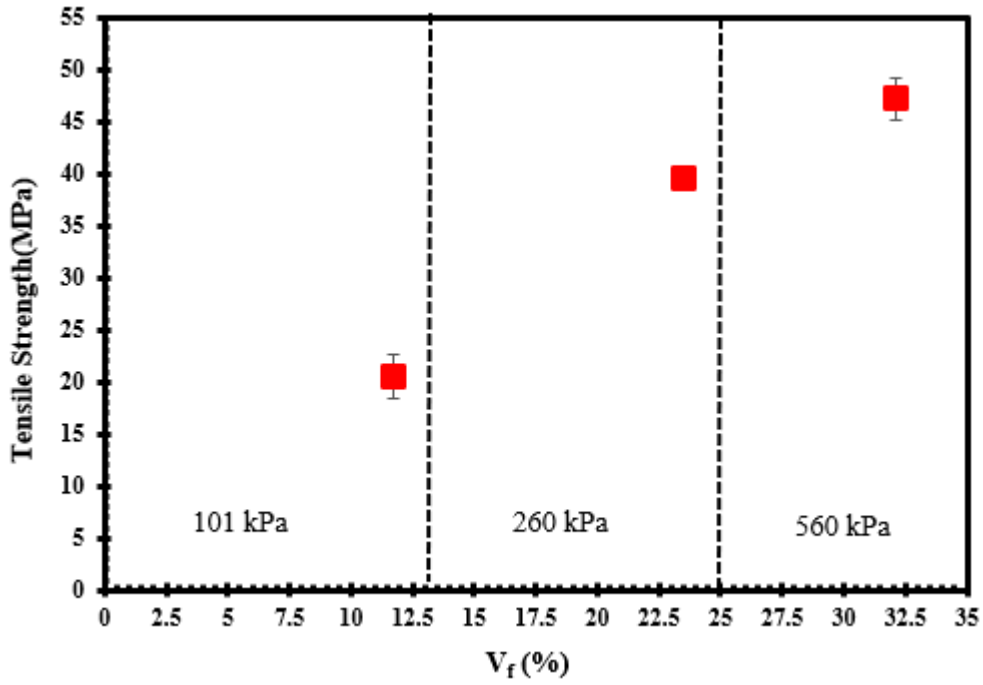

Figure 4.33 Relationship between tensile strength and fiber volume fraction of flax-hemp composite at different pressure.

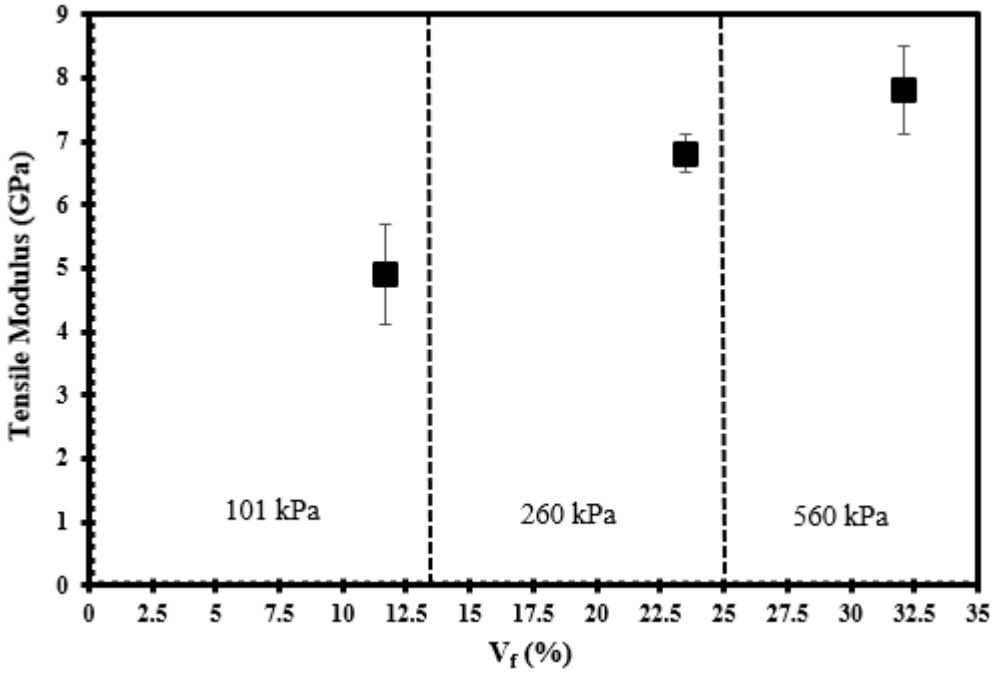

Figure 4.34 Relationship between tensile modulus and fiber volume fraction of flax-hemp composite at different pressure.

4.10.4 Statistical analysis

A statistical test was carried out to measure the significant difference of the tensile strength and tensile modulus in terms of fiber volume fraction of flax-hemp mat composite. Two tailed t-test was conducted to compare the values of tensile strength and tensile of composite in terms of fiber volume fraction measured at different consolidation pressure. T-test result for tensile strength and tensile modulus of flax-hemp composite is summarized in Table 4.12. As seen from the P-values among different groups containing different V_f % in Table 4.10, they all seem to be statistically significant due to lower P-values (<0.05) at all cases which indicates change in V_f % and change in consolidation pressure has changed the mechanical properties of composite significantly.

Table 4.12 T-test results for tensile strength and tensile modulus of flax-hemp composite.

V_f % of composite		Tensile strength			Tensile Modulus		
Group-1	Group-2	P - value	t_{stat}	Result	P - value	t_{stat}	Result
11.7	23.5	< 0.0001	19.5	Extremely statistically significant	0.0008	5.2	Very statistically significant
11.7	32.1	< 0.0001	21.6	Extremely statistically significant	0.0002	6.3	Extremely statistically significant
23.5	32.1	< 0.0001	7.7	Extremely statistically significant	0.0188	2.9	Statistically significant

CHAPTER V

CATTAIL : FIBER AND COMPOSITE CHARACTERIZATIONS – RESULTS AND DISCUSSION

5.1 YIELD PERCENTAGE OF CATTAIL FIBER

Yield percentage of cattail fiber was recorded for different extraction processes. However, as mentioned in section 3.2.2, 90^{o}C temperature and 4 hrs time was considered as optimum condition for cattail fiber yield (%), which is presented in this chapter. Cattail fiber yield % extracted using optimum condition varied at different days or extraction number ranging from 18-30% as shown in Figure 5.1. This fibre yield (%) is less than the previously reported cattail fibre yield by Hasan (2019), which is due to the use of green plant for the current study, whereas Hasan (2019) used dried plants.

Extraction 1-5 and extraction 18 exhibited higher fiber yield % than that of other extractions as shown in Figure 5.1. A test of significance was carried out in SAS using Tukey's mean comparison. Day to day fiber yield % values were fitted in Tukey's mean comparison chart to understand the significant difference. The Figure 5.2 shows the Tukey's LS means test of significance. The vertical bar of same color represents fiber yield % having no significant difference. Different color bars represent that there are slight differences in the values of the fiber yield % at different extraction stages; however, the changes are not statistically significant. Extraction number 3 in both Figure 5.1 and Figure 5.2 showed the highest yield value which is significantly higher than the other extraction processes. There are no significant changes observed in extraction trial 12,13,16,6,11. Though Extraction trial 8, 10, 9, 7, 17, 14, 15, 18 showed a slight deviation in mean value but the changes were not found to be statistically significant.

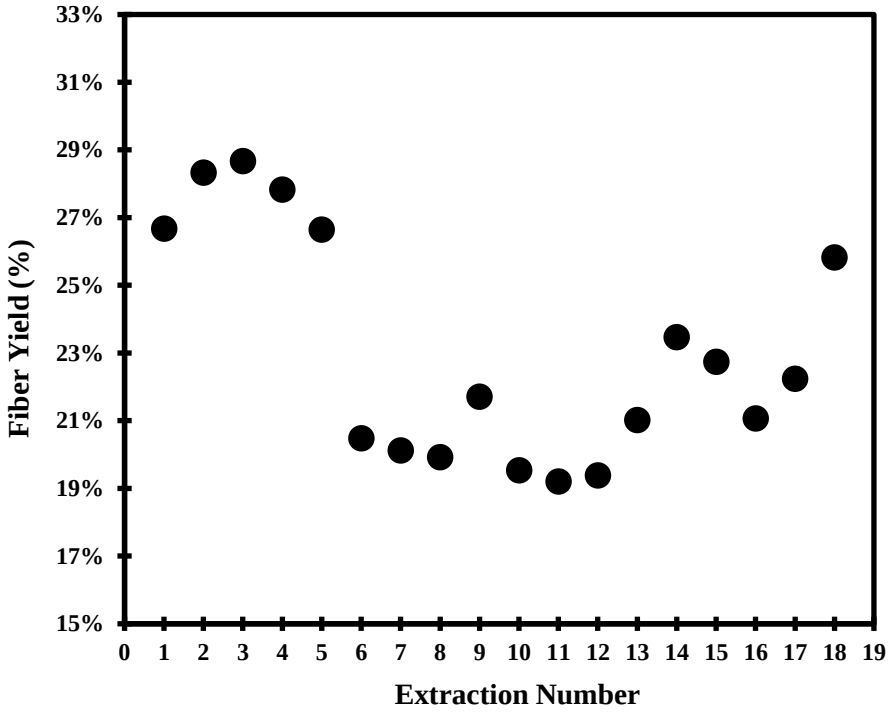

Figure 5.1 Yield % of cattail fiber at different stage of extraction.

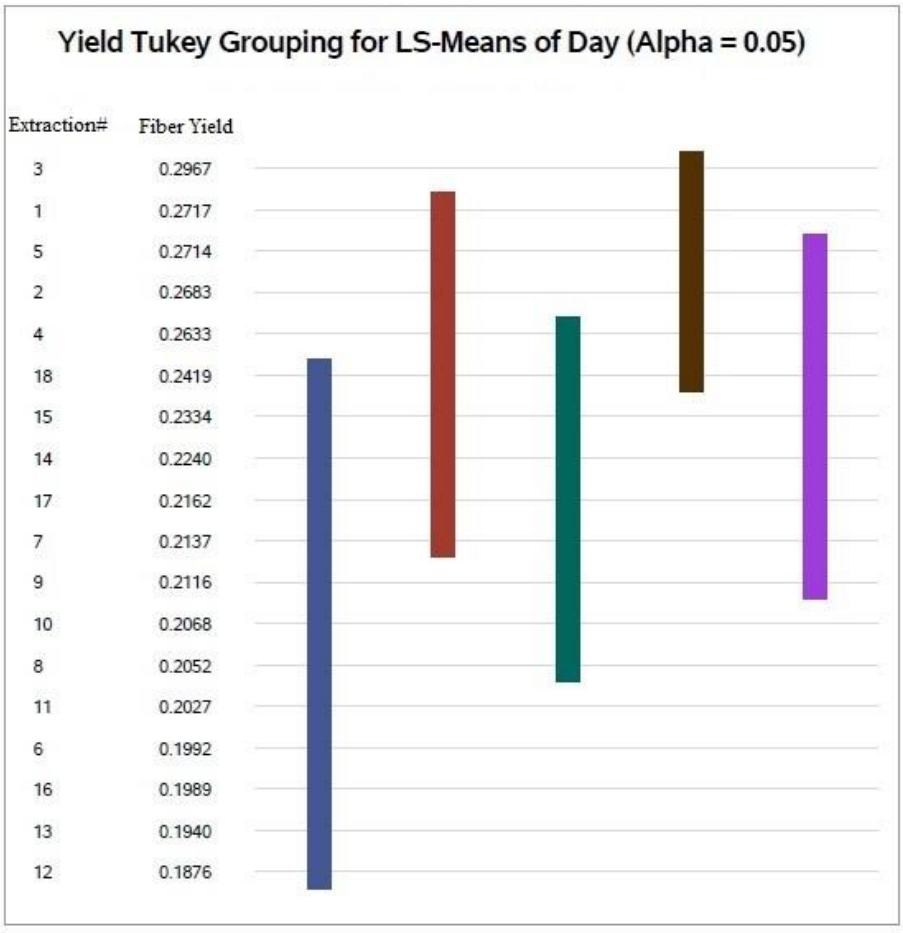

Figure 5.2 Analysis of yield of cattail fiber using Tukey chart.

5.2 PHYSICAL PROPERTIES OF CATTAIL FIBER

The length of the extracted cattail fiber varied between 4 to 10 cm while the diameter varied between 13 to 53 μm. The measured value of fiber length and diameter were used to determine the normal frequency distribution histogram. The frequency distribution was plotted as a function of fiber length and fiber diameter as shown in Figures 5.3 and 5.4, respectively. Length and diameter of cattail fiber were normally distributed. A normal curve was fitted through the experimental data points using *Analyse-it* software in the distribution of both length and diameter.

The average fiber length and diameter of a normal frequency distribution model were calculated using Eq. (5.1) and (5.2) respectively, where n_f is the frequency of fibers for a given fiber length and diameter. The calculated average fiber length of cattail fiber using normal frequency distribution is 6.98 cm and average fiber diameter is 32.1 μm. These values are close to the mean fiber length (6.83 cm) and mean fiber diameter (30.6 μm) values of experimental results.

$$\bar{L} = \frac{\sum nf\ Lf}{\sum nf} \tag{5.1}$$

$$\bar{D} = \frac{\sum nf\ Df}{\sum nf} \tag{5.2}$$

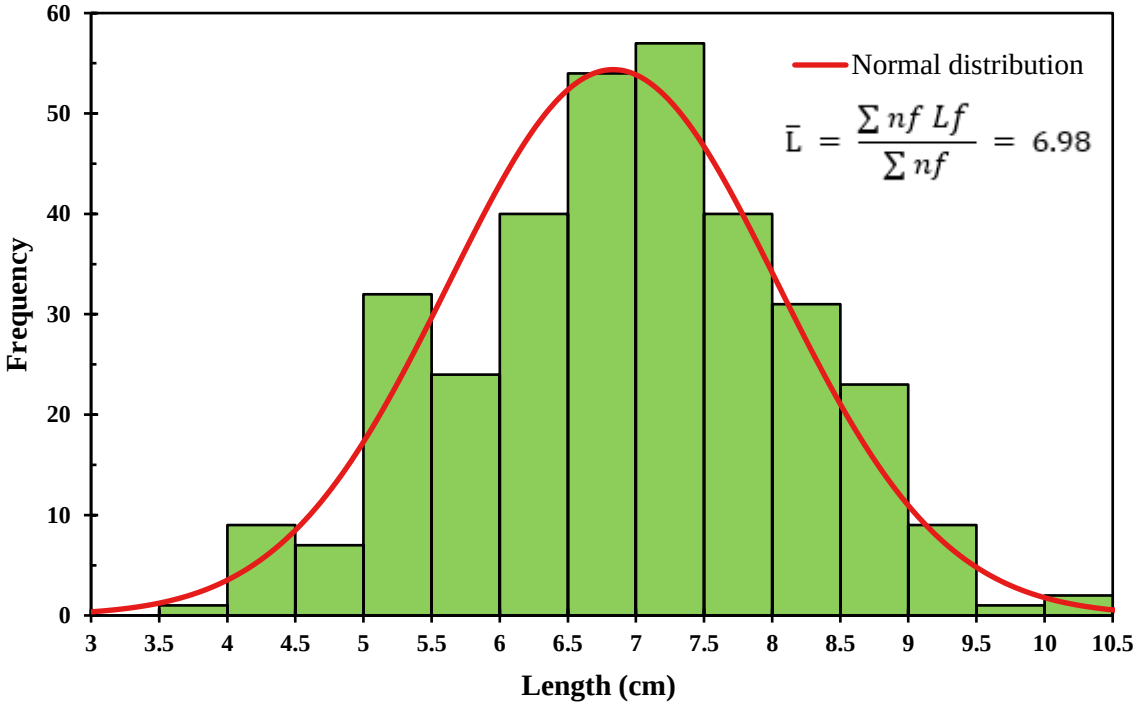

Figure 5.3 Normal distribution in length of cattail fiber.

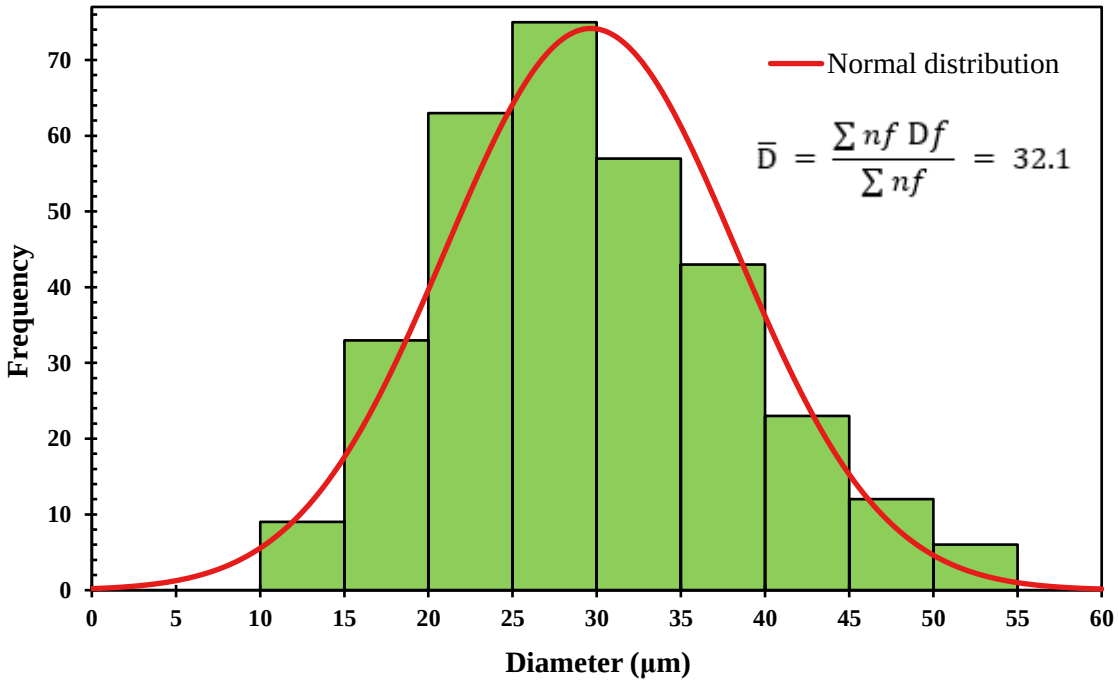

Figure 5.4 Normal distribution in diameter of cattail fiber.

5.3 FIBER CHARACTERISATION - APPLICATION OF WEIBULL DISTRIBUTION TO STUDY THE EFFECT OF MOISTURE CONTENT ON THE TENSILE PROPERTIES OF CATTAIL FIBER

5.3.1 Relationship between relative humidity and moisture content of cattail fiber

The moisture content value of cattail fiber at different relative humidity is measured on this study and the relationship between MC and relative humidity (%) for cattail fiber is shown in Figure 5.5. The moisture content of WBFs increases as the relative humidity increases, which is in agreement with the published data for other natural cellulosic fibres (for example, flax), where the MC is increased with the increasing RH (%) reaching a maximum value at 95% RH (Moudood et al., 2019). It can be seen from the figure that the equilibrium moisture content increased approximately linearly with the RH (%) up till about 70% RH and then accelerated rapidly. This relationship can be explained using the Peirce's two phase model where in phase one, water molecules associated with the glucose unit in the cellulose chain $[(C_6H_7O(OH)_3]n$ and in phase two, the water molecules fill the spaces available under attractive forces (Peirce, 1929). Further, the relationship appears to follow the type II sorption isotherm similar to other cellulosic natural fibers (cotton, flax, hemp, jute, and sisal) [Xie et al., 2011].

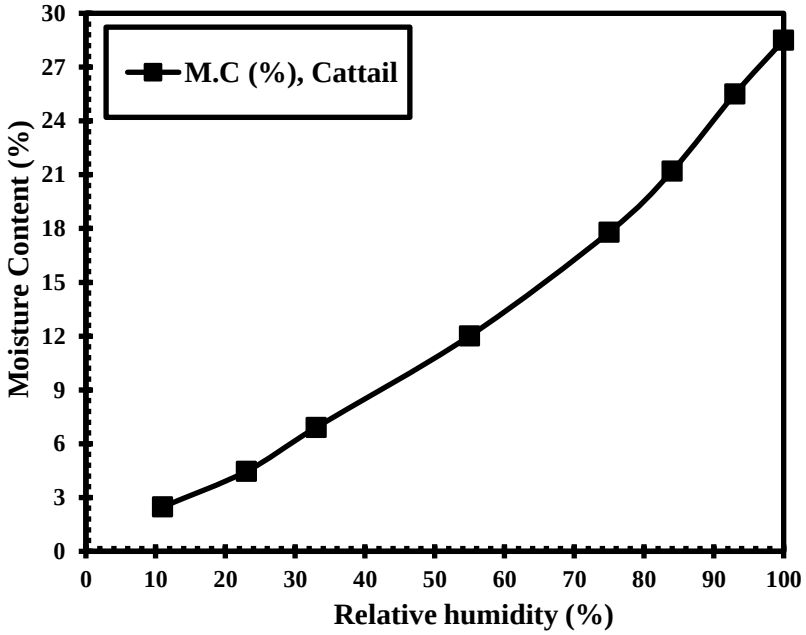

Figure 5.5 Relationship between relative humidity and moisture content of cattail fiber.

5.3.2 Effect of RH (%) on the mechanical properties of cattail fiber

The mechanical properties of cattail fiber is shown in Table 5.1. For cattail fibre, with the increase in relative humidity both tensile stress and modulus increase up to the relative humidity of 75% and at above this point of RH% these two properties decrease. There is a slight trend of increasing strain (%) with the increase in relative humidity. No relationship data between relative humidity and tensile stress values was found for cattail fiber. Generally, the value of tensile properties is increased with the increases in relative humidity conditions for bast and cotton fibers. For cotton, the ratio of tenacity value at 100% and 65% RH is 1.11 (Morton & Hearle, 2008) while for flax, the tensile strength is increased with the increase in relative humidity up to 95% (Nilsson, 2006). Further analysis of the data for other bast fibres revealed that for hemp, the highest modulus value was obtained at 80% RH while the tensile stress was found to be at 50% RH condition (Placet et al., 2012). For flax, the optimum value is found to be 66% RH (Stamboulis et al, 2001) while others reported the reduction in modulus at rate of 0.39 GPa/RH% when measured using the constant rate of loading principle (Davies & Bruce, 1998).

Table 5.1 Mechanical properties of cattail fiber at different relative humidity.

Relative Humidity (%)	Tensile strength (MPa) (S.D)*	Modulus of elasticity (GPa)	Strain at break (%)
11.3	486 (281)	54.9 (28.3)	1.81 (1.34)
33	833 (453)	64.4 (30.3)	1.97 (1.39)
55	963 (500)	69.2 (35.3)	1.93 (0.54)
75.5	1106 (565)	74.7 (34.4)	1.88 (0.51)
84.3	720 (495)	57.9 (40.2)	1.92 (0.69)
93.6	830 (411)	57.0 (30.1)	2.37 (0.78)
100	600 (335)	48.7 (39.6)	2.14 (0.98)

(S.D)* = Standard deviation

The large standard deviation in the mechanical properties of the cattail fiber at different relative humidity points to a wide variation of strength and modulus from one fiber to another (Table 5.2). This is common for all bast fibres; for example, the Young's modulus (GPa) of flax, ramie, hemp and kenaf fibre is reported between 27.6-80 (Li et al., 2007) and 25-160 (Joffea et al., 2003), 44-128 (Ali, 2013), 20–70 (Ali, 2013) and 75-175 (Ibrahim et al., 2018), respectively. The wide dispersion in the mechanical properties of cattail and other natural fibers obtained from the same stem is the result of a number of factors that include fiber extraction and retting parameters (Foulk et al., 2003), differential fiber cross-section along the single fiber length (Thomason et al., 2011), fiber defects like knots, thick and thin places (Sparnins, 2006) and drying conditions prior to tensile properties measurement. Most of the factors that affect the tensile properties can be controlled except fibre cross-section variation and defects. In this study, it was noticed that during tensile properties measurement, the majority of the fiber did not break at the average inserted diameter. This point is discussed later in this section.

While the tensile stress data for cattail falls within the range from previous research group (Hasan, 2019) of Biosystems Engineering department, the modulus values are much

higher in this research than the previously studied modulus value. For this research, we had to oven dry the samples at 105°C for 24 hours to measure the moisture content before tensile properties measurement. It was noticed that the fiber samples became stiff when removed from the oven, which might be responsible for the higher modulus values for cattail. This is supported by the work of Hart and Summerscales (2017), who found that the modulus was doubled for jute fiber from 650 MPa at room temperature to 1250 MPa at 180°C when the heating was conducted for 15 minutes. Similarly, an increase in strength and modulus for thermally treated (140°C and 190°C) flax fiber was also found by Gourier et al., (2014). Also, the high modulus value for hemp (70 GPa, Ku at al., 2011) and kenaf (175 GPa – Ibrahim et al., 2018) was also obtained for oven dried samples. It is possible that due to heating for such a long time, some of the microfibrils (theoretical modulus for 100% microfibrils is 70 GPa) converted into crystallites (theoretical modulus for 100% crystallites is 250 GPa), which is almost 3.5 times stiffer than the microfibrils (Bledzki & Gassan, 1999). This behaviour can be further explained by the 'stiffening effect' by the fringed micelle theory where due to the heat the 'fringe' in the amorphous regions is found to be increased (Levine & Slade, 1988).

One of the sources of variation in mechanical properties for cattail is the diameter, as the methodology is being used to measure the tensile properties i.e., the single fiber method according to ASTM D 3822 (ASTM, 2020), and it is used widely to determine the modulus and stress of natural fibrers (Li et al., 2009; Park et al., 2006; Beckermann et al., 2009; Xia et al., 2009; Baley, 2002; Lamy & Baley, 2000; Symington et al., 2009; Virk et al., 2010). The methodology calculates the tensile properties based on the inserted fiber diameter – this is the point at which the fiber is theoretically predicted to break. In order to determine the exact location of the breaking point, the two broken parts of the fiber was joined together and diameter of these broken ends were measured. Our results showed that around 80% of fibers broke at a point that was different from the predicted point of breakage as shown in Figure 5.6. Measuring

the diameter of the breakage point was also a challenge due to the irregular breakage pattern. While most of the samples had tensile failures (fibrillary/granular/brittle nature – Figure 5.7(a)), few samples broke with multiple splitting (Figure 5.7(b)), axial split (Figure 5.7(c)), or tensile break with single and multiple steps at the end (Figure 5.7(d, e)). It was not possible to calculate the accurate cross-sectional area, as cattail fibers are not exactly circular. The cross section of the cattail fiber consists of numerous small elliptical (polygonal) cells, each about 4.5 – 6.0 µm (Rahman et al, 2020). A similar polygonal shape in the cross-section exists in flax and hemp fibres (Hatch, 2006). However, when we check the variation for the strain at the break (%) which is not dependent on the fibre cross-section, it was found that the standard deviations are also very large as shown in Table 5.1.

With this large variation in tensile properties in the cattail and since the complete variation sources are unknown, it is essential that probability analysis be carried out. The two-parameter Weibull distribution was conducted which is reported to have good agreement with single fiber strength data for other natural cellulosic fibers (Joffe et al., 2003; Pan et al., 1997).

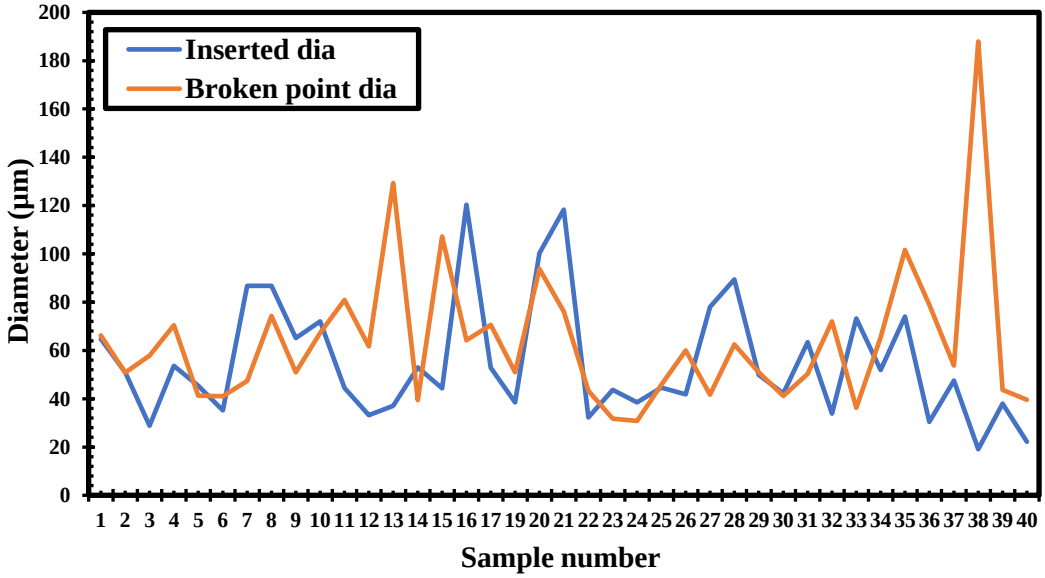

Figure 5.6 Inserted diameter and breakage point diameter at 33% RH (Canola fiber).

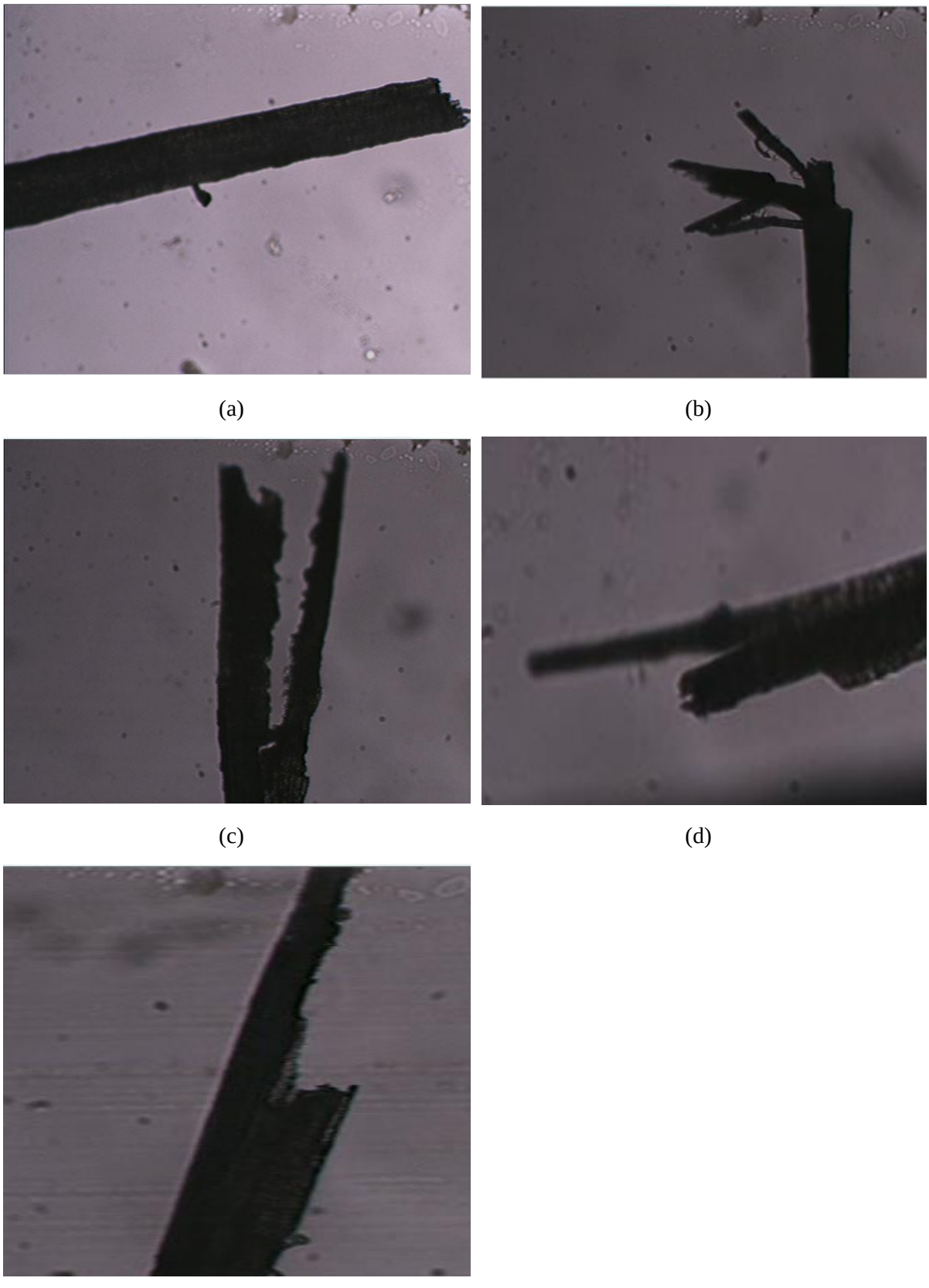

Figure 5.7 (a) Granular/fibrillar break at 11% RH; (b) Fiber breakage with multiple splitting at 11% RH; (c) Axial spit (75% RH); (d) Tensile break – multiple ends (11% RH); (e) Tensile break – (b) single end (75% RH).

5.3.3 Weibull distribution and calculating Weibull parameters

Weibull distribution, which characterize an entire strength distribution rather than simply estimate a mean strength value, widely used for modelling failure behaviour and reliability analysis of a tested subject. The probability of failure for a random stress state can be predicted using Weibull statistical theory when the failure statistics are known for a given stress state (Roy et al., 2012). The cumulative distribution function of the two-parameter Weibull distribution used in this study can be stated using eq. (5.3) (Quinn & Quinn, 2010; Barsoum, 2019).

$$F(x) = 1 - \exp(-x/\beta)^{\alpha} \tag{5.3}$$

Where, F(x) is the cumulative probability of failure (P_f) of a fibre at an applied stress x, β is the scale parameter and α is the shape parameter or Weibull modulus. Considering double logarithm of eq. (5.3), it can be simplified to eq. (5.4).

$$\ln\left[\ln\frac{1}{1 - F(x)}\right] = \alpha \ln(x) - \alpha \ln(\beta) \tag{5.4}$$

The reason for using double logarithm in the Weibull equation for strength and modulus analysis is the ease of accessing information. The eqn. (5.4) can be compared with the straight-line equation using linear regression (LR) and represented in the form of eq. (5.5).

$$Y = mX + c \tag{5.5}$$

Where, $Y = \ln[\ln(1/(1-F(x))]$

$X = \ln(x)$

$c = -\alpha \ln(\beta)$

To determine the probability of failure, experimental values of tensile strength and tensile modulus were ranked in ascending order, *i*=1, 2, 3, . . ., N, where N is the total number of test

specimens and *i* is the i^{th} datum. Thus, the lowest strength or modulus for each configuration represents the first value (i = 1), the next lowest stress value is the second datum (i = 2), etc., and the highest stress is represented by the Nth value. In this study the probability of failure or F(x) is calculated based on the median rank position of the data points [19] using eq. (5.6). This median rank estimator (we called it as Estimator 1) is the most widely used for Weibull distribution than other probability estimators (Zafeiropoulos & Balillie, 2007).

$$F(x) = \frac{i - 0.3}{N + 0.4} \tag{5.6}$$

To determine the shape parameter or Weibull modulus and scale parameter or characteristic strength, ln [ln (1/(1-F(x))] is plotted in graph as a function of ln (strength) or ln (modulus) of cattail fibre. Finally, a line is fitted through the plotted data points. Linear regression analysis is used on this research to determine the Weibull parameters.

In Weibull statistical modelling, the tensile strength value would be equal to average Weibull tensile strength (σ_{avg}) when the probability of failure is 50% (Quinn & Quinn, 2010). Using this condition, average Weibull strength can be calculated from Weibull distribution model. Therefore, $x = \sigma_{avg}$, when F(x) = 0.5. Putting these values in eq. (5.4) would result in eq. (5.7)

$$\ln \left[\ln \frac{1}{1 - 0.5} \right] = \alpha \ln (\sigma_{avg}) - \alpha \ln (\beta) \tag{5.7}$$

Now, eqn. (5.7) can be simplified further and for a given shape parameter (α) and scale parameter (β) average Weibull tensile strength, σ_{avg} can be determined using eq. (5.8). Similarly, the average Weibull tensile modulus of cattail fibre, E_{avg} is determined.

$$\sigma_{avg} = \exp \frac{[\alpha \ln (\beta) - 0.3665]}{\alpha} \tag{5.8}$$

Reliability analysis can also be evaluated using Weibull statistical model. For a given shape parameter or Weibull modulus (α), and scale parameter (β), the probability of survival can be determined by Benard's approximation using eq. (5.9).

$$R(x) = 1 - F(x) = 1 - \frac{i - 0.3}{N + 0.4} = \exp(-x/\beta)^{\alpha} \quad (5.9)$$

Where, R(x) is the reliability or the probability of survival of the variable x.

5.3.4 Weibull analysis of tensile strength of cattail fiber at different relative humidity conditions

The plot between ln [ln (1/(1-F(x))] and ln (Tensile strength) is represented in Figures 5.8. The Weibull shape parameter (α), scale parameter (β), average Weibull tensile strength (σ_{avg}) and coefficient of determination of tensile strength (R^2_{σ}) of the Weibull distribution of cattail fiber at different relative humidity conditions are given in Table 5.2.

The Weibull tensile strength (σ_{avg}) closely follows experimental tensile strength of cattail fiber (Tables 5.2) at different R.H. The correlation coefficient (R^2_{σ}) is greater than 0.90 in all conditions. This R^2_{σ} is used to determine whether the tensile properties data for cattail fiber follow Weibull distribution by calculating the critical value of R^2 with a 95% significant level ($R^2_{0.05}$) using eq. (5.10) (Tiryakioglu et al., 2009).

$$R^2_{0.05} = 1.0637 - \frac{0.4174}{n^{0.3}} \quad (5.10)$$

Where $R^2_{0.05}$ is the critical value for R^2 and n is the number of samples for each relative humidity condition. The value for $R^2_{0.05}$ is also given in Table 5.2. All except one of the calculated R^2 values from the Weibull plot is larger than the critical $R^2_{0.05}$ for cattail fiber. Further, in order for data to follow the Weibull distribution, the Weibull shape parameter should be greater than 0.5 (Monterio et al., 2013; NCSS Statistical Software, nd) and all the shape

parameter data are higher than this threshold value (Table 5.2), which is discussed further in the following section. Therefore, it was determined that the tensile properties come from the Weibull distribution.

The Weibull shape parameter (α) for cattail ranged from 1.67 to 1.99. The shape parameter was the highest at 93.6% R.H. Higher shape parameter values are preferable in the Weibull distribution model as a lower shape parameter value indicates higher scattering in tensile strength whereas a higher value designates lower variability in the tensile strength [30]. The values of (α) when measuring tensile strength are found to be 1.19 for jute (gauge length: 20 mm) (Xia et al., 2009), 2.48 for kenaf (gauge length: 20 mm) (Ibrahim et al., 2018), 3.7 for sisal (gauge length: 20 mm) (Silva et al., 2008), and 2.6 for flax (gauge length: 10 mm, 140°C treated) (Gourier et al., 2014). One of the reasons for slightly higher shape parameter for other bast fibers, is that the authors used lower gauge length (10 to 20 mm) than the used in the current study (25 mm).

The probability of survival calculated using eq. (5.9) was plotted as a function of experimental tensile strength values to understand the reliability of tested specimen as shown in Figures 5.8 for cattail fibers. The experimental tensile strength values of cattail fiber corresponding to 50% probability of survival ranges between 500 – 1000 MPa (Figure 5.9). These range values lie within the average tensile strength values at different R.H (Table 5.2). The differences in tensile strength at different humidity conditions seem to be reduced to a great extent when the probability of survival increases. The survival probability in terms of tensile strength is the highest at 75% relative humidity for cattail fiber. However, for engineering applications, the higher strength values from these conditions should be counter institutive.

Table 5.2 Weibull parameters of tensile strengths for cattail fiber at different relative humidity based on Weibull distribution model.

R.H (%)	α	β (MPa)	σ_{avg} (MPa)	R^2_σ	[a]$R_{0.05}$
11	1.67	551	443	0.99	0.92 (38)
33	1.87	953	783	0.98	0.92 (39)
55	1.93	1098	908	0.98	0.93 (41)
75	1.94	1259	1043	0.97	0.93 (42)
84	1.76	804	653	0.97	0.93 (40)
93	1.99	948	789	0.97	0.93 (41)
100	1.85	677	556	0.99	0.93 (40)

[a]:number of samples in the parentheses;

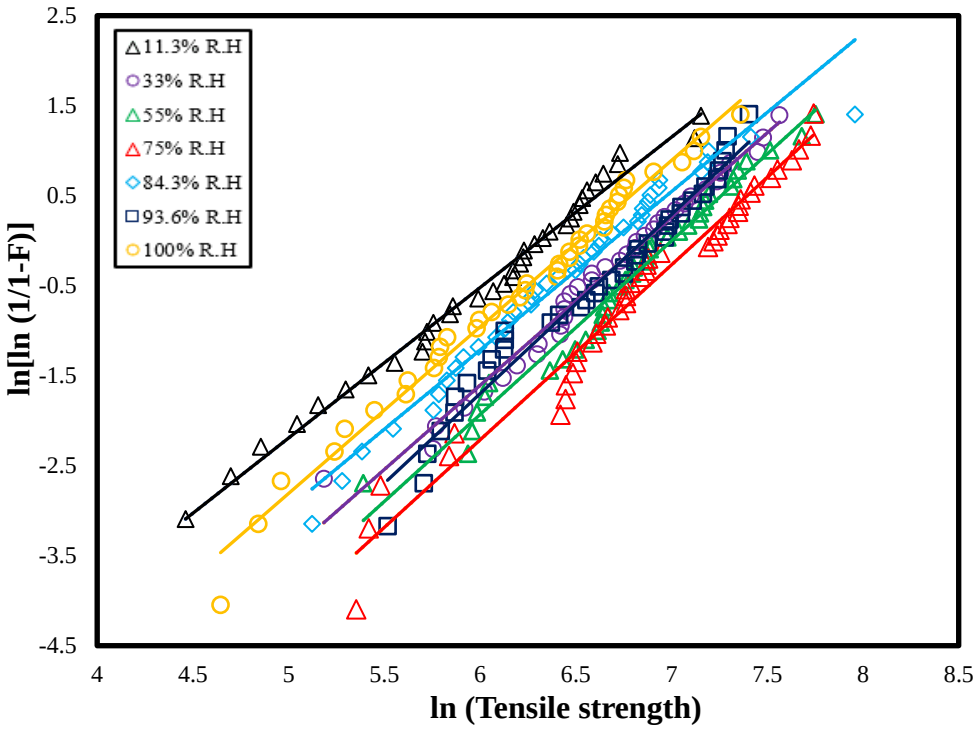

Figure 5.8 Weibull plots of the tensile strength of cattail fiber at different relative humidity.

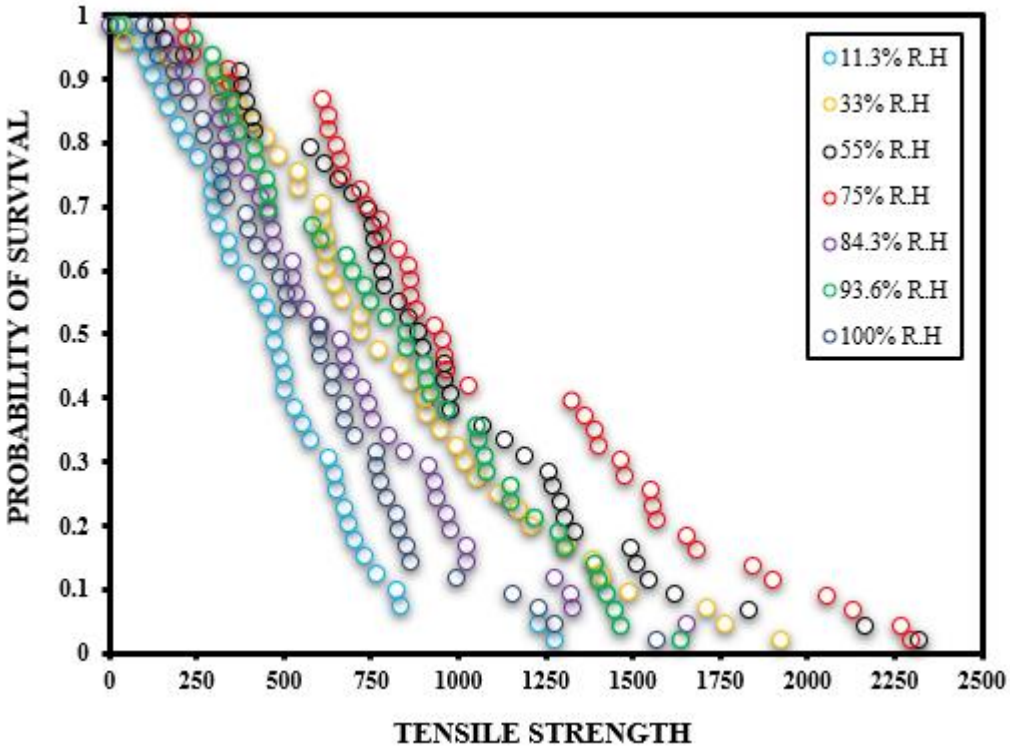

Figure 5.9 Reliability analysis of tensile strength of cattail fiber at different relative humidity using Weibull distribution.

5.3.5 Weibull analysis of elastic modulus of cattail fiber at different relative humidity conditions

The values of the Weibull parameters (α and β), and average Weibull elastic modulus (E_{avg}) obtained from ln[ln(1/1-F)] versus ln(elastic modus) for cattail fiber are shown in Figure 5.10. These parameters are listed in Table 5.3. The predicted average elastic modulus (E_{avg}) follows closely with the experimental modulus with the R^2_E being 0.95 or higher.

The shape parameter (α) for the elastic modulus of cattail fibre ranges between 1.73 to 2.49 with the top two values (2.49 and 2.38) belonging to 33.0 and 75% R.H. The Weibull shape parameter (α) for cattail falls within the values for flax (1.64-2.14, Ahmed, 2017) and Curaua fiber (1.59 – 2.23, Monteiro et al., 2013). The lower Weibull shape parameters for WBFs and BFs indicated larger variability in the modulus than the synthetic fibers as a much higher value was recorded for Nextel 312 (4.6) and Nextel 610 (10.5) (Chawlaw & Kerr, 2005).

The reliability analysis for the elastic modulus of cattail fiber using Weibull distribution is presented in Figures 5.11 and is determined by plotting the probability of survival and experimental elastic modulus. The elastic modulus corresponding to a 50% probability of survival lies within the mean values listed in Table 5.3. The survival probability in terms of the elastic modulus was found to be the highest at 75% relative humidity for cattail and canola fibers.

Table 5.3 Comparison of Weibull parameters and elastic modulus of cattail fiber at different relative humidity based on experimental data and Weibull distribution model.

RH (%)	α	β (GPa)	E_{avg} (GPa)	R^2_σ	[a]$R_{0.05}$
11	2.18	62.23	52.58	0.96	0.92(38)
33	2.49	72.37	62.44	0.96	0.92(37)
55	1.95	79.1	65.56	0.98	0.93(41)
75	2.38	84.41	72.35	0.97	0.93(41)
84	1.79	62.69	51.09	0.99	0.93(40)
93	1.99	64.32	53.51	0.98	0.93(44)
100	1.73	51.07	41.34	0.95	0.93(41)

[a]:number of samples in the parentheses;

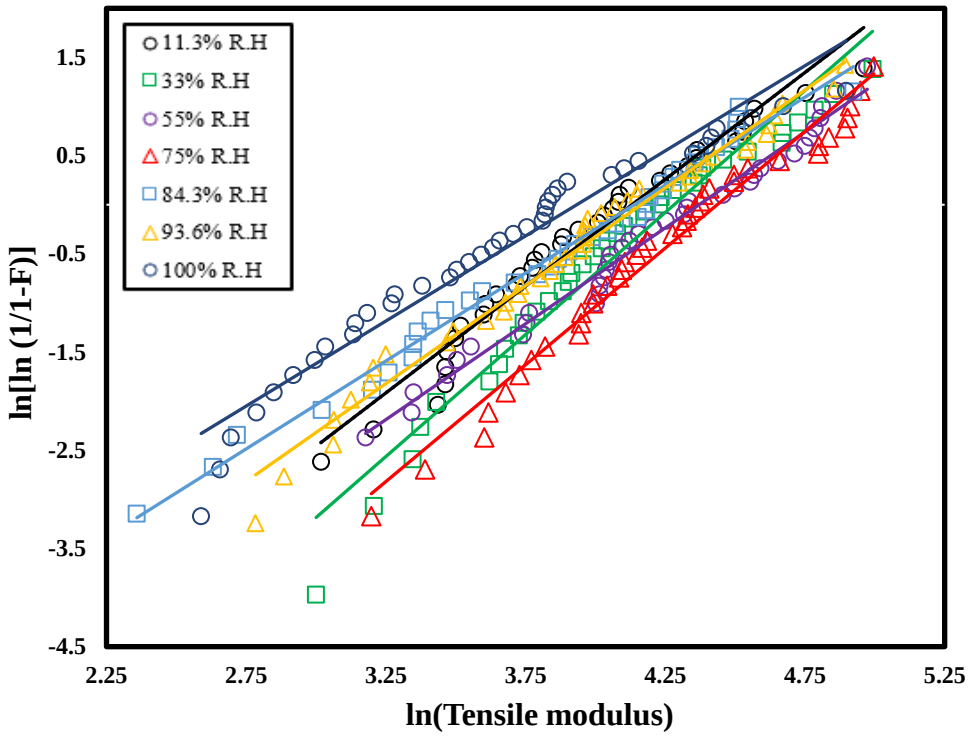

Figure 5.10 Weibull plots of the elastic modulus of cattail fiber at different relative humidity.

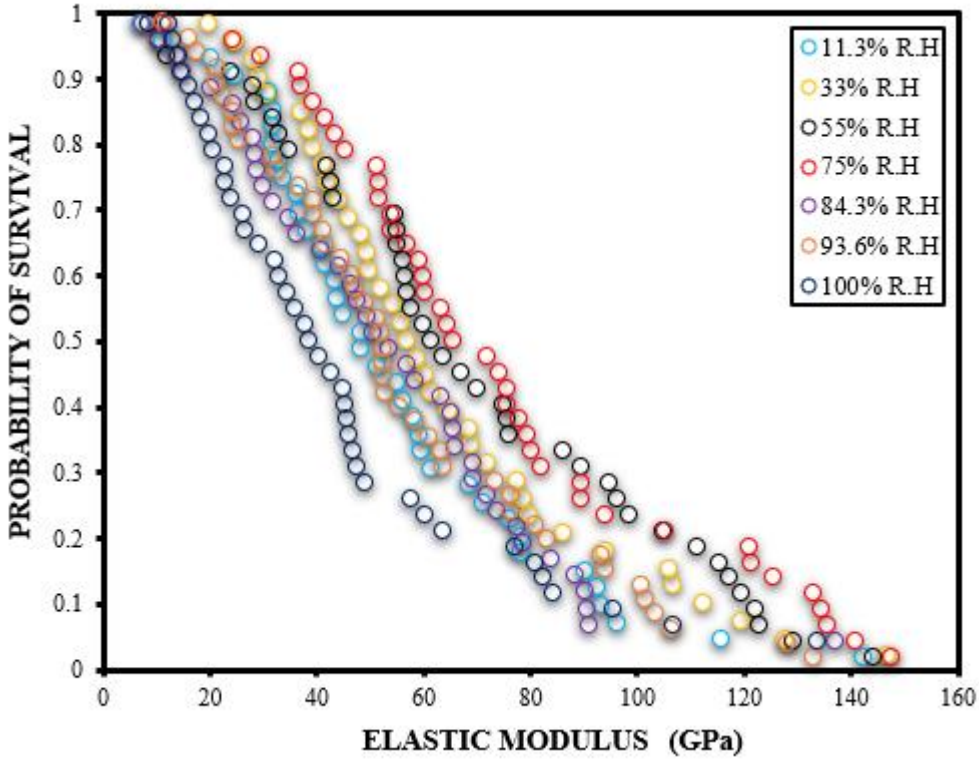

Figure 5.11 Reliability analysis of elastic modulus of cattail fiber at different relative humidity using Weibull distribution.

5.3.6 Effect of fiber length on Weibull distribution (cattail fiber)

Three different cattail fiber lengths (25 mm, 35 mm, and 45 mm) were chosen to determine the length effect on the Weibull distribution. The mechanical properties and Weibull parameters are shown in Table 5.4. The Weibull parameters calculated from the ln(ln(1/1-F)) versus ln(Tensile strength) plot are given in Figure 5.12. The Weibull modulus is slightly better for 35 mm and 45 mm lengths compared to 25 mm, however, the $R^2\sigma$ is better for 25 mm length data. The effect of length result on the Weibull Modulus in the current study is in agreement with other published results that used similar fiber length (Naik & Fronk, 2016; Pan et al., 1997). This is because the effect of defect beyond a specific gage length and larger strain rate (100 mm^{-1}) does not follow the Weakest Link Theory. However, others found an increase in the Weibull modulus and tensile strength with the increasing gage length. For example, Xia et al. (2009) reported a Weibull Modulus of 2.18 and 1.19 for 5 mm and 20 mm gage length jute fiber.

Using such a shorter fiber length to predict the performance of natural fiber composites, particularly those that are made from needle punched non-woven fabric, would be inaccurate. During needle punched non-woven fabrication, the fibers must reach the bottom of the fabric with the needle to make the pillar structure, which is formed when the needle is capable of bridging the fibers that makes a stich structure (Ishikawa et al, 2019). These stich structures are essential because they absorb the external force applied to the fabric. Usually, 40 to 80 mm long fibres are required to make needle punched non-woven fabrics as the longer fibers increase the fabric grab strength (Ghosh et al., 1994), fiber to fiber cohesion and fiber interlock (Hearle & Sultan, 1968) and decrease air permeability (Luenenschloss, 1972). Most importantly, it was found that about 33% of the fiber strength is utilized in a needle-bonded fabric (Hearle & Sultan, 1968).

Although the Weibull modulus (shape of the slope) is the lowest for the shorter gage length test, for all (Table 5.4), the characteristics strength (distribution location) is increased with the increasing fiber length (Figure 5.13). Usually, a lower Weibull modulus demonstrate that the samples are more likely to break at lower stress, however, this is not the case as the experimental tensile strength and Weibull characteristics strength decreased with the increasing gage length (Table 5.4). This indicates the flaws present in all three specimen sets; however, the types of flaw may be different as can be seen from their breakage pattern (Figures 5.7). These multiple flaws might contribute to the breakage as well as cause the wriggle effects in the survival graph (Figure 5.13). Further, the characteristics strength for the shorter length samples is high due to these specimens being highly stressed. While this behaviour is more pronounced at the higher strength data points, at the lower strength data points and at 98% reliability the values are almost similar (≈155 MPa) (Figure 5.13). This is due to the use of the LR method that 'chases' the lower strength data points (Quin & Quin, 2010).

Table 5.4 Effect of fiber length on the Weibull Parameters of cattail fiber.

Fibre length (mm)	Mechanical Properties			Weibull Parameters				
	Tensile strength (MPa)	Tensile modulus (GPa)	Strain at break (%)	Shape parameter (α)	Scale parameter (β, MPa)	Weibull tensile strength ($\sigma_{avg,}$ MPa)	R^2_{σ}	$R^2_{0.05}$
25	787.3 (386.9)	61.9 (19.4)	3.1 (2.6)	1.5	1906	1493	0.98	0.87
35	737.4 (254.3)	67.1 (19.8)	1.8 (0.5)	1.77	1626	1321	0.86	0.87
45	600.2 (274.9)	56.4 (23.6)	2.2 (1.7)	1.66	998	800	0.96	0.87

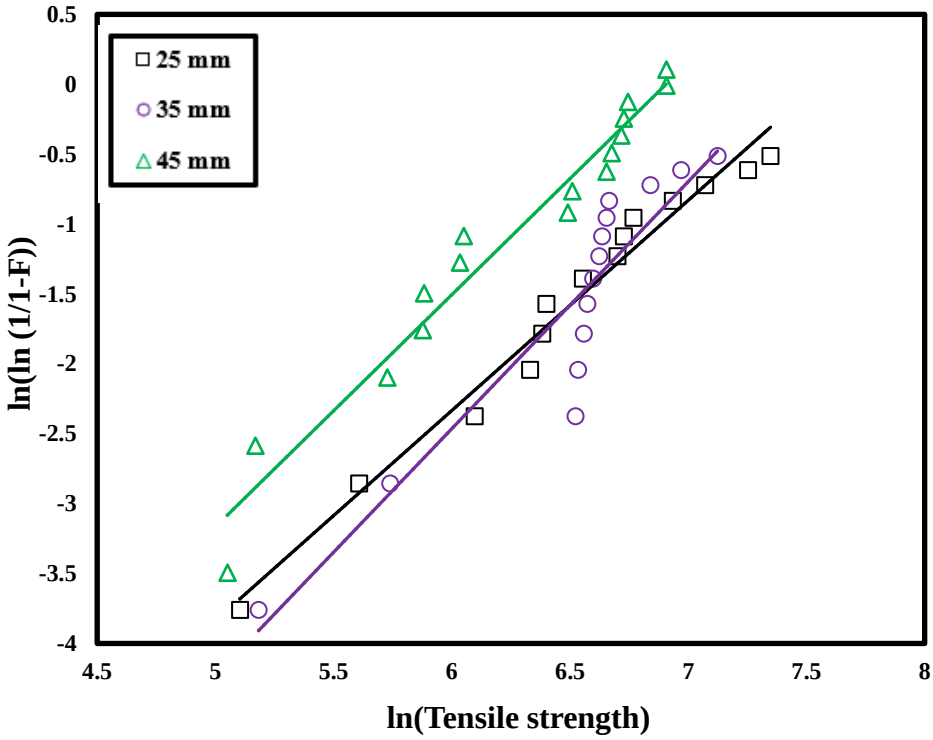

Figure 5.12 Weibull analysis of tensile strength of virgin cattail fiber using different fiber length.

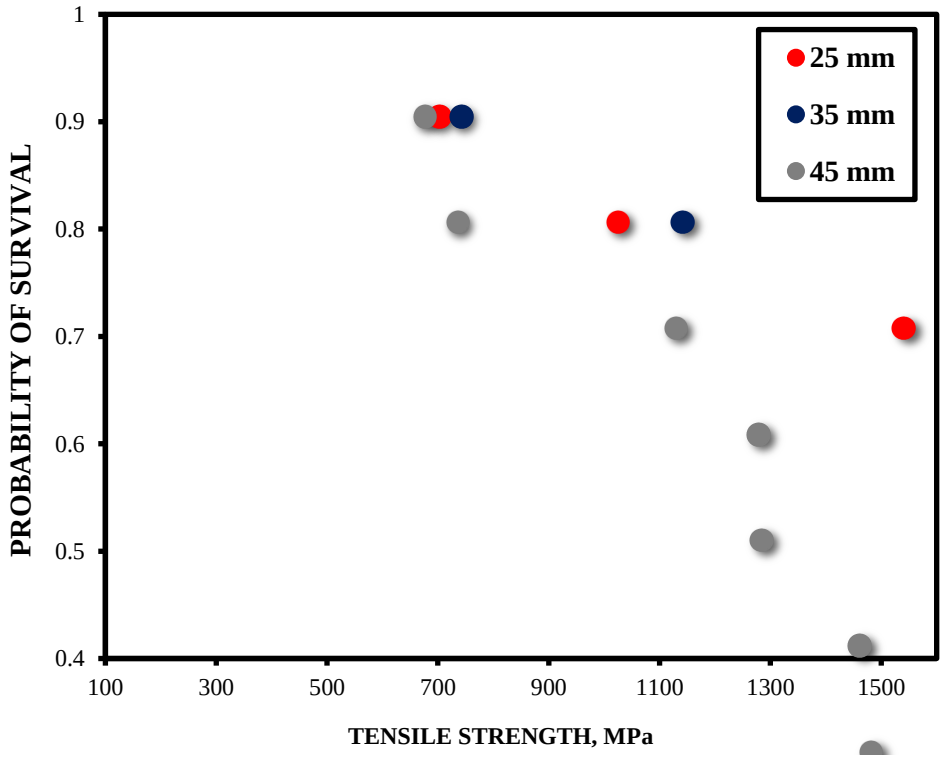

Figure 5.13 Reliability analysis of tensile strength of cattail fiber for different fiber length using Weibull distribution.

5.3.7 Effect of estimator on the Weibull distribution (cattail fiber)

The probability index was also calculated by three other estimators given in eq. 5.11 (Hazen'-Estimator 2), eq. 5.12 (Mean Rank – Estimator 2) and eq. 5.13 (Small Sample – Estimator 4) and the Weibull parameters calculated are given in Table 5.5. Probability estimators 1, 2 and 4 produced an almost similar α as well as $R^2\sigma$ while E3 revealed larger variation (lower α) in the samples, particularly at 33% and 84% relative humidity samples. Also, $R^2\sigma$ values for these two RH (%) samples are lower than for other relative humidity samples. The predicted values for strength (σ_{avg}) are almost close to each other for all four estimators, however, the most conservative estimation (lowest) was obtained from the probability estimator E3 and the predicted strength value is the lowest at the 11% RH condition. Conservative strength estimates are preferred for engineering applications. Also, the goodness-of-fit value for cattail fibre at 11% relative humidity is the highest (0.99) of any other RH conditions for all four estimators that is obtained from LR analysis of ln [ln (1/(1-F(x))] and ln (Tensile strength).

Estimator 2 (Hazen's):

$$P(\sigma) = \frac{i - 0.5}{n} \tag{5.11}$$

Estimator 3 (Mean Rank):

$$P(\sigma) = \frac{i}{n + 1} \tag{5.12}$$

Estimator 4 (Small Sample):

$$P(\sigma) = \frac{i - \frac{3}{8}}{n + 0.25} \tag{5.13}$$

Table 5.5 Effect of different estimators on the Weibull parameters.

RH (%)	Estimator 2				Estimator 3				Estimator 4			
	α	β	σ_{avg}	R^2_σ	α	β	σ_{avg}	R^2_σ	α	β	σ_{avg}	R^2_σ
11	1.74	547.9	443.8	0.99	1.59	555.3	441	0.99	1.69	549.8	442.9	0.99
33	1.92	948.8	783.2	0.98	1.32	1004	759.6	0.91	1.41	988.7	762.6	0.92
55	1.96	1093	906.9	0.98	1.8	1106	902.6	0.98	1.92	1097	905.9	0.98
75	2.01	1254	1045	0.96	1.86	1266	1039.6	0.97	1.97	1258	1044	0.97
84	1.8	801.2	653.8	0.97	1.15	886.2	644.2	0.83	1.78	803.4	653.5	0.97
93	1.63	980.6	782.6	0.91	1.93	951.7	787.1	0.97	2.01	946.9	788.9	0.97
100	1.92	674.9	557.5	0.98	1.77	681.2	553.6	0.99	1.87	676.2	556.1	0.99

This study examined the effects of pre-moistened cattail fiber on their breaking strength and Young's modulus. Both tensile strength and modulus data were successfully described with a 2-parameter Weibull distribution for cattail using the widely used Bernard's median rank approximation estimator (E1). The tensile stress data was further validated using three other estimators. The Weibull modulus of cattail fiber is similar to those of flax and hemp when compared with the similar test length. The predicted tensile strength (σ_{avg}) and modulus (E_{avg}) closely follow the experimental values for all relative humidity conditions. However, the predicted values at 11% relative humidity is the most conservative for cattail fiber, the goodness-of fit is the highest for cattail fiber for four estimators. At this relative humidity, the value of strength at 50% reliability is 442 MPa and 245 MPa while the value of the modulus is 52.9 GPa and 25.9 GPa for cattail fiber. At 90% reliability, the value for strength and modulus is reduced to 155 MPa and 20 GPa respectively. The 90% reliability values for strength and modulus for cattail fibre is within the strength range of hemp when compared with the similar diameter fiber and measurement technique (Shahzad, 2013) and hemp as quoted by (Gurunathan et al., 2015).

The Weibull modulus was lower for shorter gage length (25 mm), although the experimental strength, modulus and characteristics strength are higher as the gage length increased. Taking the results of the gage length, future research should be conducted by using the appropriate (40 to 80 mm) fiber length that is used to make needle punch non-woven fabric for composite applications. Finally, the variation and survival probability of cattail fiber are comparable with the bast fibers.

5.4 INFLUENCE OF FIBER DIAMETER ON THE MECHANICAL PROPERTIES OF CATTAIL FIBER

A dependence between the mechanical properties and fiber diameter has been found in previous studies for natural fibers which indicated an inverse relationship between mechanical properties (e.g. elastic modulus and tensile strength) and fiber diameter (Baley, 2002; Charlet et al., 2007). The increase in fiber diameter results in a decrease in tensile strength for flax fiber stated by Andersons et al., (2005) in terms of Weibull statistics because the larger fibers of flax fall more prematurely than the smaller fibers as the probability of containing a defect is higher in larger fibers.

For cattail, the experimentally measured tensile modulus or modulus of elasticity (E_f) varied with the variation in diameter of cattail fibers (D_f). These variations are illustrated in Figure 5.14 by plotting the tensile modulus as a function of cattail fiber diameter. The tensile modulus of cattail fiber exhibits a larger variation as mentioned in Table 5.1. The experimental data points in Figure 5.2 were empirically fitted using the non-linear regression function and an equation was derived with the fitted values for predicting the cattail fiber modulus using fiber diameter. The derived equation is shown in eq. (5.12). From Figure 5.14, a decreasing trend in modulus is observed with the increase in cattail fiber diameter which is in agreement with the

negative correlation between fiber diameter and fiber modulus in eq. (5.14). The correlation or R^2 value is found 0.81 from the regression analysis.

$$E_f = 241.4 \exp [- 0.044 (D_f)] \quad (5.14)$$

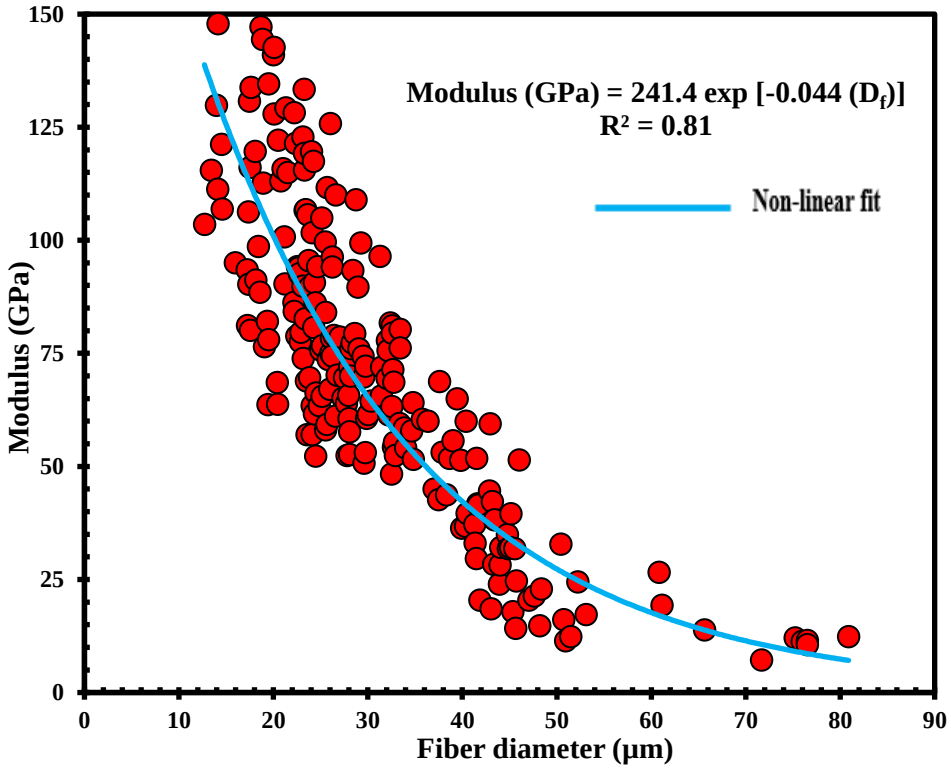

Figure 5.14 Variation of elastic modulus of cattail fiber with fiber diameter.

5.5 EFFECT OF SURFACE MODIFICATIONS

5.5.1 Evaluation of chemical changes

Fourier infrared spectrometer (FTR) – Attenuated total reflection (ATR)

The FTIR spectra of virgin cattail fiber and cattail fiber treated with DIH and HEA at 2.5, 5, and 10% concentration for 20 minutes are shown in Figure 5.15. It can be seen from the figure that virgin cattail fibre has very weak peaks in the carbonyl stretching regions whereas all the treated cattail fibres have strong peaks, particularly at 1625 cm^{-1}, 1680 cm^{-1}, and 1716 cm^{-1}. The peak at 1716 cm^{-1}, which is due to the formation of strong bond between fibers and DIH-HEA, belongs to carbonyl peak, and the group 1680 cm^{-1} belongs to amide group associated at

1630 cm^{-1} (Sigma Aldrich, 2020). The isocyanate group is also present in the treated cattail fibers in the 2270 cm^{-1} to 2360 cm^{-1} regions.

When a sample (10%, 30 minute) was washed with alkali (the pH of the solution is 5.7) and water, the carbonyl group at 1716 cm^{-1} and amide groups were still strong and did not wash away (FTIR graphs are not shown). Also, the intensity of the peak at 1716 cm^{-1} increased with the increasing chemical concentration. The immediate conclusion is that the solution of DIH-HEA was covalently bonded with cattail fibre and Structure-I is formed as shown in Figure 5.16. Further, the conjugated C=C in the Structure-I is expected to form covalent linkages with the Stypol resin via the styrene unit during free radical polymerization curing of the Stypol resin system by Lupeprox initiator and resulted in the proposed structure II in modified surface cattail composite (Figure 5.16).

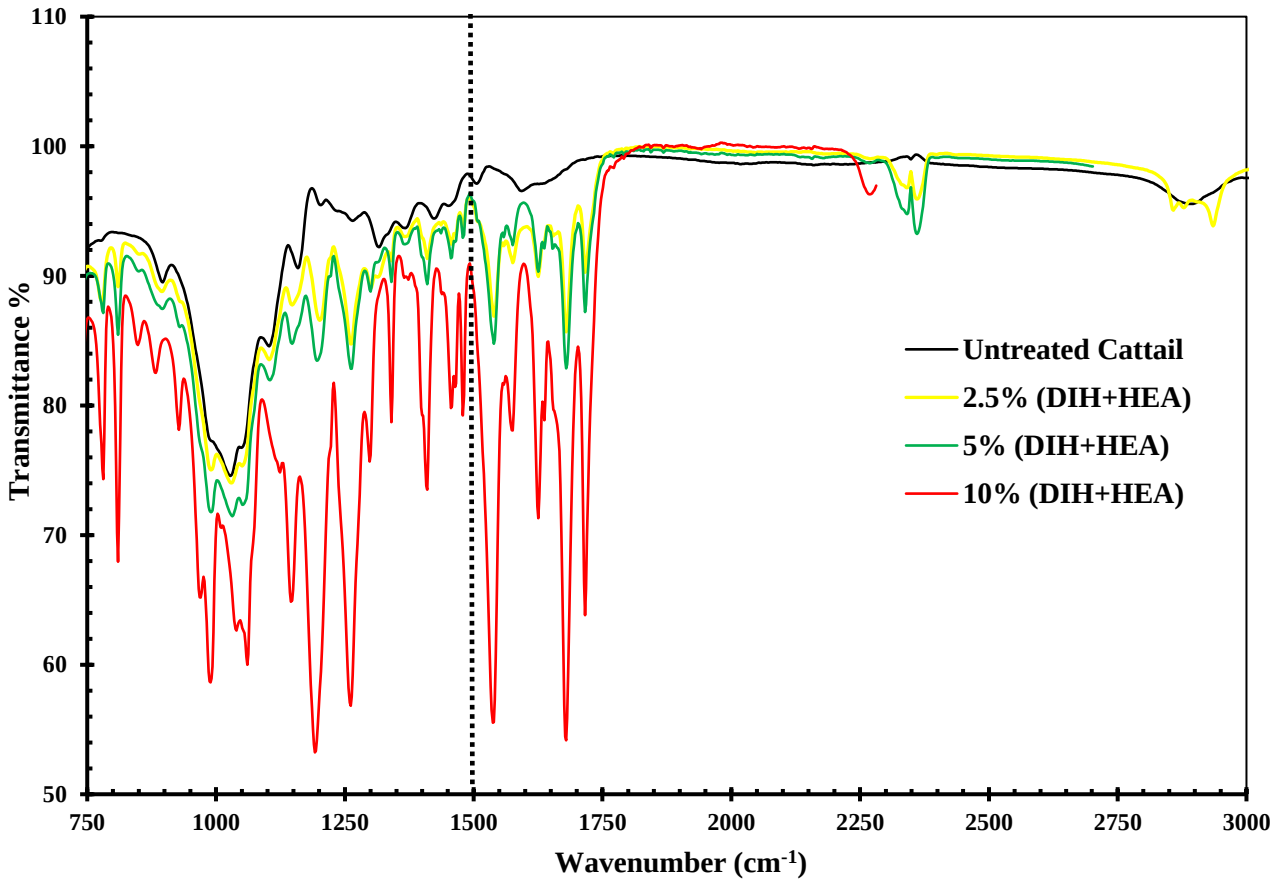

Figure 5.15 FTIR spectra of untreated cattail fiber and cattail fiber treated with DIH and HEA at 2.5, 5, and 10% concentration for 20 minutes.

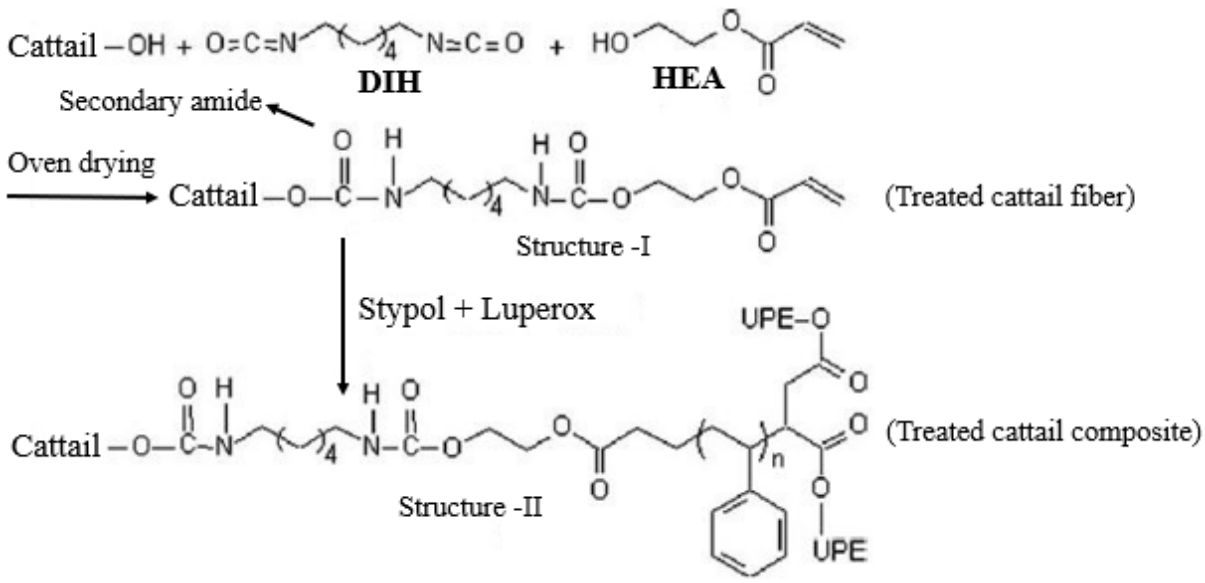

Figure 5.16 Proposed reactions in the DIH-HEA-treated cattail fibers and cattail-stypol composites.

5.5.2 Evaluation of moisture regain of the treated samples

Hydrophilic or hydrophobic characteristics of treated cattail fiber can be examined by understanding their behaviour when exposed to different moisten conditions. For the moisture regain measurement, nine different samples were prepared that included three different concentrations (2.5, 5, and 10%) of DIH-HEA and three different immersion times (10, 20, and 30 min) at each concentration condition. Treated cattail fiber along with a virgin cattail fiber sample were dried in an oven at 105 °C for 24 hrs and kept in a desiccator having 11% relative humidity. The 11% relative humidity was chosen because this condition should be used for the fiber condition before any mechanical test for composite application as discussed in Section 5.13. The moisture regain value of virgin and treated cattail fiber was recorded after 24 hrs desiccation at 11% RH. The moisture regain values of treated cattail fiber were plotted as a function of concentration % in Figure 5.17 for the different immersion time. For treated fibers, the maximum recorded moisture regain value is 1.8 % and the lowest value is 0.93 %, which are lower than the moisture regain of virgin cattail fiber (2.3 %) in this experiment. HEA is a long chain carbonyl compound, which is hydrophobic in nature (Stavber & Stavber, 2010). The

incorporation of carbonyl groups in cattail fiber while under chemical treatment improves the hydrophobic nature of cattail fiber, which resulted in a decrease in the moisture regain value of the treated cattail fiber. The rate of decrease in moisture regain of the treated fiber increases when the concentration of DIH-HEA increased from 2.5 to 10 % as seen in Figure 5.17. Also, for a given concentration, the moisture regain value of the treated cattail fiber decreases with the increase in immersion time. However, differences of regain value at different immersion times become less prominent at 10 % concentration. Overall, the water behaviour of DIH-HEA treated cattail fiber follows the behaviour of treated hemp (Qiu et al., 2011), bamboo (Liu et al., 2014), and flax (Arbelaiz et al., 2005).

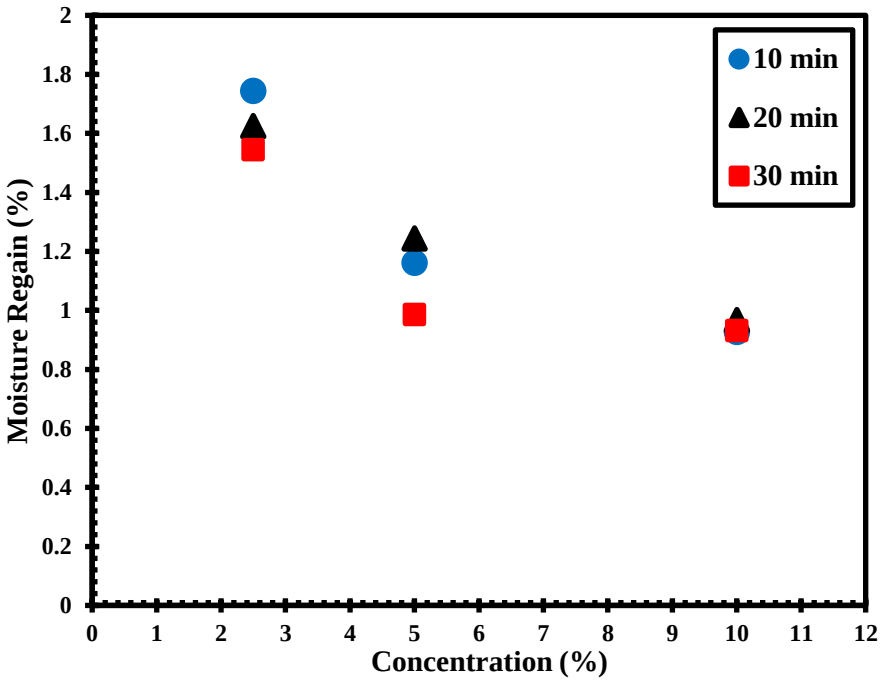

Figure 5.17 Moisture regain of treated cattail fiber at different DIH-HEA concentration and immersion time.

5.6 CATTAIL MAT CHARACTERIZATION

5.6.1 Density of cattail fiber

The experimental density value of cattail fiber measured from helium Pycnometer is found to be 1.39 gm/cc (Table 5.6). Looking at the density values, it appears that cattail fiber is lighter than flax (1.49 g/cc, Table 4.5) and hemp (1.57 g/cc, Table 4.5) fiber which could be because of the hollow fiber structure of cattail (Rahman et al, 2020). This phenomenon also can be seen in the SEM micrographs (Figures 5.35-5.39).

Table 5.6 Density of cattail fiber.

Content	Density (gm/cc)	S.D (N=3)
100% Cattail	1.39	0.005

5.6.2 Physical properties of non-woven cattail mat

The areal density, mat thickness, permeability, and fiber volume fraction percentage of nonwoven mats are the key parameters that determines the mat design and influences the mechanical properties of manufactured composites. The physical properties of nonwoven cattail mats are listed in Table 5.7. Table 5.8 shows a comparison of properties among flax, hemp, and flax hemp mats.

The large standard deviation in areal density in cattail mats is due to the uneven fiber distribution that occurred while laying up the fibers manually during mat preparation before making zero punched nonwoven. Comparing the mat properties of zero punched 100% flax, 100% hemp and 50%flax+50% hemp (Table 5.8) with the 100% cattail mat (Table 5.7), it can be stated that the areal density of all four fibers and fiber combination are nearly the same. The thickness of the nonwoven mat is higher for cattail when compared to flax, hemp, and flax-

hemp blended mats. Since, all these mats were subjected to a similar dead-weight force, the higher thickness of cattail mat indicates low compaction achieved after dead-weight application. This is believed to be due to the higher length of cattail fibers used in making mats compared to that of flax and hemp mats. A bundle of individualized cattail and flax fibers is illustrated in Figure 5.19. This could be also due to the nature of cattail fiber as cattail is slightly less flexible when compared to flax and hemp fiber. Regardless of fiber content, all these mats are thicker than the 20, 30, and 72 punch density flax mats despite having similar areal density which indicates that the needle punching process reduces the thickness of mats (discussed in Chapter 4).

Cattail fiber had the least fiber volume fraction among all these mats. The fiber volume fraction percentage (V_f) in the manufactured nonwoven mat depends on the mat thickness, areal density, and density of fiber content. For a given areal density, the cattail fiber could result in a higher fiber volume fraction % where all the mats are manufactured in similar thickness as the density of cattail is low compared to flax and hemp fiber. For the fibers with a similar density, a higher starting areal density and lower thickness of mat would result in higher V_f (%). The fiber volume fraction percentage of the nonwoven cattail mat was plotted as a function of corresponding mat thickness in Figure 5.18. Instead of the mean values with standard deviations (N=3), the raw data of thickness and permeability for various cattail mats are plotted in Figure 5.18 which showed a nearly inverse relationship between them although the neat V_f (%) of mat as a whole would depend on other factors as well as those discussed above.

Table 5.7 Physical properties of nonwoven cattail mat.

Mat content	Punch density (p/cm^2)	Areal density of mat (g/m^2)	Mat thickness before consolidation (mm)	Fiber volume fraction in mat, V_f %
100% Cattail	0	913.5 (52.8)	19.1 (1.6, N=3)	3.5 (0.4, N=3)

Table 5.8 Physical properties of nonwoven flax, hemp, and flax-hemp hybrid mat.

Mat content	Punch density (p/cm^2)	Areal density of mat (g/m^2), (SD)*	Mat thickness before consolidation (mm), (SD)*	Fiber volume fraction in mat, V_f %, (SD)*
100% Flax	0	931.1 (67.1)	16.3 (0.7)	3.8 (0.2)
100% Hemp	0	941.3 (17.9)	12.5 (3.1)	6.6 (1.6)
100% Hemp	2.6	1021.6 (7)	8.1 (1.5)	8.7 (1.6)
50% Flax-50% Hemp	0	993.3 (4.3)	13.9 (0.5)	4.7 (0.2)

(SD)* - Standard deviation

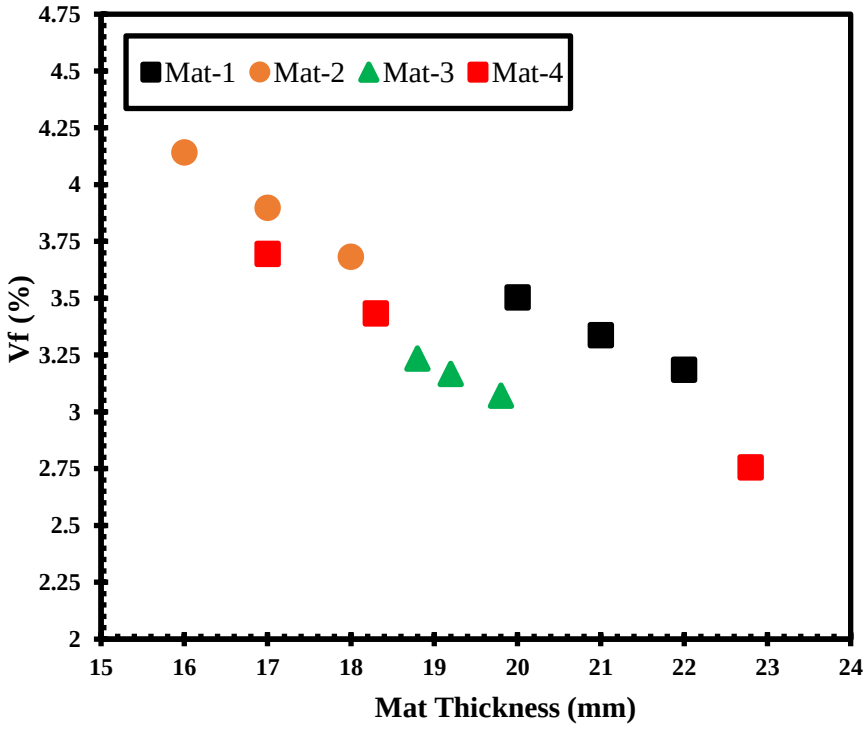

Figure 5.18 Relationship between mat thickness and fiber volume fraction % of cattail mat.

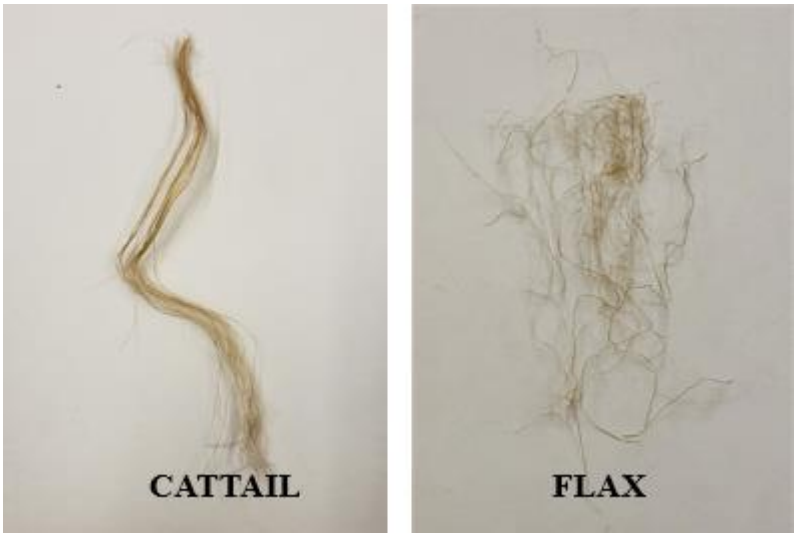

Figure 5.19 Individualised cattail and flax fiber for preparing zero punched nonwoven mat.

5.6.3 Cattail mat permeability

Mat permeability (transverse permeability or out of plane permeability or through-the-thickness permeability) is one of the most significant properties of nonwoven materials for the application in dry filtration. The permeability in a nonwoven cattail mat determines the rate of flow of resin, the amount of resin impregnated, and the mold filling time during resin transfer molding. The higher permeability in the mat helps to reduce the mold filling time and increase the rate of flow during VARTM process. The transverse permeability of each cattail mat was recorded at three different locations prepared for manufacturing composite at different pressures. The mean values of transverse mat permeability for each cattail mat and corresponding V_f % of the mat is listed in Table 5.9.

The transverse permeability of the zero punched cattail mat (Table 5.9) is higher than those of zero punched flax and flax-hemp hybrid mats (Table 5.10). The transverse permeability or out of plane permeability depends on several factors, for example – thickness of mat, fiber volume fraction, and area of reinforcement specimen. The higher permeability values of the

cattail mat compared to those of flax and flax-hemp hybrid mats (Table - 5.9, 5.10) is believed to be due to the higher thickness and lower V_f of the cattail mat as shown in Tables 5.7- 5.8). Further comparison among these three fibers is given in Chapter – 6 (Section – 6.2).

To understand the effect of V_f and void fraction content of mats on the transverse permeability, the experimental permeability values are plotted as a function of corresponding mat void fraction content as shown in Figure 5.20, which exhibits a non-linear increase of mat permeability with the increase of void fraction and it would be the opposite when plotted against the V_f % of the mat. So, the out of plane permeability of the cattail mat is a function of V_f and void fraction content of cattail mat. However, the error in the experimental values of the cattail mat permeability appears to be very much less at the void fraction content indicating a higher permeability-void fraction correlation. So, it could be stated that mat permeability increases with the decrease in V_f % of the mat which is the possible reason for the higher out of plane or transverse permeability value of the cattail mat compared to those of flax and flax-hemp mats (Tables - 5.9, 5.10) despite having a smaller diameter in the cattail fiber when compared to flax and hemp (Table 6.1).

Table 5.9 Transverse permeability of cattail mat and corresponding V_f % of mat prepared for manufacturing composite at different pressures.

Mat content	Pressure (kPa)	Fiber volume fraction in mat, V_f (%),(SD)[1]	Transverse permeability, k x (10^{-11}) (m^2), (SD)[1]
100% Cattail	101	3.2 (0.06)	5.9 (0.03)
100% Cattail	260	3.9 (0.1)	4.7 (0.2)
100% Cattail	560	3.3 (0.1)	4.9 (0.3)

(SD)[1] – Standard deviation, N = 3

Table 5.10 Transverse permeability of flax and flax-hemp hybrid nonwoven mat.

Mat content	Punch density (p/cm^2)	Transverse permeability, k_z x (10^{-11}) (m^2), $(SD)^1$
100% Flax	0	2.5 (0.04)
50% Flax-50% Hemp	0	2.3 (0.1)

$(SD)^1$ – Standard deviation, N = 3

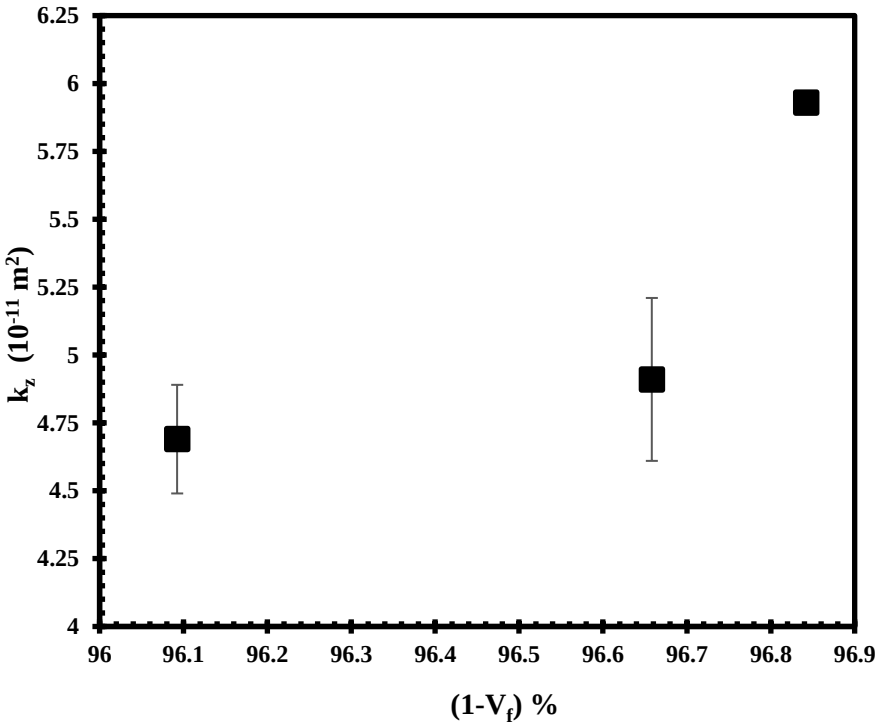

Figure 5.20 Effect of void fraction content on the experimental transverse permeability of cattail mat.

5.7 COMPOSITE PROPERTIES

5.7.1 Effect of consolidation pressure during manufacturing on structure of composite

Since the cattail non-woven mat was prepared with a zero needle punch, numerous problems were faced to make a homogeneous cattail-resin composite structure, particularly in the VARTM pressure. The zero punched nonwoven cattail mats used in this study were prepared in a lab where the fiber distribution was uneven across the mat when compared to needle

punched non-woven flax mats that are manufactured by the needle loom technique. For the zero punched cattail mat at VARTM pressure (101 kPa), resin quickly flew through the higher porous regions and filled the mold immediately leaving the less porous region of the mat not infiltrated with resin. As a result, it caused dry spots in the cured composite as shown in Figure 5.22. Such problem was not observed for the needle punched (20-P, 30-P and 72-P) flax mat at VARTM pressure (Figure 5.21).

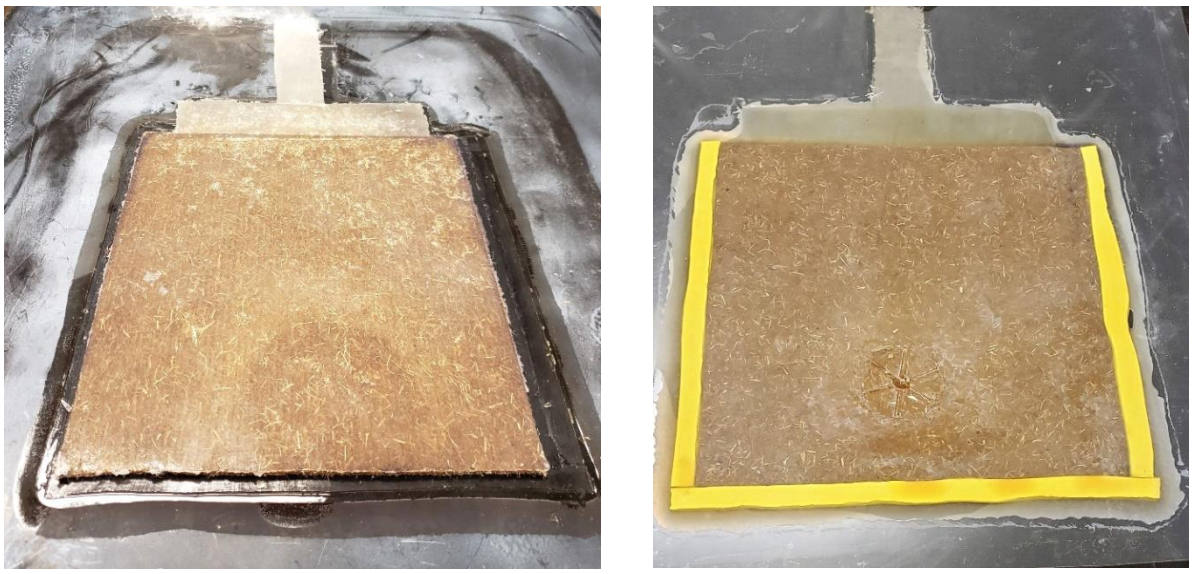

(a) (b)

Figure 5.21 Cured flax composite manufactured at VARTM pressure for (a) 20-punch density and (b) 30-punch density mat.

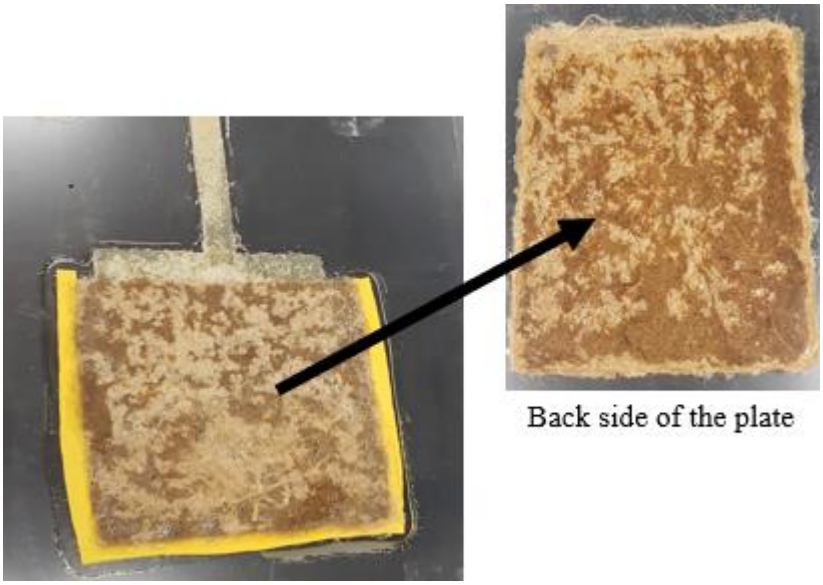

Figure 5.22 Dry spots in cured zero punched cattail mat composite manufactured at VARTM pressure.

However, the cured composite didn't show up any dry spots in the compression molding process when manufactured from the same zero punched nonwoven mat at 260 and 560 kPa pressures. The uniformity of the uneven resin impregnated mat from VARTM improved when sandwiched between a silicon pad, metal plate, and release film in the compression molding process, therefore more uniform cured composites developed as the silicon pad and metal plate usually compensate on the thickness non-uniformity of cured composite (figure not shown here). Moreover, the higher pressure used in the compression molding made the excess resin to be squeezed out thus filling the dry spots and voids in the mat. A cured cattail composite manufactured in compression molding process at 260 kPa is shown in Figure 5.23.

To overcome this problem in the VARTM process, a good control over resin flow and mold filling time while manufacturing is required. This was obtained by using the vertical glass strand that connects the vacuum pump in the VARTM setup to control the rate of resin flow. Further, a thinner (22.5 mm) glass strand mat in vertical direction was used instead of 45 mm which prolong the mold filling time by reducing the speed of resin flow. Also, the vacuum pump was allowed to run at least for 10 minutes before resin impregnation to exhaust all the air trapped inside and to identify any leakage in the VARTM set up.

Figure 5.23 Cured cattail composite manufactured in compression molding process at 260 kPa.

5.7.2 Composite thickness

The consolidation pressure used in VARTM and compression molding had a significant influence on the final part thickness of cattail-reinforced composites manufactured using various mats. The thickness of the nonwoven cattail mat at zero consolidation pressure and the thickness of cured cattail composite plates at different consolidation pressures are plotted as a function of molding pressures as illustrated in Figure 5.24. The increase in consolidation, indicated by the decrease in thickness, is highest when the pressure was increased from 101 kPa to 260 kPa. However, the rate of increase was relatively gradual when the pressure was increased from 260 to 560 kPa. Higher variation in thickness was observed before consolidation (virgin mat) (standard deviation: 1.6, Table 5.7) which was reduced to a significantly lower value in the final cured composite at 260 (standard deviation: 0.04 mm, Figure 5.24) and 560 kPa pressure (standard deviation: 0.04 mm, Figure 5.24).

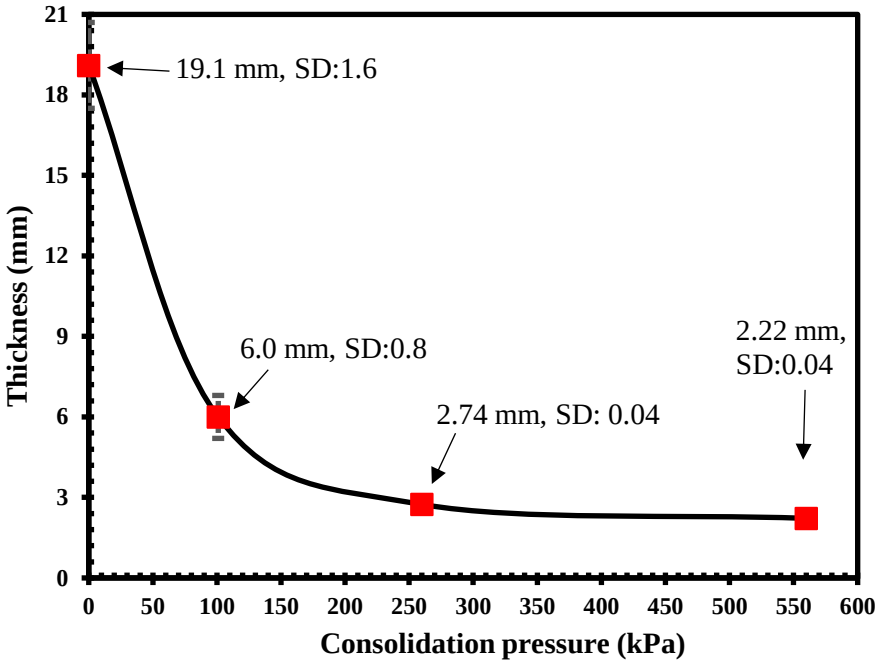

Figure 5.24 Effect of consolidation pressure on composite thickness during manufacturing.

5.7.3 Density and fiber volume fraction of composite

The density results of the cattail mat composite (obtained from helium Pycnometer) manufactured at different molding pressures are tabulated in Table 5.11 along with their corresponding fiber volume fraction % values. The experimentally measured fiber volume fraction of the cattail mat composites is plotted in Figure 5.25 as a function of consolidation pressure. In this figure, the fiber volume fraction value at zero pressure corresponds to the fiber volume fraction in zero punched dry mats before resin infiltration. Although the V_f (%) increased with the consolidation pressure as expected, the rate of increase varied with the change in manufacturing pressure. The maximum fiber volume fraction value is observed for the cattail mat composite when the manufacturing pressure increased from 101 to 260 kPa. It appears that the maximum compaction achieved at 260 kPa for the cattail mat composite and V_f % decreased at 560 kPa as seen in Figure 5.25.

Although the cattail mat composite with a modified surface (DIH-HEA treated fibers) was manufactured at 260 kPa, the fiber volume fraction of the untreated composite (V_f%: 30.4)

that was also manufactured at 260 kPa, is higher than that of the treated composite (V_f %: 26.1). This could be due to the lower starting areal density (shown in Table 5.11) of the treated mat composite. The fiber volume fraction % of the manufactured cattail composite truly depends on the density of the composite. The higher density value would result in a higher fiber content in the composite. On the other hand, the mat design or properties of the nonwoven mat, such as the areal density, and the fiber content highly influence these density values. The experimentally measured density values of composites are plotted in Figure 5.26 as a function of their corresponding mat fiber volume fraction % respectively which exhibits a linear relationship between V_f % of nonwoven mat and composite density. From Figure 5.26, it is seen that an untreated cattail mat composite was manufactured from a mat had 3.91 % fiber content in it whereas the treated one from a mat had 3.3 % fiber content in it which is the possible reason for the low density value and low V_f % of the treated cattail mat composite manufactured at 260 kPa.

Table 5.11 Density and fiber volume fraction of cattail composite at different manufacturing pressure.

Mat content	Needle Punch density (p/cm^2)	Consolidation pressure (kPa)	Starting areal density of Mat (gm/m^2)	Composite density (gm/cm^3)	Fiber volume fraction in composite (V_f %)
100% Cattail	0-P	101	845.3	1.19 (0.002)	11.2
100% Cattail	0-P	260	921.2	1.23 (0.005)	30.4
100% Cattail	0-P	560	974	1.22 (0.002)	26.1
100% Cattail (Modified surface)	0-P	260	873.2	1.22 (0.005)	26.1

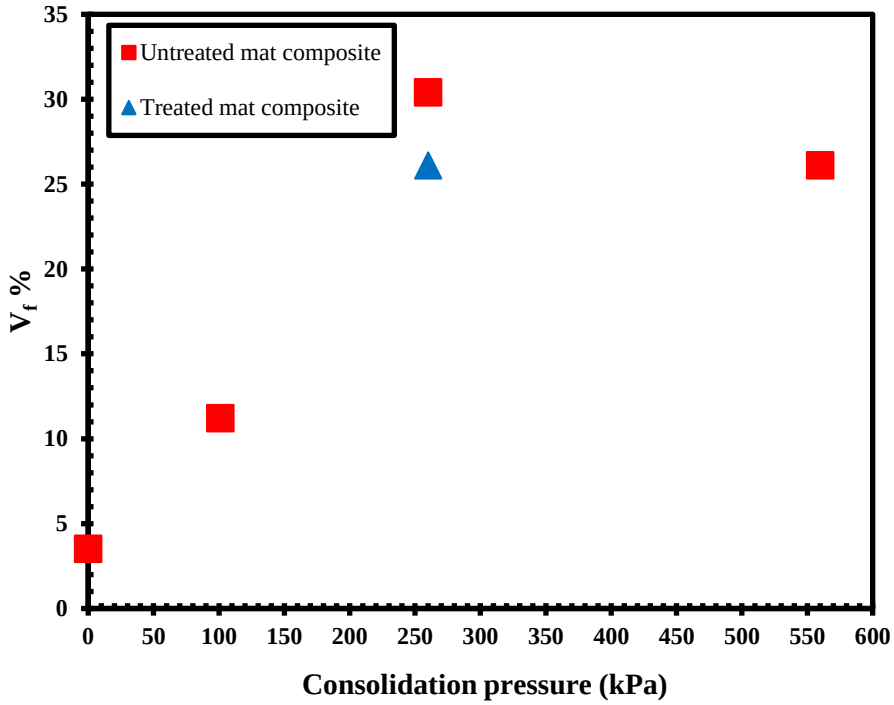

Figure 5.25 Effect of consolidation pressure on fiber volume fraction of cattail mat composite.

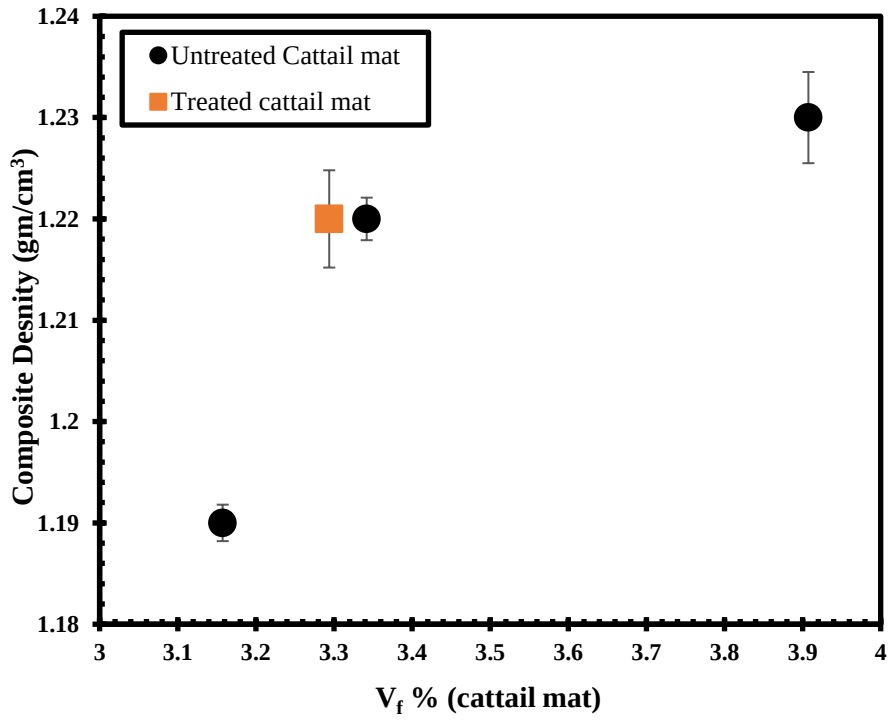

Figure 5.26 Relationship between fiber volume fraction % of nonwoven mat and composite density.

5.7.4 Stress-strain curve

The mechanical properties of the composites would mostly depend on the nonwoven design, composite manufacturing parameters, fiber content and interfacial bonding strength between the matrix and fiber. The unsaturated polyester resin used with the cattail reinforcing system influences the characteristics of the composite as well. The mechanical properties of the unsaturated polyester resin depend on the type of crosslinking monomer used during synthesis, their chemical structure, and molecular weight (Chabros, 2019). The modulus of the unsaturated polyester resin varied from 1 to 2.6 GPa (Chabros, 2019; Davallo, 2010).

The mechanical properties of the manufactured cattail composite are tabulated in Table 5.12. The corresponding stress value of the cattail fiber reinforced composite manufactured at different molding pressures and the stress value of stypol resin obtained from experimental tensile testing results is plotted as a function of strain to fit the stress-strain curve (Figure 5.28). Also, a representative tensile stress-strain curve for cattail fiber is shown in Figure 5.27. Comparing the stress-strain curve of pure polyester resin (Stypol) with the cattail fiber reinforced composite curve, it can be stated that the cattail fiber reinforced the neat resin significantly, however, the level of reinforcement or stress-strain behavior of the cattail fiber reinforced composite varied with the manufacturing pressure.

The level of reinforcement was less for 101 kPa when compared to 260 kPa and 560 kPa. As mentioned in section 5.4.3, the maximum compaction was achieved at 260 kPa for the cattail mat composite which could be understood from the stress-strain curve at 260 and 560 kPa. The cattail composite exhibited a similar level of reinforcement at 260 and 560 kPa as the curves at both pressures superposed and they could barely be distinguished from each other. However, the line fitted for the cattail composite with a treated surface was slightly steeper than those of the untreated composite indicating an increase in the reinforcement level for the treated composite.

So, it is clear that the consolidation pressure and chemical treatment of the cattail fiber surface played a significant role for reinforcing the neat resin with the cattail fiber as the level of reinforcement is higher for the higher manufacturing pressure and treated composite.

Table 5.12 Mechanical properties of stypol resin and cattail fiber reinforced composite (N=5).

Content	Needle Punch density (p/cm^2)	Consolidation pressure (kPa)	Longitudinal modulus (GPa)	Tensile strength (MPa)	Strain at break (%)
Stypol 8086	N/A	N/A	1.87 (0.09)[a]	34.6 (1.5)[a]	2.54 (0.8)[a]
100% Cattail	0-P	101	4.6 (0.6)[b,c,d]	18.6 (3.2)[b,c,d]	0.4 (0.1)
100% Cattail	0-P	260	7.0 (0.2)[b,e]	34.0 (3.8)[b,e]	0.5 (0.1)
100% Cattail	0-P	560	6.5 (0.2)[c,e,f]	44.1 (2.7)[c,e,f]	1.0 (0.1)
100% Cattail (modified surface)	0-P	260	7.2 (0.3)[d,f]	35.6 (0.5)[d,f]	0.6 (0.01)

[a]Fahimian, 2013; [a,b,c,d,e,f]: statistically significant ($p<0.05$).

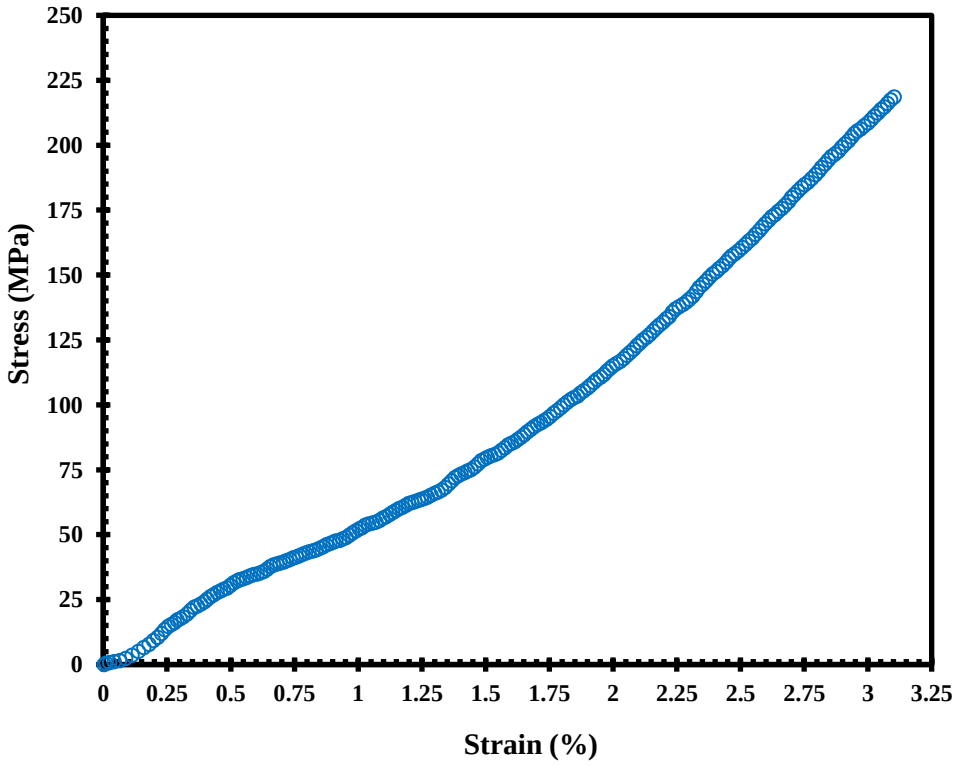

Figure 5.27 A representative tensile stress -strain curve for cattail fiber.

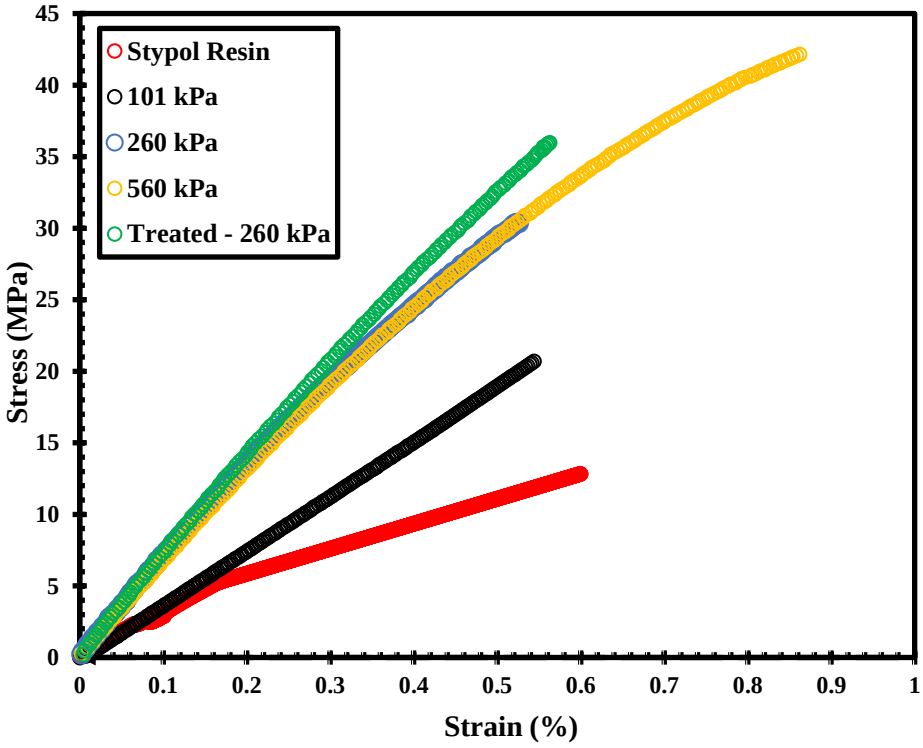

Figure 5.28 Stress-strain curve for stypol resin and cattail mat composite manufactured at different pressure.

5.7.5 Tensile modulus

The stress-strain graphs from the tensile test results show a non-linear relationship (Figure 5.28). The tensile modulus of manufactured composite was calculated from the slope of the stress-strain curve from the initial linear portion (in the strain range of 0.1%) as indicated in Figure 5.28. In order to verify the modulus calculation, a line was fitted to data points up to 0.1% strain using the linear regression function. The correlation (R^2) values between the fitted lines and experimental data points for up to 0.1% strain range is found to be 0.999 for all four cattail composites.

The experimentally determined longitudinal modulus of cattail composites manufactured at different manufacturing pressures are plotted in Figure 5.29 as a function of corresponding fiber volume fraction (V_f %) values which were tabulated in Table 5.11. The

measured fiber volume fraction in each of the tested samples for a single compaction pressure varied. The V_f of cattail composites increased with the consolidation pressure, however, the increase was linear until pressure increased to 260 kPa and it followed a decreasing trend when the pressure was further increased to 560 kPa. The difference in Vf observed at 260 and 560 kPa pressure depends on the fiber length, fiber distribution, orientation, starting areal density, and fiber fraction of the corresponding nonwoven mats that were manufactured. The maximum Vf % for the cattail composite (30.4%) was observed at 260 kPa pressure. Despite having a lower volume fraction value for treated composite than those of the untreated cattail composite at 260 kPa, the treated composite exhibited a higher modulus value as shown in Figure 5.29. This indicates the enhancement of cattail composite mechanical properties due to chemical treatment on the cattail mat (a proposed mechanism is given in Figure 5.16).

Apparently, the tensile modulus of the cattail mat composite is a function of V_f. A line was fitted through the experimental tensile modulus data points of the untreated cattail composite in Figure 5.29 using a linear regression function. The equation of the best fitted line is shown in Eq. (5.13). The correlation or R^2 value of this equation is 0.997. For a given fiber volume fraction (V_f %), the tensile modulus of cattail composite can be predicted using eq. (5.15).

$$\textit{Tensile Modulus, } E_c = 0.1274 \times V_f\% + 3.1918 \qquad (5.15)$$

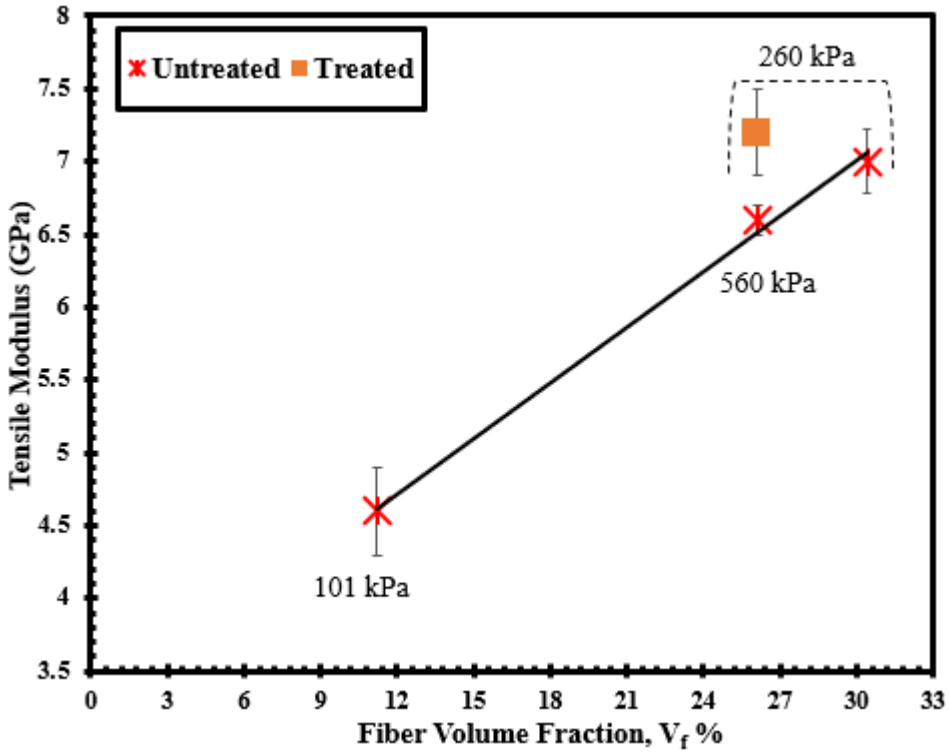

Figure 5.29 Relationship between fiber volume fraction and tensile modulus of cattail composite at different pressure.

5.7.6 Tensile strength

The tensile strength of the results of the zero punched cattail mat composite manufactured at VARTM and the compression molding pressures were tabulated in Table 5.12. For the cattail, no clear trend was observed in tensile strength with the change in V_f % at different manufacturing pressures. In order to understand the change in tensile strength value of the cattail composite, the experimental values of the tensile strength are plotted as a function of the manufacturing pressures in Figure 5.30. An increase in tensile strength of the cattail composite was observed with the increase in consolidation pressure, which is statistically significant (Table 5.12, the statistical analysis table is provided in the Appendix). For composites manufactured with VARTM pressure (101 kPa), the tensile strengths were lower than that of the strength in 260 and 560 kPa indicating a low reinforcement of the matrix by the fiber. The maximum longitudinal tensile strength value was recorded for cattail composites cured at 560

kPa, in the range of 41–48 MPa, which is in the comparable range of both flax and hemp composites (Table 4.6; Fahimian, 2013).

The tensile strength value of treated and untreated cattail composites manufactured at 260 kPa reveals that chemical treatment on the cattail mat marginally increased the strength value of the composite as the mean strength value increased from 34.0 to 35.6 MPa. However, it is found that the composites that were prepared from the treated cattail mat (tensile strength: 35.6±0.5 kPa) exhibited larger homogeneity, based on the standard deviation, in tensile strength than the untreated composite (tensile strength: 34.0±3.8 kPa) as shown in Table 5.12.

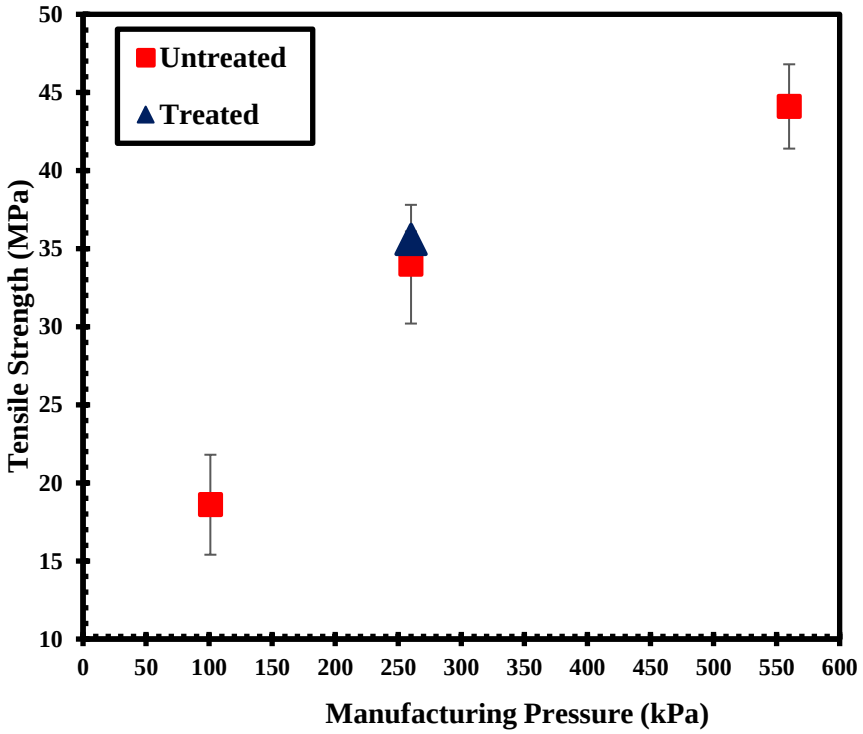

Figure 5.30 Effect of manufacturing pressure on tensile strength of cattail composite.

5.7.7 Image analysis of cattail composite

Microscopic images of the cattail composite captured from VHX Digital Microscope for VARTM pressure (101 kPa), 260 kPa, and 560 kPa are shown in Figure 5.31, 5.32, and 5.33, respectively. The x30 image shows that VARTM samples have a resin rich top layer as

compared to 260 and 560 kPa as more resin was squeezed out at the higher consolidation pressure. It appears that cattail fibers are more soaked in resin in the composite manufactured at 560 kPa (x100) – Figure 5.33 than those of VARTM pressure (x100) – Figure 5.31. From these images, it is also apparent that variation in the cattail fiber diameter is less compared to the flax mat composite (Appendix - Figure B1, B2, B3, B4).

Also, these images show that a higher number of fibers are present in a given area at pressure 260 and 560 kPa than VARTM pressure due to the higher consolidation achieved at 260 and 560 kPa. Also, there are variations in fiber length in these images from one pressure to another. Apparently, the cattail composite manufactured at 560 kPa contains longer cattail fibers than that of 260 kPa as revealed in these images, which could be one of the reasons for less compaction achieved at 560 kPa pressure and a lower fiber volume fraction value.

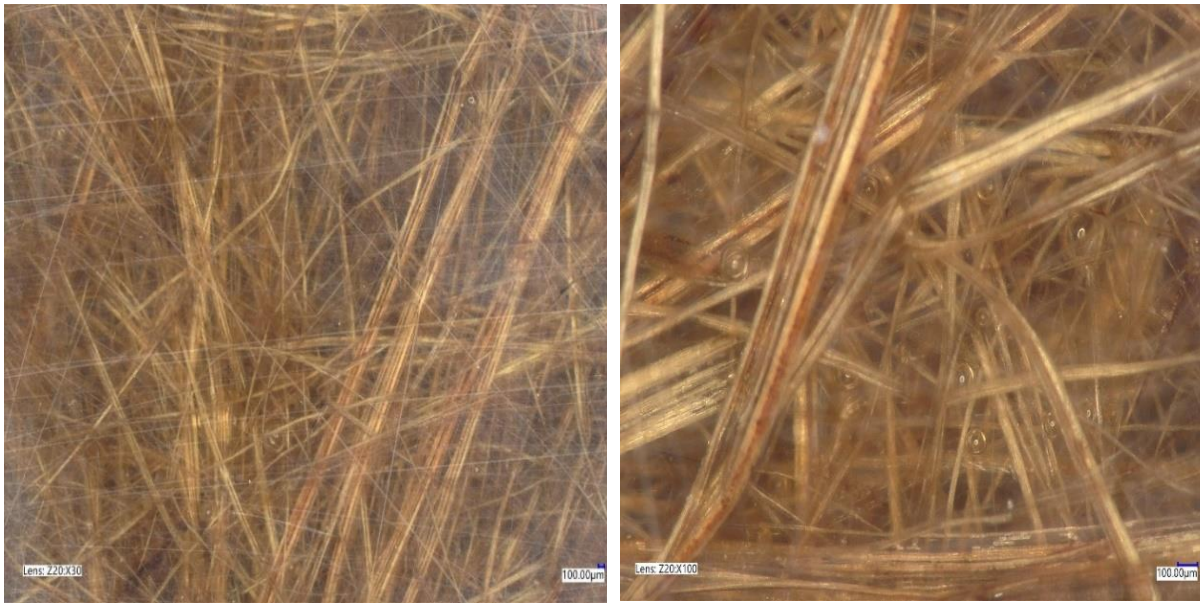

(a) (b)

Figure 5.31 Microscopic images of cattail composite – (a) 30X magnification and (b) 100X magnification; manufactured at VARTM pressure.

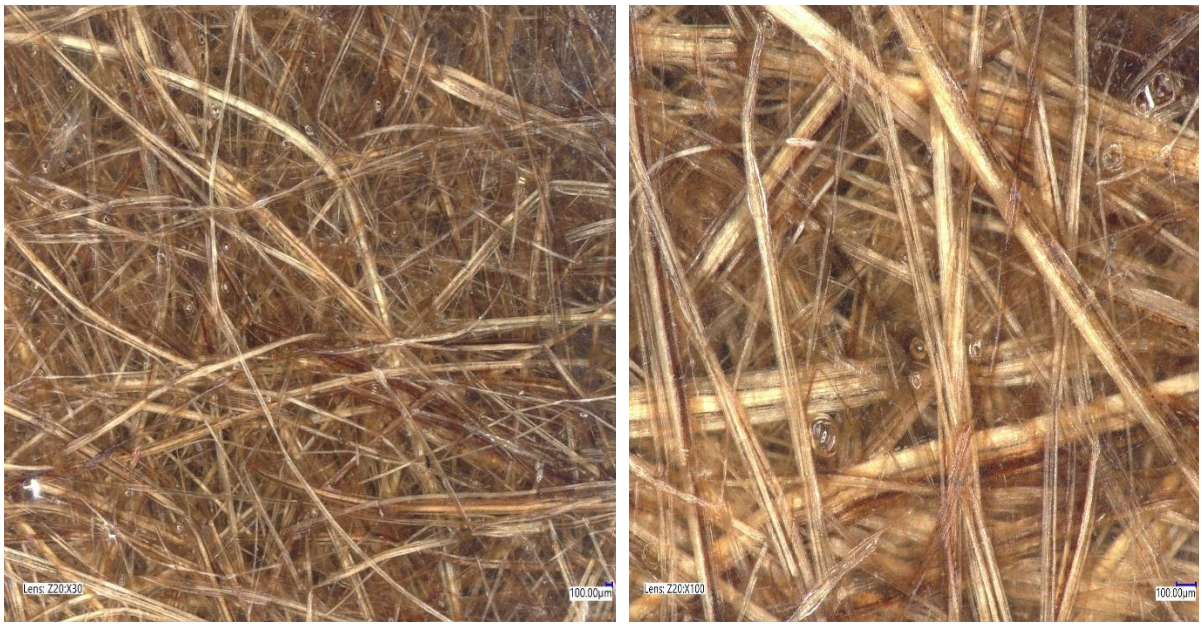

(a) (b)

Figure 5.32 Microscopic images of cattail composite – (a) 30X magnification and (b) 100X magnification; manufactured at 260 kPa molding pressure.

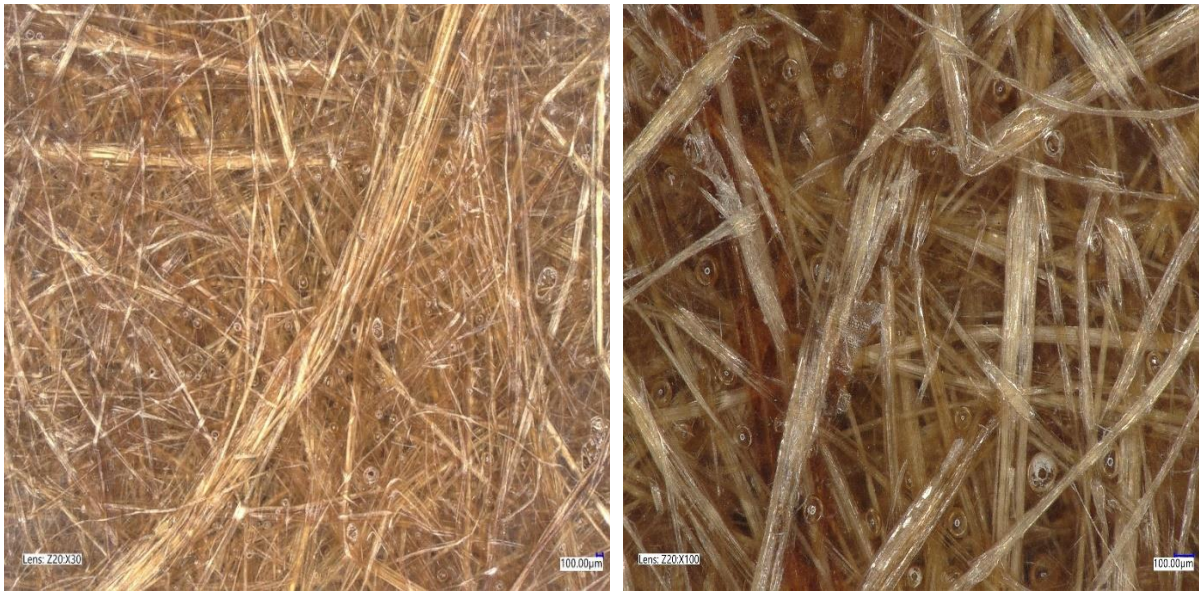

(a) (b)

Figure 5.33 Microscopic images of cattail composite – (a) 30X magnification and (b) 100X magnification; manufactured at 260 kPa molding pressure.

5.7.8 Scanning Electron Microscopy (SEM)

The scanning electron microscopy of cattail fiber is shown in Figure 5.34. The rectangular calcium oxalate plates and pit areas (without oxalate plates) can be seen all over the fiber surface (Witztum & Wayne, 2014, 2015; Yu & Rahman, 2020. These plates lie in the longitudinal direction and their length and width are different.

Since cattail is a novel fiber, the major objective of conducting the SEM is to find out the adhesion between fiber and resin in a composite structure. The cattail fibers from the composite fracture surface show that the fibers are covered by the resin (Figure 5.35) as no oxalate plates can be seen as in the virgin cattail fiber in Figure 5.34. The adhesion between the fiber and resin is clearly shown in Figure 5.36 and 5.37 as well as the fiber hollowness in the centre. Due to this hollowness, the density of the cattail fiber (Table 5.6) is much lower than that of other bast fibers.

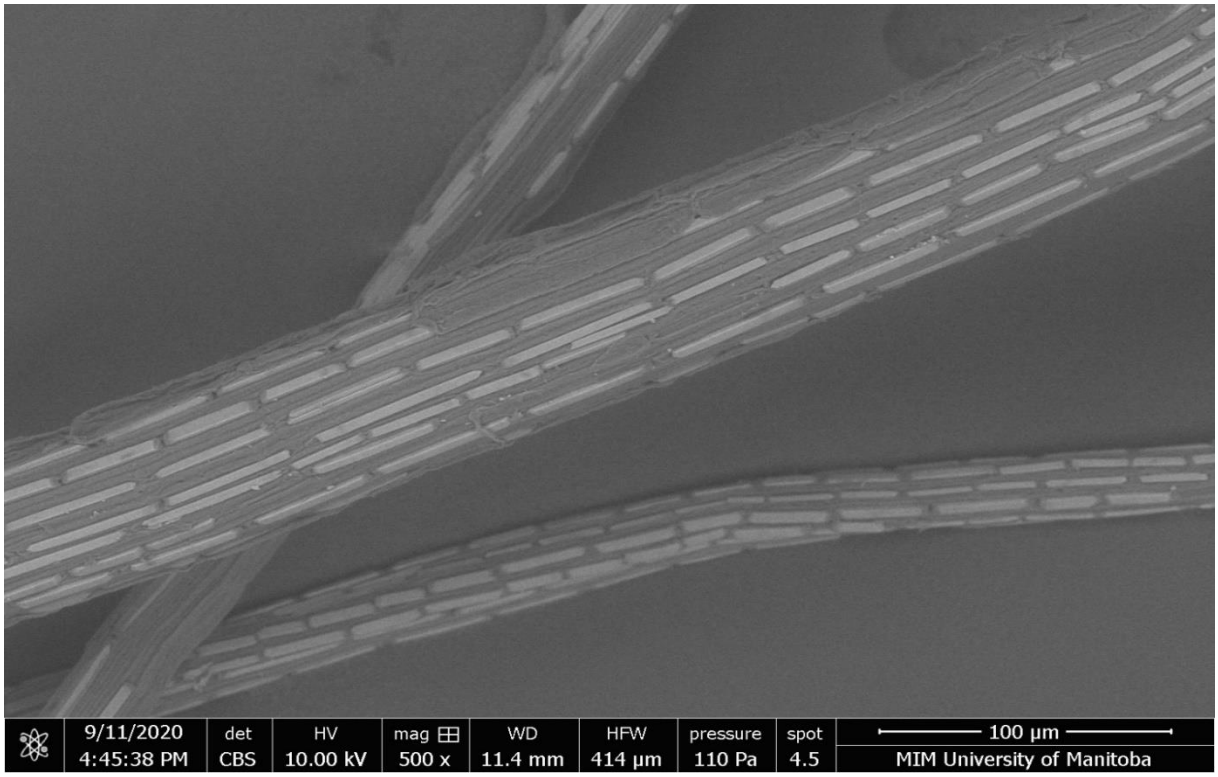

Figure 5.34 Scanning electron microscopy of cattail fibre (chemically extracted, Yu and Rahman, 2020)

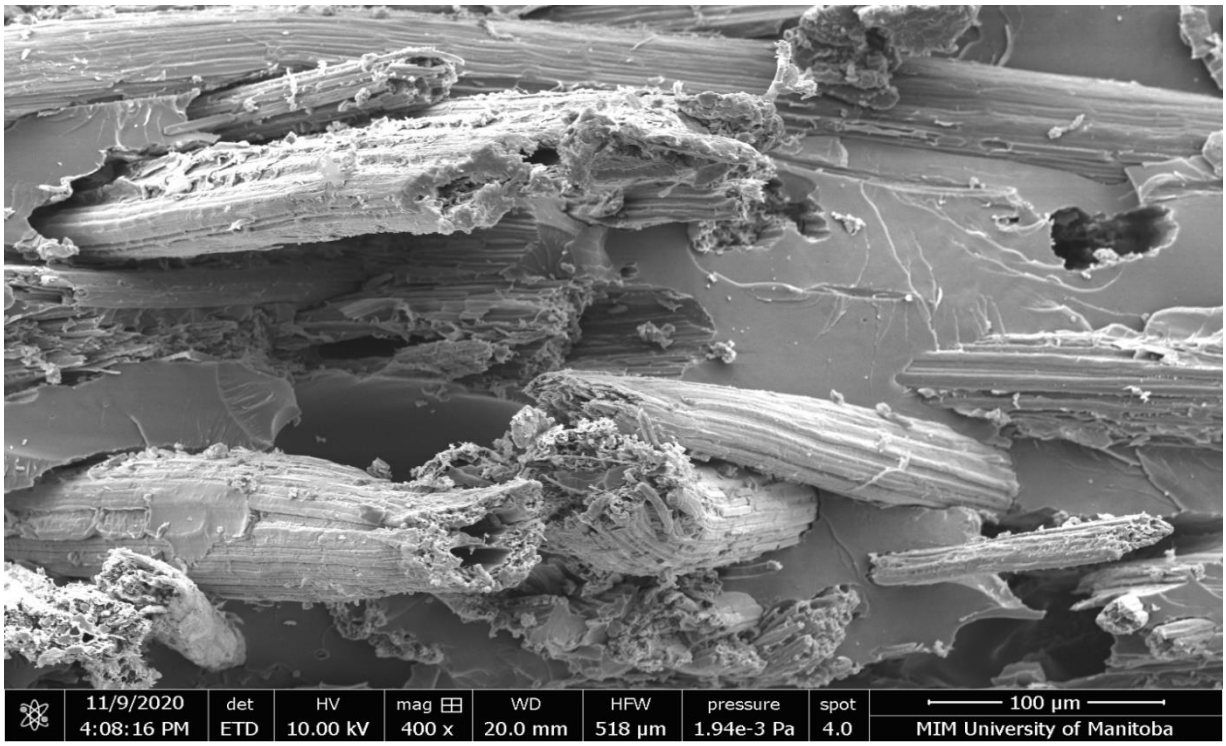

Figure 5.35 Scanning electron micrograph of fracture surface for cattail composite (560 kPa).

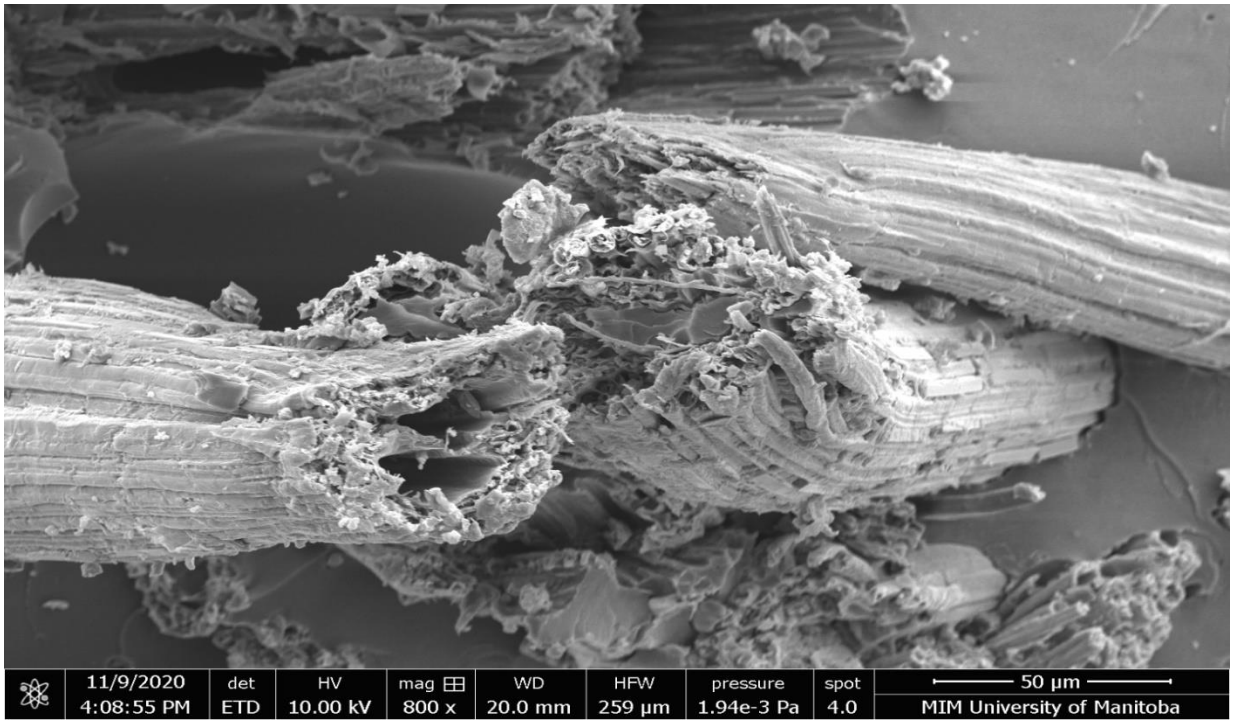

Figure 5.36 Scanning electron micrograph of fracture surface for cattail composite (560 kPa) showing fiber covered with resin.

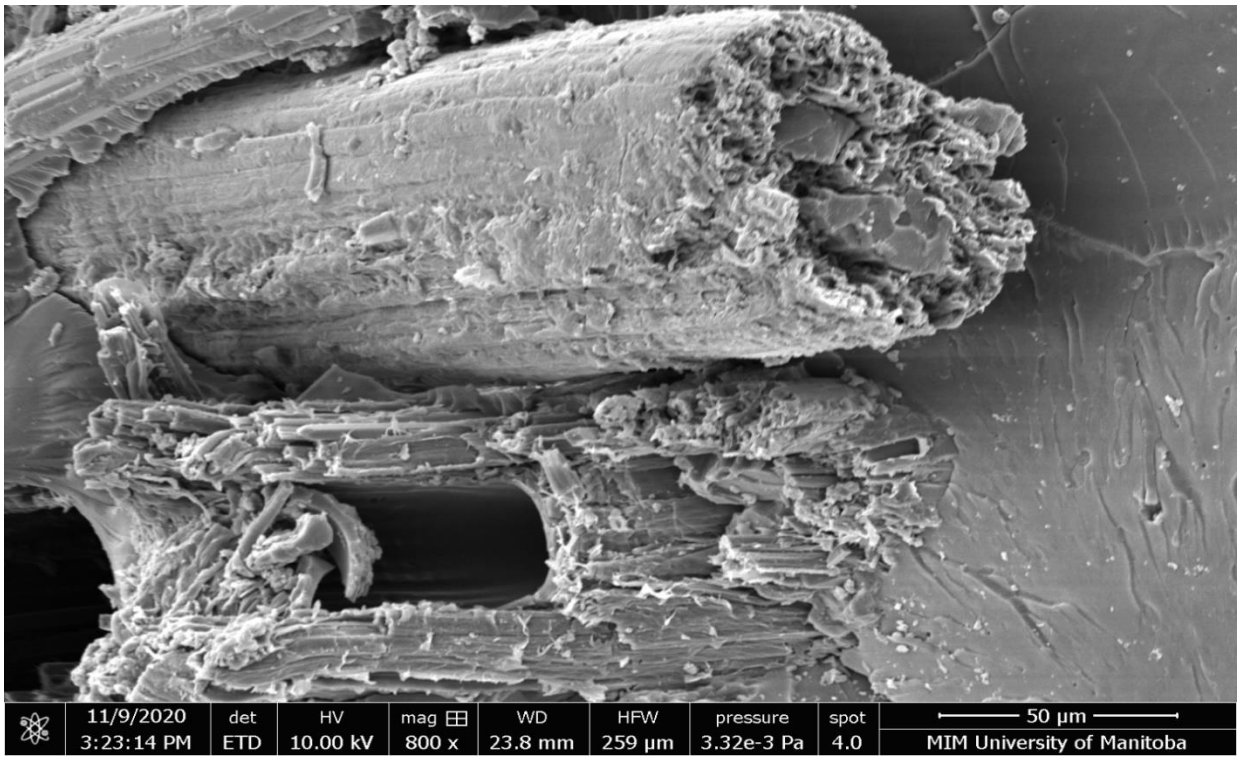

Figure 5.37 Scanning electron micrograph of fracture surface for cattail composite (260 kPa) showing fiber covered with resin.

The fracture surface of the cattail composites shows numerous empty fiber regions with different dimensions due to the tension loading (Figure 5.38). The different sizes of the empty fiber regions indicate the presence of fiber with different which has already been reported (Rahman, et al, 2020). The serrated structure of the empty fiber regions (Figure 5.36) is due to the fiber adhesion with the matrix, particularly of the calcium oxalate plates. The pull out fibres with different dimensions can also be seen in this micrograph. The fracture surface of the pull out fibers is fibrillar in nature (Figure 5.37) and the debonding distance (crack between matrix and pull out fiber) is less than 1.23 µm (Figure 5.36).

While most of the pull out fibers show a fibrillar nature and hollowness in the centre, the tip of the few pull out fibres is covered with resin which is more common in the treated fiber composite (Figure 5.40) than in the untreated fiber composite (Figure 5.39). This is due to the fiber pulling out of the composite structure instead of breakage. The matrix surface in all

composites shows a ‘wrinkly effect’ and since the strength of fibre along the length is variable, the fiber is able to break some distance from the ‘wrinkly matrix’ and after composite breakage the fibers show pull out effect. It is worth mentioning here that no such wrinkle effect was observed when the surface of the cattail composites was observed (Figures 5.31-5.32).

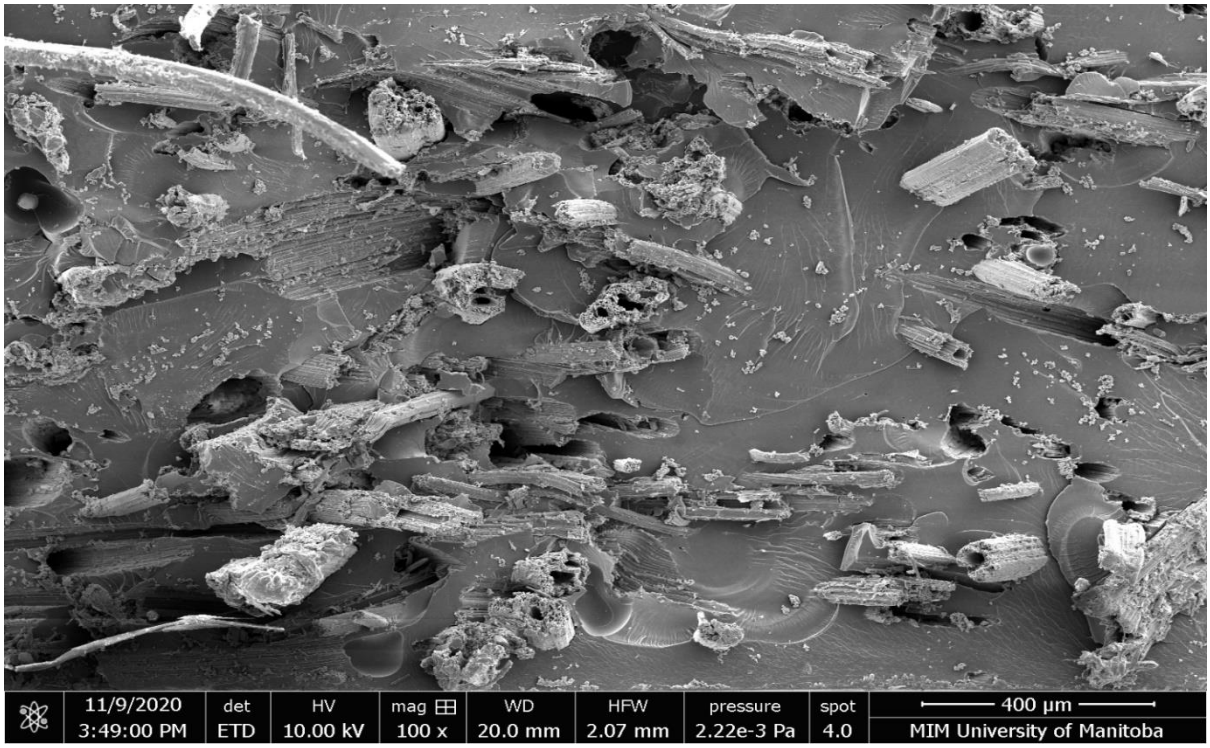

Figure 5.38 Scanning electron micrograph of fracture surface for cattail composite (260 kPa) showing empty fiber regions.

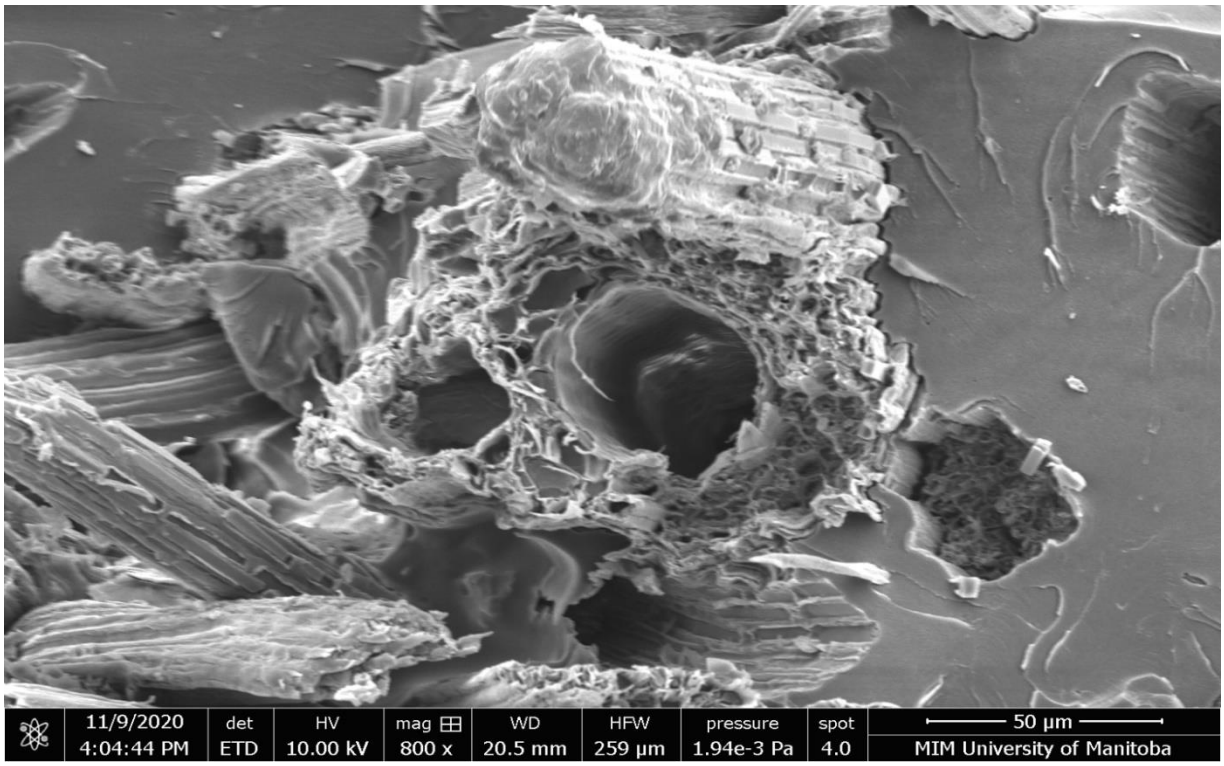

Figure 5.39 Tip end of fiber covered with resin (560 kPa).

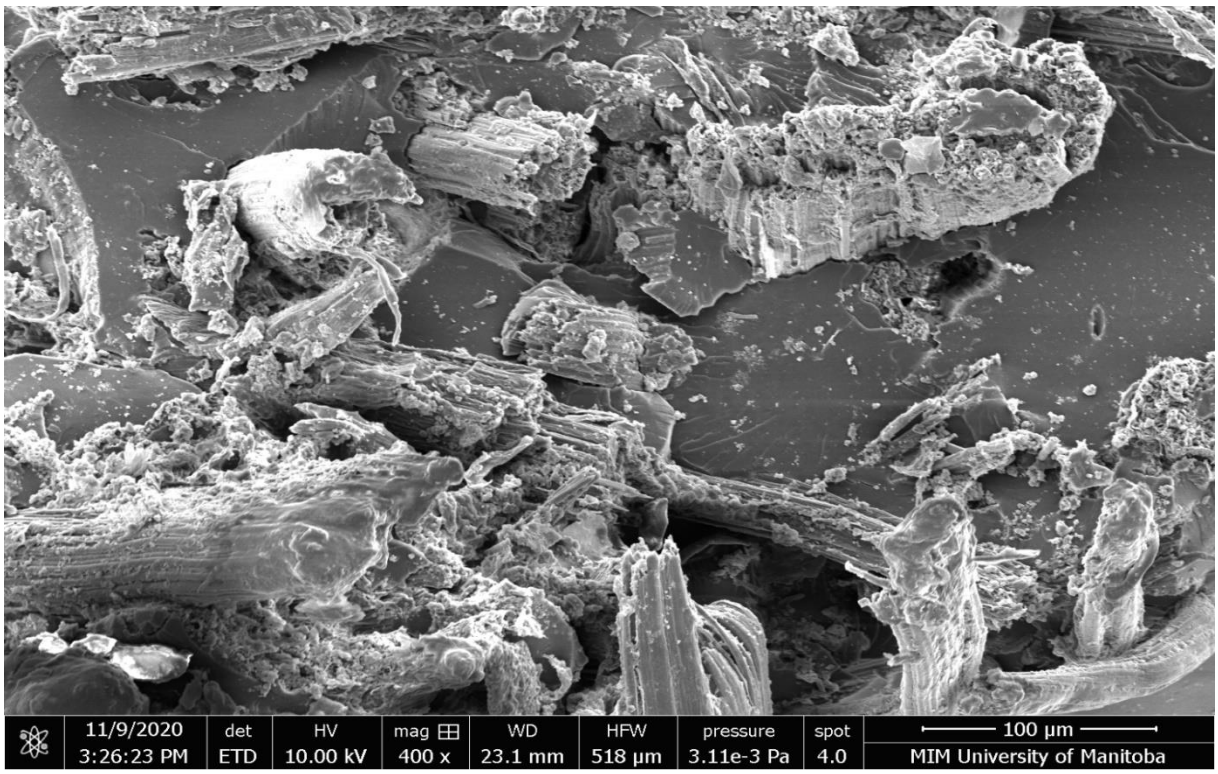

Figure 5.40 Tip end of fiber covered with resin (260 kPa – treated fiber).

CHAPTER VI

COMPARITIVE ANALYSIS

This chapter has three sections. A brief comparison of properties of cattail, flax, and hemp fibers that were used to make nonwoven mats. Effect of mat manufacturing parameters on the mat properties is analysed for mats with three different fibers. Mechanical properties of flax, cattail, flax-hemp, and hemp composite manufactured using zero punched mat is compared. Finally, a brief comparison was caried out between flax and hemp composite manufactured from needle punched mat. The properties of hemp fiber, needle punched hemp mat, and hemp composite is taken from Fahimian (2013) for comparison.

6.1 FIBER PROPERTIES

Table 6.1 summarizes the physical and mechanical properties of flax, hemp, and cattail fibers. The properties for cattail and flax have been measured during the current study while the hemp fiber properties obtained from Fahimian (2013). The tensile strength of cattail fiber is similar to flax and hemp fiber. However, tensile modulus of hemp fiber is higher than that of flax and cattail fiber and strain at break percentage of cattail is less than that of flax fiber. A similar trend of modulus and strain is also observed in the mechanical properties of flax, hemp, and cattail composite. Cattail fiber is finer and lighter than the flax and hemp. Further, cattail fiber can be obtained from waste sources and fiber yield percentage is much higher than the flax and hemp. Perhaps the most important advantage of cattail fiber is the much less greenhouse gas emission than that of flax and hemp if the fiber can be obtained from the naturally growing areas. Despite having similar tensile strength in all three fibers, cattail fibers possess higher specific strength than flax and hemp due to lower density values of cattail fiber; however, specific modulus

followed the same trend observed for tensile modulus ($E_{flax} < E_{cattail} < E_{hemp}$); it should be noted that the weight of the composite part decreases with increase in specific properties of the fiber.

Table 6.1 Physical and mechanical properties of flax, hemp, and cattail fiber.

Parameters	Flax	Hemp	Cattail
Length (cm)	6.64 (2.3)	0.4 - 21 [a]	6.98 (1.2)
Diameter (μm)	80.2 (32.7)	138.3 (31.9) [a]	32.1 (8.6)
Density (gm/cm^3)	1.49 (0.004)	1.57 (0.003)	1.39 (0.005)
Tensile strength (MPa)	180.1 (126.1)	172.1 [a]	172.3 (99.3)
E - Modulus (GPa)	11.3 (10.7)	28.5 [a]	18.1 (9.7)
Specific strength	120.87	110.32	123.96
Specific modulus	7.58	18.27	13.02
Strain at break (%)	3.1 (1.5)	-	1.8 (1.4)

[a] Fahimian, 2013

6.2 NONWOVEN MAT PROPERTIES

The physical properties of all nonwoven mats investigated on this study is summarised in Table 6.2. These include flax, cattail, and flax-hemp hybrid mat. Fahimian (2013) studied the properties of zero punched and needle punched hemp mat. However, Fahimian (2013) measured the transverse permeability of hemp mat using water whereas transverse permeability of flax, cattail, and flax-hemp mat was evaluated using air in this study. Hence, the difference in permeability results are expected while using two different media. So, to compare the results flax, cattail, and flax-hemp mat, the transverse permeability of zero punched hemp mat was also investigated in this study (Table 6.2).

Needle punched flax mat exhibited much higher deviation in areal density than that of any other zero punched nonwoven mat manufactured in this study. Highest mat thickness was observed in zero punched cattail mat thus resulting in lower V_f when compared to zero punched flax, hemp, and flax-hemp mat (Table 6.2), which is believed to be due to longer fiber length. Transverse permeability of cattail mat was found higher than that of flax mat with similar V_f and higher than that of hemp mat with slightly higher V_f.

Table 6.2 Physical, properties of nonwoven cattail, flax, hemp, and flax-hemp hybrid mat.

Mat content	Needle punch density (p/cm^2)	Areal density of mat (g/m^2)	Mat thickness before consolidation (mm)	Fiber volume fraction in mat, Vf %	Transverse Permeability x 10^{-11} (m^2)
100% Cattail	0	913.5 (52.8)	19.1 (1.6)	3.5 (0.4)	5.2 (0.5)
100% Hemp	0	941.3 (17.9)[a]	12.5 (3.1) [a]	6.6 (1.6) [a]	2.8 (0.07)[b]
50% Flax-50% Hemp	0	993.3 (14.3)	13.9 (0.5)	4.7 (0.2)	2.3 (0.2)
100% Flax	0	931.1 (67.1)	16.3 (0.7)	3.8 (0.2)	2.5 (0.04)
100% Flax	20	814.7 (88.3)	4.6 (0.3)	11.6 (0.7)	0.4 (0.05)
100% Flax	30	823.6 (97.4)	4.7 (0.5)	11.4 (1.4)	0.5 (0.01)
100% Flax	72	885.2 (108.5)	6.8 (0.4)	8.7 (1.4)	0.9 (0.3)

[a] Fahimian, 2013; [b] Transverse permeability of hemp mat measured using air flow.

6.3 COMPARISON AMONG MECHANICAL PROPERTIES OF ZERO PUNCHED MAT COMPOSITE

6.3.1 Stress-strain behavior

Figure 6.1 and Figure 6.2 shows the stress – strain behaviour of zero punched flax, cattail, and flax-hemp hybrid mat composite manufactured at 260 kPa and 560 kPa respectively. Cattail, flax, and flax-hemp fibers reinforce the pure resin significantly. At both 260 and 560 kPa

manufacturing pressure, cattail and treated cattail mat composite exhibited steeper stress-strain curve than flax and flax-hemp hybrid mat composite indicating higher stiffness and higher degree of reinforcement. However, cattail mat exhibited a poor strain to failure than flax and flax-hemp hybrid mat composite. Zero punched flax composite exhibited highest strain at fracture value at all consolidation pressure.

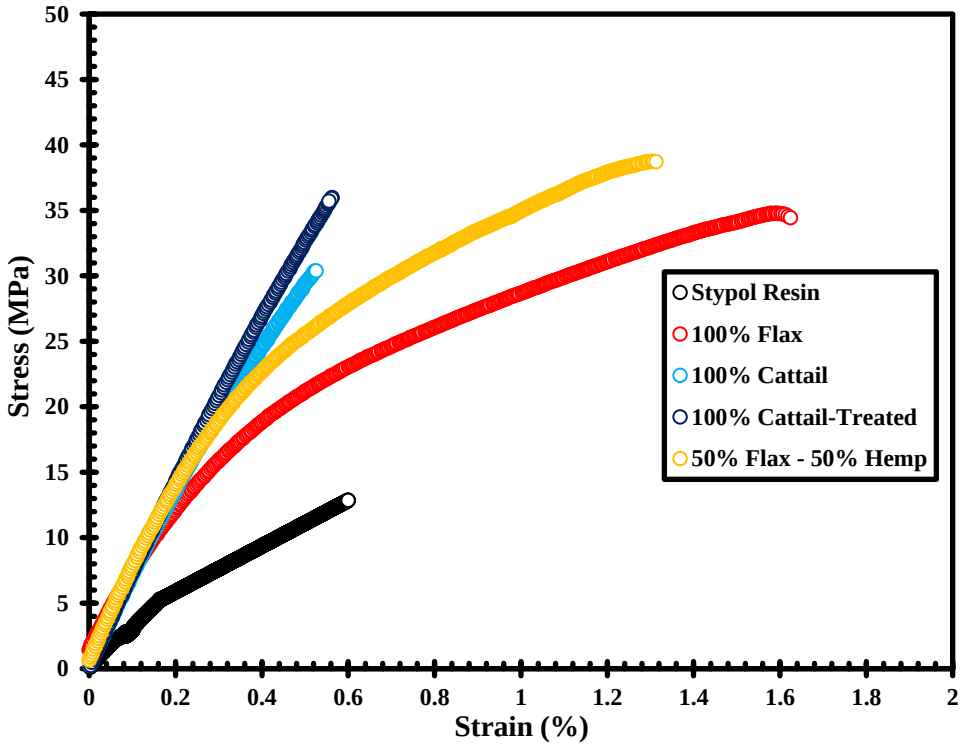

Figure 6.1 Stress-strain behavior of flax, cattail, and flax-hemp hybrid mat composite manufactured at 260 kPa.

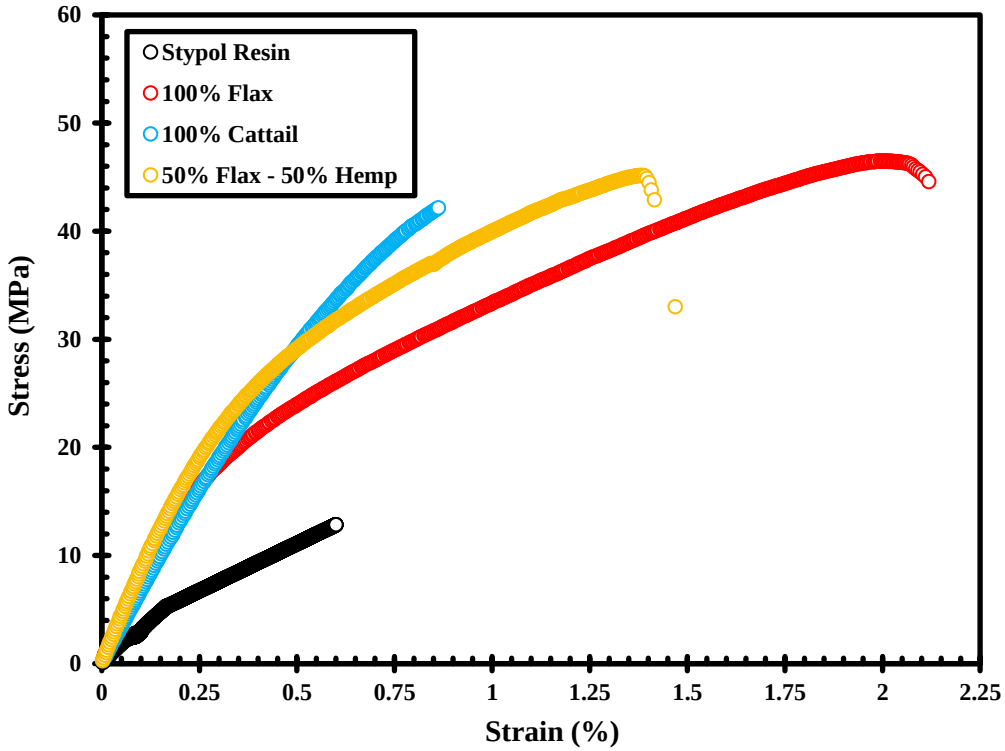

Figure 6.2 Stress-strain behavior of flax, cattail, and flax-hemp hybrid mat composite manufactured at 560 kPa.

6.3.2 Tensile modulus and tensile strength

The measured fiber volume fraction of various (flax, cattail, hemp, flax-hemp) zero punched mat composite at different consolidation pressure is tabulated in Table 6.3. Also, the percentage of V_f is plotted as a function of average experimental tensile modulus value of each composite in Figure 6.3. The experimental values of zero punched hemp mat composite have been taken from Fahimian (2013) for comparison.

Zero punched hemp composite achieved much higher V_f % (Table 6.3) at 260 and 560 kPa than that of zero punched flax, cattail, and flax-hemp mat composite. For a given fiber volume fraction, composites manufactured using the three fibers exhibited similar modulus at 101 kPa. With increased in compaction pressure, the consolidation level differs with fiber type, resulting in differing V_f and modulus. At 260 and 560 kPa, the modulus of cattail fiber composites is higher than that of flax but less than that of flax-hemp fiber composites due to higher modulus of 100% hemp fiber composites.

The tensile strength of flax and flax-hemp composite increased with the increase in V_f (%) as shown in Figure 6.4. At 101 kPa, the tensile strength of composites manufactured with three fibers are similar. With increased in compaction pressure, the consolidation level differs with fiber type, resulting in differing V_f and strength. At 260 kPa, the hemp fiber composites exhibited the highest strength due to higher V_f. The other composites had similar V_f, with cattail fiber composites exhibiting the higher strength. At 560 kPa, the strength of cattail and hemp fiber composites decreased (when compared to the values at 260 kPa), the reason for which is not known at this time. The strength of flax and flax-hemp fiber composites increased when the pressure was increased from 260 to 560 kPa due to marginal increase in V_f.

Table 6.3 Fiber volume fraction of flax, hemp, cattail, and flax-hemp mat composite manufactured at different pressure.

Mat content	Consolidation pressure (kPa)	V_f (%) of composite
100% Flax	101	11.2
100% Flax	260	26.9
100% Flax	560	32.6
100% Cattail	101	10.9
100% Cattail	260	30.4
100% Cattail	560	26.1
50% Flax - 50% Hemp	101	11.7
50% Flax - 50% Hemp	260	23.5
50% Flax - 50% Hemp	560	32.1
100% Hemp	101	12.5 [a]
100% Hemp	260	42.5 [a]
100% Hemp	560	47 [a]

[a] Fahimian, 2013

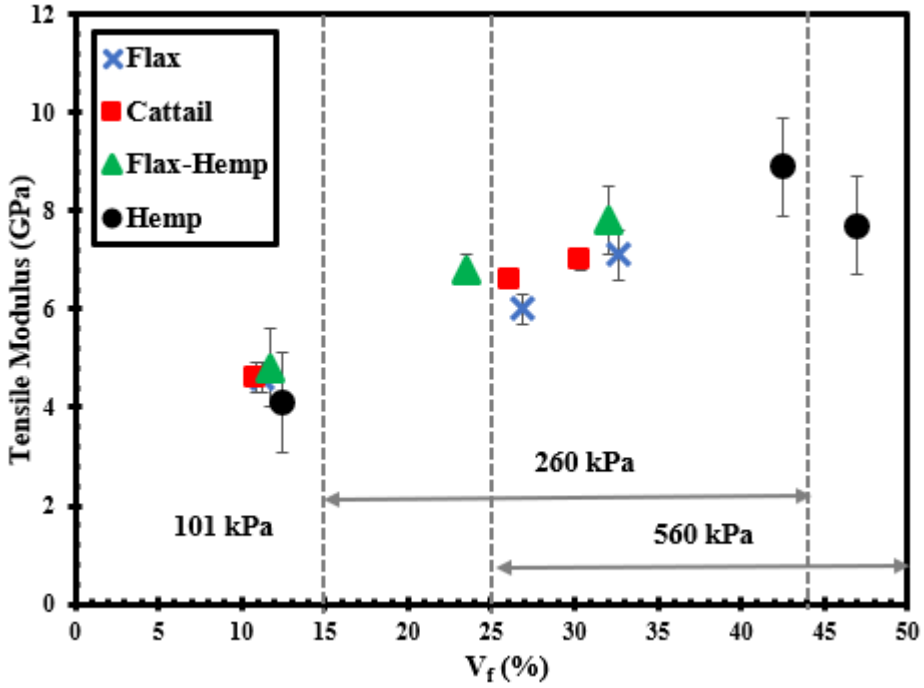

Figure 6.3 Relationship between V_f and experimental tensile modulus of zero punched mat composite.

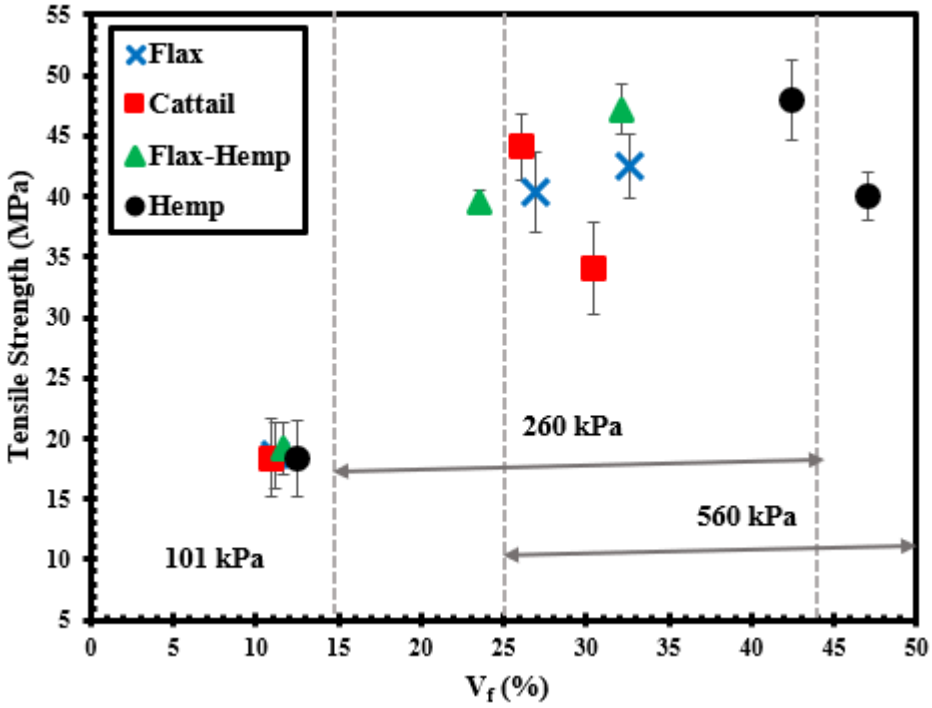

Figure 6.4 Relationship between V_f and experimental tensile strength of zero punched mat composite.

6.4 COMPARISON OF NEEDLE PUNCHED FLAX AND HEMP MAT COMPOSITES

The experimental longitudinal tensile modulus value of flax composite manufactured from needle punched mat having 20, 30, and 72 punches/cm^2 needle punching density are listed in Table 6.4 along with the corresponding experimental longitudinal tensile modulus value of 7-P, 30-P, and 70-P needle punched hemp composite for comparison. Experimental longitudinal tensile modulus value of needle punched hemp composite were taken from Fahimian (2013).

The Table 6.4 appears difficult to read for comparison as V_f is varying at all pressure and punch density for both flax and hemp; hence, tensile modulus of needle punched flax and hemp mat composite is plotted as a function of V_f and presented in Figure 6.5 for comparison. Longitudinal modulus of needle punched flax and hemp fiber composites at VARTM pressure (101 kPa) increased with the increase in punch density from 0 to 30 P/cm^2. Hemp composite exhibited much higher longitudinal modulus value at VARTM pressure for 7-P and 30-P than that of 20-P and 30-P flax composite despite having lower V_f % for 7-P hemp composite. At 260 kPa and 560 kPa manufacturing pressure, both V_f and longitudinal modulus of 30-P and 70-P hemp composite was higher than that of 30-P and 72-P flax composite respectively. Although gradual increase in Vf was observed in 7-P hemp composite when pressure increased from 101 to 260 and 560 kPa; surprisingly modulus of 7-P hemp composite was less both in 260 and 560 kPa pressure compared to VARTM pressure. However, longitudinal modulus of 20-P flax composite increased or decreased followed by an increase or decrease in V_f % with the change in consolidation pressure.

Table 6.4 Longitudinal tensile modulus of needle punched flax and hemp composite.

100% Flax				100% Hemp			
Needle Punch density	Pressure (kPa)	V_f (%)	Longitudinal modulus (GPa)	Needle Punch density	Pressure (kPa)	V_f (%)	Longitudinal modulus (GPa)
20	101	15.6	4.9 (0.2)	7	101	13.9	6.8 (0.2) [a]
20	260	25.8	6.1 (0.8)	7	260	22.5	4.3 (0.5) [a]
20	560	22.5	5.6 (0.5)	7	560	35.5	5 (0.4) [a]
30	101	20.9	5.9 (0.5)	30	101	25	8.2 (0.2) [a]
30	260	25	6.9 (0.5)	30	260	31	7.5 (0.4)
30	560	23.6	6 (0.4)	30	560	39	9.4 (0.5) [a]
72	101	18.1	5.9 (0.3)	70	101	20	4.9 (0.3) [a]
72	260	24.7	6.2 (0.2)	70	260	32.5	9.5 (2.5) [a]
72	560	31.5	8 (0.7)	70	560	39	9.7 (0.4) [a]

[a] Fahimian, 2013

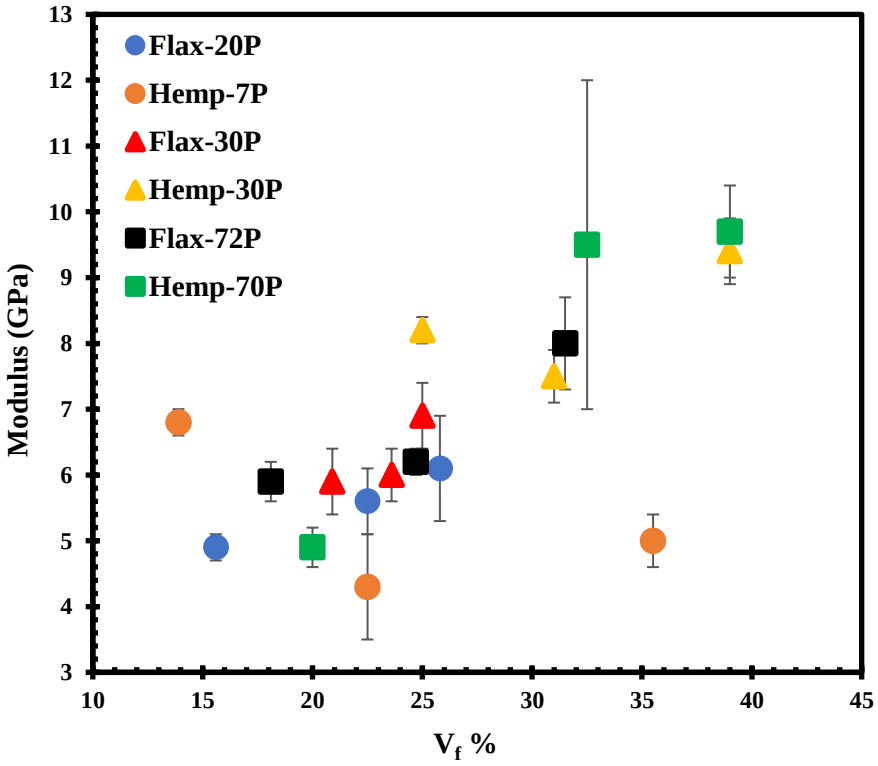

Figure 6.5 Relationship between V_f and modulus of flax and hemp composites at various punch density.

CHAPTER VII

CONCLUSION

The goal of this thesis was to perform a comparative evaluation of properties of discontinuous natural fiber composites manufactured using flax, hemp, and cattail fibers. The three objectives identified in Chapter 2 to realize this goal have been successfully executed.

In this study, flax fibers were bound by needle punching process to manufacture nonwoven mats. The needle punching density, depth of needle penetration, and areal density of flax mat were varied that resulted in different mat structure with different thickness, fiber volume fraction, and permeability. The effect of these variations on the composite properties was studied. Cattail fiber were extracted from leaves, tested for mechanical properties, and surface treated to improve the bonding with the polymer matrix. Similar to flax, cattail mat composite was manufactured using VARTM and compression molding pressures; nonwoven cattail mat was restricted to zero punch. Zero punch cattail mat was prepared in the laboratory using a mini carding machine and a customized fiber lay-up mold. Same method was followed to manufacture zero punch flax, and zero punch flax-hemp hybrid mat. Effect of consolidation pressure on composite properties such as fiber volume fraction, tensile strength, and tensile modulus was investigated. Finally, a detailed comparison of fiber, mat, and composite properties was made for flax, cattail, and hemp fibers.

7.1 SUMMARY AND CONCLUSIONS

A summary of results and conclusion based on these results are presented below.

1. Conclusions based on tasks completed to realize Objective 1:

- Flax fiber mechanical properties increased with decrease in diameter and the length and diameter of fibers in the mat showed a distribution.

- Increase in needle punch density decreased the thickness of the flax mat and increased the V_f in the mat.

- The out-of-plane permeability of flax mat decreased with increase in punch density, for a given needle depth, due to decrease in percenatge of void fraction. While the magnitude of consolidation during composite manufacturing decreased with increase in punch density due to the increase in V_f of the mat with punch density. This along with the variation of V_f in the starting mat, resulted in complex variation in the V_f in the final composite. For example, at 101 kPa, the V_f in the composite increased with punch density while the opposite trend was observed at 260 kPa. Only mats with loosely bound fibers, such as 0-P and 72-P, exhibited a higher V_f at 560 kPa when compared to that at 260 kPa.

- Higher needle punch density resulted in higher modulus and strength in flax fiber composites at pressures < 260 kPa and lower needle punch densities resulted in higher strength and modulus at pressures > 260 kPa.

- The modulus and strength of composites manufactured using the 0-P 50% Flax-50% Hemp fiber mat, increased with increase in consolidation pressure due to increase in V_f.

2. Conclusions based on tasks completed to realize Objective 2:

- Cattail fiber exhibited higher yield percentage than that of conventional bast fibers used in composite applications. Similar to flax fibers, the modulus and strength varied with fiber diameter and length. The modulus increased with decrease in fiber diameter. Despite large SD, the average modulus and strength increased with relative humidity until 75% beyond which they decreased, a trend observed in other natural fibers too.

- Similar to that of flax, transverse (out-of-plane) permeability of cattail mat decreased with increase in percentage of void fraction in the mat.

- Similar to flax fiber composites, the modulus and the strength of cattail fiber composite increased with compaction pressure (up to 260 kPa) due to increase in V_f. With further increase in pressure to 560 kPa, the V_f decreased, the modulus decreased slightly and the strength increased. The reason for decrease in V_f is not known at this time.

- Treating the surface of cattail fiber with 5% DIH-HEA resulted in higher modulus and strength than untreated fiber composite, manufactured at 260 kPa, despite having lower V_f. Further optimization on chemical treatment is required in future studies.

3. Conclusions based on tasks completed to realize Objective 3:

- The cattail fibers have a lower density than flax fibers, which in turn have a lower density than hemp fibers.

- While strength of the three fibers are similar, the modulus increases as follows: $E_{flax} < E_{cattail} < E_{hemp}$.

- The specific strength and modulus increases in this order $\sigma_{hemp} < \sigma_{flax} < \sigma_{cattail}$ and $E_{flax} < E_{cattail} < E_{hemp}$; it should be noted that the weight of the composite part decreases with increase in specific properties of the fiber.

1. The transverse permeability of cattail fiber mat is the highest, followed by hemp fiber mat and the flax fiber mat's permeability was the least.

2. At VARTM pressure (101 kPa) the properties of composites with three fibers are similar.

7.2 RECOMMENDATIONS FOR FUTURE WORKS

1. Since the effect of needle punching on the mechanical properties (longitudinal) of flax and flax/hemp composites was established, future work should be conducted on developing a model that could predict the modulus and the strength of needle-punched mat composites. Further, both longitudinal and transverse modulus of elasticity influences the total stiffness of manufactured composite; the transverse mechanical properties of composites should be measured.

2. It was found that the variations in the areal density of the needle punched mats were high that might have contributed to the composite properties. Studies should be conducted to minimize the variation in areal density while manufacturing needle punched non-woven mat.

3. For cattail, only zero punched mat was used to make composites. This would help the researchers explore this novel fiber further for composites and other industrial applications. However, research in this area should be conducted further by using different needle punched non-woven mat.

4. Although DIH-HEA treatment improved the hydrophobicity of fiber, however, this has not contributed to the mechanical properties of cattail composites, perhaps, the increased hydrophobicity was not enough to have a significant impact on the mechanical properties. Therefore, future work should be carried out to optimize the chemical modification that would increase the mechanical properties of cattail composites.

REFERENCES

Ahmed, S. (2017) Mechanical and Surface Properties of Technical and Single Flax Fiber in Micro and Nano Scale, M.Sc. thesis, North Dakota State University, USA).

Akil, H., Omar, M. F., Mazuki, A. A. M., Safiee, S. Z. A. M., Ishak, Z. M., & Bakar, A. A. (2011). Kenaf fiber reinforced composites: A review. *Materials & Design, 32*(8-9), 4107-4121.

Ali, A. (2013). Surface Modification of Hemp Fiber to Improve Spinning Properties. M.Sc. thesis, University of Manitoba.

Alzeer, M., & MacKenzie, K. (2013). Synthesis and mechanical properties of novel composites of inorganic polymers (geopolymers) with unidirectional natural flax fibres (phormium tenax). Applied Clay Science, 75, 148-152.

Andersons, J., Sparniņs, E., Joffe, R., & Wallstrom, L. (2005). Strength distribution of elementary flax fibres. Composites science and technology, 65(3-4), 693-702.

Andre, N.G., Ariawan, D., & Mohd Ishak, Z. A. (2017). Mechanical properties and micromechanical analysis of nonwoven kenaf fibre/epoxy composites produced by resin transfer moulding. *Journal of Composite Materials*, 51(13), 1875-1885.

Arbelaiz, A., Fernandez, B., Ramos, J. A., Retegi, A., Llano-Ponte, R., & Mondragon, I. (2005). Mechanical properties of short flax fibre bundle/polypropylene composites: Influence of matrix/fibre modification, fibre content, water uptake and recycling. Composites science and technology, 65(10), 1582-1592.

ASTM (2020). ASTM D 3822: Standard Test Method for Tensile Properties of Single Textile Fibers, ASTM International, West Conshohocken, PA 19428-2959. United States.

Averink, J. 2015. Global Water Footprint of Industrial Hemp Textile, Water Engineering and Management, University of Twente, Enschede, Nederland, https://essay.utwente.nl/68219/1/Averink,%20J.%200198501%20openbaar.pdf (accessed through internet, August 13, 2020).

Baley, C. (2002). Analysis of the flax fibers tensile behaviour and analysis of the tensile stiffness increase. Composites Part A: Applied Science and Manufacturing, 33(7), 939-948.

Baran, G. R., Mccool, J. I., Boberick, K. G., & Zhang, H. (1999). Size effect in resin/glass composite flexure strengths. Journal of oral rehabilitation, 26(10), 775-780.

Barsoum, M. W. (2019). Fundamentals of ceramics. CRC press.

Beckermann, G.W., Pickering, K.L. (2009). Engineering and evaluation of hemp fibre reinforced polypropylene composites. Composites Part A, 40:210–7.

Bharath, K. N., & Basavarajappa, S. (2016). Applications of biocomposite materials based on natural fibers from renewable resources: a review. *Science and Engineering of Composite Materials*, 23(2), 123-133.

Biswas, S., Kindo, S., & Patnaik, A. (2011). Effect of fiber length on mechanical behavior of coir fiber reinforced epoxy composites. *Fibers and Polymers*, 12(1), 73-78.

Bledzki, A. K., Gassan, J. (1999). Composites reinforced with cellulose based fibres, Prog. Polym. Sci. 24, 221–274.

Canadian Encyclopedia, The (n.d.). Wetlands, https://www.thecanadianencyclopedia.ca/en/article/wetlands, retrieved March 18, 2019.
Canola Council of Canada (n.d.). Industry Overview, https://www.canolacouncil.org/markets-stats/industry-overview/, retrieved March 18, 2019.

Chabros, A., & Gawdzik, B. (2019). Methacrylate monomer as an alternative to styrene in typical polyester–styrene copolymers. Journal of Applied Polymer Science, 136(27), 47735.

Chakma, K., Rahman, M. (2018). “Extraction efficiency, quality and characterization of Typha latifolia L. fibres for textile applications.” Masters thesis, University of Manitoba, 2018.

Charlet, K., Baley, C., Morvan, C., Jernot, J. P., Gomina, M., & Bréard, J. (2007). Characteristics of Hermès flax fibres as a function of their location in the stem and properties of the derived unidirectional composites. Composites Part A: Applied Science and Manufacturing, 38(8), 1912-1921.

Charlet, K., Jernot, J.P., Gomina, M., Bréard, J., Morvan, C., Baley, C. (2009). Influence of an Agatha flax fibre location in a stem on its mechanical, chemical and morphological properties, Composite Science and Technology, 69, 1399-1403.

Charlet, K., Baley, C., Morvan, C., Jernot, J. P., Gomina, M., & Bréard, J. (2007). Characteristics of Hermès flax fibres as a function of their location in the stem and properties

of the derived unidirectional composites. *Composites Part A: Applied Science and Manufacturing*, *38*(8), 1912-1921.

Chawla, K. K. (2012). Composite materials: science and engineering. *Springer Science & Business Media*. p. 378-381.

Chawlaw, N and Kerr, M. (2005). Monotonic and Cyclic Fatigue Behavior of High-Performance Ceramic Fibers, Journal of American Chemical Society, 88 (1), 101-108.

Chekurthi, S. (2018). "Fracture criterion to predict strain-rate dependent failure of unidirectional carbon fiber composites under multi-axial state of stress." Masters thesis, University of Manitoba, Winnipeg, Canada. http://hdl.handle.net/1993/32961

Cristaldi, G., Latteri, A., Recca, G., & Cicala, G. (2010). Composites based on natural fibre fabrics. *Woven fabric engineering*, *17*, 317-342.

Cook JG. (1984). Handbook of textile fibers. Shildon: Merow, 1984. p. 35-73.

Collier, B.J., Epps, H.H. (1999). Textile Testing and Analysis, Prentice Hall Inc, New Jersey, USA.

Dao M and Asaro R., (1999). A study on the failure prediction and design criteria for fibre composites under fire degradation. Compos A: Appl, 30: 123–131.

Davallo, M., Pasdar, H., & Mohseni, M. (2010). Mechanical properties of unsaturated polyester resin. International Journal of ChemTech Research, 2(4), 2113-2117.

Davis, G.C., and Bruce, D.M. (1998). Effect of Environmental Relative Humidity and Damage on the Tensile Properties of Flax and Nettle Fibers, Textile Research Journal, 68(9), 623-629.

de Beus, N., Carus, M., Barth, M (2019)."Carbon Footprint and Sustainability
of Different Natural Fibres for Biocomposites and Insulation Material." MSc Thesis, Nova Institute, accessed through internet at http://eiha.org/media/2019/03/19-03-13-Study-Natural-Fibre-Sustainability-Carbon-Footprint.pdf.

Dev, V. G., & Dhanakodi, A. K. P. (2018). Studies on mechanical properties of thermoplastic composites prepared from flax-polypropylene needle punched nonwovens. *Science and Engineering of Composite Materials*, 25(3), 489-499.

Djeghader, D., Redjel, B. (2019). Effect of water absorption on the Weibull distribution of fatigue test in jute-reinforced polyester composite materials, Advanced Composites Letters, 28: 1–11.

Duval, A., Bourmaud, A., Augier, L., & Baley, C. (2011). Influence of the sampling area of the stem on the mechanical properties of hemp fibers. Materials Letters, 65(4), 797-800.

Ebskamp, M. J. M. 2002. Engineering flax and hemp for an alternative to cotton. *Trends in Biotechnology* 20: 229–230. doi:10.1016/S0167-7799(02)01953-4.

Euliss, N. H., Gleason, R. A., Olness, A. et al. (2006). North American prairie wetlands are important nonforested land-based carbon storage sites. *Science of the Total Environment*, 361(1-3): 179-188. https://doi.org/10.1016/j.scitotenv.2005.06.007.

Facca, A. G., Kortschot, M. T., & Yan, N. (2006). Predicting the elastic modulus of natural fibre reinforced thermoplastics. *Composites Part A: Applied Science and Manufacturing*, 37(10), 1660-1671.

Fahimian, M. (2013). "Processing-Structure-Property Relationship in Needle-Punched Nonwoven Natural Fibre Mat Composites." PhD diss., University of Manitoba, Winnipeg, Canada. http://hdl.handle.net/1993/22207

Fan, M., & Weclawski, B. (2017). Long natural fibre composites. In *Advanced High Strength Natural Fibre Composites in Construction* (pp. 141-177). Woodhead Publishing.

Faruk, O., Bledzki, A. K., Fink, H. P., & Sain, M. (2012). Biocomposites reinforced with natural fibers: 2000–2010. *Progress in polymer science*, *37*(11), 1552-1596.

Foulk, J., Akin, D., Dodd, R. (2003). Influence of pectinolytic enzymes on retting effectiveness and resultant fibre properties, *BioResources*, 3(1), 155-169.

Gassan, J., Chate, A., and Bledzki, A. (2001). Calculation of elastic properties of natural fibers, *Journal of Materials Science*, 36, 3715 – 3720.

Ghosh, A., Dever, M., Thomas, H., Tewksbury, C. (1994). Effects of selected fibre properties and needle punch density on thermally-treated nonwoven fabrics, *Indian Journal of Fibre and Textile Research*, 19, 203-208.

Gillies, M. (1979). "Nonwoven Materials: Recent Developments", Noyes Data Corporation Park Ridge, NJ, USA.

Gourier, C., Le Duigou, A., Bourmaud, A., Baley, C. (2014). Mechanical analysis of elementary flax fibre tensile properties after different thermal cycles, *Composites: Part A*, 159-166.

Gurunathan, T., Mohanty, S., Nayak, S. (2015). A review of recent developments in biocomposites based on natural fibres and their application perspectives, *Composites: Part A*, 77, 1-25.

Hargitai, H., Racz, I., & Anandjiwala, R. (2006, June). Development of hemp fibre–PP nonwoven composites. In *Macromolecular symposia* (Vol. 239, No. 1, pp. 201-208). Weinheim: WILEY-VCH Verlag.

Hargitai, H., Rácz, I., & Anandjiwala, R. D. (2008). Development of hemp fiber reinforced polypropylene composites. *Journal of Thermoplastic Composite Materials*, 21(2), 165-174.

Hart, A., Summerscales, J. (2017). Effect of time at temperature for natural fibre, Procedia Engineering, 200, 269 – 275.

Hasan, M. (2019). Optimization of Typha fibre extraction and properties for composite applications using desirability function analysis. University of Manitoba, 2019. http://hdl.handle.net/1993/34381

Hasan, M., Ying, C., Cicek, N. (2019). Desirability Analysis for Optimization of Typha Fibre Extraction and Properties for Composite Applications, CSBE/SCGAB Conference, Vancouver, July 14-17.

Hasan, M. (2019). Optimization of Typha Fibre Extraction and Properties for Composite Applications Using Desirability Function Analysis, M.Sc. thesis, University of Manitoba, Winnipeg, Canada.

Hearle, J.W.S. & Sultan, M.A.I. (1968) A Study of Needled Fabrics. Part V: The Approach to Theoretical Understanding, *Journal of the Textile Institute*, 59:4, 183-201

Hearle, J. W. S. (1972). A theory of the mechanics of needled fabrics. *Needle-felted Fabrics, Textile Trade Press,* Manchester, 51.

Hoa, S. V. (2009). Principles of the manufacturing of composite materials. DEStech Publications, Inc.

Hoareau, W., Trindade, W. G., Siegmund, B., Castellan, A., & Frollini, E. (2004). Sugar cane bagasse and curaua lignins oxidized by chlorine dioxide and reacted with furfuryl alcohol: characterization and stability. *Polymer Degradation and Stability*, 86(3), 567-576.

Ho, M. P., Wang, H., Lee, J. H., Ho, C. K., Lau, K. T., Leng, J., & Hui, D. (2012). Critical factors on manufacturing processes of natural fibre composites. *Composites Part B: Engineering*, *43*(8), 3549-3562.

Hoekstra, A. Y. (2013). The water footprint of modern consumer society. London, UK: Routledge.

Hughes, M. (2012). Defects in natural fibres: their origin, characteristics and implications for natural fibre-reinforced composites. *Journal of materials science*, 47(2), 599-609.

Ishikawa, T., Ishii, Y., Nakasone, K., Ohkoshi, Y. and Kim, K.H. (2019). Structure analysis of needle-punched nonwoven fabrics by X-ray computed tomography, *Textile Research Journal*, 89, 20-31.

Jawaid, M., & Khalil, A. (2011). Cellulosic/synthetic fibre reinforced polymer hybrid composites: A review. *Carbohydrate polymers*, 86(1), 1-18.

Joffea, R., Andersons, J., Wallstro¨m, L. (2003). Strength and adhesion characteristics of elementary flax fibres with different surface treatments, *Composites: Part A*, 34, 603-612.

John, M. J., & Thomas, S. (2008). Biofibres and biocomposites. *Carbohydrate polymers*, 71(3), 343-364.

Kanade, P.S. (2016). Role of Instrumental Parameters on Yarn Properties, IJIRSET, 5(3), 3202-3207.

Karaki, M., Younes, R., Trochu, F., & Lafon, P. (2019). Progress in Experimental and Theoretical Evaluation Methods for Textile Permeability. *Journal of Composites Science*, *3*(3), 73.

Karnani, R., Mohan, K. & Ramani, N. (1997). "Biofibre-reinforced polypropylene composites." *Polymer Engineering & Science*, 2, 476-483. doi:10.1002/pen.11691.

Keller T, Tracy C and Zhou A. (2006). Structural response of liquid-cooled GFRP slabs subjected to fire. Part I: Material and post-fire modeling. Compos A: Appl, 37: 1286–1296.

Keller T, Tracy C and Zhou A., (2006) Structural response of liquid-cooled GFRP slabs subjected to fire. Part II: Thermo-chemical and thermo-mechanical modeling. Compos A: Appl 2006; 37: 1296–1308.

Kingdom. 2014. Fibre Flax. Retrieve from http://www.kingdom-china.com/en/products1.php#:~:text=Because%20flax%20is%20thin%20and,period%2C%2030%2D40%20days.

Kittl, P., & Diaz, G. (1988). Weibull's fracture statistics, or probabilistic strength of materials: State of the art. Res Mechanica, 24(2), 99-207.

Koronis, G., Silva, A., & Fontul, M. (2013). Green composites: A review of adequate materials for automotive applications. *Composites Part B: Engineering*, 44(1), 120-127.

Krishisewa. 2013. Jute the golden fibre-an overview. Retrieve from https://www.krishisewa.com/production-technology/327-jute.html

Ku, H., Wang, H., Pattarachaiyakoop, N., & Trada, M. (2011). A review on the tensile properties of natural fiber reinforced polymer composites. *Composites Part B: Engineering*, 42(4), 856–873.

Ibrahim, I., Sarip, S., Bani, N.A., Ibrahim, M. H., M. Z. Hassan, M. Z. (2018). The Weibull probabilities analysis on the single kenaf fiber, AIP Conference Proceedings 1958, 020009, https://doi.org/10.1063/1.5034540.

Lamy B., Baley, C. (2000). Stiffness prediction of flax fibres–epoxy composite materials. *J Mater Sci Lett*: 19: 979–80.

La Mantia, F. P., & Morreale, M. (2011). Green composites: A brief review. *Composites Part A: Applied Science and Manufacturing*, 42(6), 579-588.

Lau, K. T., Hung, P. Y., Zhu, M. H., & Hui, D. (2018). Properties of natural fibre composites for structural engineering applications. *Composites Part B: Engineering*, 136, 222-233.

Lee, C. H., Abdan, K., Lee, S. H., & Liu, M. (2019). A Comprehensive Review on Bast Fiber Retting Process for Optimal Performance in Fibers Reinforced Polymer Composites. *Advances in Materials Science and Engineering*, vol. 2020, Article ID 6074063, 27 pages, 2020. https://doi.org/10.1155/2020/6074063

Lefeuvre, A., Bourmaud, A., Lebrun, L., Morvan, C., Baley, C. (2013). A study of the yearly reproducibility of flax fiber tensile properties, *Industrial Crops and Products*, 50, 400-407.

Lewin, M., & Pearce, E. M. (1985). Handbook of fiber science and technology: volume 4-fiber chemistry.

Levine, H., & Slade, L. (1988). In Water Science Reviews, 3, Felix Franks (ed),Chapter 2: Water Dynamics, Water as a plasticizer: physio-chemical aspects of low-moisture polymeric systems, 79-185. CAM BRIDGE UNIVERSITY –PRESS CAMBRIDGE NEW YORK, USA. DOI: 10.1017/CBO9780511552083.002

Li, Y. Pickering, K.L., Farrell. R.L. (2009). Determination of interfacial shear strength of hemp fibre reinforced polypropylene. *Composites science and technology*, 69:1165–71.

Li, X., Tabil, L.P., Panigrahi, S. (2007). Chemical Treatment of Natural Fibre for Use in Natural Fibre Composites: A Review, *J Polym Environ*, 15: 25-33.

Liu, W., Qiu, R., Li, K. (2014). Effects of Fiber Extraction, Morphology, and Surface Modification on the Mechanical Properties and Water Absorption of Bamboo Fibers-Unsaturated Polyester Composites, 37 (5), 1612-1619.

Liu, M., Fernando, D., Daniel, G., Madsen, B., Meyer, A.S., Ale, M. T., Thygesen, A. (2015). Effect of harvest time and field retting duration on the chemical composition, morphology and mechanical properties of hemp fibers, *Industrial Crops and Products*, 69, 29-39.

Luenenschloss, J., (1972), "The Effect of Fiber Length, Fiber Fineness, Crimp, and Matting on the Needling Process and the Properties of Needled Non-woven", Melliand Textil., 53, 144.

Magdalena, W-K., Magdalena, C., Anna, K., Magdalena, Ż., Jacek, K., Lucyna, D., Jerzy, H., Maciej, P., Jan, S. (2012). "New biocomposites based on bioplastic flax fibres and biodegradable polymers." *Biotechnology progress*, 5, 1336-1346. doi:10.1002/btpr.1599.

MARIENFELD, M. (1995). Geotextile trends and developments. *Tappi Journal*, *78*(9), 143-146.

Marru P, Latane V, Puja C, et al. (2014). Lifetime estimation of glass reinforced epoxy pipes in acidic and alkaline environment using accelerated test methodology. *Fibre Polym*, 15: 1935–1940.

Martin, N.; Mouret, N.; Davies, P.; Baley, C. (2013). Influence of the degree of retting of flax fibers on the tensile properties of single fibers and short fiber/polypropylene composites. *Ind. Crops Prod*. 49, 755–767.

Martí-Ferrer, F., Vilaplana, F., Ribes-Greus, A., Benedito-Borrás, A., & Sanz-Box, C. (2006). Flour rice husk as filler in block copolymer polypropylene: Effect of different coupling agents. *Journal of Applied Polymer Science*, *99*(4), 1823-1831.

Mazian, B., Bergeret, A., Benezet, J-C., Malhautier, L. (2019). A Comparative Study of the Effect of Field Retting Time on the Properties of Hemp Fibres Harvested at Different Growth Stages, Fibers, 7, 108; doi:10.3390/fib7120108

Merhi, D., Michaud, V., Kämpfer, L., Vuilliomenet, P., & Månson, J. A. (2007). Transverse permeability of chopped fibre bundle beds. *Composites Part A: Applied science and manufacturing*, *38*(3), 739-746.

Miao, M., & Finn, N. (2008). Conversion of natural fibres into structural composites. *Journal of textile engineering*, *54*(6), 165-177.

Mohanty, A. K., Misra, M., & Drzal, L. T. (2001). Surface modifications of natural fibers and performance of the resulting bio composites: an overview. *Composite interfaces*, 8(5), 313-343.

Monteiro, S.N., Lopes, F.P.D., Ferreira, A.S. (2013). Weibull analysis for the diameter dependence of the elastic modulus of curaua fibers, Revista Matéria, 18(46–54).

Mortazavi, S.M., and Moghadam, M.K. (2009). Introduction of a New Vegetable Fibre for Textile Application, *J Appl Polym Sci*, 113, 3307-3312. DOI 10.1002/app.30301.

Morotn, W.E., Hearle, J.W.S. (2008). Physical properties of textile fibres, 4th edition, Woodhouse Publishing Limited and CRC Press, Cornwall, England.

Moudood, A., Hall, W., Ochsner, A., Li, H., Rahman, A., Francucci, G. (2019). Effect of Moisture in Flax Fibres on the Quality of their Composites. *Journal of Natural Fibers*, https://doi.org/10.1080/15440478.2017.1414651.

Mukhopadhyay, S., Srikanta, R. (2008). Effect of ageing of sisal fibres on properties of sisal – Polypropylene composites, *Polymer Degradation and Stability*, 93, 2048-2051.

Mwaikambo, L. A., & Ansell, M. P. (2006). Mechanical properties of alkali treated plant fibres and their potential as reinforcement materials. I. Hemp fibres. *Journal of materials science*, *41*(8), 2483-2496.

NCSS Statistical Software (nd). Chapter 550. Distribution (Weibull Fitting). https://ncss-wpengine.netdna-ssl.com/wp-content/themes/ncss/pdf/Procedures/NCSS/Distribution-Weibull-Fitting.pdf

Naik, D., Fronk, T. (2016). Weibull Distribution Analysis of the Tensile Strength of the Kenaf Bast Fiber, Fibers and Polymers, 17, 1696-1701.

Nair, G. R., Rho, D., Yaylayan, V., & Raghavan, V. (2013). Microwave assisted retting–A novel method of processing of flax stems. *Biosystems engineering*, *116*(4), 427-435.

Ngo, T.D. (2018). Chapter 7: Natural Fibres for Sustainable Bio-composites. In book: Natural and Artificial Fiber-Reinforced Composites as Renewable Sources, Gunay, E. (ed.), IntechOpen Limited, London, UK.

Nilsson, T. (2006). Micromechanical Modelling of Natural Fibres for Composite Materials, Master's thesis, Lund University, Lund, Sweden.

Nishino, T., Koichi, H., Masaru, K., Katsuhiko, N., & Hiroshi, I. (2003). Kenaf reinforced biodegradable composite. *Composites science and technology*, 9, 1281-1286. doi:10.1016/S0266-3538(03)00099-X.

Niu, H., Jiao, X., Wang, R., & Zhou, H. (2010). Direct manufacturing of flax fibers reinforced low melting point PET composites from nonwoven mats. *Fibers and polymers*, *11*(2), 218-222.

Niya, S. R., & Selvadurai, A. P. S. (2018). A statistical correlation between permeability, porosity, tortuosity and conductance. *Transport in Porous Media*, *121*(3), 741-752.

Morotn, W.E., Hearle, J.W.S. (2008). Physical properties of textile fibres, 4th edition, Woodhouse Publishing Limited and CRC Press, Cornwall, England.

Oksman, K., Lennart, W., Lars, A. B., Romildo, D. T. F. (2002). "Morphology and mechanical properties of unidirectional sisal–epoxy composites." *Journal of Applied Polymer Science*, 13, 2358-2365. doi.org/10.1002/app.10475

Pan, N., Chen, H.C., Thompson, J., Inglesby, M. K., KHATUA, S., ZHANG, X.S., Zeronian, S. H. (1997). The size effects on the mechanical behaviour of fibres, *Journal of Materials Science*, 32, 2677-2685.

Pandey, R. (2016). Fiber extraction from dual-purpose flax. *Journal of Natural Fibers*, *13*(5), 565-577.

Park, J.M., Quang, S.T., Hwang, B.S., DeVries, K.L. (2006). Interfacial evaluation of modified Jute and Hemp fibers/polypropylene composites using micromechanical technique and nondestructive acoustic emission. Compos Sci Technol, 66:2686–99.

Paridah, M. T., Basher, A. B., SaifulAzry, S., & Ahmed, Z. (2011). Retting process of some bast plant fibres and its effect on fibre quality: a review. *BioResources*, *6*(4), 5260-5281.

Peças, P., Carvalho, H., Salman, H., & Leite, M. (2018). Natural fibre composites and their applications: a review. *Journal of Composites Science*, 2(4), 66.

Peirce, F.T. (1929). A Two-Phase Theory of the Absorption of Water Vapour by Cotton Cellulose, *Journal of the Textile Institute Transactions*, 20:6, T133-T150,

DOI: 10.1080/19447022908661486.

Placet, V., Cisse, O., Boubakar, M. L. (2012). Influence of environmental relative humidity on the tensile and rotational behaviour of hemp fibres. *Journal of Materials Science*, 47(7), 3435-3446.

Preisner, M., Kulma, A., Zebrowski, J., Dymińska, L., Hanuza, J., Arendt, M., & Szopa, J. (2014). Manipulating cinnamyl alcohol dehydrogenase (CAD) expression in flax affects fibre composition and properties. *BMC plant biology*, *14*(1), 50.

Qiu, R., Ren, X., Fifield, L. S., Simmons, K. L., & Li, K. (2011). Hemp-fiber-reinforced unsaturated polyester composites: Optimization of processing and improvement of interfacial adhesion. *Journal of Applied Polymer Science*, 121(2), 862-868.

Quin, J., Quin, G. (2010). A practical and systematic review of Weibull statistics for reporting strengths of dental materials, Dental Materials, 26, 135-147.

Rahman, M., Cicek, N., Chakma, K., (2020). The Optimum Parameters for Fibre Yield (%) and Characterization of Typha latifolia L. Fibres for Textile Applications, *Fibres and Polymers*. In press.

Ramamoorthy, S. K., Skrifvars, M., & Persson, A. (2015). A review of natural fibers used in biocomposites: plant, animal and regenerated cellulose fibers. *Polymer reviews*, 55(1), 107-162.

Ramaswamy, G. N., Ruff, C. G., & Boyd, C. R. (1994). Effect of bacterial and chemical retting on kenaf fiber quality. *Textile research journal*, *64*(5), 305-308.

Rao, G. V., & Banerjee, P. K. (1997). Geosynthetics: Recent developments.

Roy, A., Chakraborty, S., Kundu, S. P., Basak, R. K., Majumder, S. B., Adhikari, B. (2012). Improvement in mechanical properties of jute fibres through mild alkali treatment as demonstrated by utilisation of the Weibull distribution model. *Bioresource technology*, 107, 222-228.

Sadrmanesh, V., Chen, Y., Rahman, M., AL-Oqla, F. (2019). Developing a decision making model to identify the most influential parameters affecting mechanical extraction of bast fibers, *J. Clean. Prod.*, 238, https://doi.org/10.1016/j.jclepro.2019.117891.

Sadrmanesh, V., & Chen, Y. (2019). Bast fibres: structure, processing, properties, and applications. *International Materials Reviews*, *64*(7), 381-406.

Sayeed, M. A., & Paharia, A. (2019). Optimisation of the surface treatment of jute fibres for natural fibre reinforced polymer composites using Weibull analysis. *The Journal of The Textile Institute*, 110(11), 1588-1595.

Schiefer, H. F., & Boyland, P. M. (1942). Improved instrument for measuring the air permeability of fabrics. *Journal of Research of the National Bureau of Standards*, *29*.

Scholz, S., Gillespie Jr, J. W., & Heider, D. (2007). Measurement of transverse permeability using gaseous and liquid flow. *Composites Part A: Applied Science and Manufacturing*, *38*(9), 2034-2040.

Sengupta, S. (2018). Study on some functional properties of mesta needle punched nonwoven fabrics using central composite rotatable design. *Journal of Natural Fibers*, *15*(1), 131-145.

Sevenhuysen, G.P. and Rahman, M. (2016). U.S. Patent, WO2015039243.

Shadhin, M., & Shuvo, I. I. (2019). Biopolymer flax (Linum Usitatissimum L.) and its prospects in biodegradable composite fabrication-a short review. *J Textile Eng Fashion Technol*, 5(5), 267-274. DOI: 10.15406/jteft.2019.05.00212

Shahzad, A. (2013). A Study of Physical and Mechanical Properties of Hemp Fibres, Advances in Materials Science and Engineering, vol. 2013, Article ID 325085, 9 pages. https://doi.org/10.1155/2013/325085.

Shamsuyeva, M.; Chang, B.P.; Vellguth, N.; Misra, M.; Mohanty, A.; Endres, H.-J. (2020). Surface Modification of Flax Fibers for Manufacture of Engineering Thermoplastic Biocomposites. *J. Compos. Sci*., 4, 64, doi:10.3390/jcs4020064

Shevidi, A.H., Taghiabadi, R., Razaghian, A. (2018). Weibull analysis of effect of T6 heat treatment on fracture strength of AM60B magnesium alloy, Trans. Nonferrous Met. Soc. China 28, 20−29.

Shih, J. G., & Finkelstein, S. A. (2008). Range dynamics and invasive tendencies in Typha latifolia and Typha angustifolia in eastern North America derived from herbarium and pollen records. *Wetlands*, *28*(1), 1-16.

Shuvo, I. I., Rahman, M., Vahora, T., Morrison, J., DuCharme, S., & Choo-Smith, L. P. I. (2019). Producing light-weight bast fibers from canola biomass for technical textiles. *Textile Research Journal*, doi.org/10.1177/0040517519886636.

Sparnins, E. (2006). Mechanical properties of flax fibers and their composites, Master's thesis, Luleå University of Technology, Sweden.

Stamboulis, A., Baillie, C. A., & Peijs, T. (2001). Effects of environmental conditions on mechanical and physical properties of flax fibres. Composites Part A: *Applied Science and Manufacturing*, 32(8), 1105-1115.

Stavber, G., & Stavber, S. (2010). Towards Greener Fluorine Organic Chemistry: Direct Electrophilic Fluorination of Carbonyl Compounds in Water and Under Solvent-Free Reaction Conditions. *Advanced Synthesis & Catalysis*, 352(16), 2838-2846.

Symington, M.C., Banks, W.M., West, O.D., Pethrick, R.A. (2009). Tensile testing of natural fibers for composite applications. *J Compos Mater*, 43(9):1083–108.

Thoman, D. R., Bain, L. J., & Antle, C. E. (1969). Inferences on the parameters of the Weibull distribution. Technometrics, 11(3), 445-460.

Thomason, J.L., Carruthers, J., Kelly, J., Johnson, G. (2011). Fibre cross-section determination and variability in sisal and flax and its effects on fibre performance characterisation, *Composites Science and Technology*, 71, 1008-1015.

Tiryakioglu, M., Hudak, D., Öktenc, G. (2009). Rapid communication On evaluating Weibull fits to mechanical testing data; *Materials Science and Engineering A,* 527: 397–399.

Van den Oever, M. J. A., Bos, H. L., & Molenveld, K. (1999). Flax fibre physical structure and its effect on composite properties: Impact strength and thermo-mechanical properties. *Die Angewandte Makromolekulare Chemie*, 272(1), 71-76.

Van den Oever, M. J. A., Bos, H. L., & Van Kemenade, M. J. J. M. (2000). Influence of the physical structure of flax fibres on the mechanical properties of flax fibre reinforced polypropylene composites. *Applied Composite Materials*, 7(5-6), 387-402.

Van der Werf, H.M.G.; Wijlhuizen, M.; de Schutter, J.A.A. (1995). Plant density and self-thinning affect yield and quality of fibre hemp (Cannabis sativa L.). *Fields Crops Res*. 40, 153–164.

Varma, D. S., Varma, M., & Varma, I. K. (1984). Coir fibers: Part I: Effect of physical and chemical treatments on properties. *Textile Research Journal*, *54*(12), 827-832.

Verma, D., Jain, S., Zhang, X., & Gope, P. C. (Eds.). (2016). Green approaches to biocomposite materials science and engineering. IGI Global.

Vetayasuporn, S. (2007). Using Cattails (Typha latifolia as a substrate for Pleurotus ostreatus (Fr.) Kummer cultivation. *J Biol Sci*, *7*, 218-221

Virk, A.S., Hall, W., Summerscales, J. (2010). Failure strain as the key design criterion for fracture of natural fibre composites. *Composites science and technology*, 70:995–9.

Wambua, P., Jan, I. & Ignaas, V. (2003). "Natural fibres: can they replace glass in fibre reinforced plastics?" *Composites science and technology*, 9, 1259-1264. doi:10.1016/S0266-3538(03)00096-4.

Wang, C., Ren, Z., Li, S., & Yi, X. (2018). Effect of Ramie Fabric Chemical Treatments on the Physical Properties of Thermoset Polylactic Acid (PLA) Composites. *Aerospace*, *5*(3), 93.

Wang, J., GangaRao, H., Liang, R., Liu, W. (2015). Durability and prediction models of fibre-reinforced polymer composites under various environmental conditions: A critical review, *Journal of Reinforced Plastics and Composites*, DOI: 10.1177/0731684415610920. Wróbel, K.,

Warner, S. B. (1995). Fiber science. New Jersey: Prentice Hall, 1995. p. 134-40.

Witztum, A., & Wayne, R. (2014). Fibre cables in the lacunae of Typha leaves contribute to a tensegrity structure. Annals of botany, 113(5), 789-797.

Witztum, A., & Wayne, R. (2015). Variation in fiber cables in the lacunae of leaves in hybrid swarms of Typha × glauca. Aquatic botany, 124, 39-44.

Wróbel, K., Magdalena, Magdalena, C., Anna, K., Magdalena, Ż., Jacek, K., Lucyna, D., Jerzy, H., Maciej, P. & Jan, S. "New biocomposites based on bioplastic flax fibers and biodegradable polymers." *Biotechnology progress*, 5(2012): 1336-1346. doi:10.1002/btpr.1599.

Xia, Z.P., Yu, J.Y., Cheng, L.D., Liu, L.F., Wang, W.M. (2009). Study on the breaking strength of jute fibres using modified Weibull distribution. *Composites Part A*, 40:54–9.

Xie, Y., Hill, C. A., Jalaludin, Z., Curling, S. F., Anandjiwala, R. D., Norton, A. J., & Newman, G. (2011). The dynamic water vapour sorption behaviour of natural fibres and kinetic analysis using the parallel exponential kinetics model. *Journal of Materials Science*, 46(2), 479-489.

Xue, D., Miao, M., & Hu, H. (2011). Permeability anisotropy of flax nonwoven mats in vacuum-assisted resin transfer molding. *The Journal of The Textile Institute*, *102*(7), 612-620.

Yan, L., Chouw, N., and Jayaraman, K. (2014). Flax fibre and its composites – A review, *Composites: Part B*, 56, 296-317.

Yan, L., Nawawi, C. & Krishnan, J. "Flax fibre and its composites–A review." *Composites Part B: Engineering* 56(2014): 296-317. doi.org/10.1016/j.compositesb.2013.08.014

Yu, C. H., Rahman, M. (2020). Working paper, Department of Biosystems Engineering, University of Manitoba, Winnipeg, Canada.

Akil, H., Omar, M. F., Mazuki, A. A. M., Safiee, S. Z. A. M., Ishak, Z. M., & Bakar, A. A. (2011). Kenaf fiber reinforced composites: A review. *Materials & Design*, *32*(8-9), 4107-4121.

Zafeiropouls, N. E., Baillie, C. A. (2007). A study of the effect of surface treatments on the tensile strength of flax fibres: Part II. Application of Weibull statistics, *Composites: Part A*, 38, 629-638.

APPENDIX A

CATTAIL

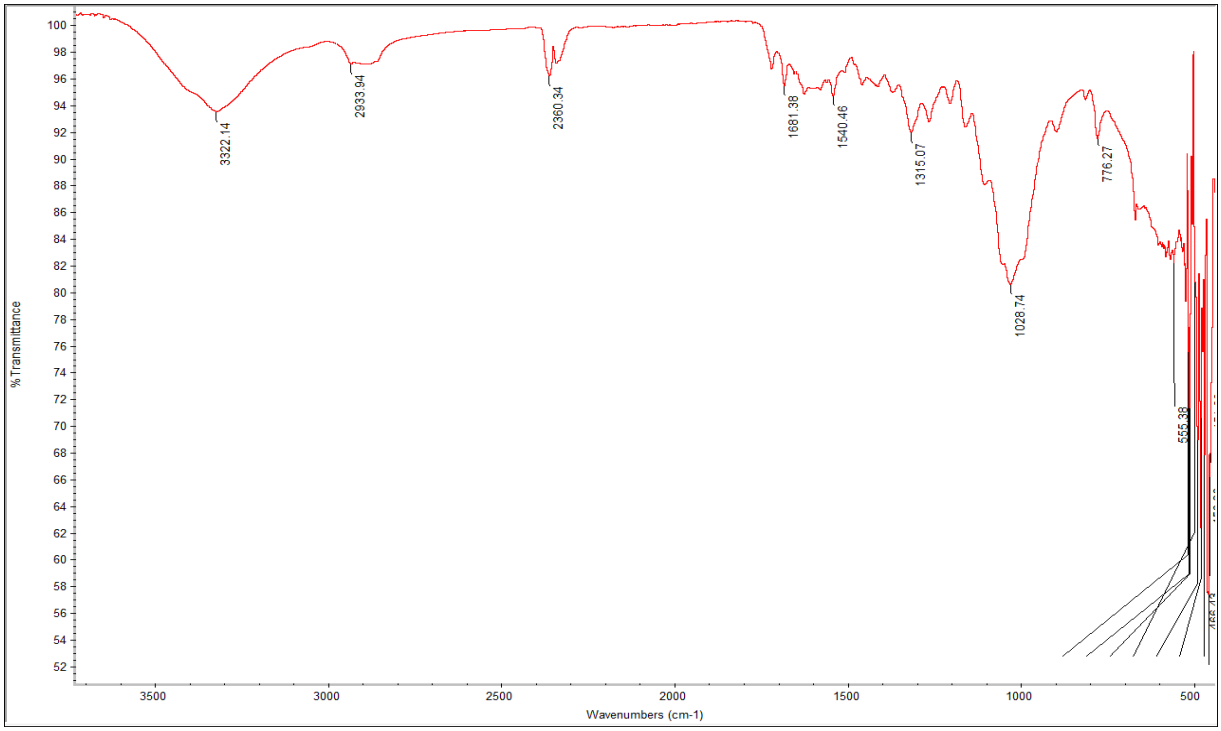

Figure A.1 FTIR spectra of cattail fiber treated with 2.5% DIH-HEA (10 min)

Figure A.2 FTIR spectra of cattail fiber treated with 2.5% DIH-HEA (20 min)

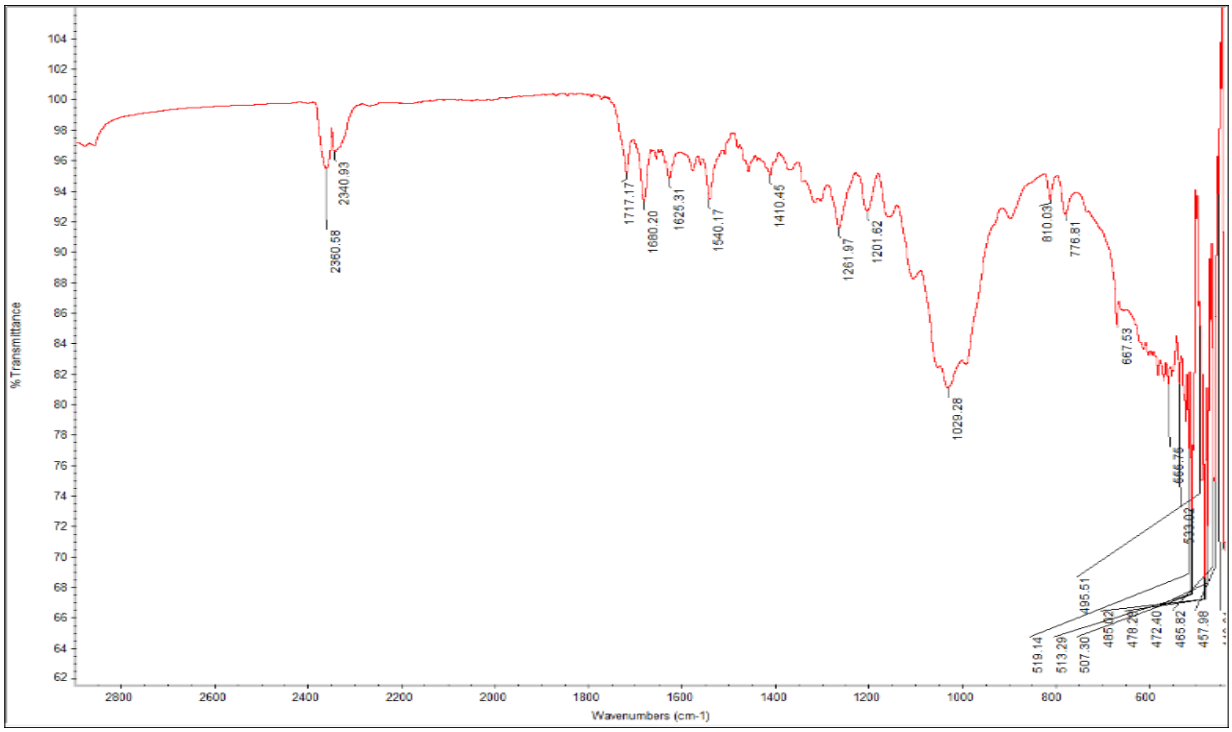

Figure A. 3 FTIR spectra of cattail fiber treated with 2.5% DIH-HEA (30 min)

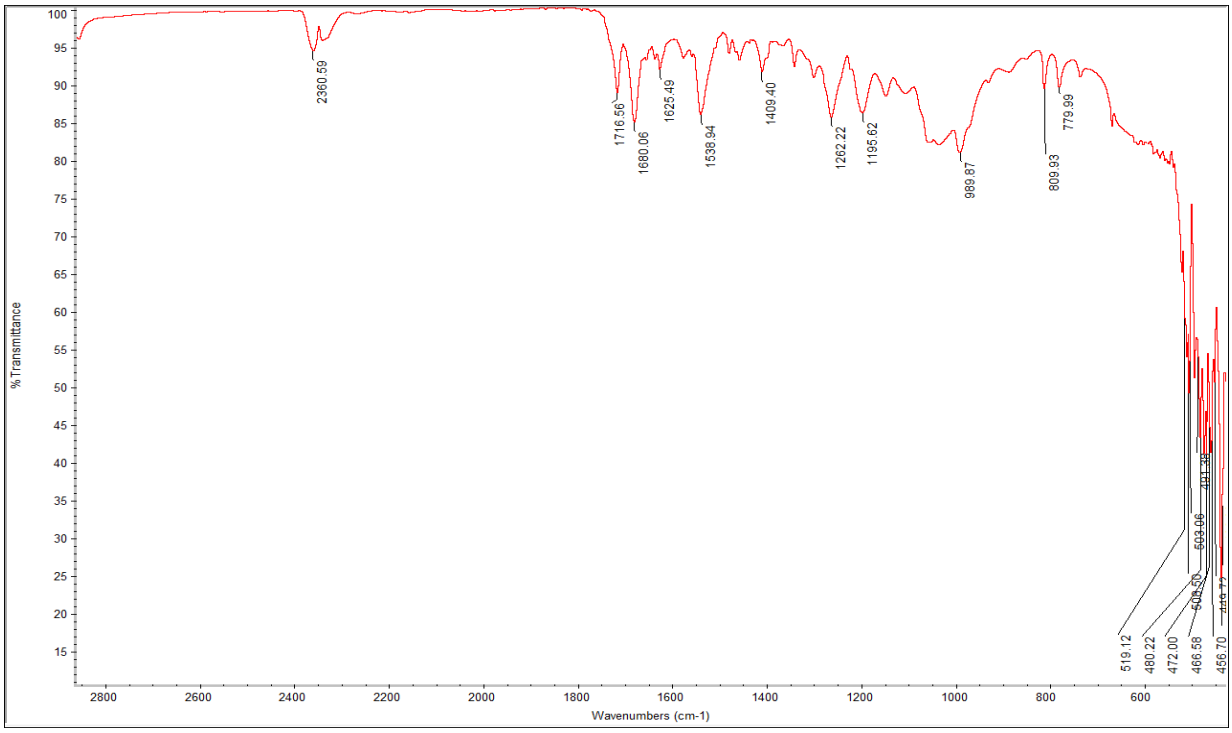

Figure A. 4 FTIR spectra of cattail fiber treated with 5% DIH-HEA (10 min).

Figure A. 5 FTIR spectra of cattail fiber treated with 5% DIH-HEA (20 min).

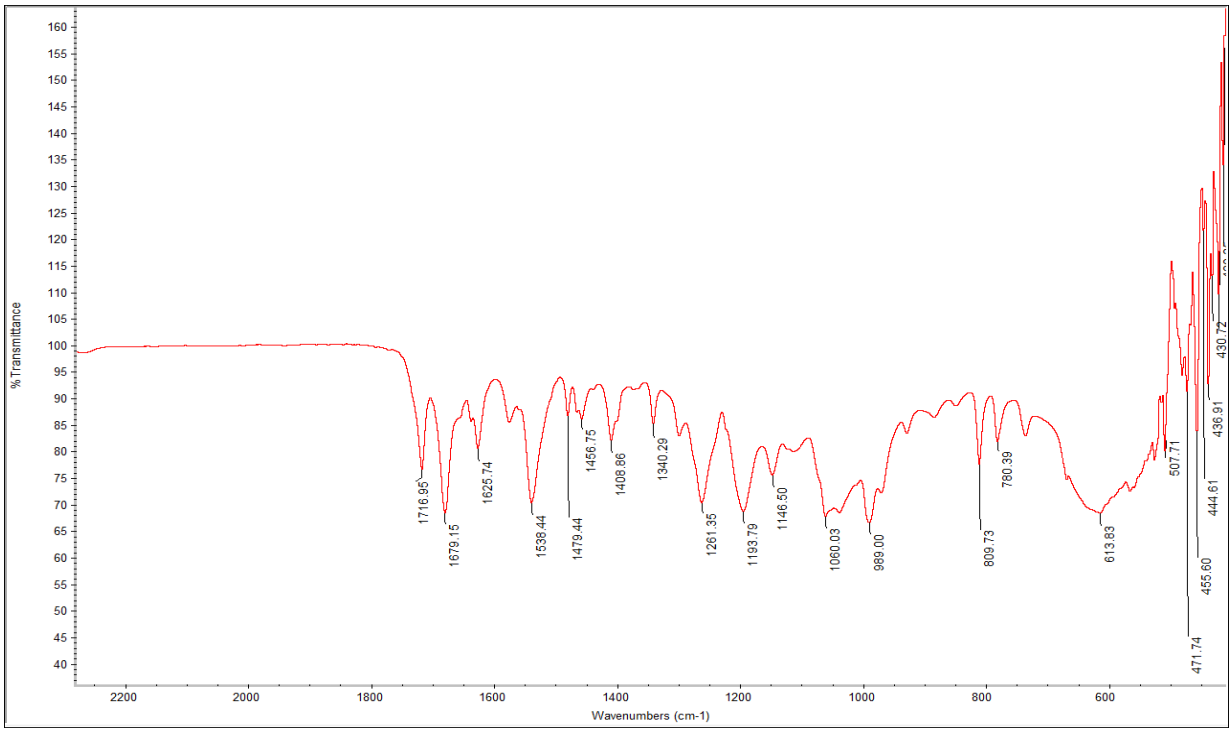

Figure A. 6 FTIR spectra of cattail fiber treated with 5% DIH-HEA (30 min).

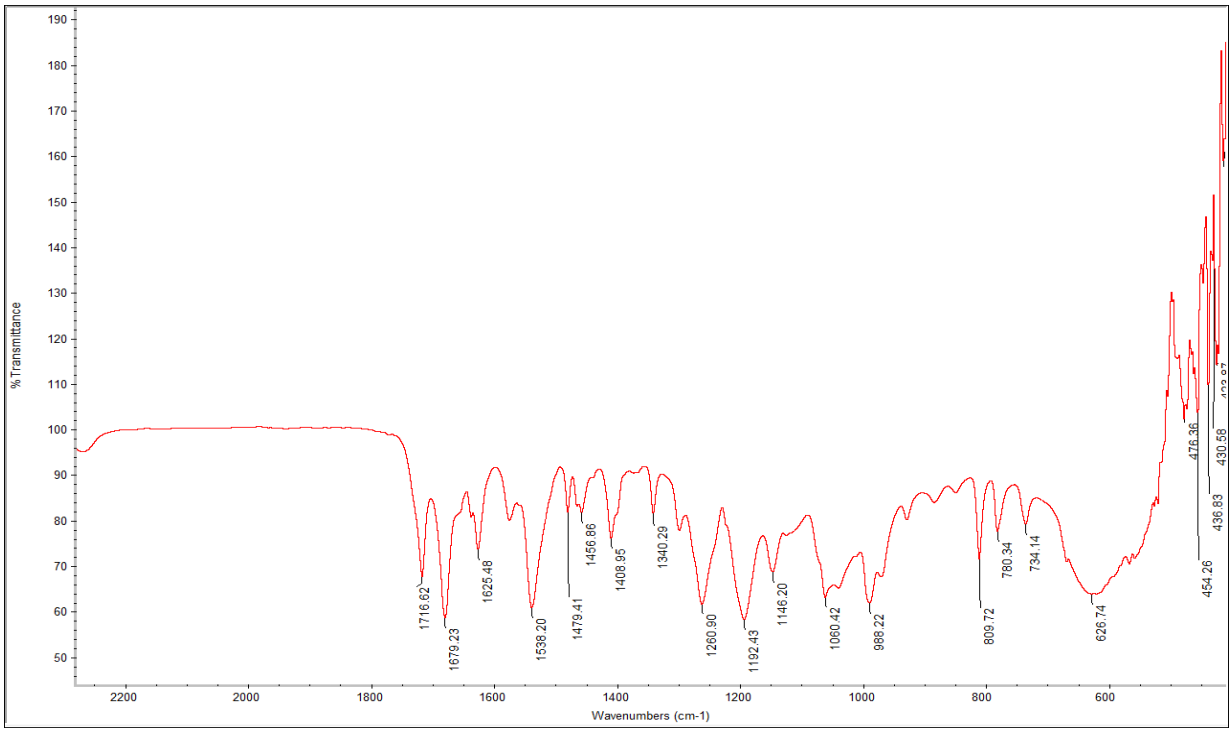

Figure A. 7 FTIR spectra of cattail fiber treated with 10% DIH-HEA (10 min).

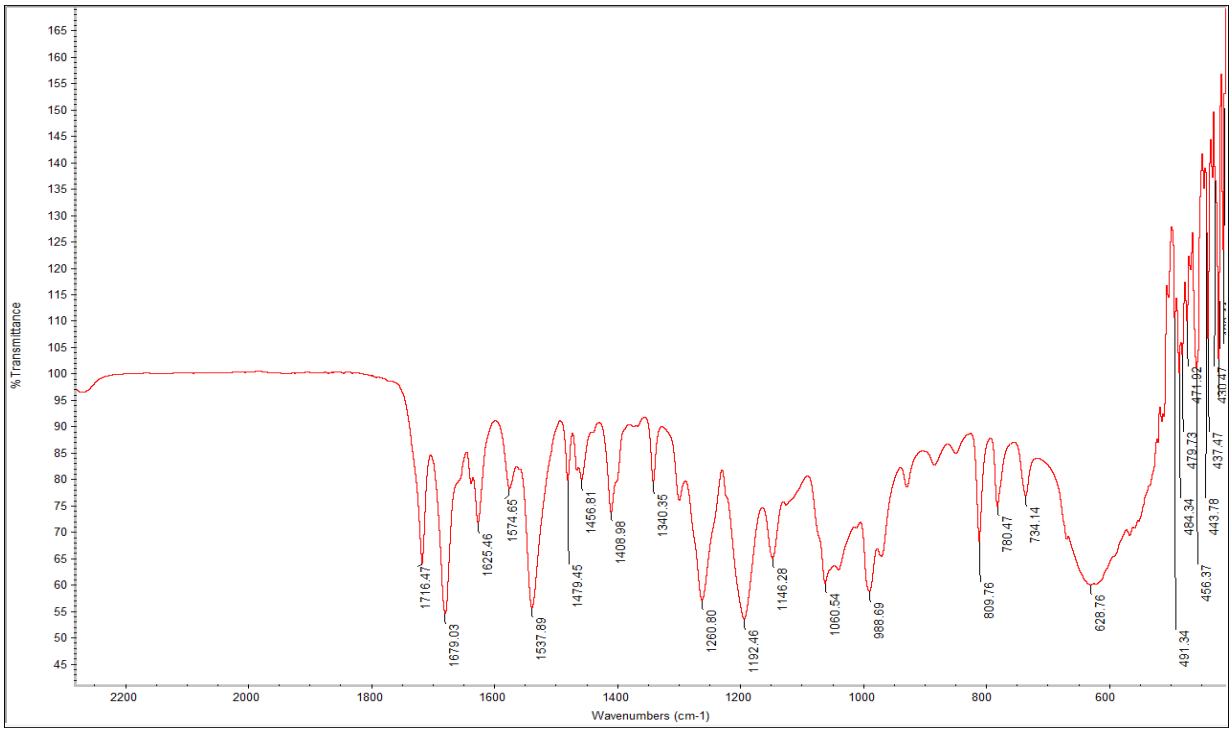

Figure A. 8 FTIR spectra of cattail fiber treated with 10% DIH-HEA (20 min).

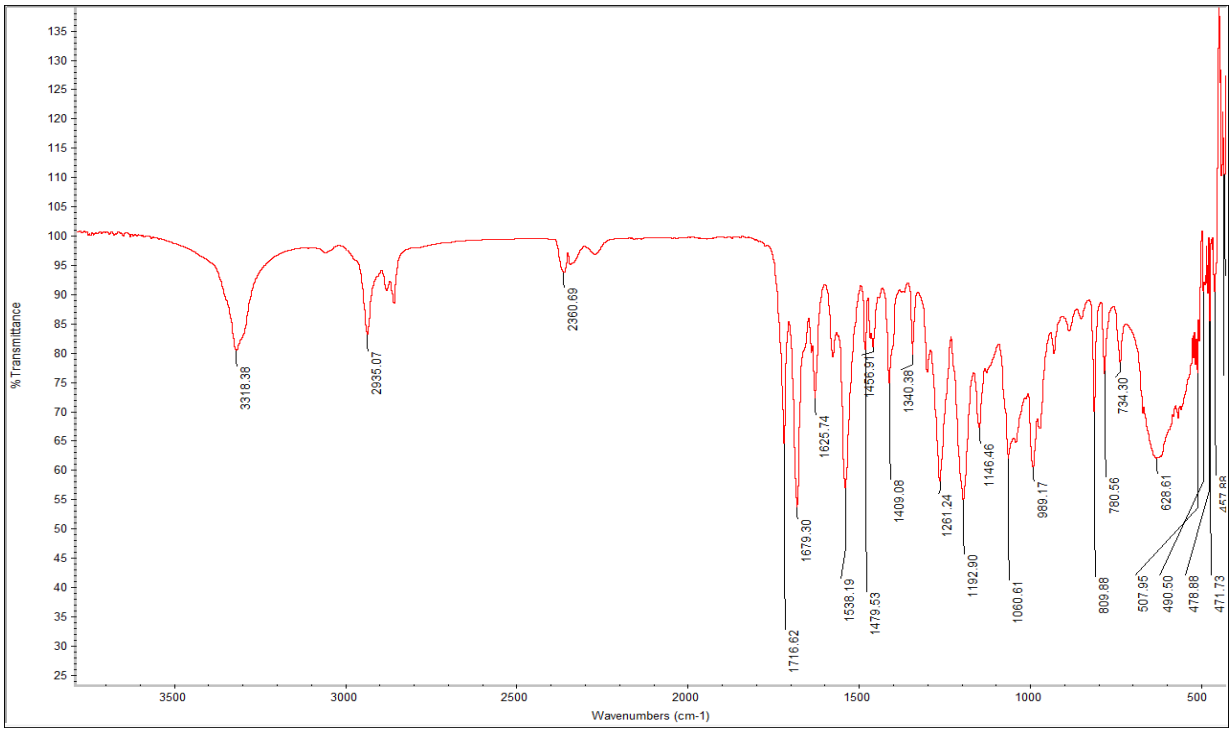

Figure A. 9 FTIR spectra of cattail fiber treated with 10% DIH-HEA (30 min).

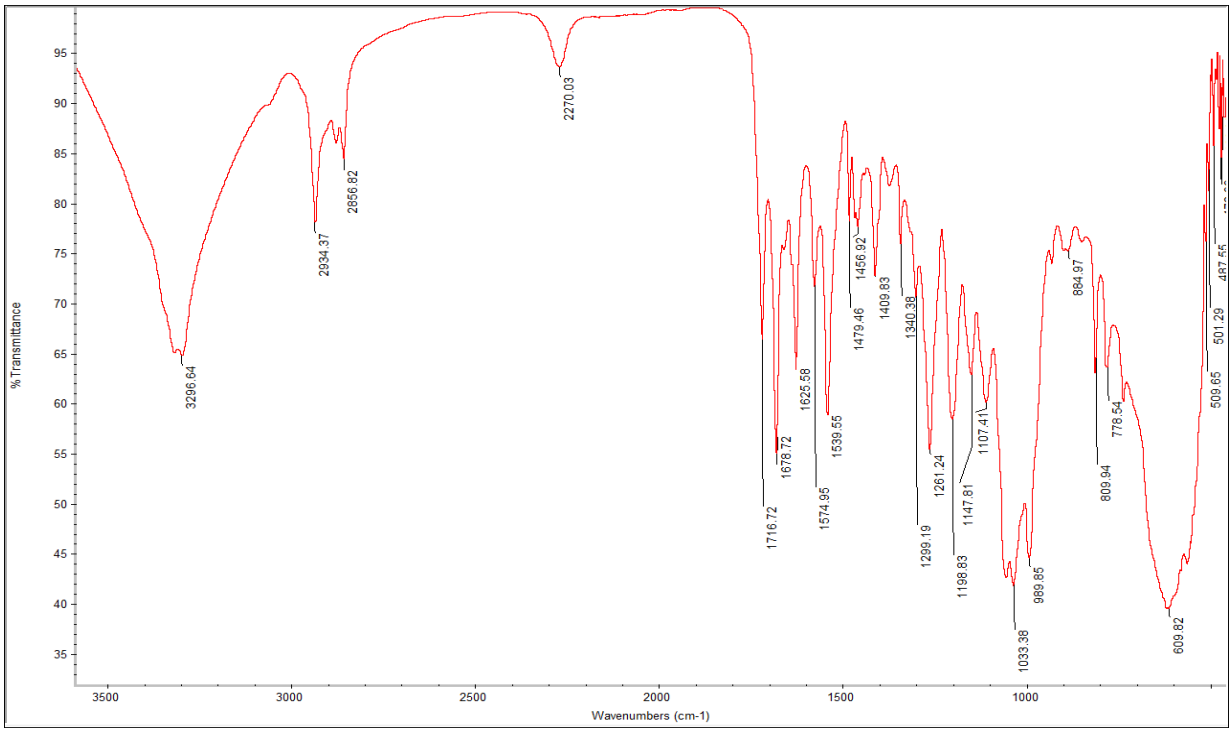

Figure A. 10 FTIR spectra of cattail fiber treated with 10% DIH-HEA (30 min – washed with water).

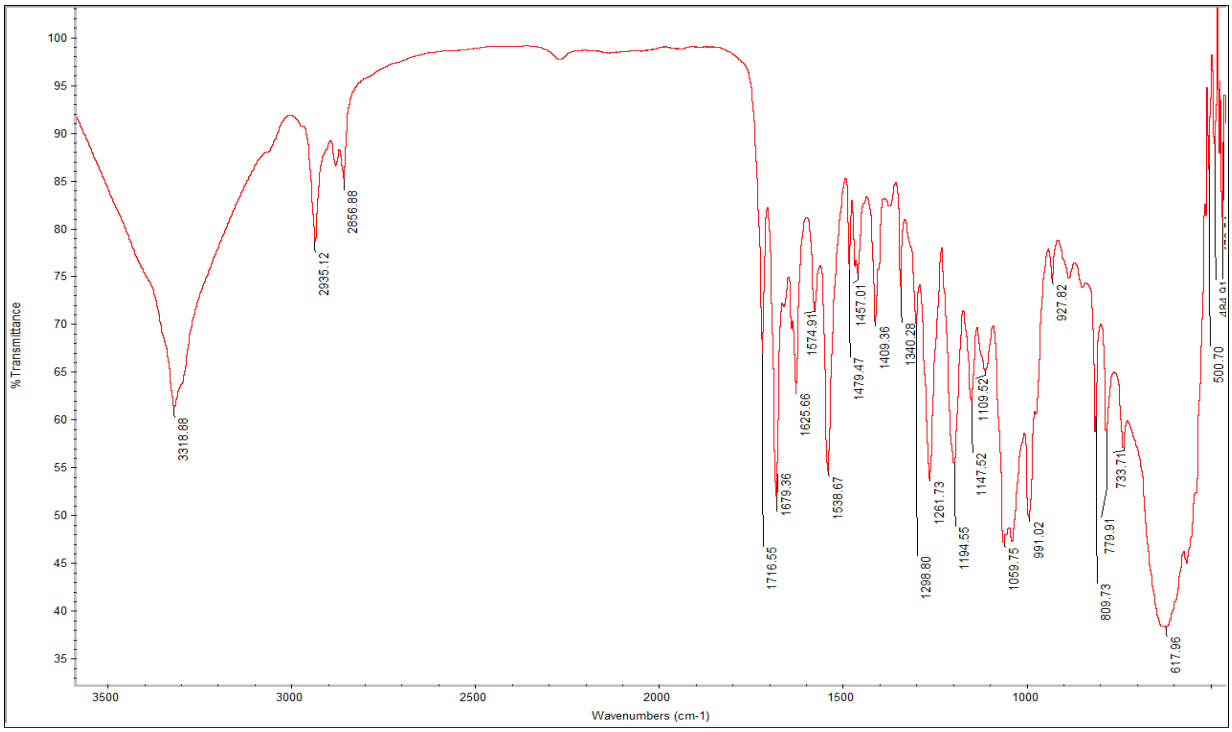

Figure A. 11 FTIR spectra of cattail fiber treated with 10% DIH-HEA (30 min – washed with alkali).

Table A.1 T-test results for tensile strength and tensile modulus of cattail composite.

V_f % of composite		Tensile strength			Tensile Modulus		
Group-1	Group-2	P - value	tstat	Result	P - value	tstat	Result
10.9	30.4	0.0003	6.2	Extremely statistically significant	<0.0001	8.5	Extremely statistically significant
10.9	26.1 (560)	<0.0001	12.7	Extremely statistically significant	<0.0001	6.7	Extremely statistically significant
10.9	26.1 (treated)	<0.0001	10.6	Extremely statistically significant	<0.0001	8.7	Extremely statistically significant
26.1 (560)	30.4	0.0013	4.8	Very statistically significant	0.0042	3.9	Very statistically significant
26.1 (treated)	30.4	0.3779	0.9	Not statistically significant	0.25	1.2	Not statistically significant

APPENDIX B

FLAX

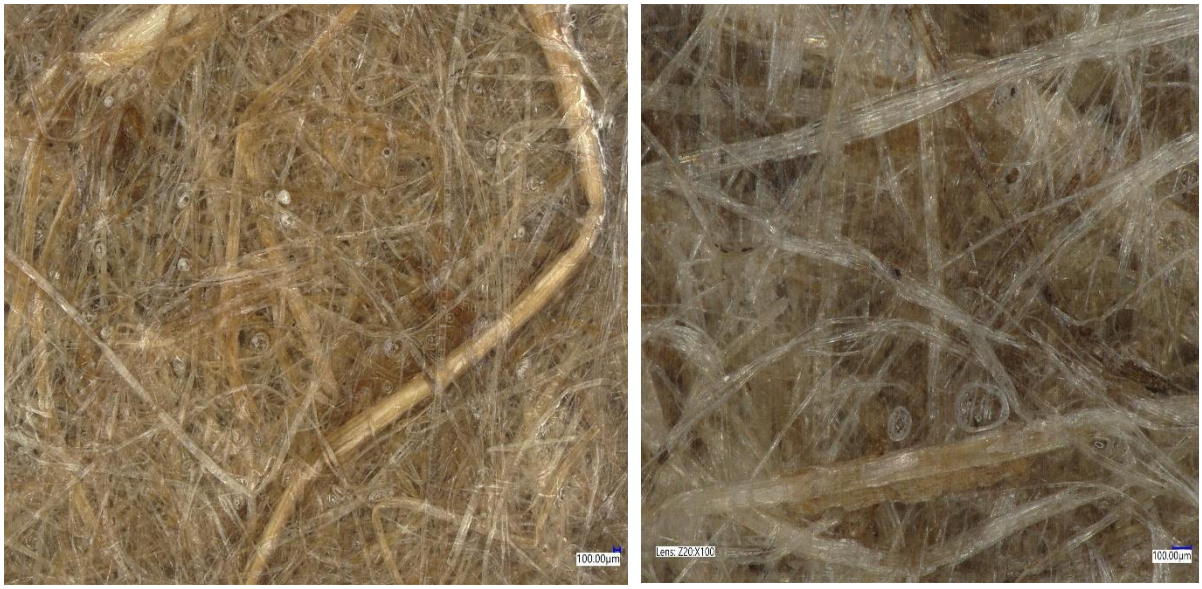

(a) (b)

Figure B.12 Microscopic images of 0-P flax mat composite – (a) 30X magnification and (b) 100X magnification; manufactured at 560 kPa.

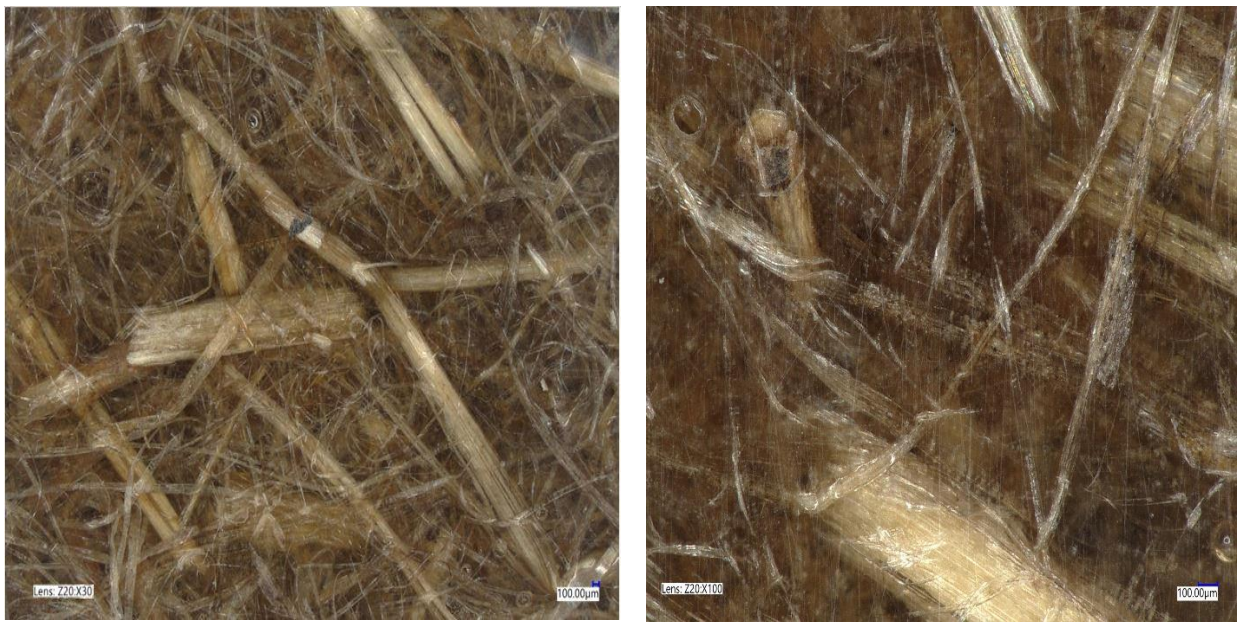

(a) (b)

Figure B. 13 Microscopic images of 20-P flax mat composite – (a) 30X magnification and (b) 100X magnification; manufactured at 560 kPa.

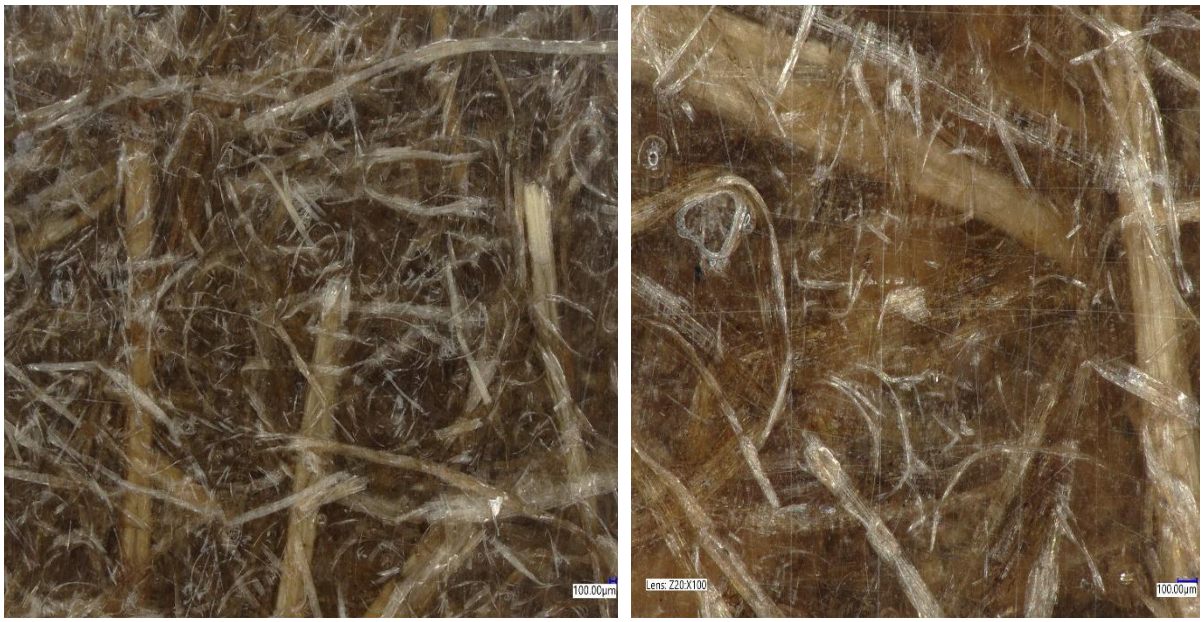

(a) (b)

Figure B. 14 Microscopic images of 30-P flax mat composite – (a) 30X magnification and (b) 100X magnification; manufactured at 560 kPa.

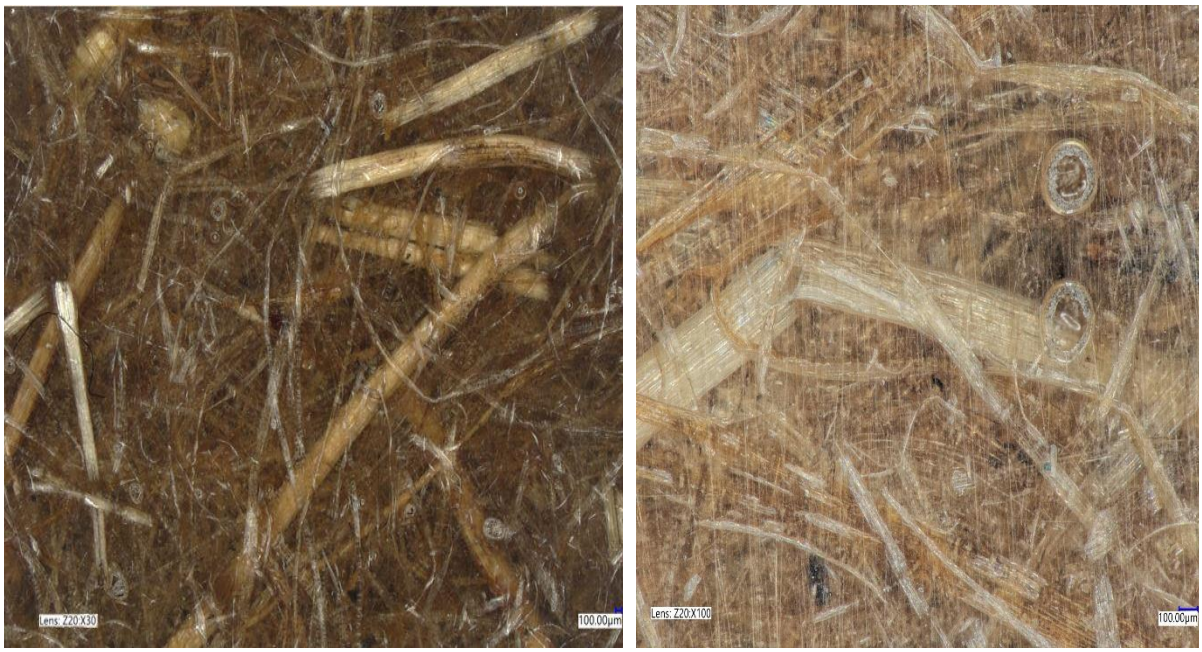

(a) (b)

Figure B. 15 Microscopic images of 72-P flax mat composite – (a) 30X magnification and (b) 100X magnification; manufactured at 560 kPa.

APPENDIX C

EXPERIMENTAL DETAIL

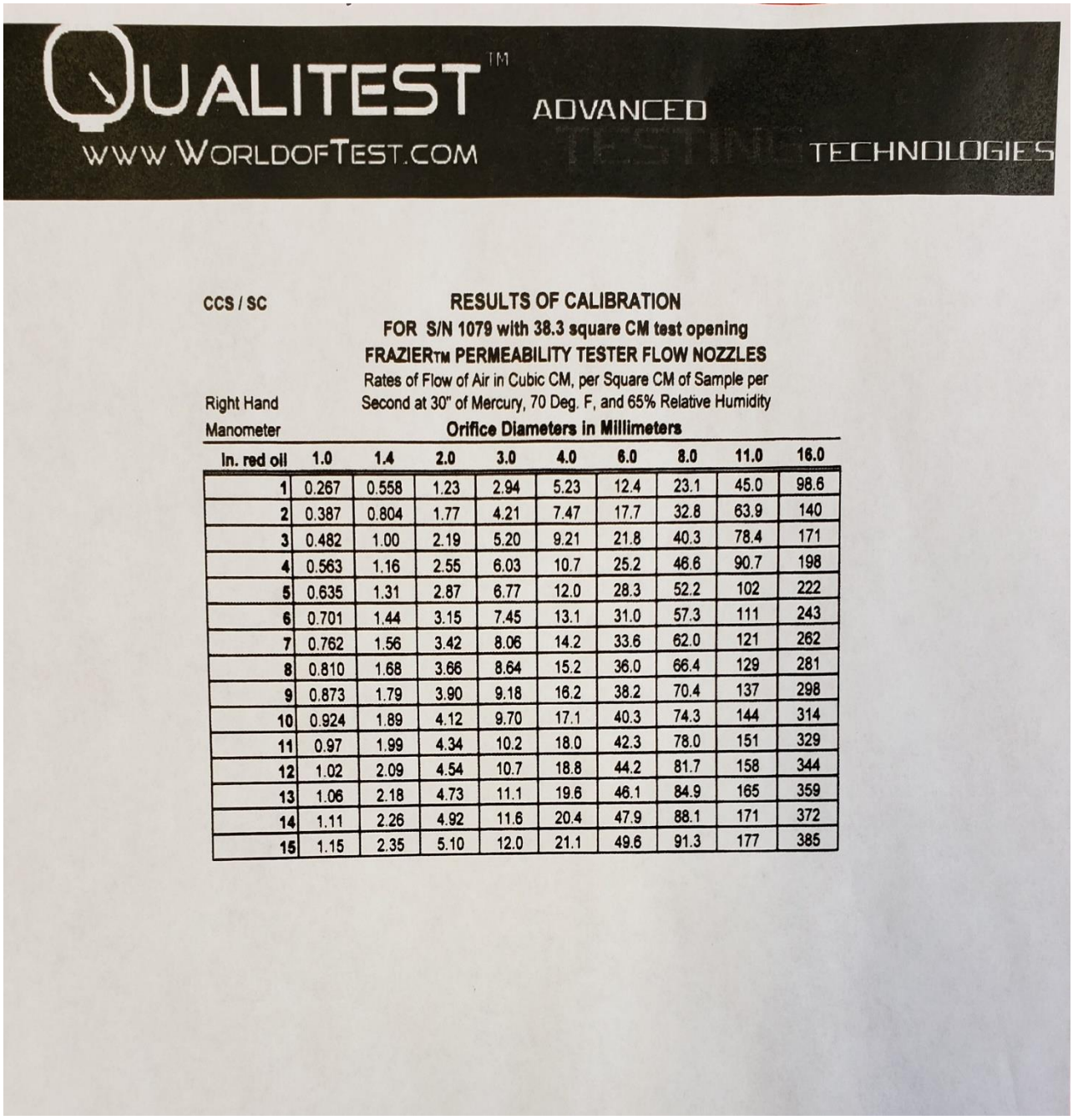

CCS / SC

RESULTS OF CALIBRATION
FOR S/N 1079 with 38.3 square CM test opening
FRAZIER™ PERMEABILITY TESTER FLOW NOZZLES
Rates of Flow of Air in Cubic CM, per Square CM of Sample per Second at 30" of Mercury, 70 Deg. F, and 65% Relative Humidity

Right Hand Manometer — **Orifice Diameters in Millimeters**

In. red oil	1.0	1.4	2.0	3.0	4.0	6.0	8.0	11.0	16.0
1	0.267	0.558	1.23	2.94	5.23	12.4	23.1	45.0	98.6
2	0.387	0.804	1.77	4.21	7.47	17.7	32.8	63.9	140
3	0.482	1.00	2.19	5.20	9.21	21.8	40.3	78.4	171
4	0.563	1.16	2.55	6.03	10.7	25.2	46.6	90.7	198
5	0.635	1.31	2.87	6.77	12.0	28.3	52.2	102	222
6	0.701	1.44	3.15	7.45	13.1	31.0	57.3	111	243
7	0.762	1.56	3.42	8.06	14.2	33.6	62.0	121	262
8	0.810	1.68	3.66	8.64	15.2	36.0	66.4	129	281
9	0.873	1.79	3.90	9.18	16.2	38.2	70.4	137	298
10	0.924	1.89	4.12	9.70	17.1	40.3	74.3	144	314
11	0.97	1.99	4.34	10.2	18.0	42.3	78.0	151	329
12	1.02	2.09	4.54	10.7	18.8	44.2	81.7	158	344
13	1.06	2.18	4.73	11.1	19.6	46.1	84.9	165	359
14	1.11	2.26	4.92	11.6	20.4	47.9	88.1	171	372
15	1.15	2.35	5.10	12.0	21.1	49.6	91.3	177	385

Figure C. 16 Chart of flow rate calculation for permeability measurement.

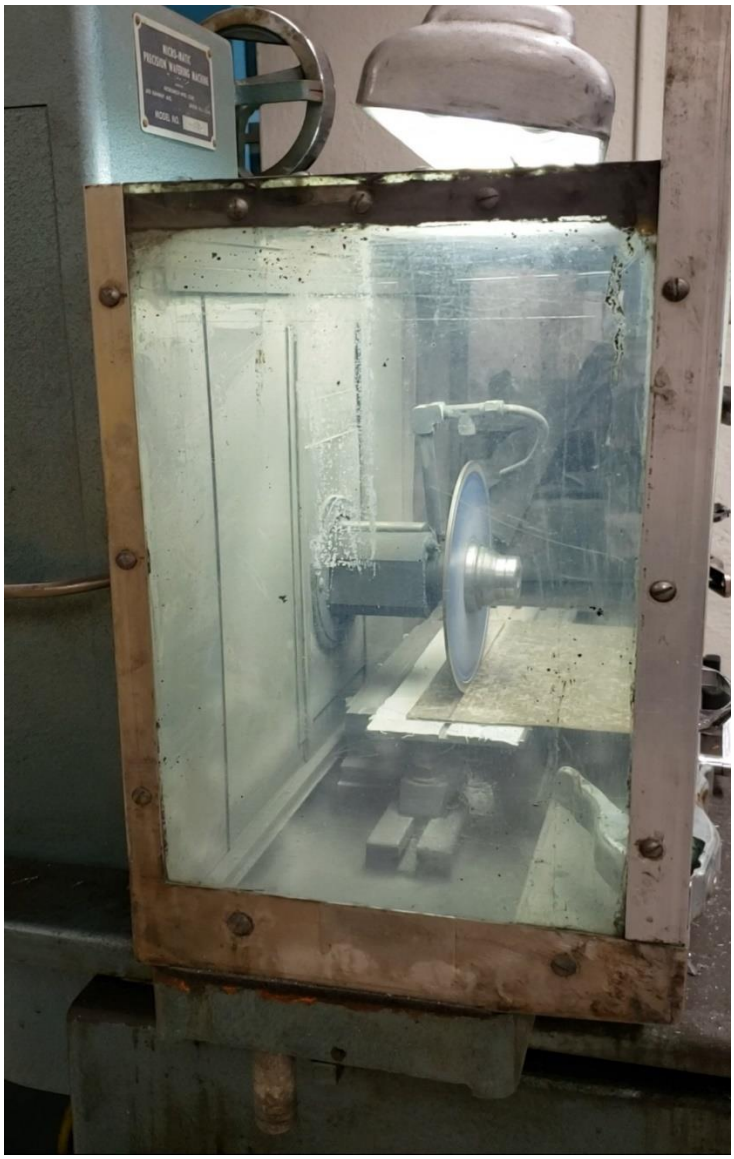

Figure C. 17 Micro-Matic Precision Wafering Machine for composite cutting.